Nonwoven and Hydrogel Poly(glycerol sebacate) (PGS)-Based Materials for Repair of Foot Plantar Defects

Michael David Phillips

Submitted in accordance with the requirements for the degree of Doctor of Philosophy

The University of Leeds, School of Design

September 2022

The candidate confirms that the work submitted is his own and that appropriate credit has been given where reference has been made to the work of others.

Acknowledgements

I would like to thank Prof. Stephen Russell and Dr. Giuseppe Tronci for their support and supervision. I would also like to thank Dr. Christopher Pask for his help and guidance with synthesis and modification of PGS and PGSLP in Chapters 4 and 5.

Abstract

Diabetic ulcers are a common and painful complication arising from diabetes, ultimately undermining the structure and functional competency of the foot. One of the consequences is the loss of soft fatty tissues on the base of the foot, referred to as the 'fat pad'. This compromises the load bearing capability of the foot leading to further dysfunction as well as pain for the patient. Current treatments involve implantation of a replacement elastomeric material to account for the lost fatty tissue. These methods are costly, have poor success rates and the results are often sub-optimal due to short implantation times, the migration of implant material and incompatibility of mechanical properties with the surrounding tissue. From a clinical perspective, the development of a new elastomeric support material suitable for implantation is highly desirable.

In this research, a new PGS-based elastomeric polymer, poly(glycerol-*co*-sebacic acid-*co*-lactic acid-*co*-polyethylene glycol) ($PGSLP_{8000}$) was developed with photo-curing capabilities. The polymer synthesis, modification and processing into hydrogels and fibres, as well as the characterisation of resulting materials are reported. $PGSLP_{8000}$ nanofibre nonwoven webs were produced for the first time by electrospinning after commixing with Poly(ε–caprolactone). Novel PGSLP Acrylate nanofibre-hydrogel matrices (composite structures) were also manufactured, and it was found that incorporation of the fibres allowed modulation of bulk compression properties.

Table of Contents

List of Figures

List of Tables

List of Equations

Abbreviations

ATR – Attenuated total reflectance

DCC – N,N'-Dicyclohexylcarbodiimide

DCM – Dichloromethane

DMAP – 4-Dimethylaminopyridine

DMPA – 2,2-Dimethoxy-2-phenylacetophenone

DSC – Differential scanning calorimetry

ECM - Extracellular matrix

ePTFE – Polytetrafluoroethylene

FDA – Food and Drug Administration

GelMA – Gelatin-methacrylamide

HAMA – Hyaluronic acid-methacrylamide

HFIP – 1,1,1,3,3,3-Hexafluoro-2-propanol

IR – Infrared

MEW – Melt Electrospinning Writing

NMR – Nuclear magnetic resonance

NPWT – Negative pressure wound therapy

OGS – Oligo(glycerol sebacate)

PBS – Phosphate buffer solution

PCL – Poly(e-caprolactone)

PDMS – Polydimethylsiloxane

PEG – Polyethylene glycol

PEGDA – Polyethylene glycol diacrylate

PET – Poly(ethylene terephthalate)

PGA – Polyglycolide

PGS – Poly(Glycerol sebacate)

PGSA – Poly(Glycerol sebacate) acrylate

PGSLP – Poly(glycerol sebacate-co-lactic acid-co-polyethylene glycol)

PGSLPA - Poly(glycerol sebacate-co-lactic acid-co-polyethylene glycol) Acrylate

PHA – Polyhydroxyalkanoates

PHBV - Poly(3-hydroxybutyrate-co-3-hydroxyvalerate)

PLA-L – Poly-L-lactic acid

PLLA – Polylactide

PMMA - Polymethylmethacrylate

RGD – Arginylglycylaspartic acid

SEM – Scanning electron microscopy

TGA – Thermogravimetric analysis

UV – Ultraviolet

Chapter 1

Introduction

1.1 Diabetic Foot Ulcers

Diabetic foot ulcers are a common complication arising from diabetes and are often developed by patients due to factors such as diabetic peripheral neuropathy, peripheral arterial disease and infection.[1] Diabetic foot ulcers affect 15% of people with diabetes[2] with follow-on complications such as soft tissue loss and the formation of cavity wounds that compromise the structure and function of the foot, resulting in chronic ulceration. While treatments for soft tissue loss and cavity wounds are available, they are costly and have poor success rates.[3]

1.1.1 Causes of Diabetic Foot Ulceration

The causes of diabetic ulceration vary between patients as there are different pathways to ulcer formation. Peripheral neuropathy related to diabetes can result in abnormal forces being applied to the foot, and this, combined with diabetic ischaemia, means that the skin is unable to withstand the loads being applied to it, which impairs healing and precipitates a break in the skin.[4] Other contributions to ulceration include genetic predisposition, limited joint mobility and cardiovascular and cerebrovascular diseases, but the most common cause is accidental trauma such as ill-fitting footwear (Figure 1.1).[5]

Another cause of diabetic ulceration is the formation of hammer toes in diabetic patients, where the flexor tendons become straight and rigid. The toes shrink back to form what is called hammer toes, which causes slippage and thinning of the plantar fat pad thereby inducing unnatural force

application throughout the foot, increasing the probability of epidermal fracture and subsequent ulceration.[6]

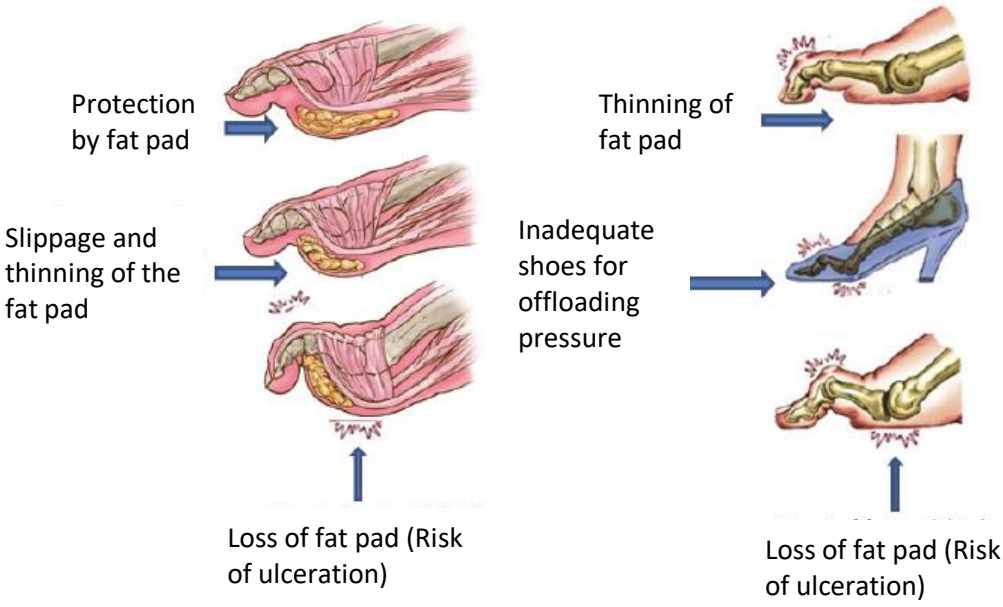

Figure 1.1 Deformation stages of an 'at risk' diabetic foot.[6]

Ulceration can become chronic in diabetic patients, resulting in serious morbidity and pain. Where a cavity wound has formed, effective treatment requires wound healing and mechanical support under compressive loading.[7]

1.1.2 Wound Healing

Treatment methods for chronic wounds can involve invasive procedures such as autologous skin grafting and tissue flap usage,[8] but such techniques carry the risk of infection and pain for the patient because of donor site morbidity. The objective is to manage the wound, particularly wound exudate, to prevent desiccation and infection. This is normally addressed in the clinic and in community nursing by the application of topical and cavity wound dressings, as well as negative pressure wound therapy (NPWT).

Unfortunately, none of the currently used wound dressing materials contribute to mechanically supporting the foot after fat pad tissue has been lost due to disease.

1.1.3 Mechanical Support

The structural and material composition of the human heel fat pad determines the transmission of plantar loading to the lower limb across a wide range of loading scenarios, from locomotion to injurious incidents.[9]

At present, abnormal loading of the foot is routinely addressed in a clinical setting by the provision of customised orthotics for patients. Alternatively, the site can be injected with materials such as silicone (typically polydimethylsiloxane (PDMS)-based)[10] to offset the abnormal loading when soft tissue loss has already occurred. In both cases, this can result in the alleviation of pain and discomfort in patients.

1.1.4 Clinical Use of poly(dimethylsiloxane) Injections

From a mechanical standpoint, injection of PDMS into the affected wound site offsets the loss of tissue. Several 'beads' of silicone are injected at various points to provide some structural support. The load imposed over the wound site by the patient can be of the order of 30 – 300 N mm^{-1}.[11] The load distribution on the plantar weight bearing surface is non-uniform (Figure 1.2 Vertical force component of reaction forces during normal gait.[12]

), with peak forces experienced at the front and heel of the foot.

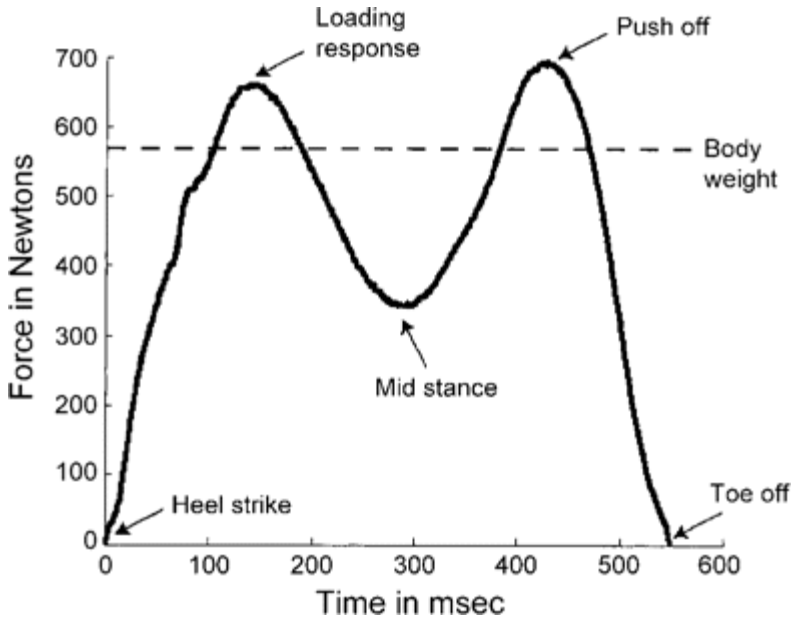

Figure 1.2 Vertical force component of reaction forces during normal gait.[12]

The load imposed over the wound site by the patient relates directly to their body weight, standing patients distribute 50% of their mass across each foot plantar weight bearing surface.[12] While at fast walking pace the mass distribution on each foot can be up to 150%.

Although the silicone (PDMS) is biocompatible and is not generally associated with toxicity concerns, the injection treatment is a temporary solution, and success rates vary between patients.

Clinically, the issue is that silicone implants disintegrate over time, fragmenting and forming microbeads, which then migrate.[10, 13] This is because the mechanical properties of the silicone do not match those of the surrounding tissue. While the mechanical properties of silicone contribute initially to the structural support needed at the wound site, they are not sufficiently well matched to the surrounding tissues, and this may explain the fragmentation of the material and formation of microbeads under compressive loading. Additionally, the migration of the microbeads is problematic in terms of long-term function and implant efficacy.

In some patients, the silicone injection treatment is functional for up to 12 months, following which time implant failure occurs, resulting in further silicone injections being required to restore implant clinical functionality.[14] The short lifetime of the implant and the application of multiple silicone injections lead to risk of secondary infections.

Silicone has also been shown to undergo degradation *in-vivo* in animal studies, forming hydrolysed and oxidised compounds.[15]

While mechanical support may be initially provided by the silicone, the material has no regenerative function in the wound site. Although the tissue may increase in volume, this is due to the body's natural healing processes, rather than any bioactivity associated with the silicone.[16]

1.2 Summary, Aims and Objectives

In summary, there is a need for improved treatments to meet the combined needs of regenerative wound healing, and the provision of mechanical support under compressive loading.

In response to clinical need defined by Mr. David Russell MD, a vascular surgeon leading the Diabetic Leg and Foot clinic at St. James' Hospital in Leeds, this research seeks to develop a replacement fat pad construct suitable for the restoration/replacement of diseased tissue in diabetic wounds of the foot. The overall aim is to develop an alternative elastomeric construct to silicone suitable for implantation, with controlled chemical composition and mechanical properties. The approach will involve the design of a new composite system in which an elastomeric polymer is combined with fibre reinforcement to enable customisation of mechanical properties according to clinical needs.

The specific objectives are:

- To review biocompatible elastomers suitable for the replacement of silicone.

- To design, manufacture and characterise biocompatible, elastomeric materials combined with fibres as a reinforced composite, capable of injection and curing *in situ*.
- To characterise key properties of the new polymer materials in relation to degradation, physical and mechanical properties, relevant to clinical requirements.

Chapter 2

Review of Literature

2.1 Material Requirements

A biomaterial suitable for repair and regeneration of fat pad tissue must ideally address the limitations associated with current silicone injection treatments, and satisfy basic clinical needs in terms of safety, mechanical function, and biological stability. It should also be compatible with the intended surgical procedure, which is delivery by injection.

Native fat pad material is a natural composite consisting of collagen-rich and elastin–rich septa, which envelope adipocytes to confine their movement.[9, 11, 17] As part of a biomimetic approach, formulation of a new composite material should therefore ideally mimic the tissue's natural elasticity, whereby compressive loading is withstood by an amorphous polymer network reinforced by a rigid 'filler' material, which could take the form of appropriately oriented fibres to enhance the structural support. Matching of mechanical properties to those of the surrounding soft tissues is paramount to ensure mechanical compatibility.

The scientific literature highlights a lack of consensus around the properties of human fat pads,[11, 18-24] which may reflect the difficulties involved in studying their behaviour under representative dynamic conditions. Wearing *et al.*[11] used a digital fluoroscope, synchronised with a pressure platform, to obtain force–deformation data of the human heel pad during gait. He reported that the initial stiffness (32 $N.mm^{-1}$) of the heel pad was an order of magnitude lower than its final stiffness (212 $N.mm^{-1}$). The energy dissipating ratio of the heel pad was found to be ~ 0.66 ± 0.12, and the peak deformation of the fat pad was 10.3 mm. This was near to the predicted limit of pain tolerance (10.7 mm), suggesting that during walking, the heel pad operates near to its physiological maximum.

Bennet *et al.*[23] subjected fat pads to cyclic compressive loading with the aim of simulating the forces the pads would be exposed to during locomotion. The reported deformation was much lower (2.1 – 4.7 mm) than other studies, similarly the energy dissipation was much lower at ~0.286 ± 0.069 %. Stiffness however was reported as much higher when compared to Wearing, with a value of 1160 ± 170 $N.mm^{-1}$. Kinoshita *et al.*[22] used a drop impact tester to examine the dynamic properties of the human heel pad. Reporting a similar deformation value to Wearing of 11.3 mm, although over the predicted limit of pain tolerance (10.7 mm). Energy dissipation was also reported to be higher with a range of 0.75 – 0.89 %. Aerts *et al.*[21] used two different methods of testing to determine stiffness and energy dissipation, using an instrumented pendulum and an Instron servo-hydraulic testing machine. Stiffness was determined to be 900 $N.mm^{-1}$ with energy dissipation ranging from 0.46 – 0.66 %.

Pai *et al.*[19] reported the modulus of plantar soft tissue to be 593 ± 205 vs 1147 ± 446 kPa for healthy and diabetic patients respectively which isn't significantly different to the value for healthy tissue reported by Ledoux *et al.*[24] (750 kPa). However Hsu *et al.*[18] reported an even higher modulus for healthy tissue (1140 ± 931 kPa). Kassab *et al*.[20] report an initial modulus of 105 ± 11 kPa initially, and then 306 ± 16 kPa at 30% strain.

In summary the stiffness determined through various studies points to a value approaching $1kN.mm^{-1}$; consequently, a suggested range of 0.9 – 1.2 $kN.mm^{-1}$ would be optimal. An energy dissipation ratio of 46 – 66 ± 0.15 % and maximum deformation of 12 mm is also suitable based upon the reviewed literature. In regard to the desired elastic modulus, without a consensus[18, 19, 24] on a definitive target a material with the ability to display elastic moduli of up to 1.5 MPa would be optimal. Tailoring of the mechanical properties of the material on an individual patient basis is beneficial. Each patient will require a material with different mechanical properties, relating directly to patient's mass index; however other variables will inform material selection, such as the mass of

tissue lost due to ulceration, the patient's gait (which relates to how forces are applied throughout the patient's foot) and mechanical properties of the tissue in the patient's foot.

By addressing the mechanical stability requirements, temporal disintegration of the implant can be minimised, and by controlling the degradation profile of the material, structural integrity and function of the construct could be maintained for a period longer than the one achieved by silicone injection.

Additionally, it is important to recognise that the implantation of biomaterials results in an immune response, and the nature of the response elicited needs to be carefully considered aiming to ensure long-term clinical function *in-vivo*.[25] This requires a detailed understanding of the host inflammatory and wound healing response to implanted materials, which has been detailed in numerous previous studies.[26-28] Immediately after implantation and contact with tissue, blood proteins and interstitial fluids adsorb to the biomaterials surface. This provisional matrix is the starting point of the induced immune response.[29] The specific pattern in which the proteins absorb elicits a specific cellular reaction and the nature of the interaction between cells and these surface proteins contributes towards the inflammatory response. The adsorbed protein layer can therefore stimulate a constructive response in the form of repair and tissue integration or can be detected as a foreign body, prompting the body to either remove or isolate the object.

If the implanted device is a scaffold with the intended purpose of complete integration and tissue regeneration, the material must be compatible and support cell adhesion, migration, and proliferation throughout the scaffold network. However, mild cellular reaction to implanted biomaterials can be beneficial, potentially leading to improved implant performance.[30] Fibrosis is an immune response whereby materials are encapsulated in fibrous tissue. All inert biomaterials

are recognised as foreign and are encapsulated resulting in them remaining unchanged and tolerated within the host.[31]

2.2 Regenerative Devices for Diabetic Foot Ulcer Management

Regenerative medicine is a comparatively new field in modern medicine where endogenous cells, biomaterials and biochemical and physical factors are used to augment, repair, or guide the development of living tissues *in-vivo*. Although tissue engineering and regenerative medicine are used interchangeably in some contexts, there is an important distinction. Tissue engineering involves harvesting of biological tissue with the aim of subsequent implantation of cells or tissues, often combined with a biomaterial, whereas regenerative medicine involves direct implantation of a medical device to restore, maintain or improve tissue function.[32] Today, regenerative rather than classical tissue engineering approaches are preferred, because they avoid the need for harvesting and manipulating cells *ex vivo*, on the one hand, and additional complexities in the regulatory pathway, on the other hand.

Soft tissue repair in diabetic foot ulcers may therefore potentially be achieved *via* the implantation of regenerative devices made of biocompatible, mechanically competent materials to immediately restore function, but also to facilitate longer-term regeneration and replacement of the damaged tissue. Such a strategy requires careful consideration of the cellular and biological processes involved in material-induced tissue regeneration, such as cell attachment, migration and proliferation, expression and retention of biochemical factors and diffusion of nutrients and waste.[33] In regenerative approaches involving the implantation of a medical device, encouraging the homing of proximal cells to the wound site can be a useful strategy for accelerating wound healing and tissue repair.

Plantar fat pads contain a network of collagen and elastin fibrous compartments that surround and retain adipose tissue.[9, 11, 17] Regeneration of tissue is closely tied to the adsorption of proteins in specific patterns onto a materials surface,[29] the interaction between the surrounding tissue cells and the adsorbed proteins dictates cell behaviour and ultimately cellular regeneration. Constructive interactions between surrounding tissue cells and adsorbed proteins yields cell growth and/or differentiations.[34] Further improvement can be made to the regenerative properties of implants with inclusion of growth factors. Hiraoka *et al*.[35] demonstrated *in situ* regeneration of adipose tissue in rat fat pads by introduction of a collagen scaffold combined with gelatin microspheres containing basic fibroblast growth factor. Adipogenesis (cellular differentiation of pre-adipocytes into adipocytes) was enhanced with the inclusion of the growth factor, however, use of microspheres compared to free growth factor demonstrated a significant increase – indicating that the method of growth factor delivery is important. The structure of the material is important in the promotion of cellular regeneration, as has been shown in various studies with nanostructured materials and their efficacy in promoting new bone growth.[36-38] Three dimensional scaffold structures with ordered structures in terms of porosity, pore size, pore morphology and orientation better facilitate migration and infiltration of homed cells.[34]

Traditionally, fibrous polymeric regenerative devices and scaffolds for implantation approved by the Food and Drug Administration (FDA) have been made from synthetic resorbable aliphatic polyesters such as polylactide (PLLA), polyglycolide (PGA), poly(ε–caprolactone) (PCL) and related copolymers. These materials are still routinely used in implantable meshes and sutures, as well as scaffolds. They are inert materials, and although FDA approved are known to hydrolytically degrade *in vivo* by bulk or surface erosion to produce acidic compounds that may be toxic to cells and tissues.[39] Other synthetic polymers have also been used in implantable devices to aid tissue repair, including Poly(3-

hydroxybutyrate-*co*-3-hydroxyvalerate) (PHBV),[40, 41] Poly(ethylene terephthalate) (PET)[42] and polytetrafluoroethylene (ePTFE).[43]

Other fibrous scaffolds are based on materials found in natural extracellular matrix (ECM) such as collagen, fibrin, elastin and hyaluronic acid.[44-46] Such materials inherently possess cell-binding cues, which has garnered significant interest due their potential role in guiding regenerative processes post implantation.[47] Such materials present in the extra cellular matrix can play a critical role in how the scaffold interacts with the surrounding tissues, particularly in respect of increased cell adhesion, compatibility and proliferation, and ultimately wound healing capacity.[48]

2.3 Dermal Fillers

Dermal fillers are applied as treatments to volume deficiency, scars, facial sculpting and facial contouring and their utilisation in fat pad replacement has been considered.[49-51] One representative example is Artefill®, which is a FDA approved permanent dermal filler, based on injectable polymethylmethacrylate (PMMA) for the treatment and correction of the nasolabial fold.[52] It consists of PMMA beads suspended in bovine collagen solution. The PMMA beads are not absorbed by the body, but they induce fibroplasia, a wound healing foreign body reaction, wherein the beads become encapsulated in newly formed collagen tissue. The encapsulation prevents subsequent migration of the beads away from the implantation site.

The main concerns associated with permanent dermal fillers are the potential for delayed onset of an immune response or structural disintegration over time of the implanted material.[53] For example, as the face structure changes due to aging, bioinert non-resorbable implants will not adapt, leading to unacceptable aesthetics. To address this issue, non-permanent dermal fillers composed of poly-L-lactic acid (PLA-L) are used to provide soft tissue augmentation through the stimulation of fibroblast production.[52] Although such fillers are routinely used in cosmetic surgery,

they have rarely been considered in respect of replacing lost fat pad tissue in the foot, and their suitability for load bearing has not been the subject of detailed study.

2.4 Cell Adhesion

In any regenerative device that is to be surgically implanted or injected subcutaneously into a defect site, cell adhesion is of critical importance to enable subsequent cell proliferation and differentiation. Promotion of cell adhesion and proliferation on the surface of a biomaterial can be accomplished in numerous ways, including direct manipulation of surface chemistry such as polyelectrolyte multilayer deposition[54-57], plasma treatment [58, 59], and plasma treatment combined with grafting of functional molecules.[60] Functional molecules can also be covalently attached *via* reactive sites present in the material's molecular structure (Figure 2.1).

Cell adhesion to biomaterials occurs from the interaction between the cell-surface receptors and cell-adhesion proteins bound to the material surface.[61] A common approach of improving cell adhesion properties is to modify the surface of a biomaterial with cell adhesion moieties. Fibronectin and collagen are cell adhesion proteins found in the extracellular matrix, both having excellent biocompatibility and adhesion properties.[62] Rather than the full protein, short amino acidic sequences can be covalently linked to the surface in an economically-affordable and controllable fashion. Arginylglycylaspartic acid (RGD) is a tripeptide sequence present in fibronectin, and is the most common peptide motif responsible for cell adhesion.[63] Cell adhesion proteins called integrins bind to this sequence, although the binding is weaker than integrin-fibronectin interactions, likely due to a lack of secondary structure in the adhesion protein.[64]

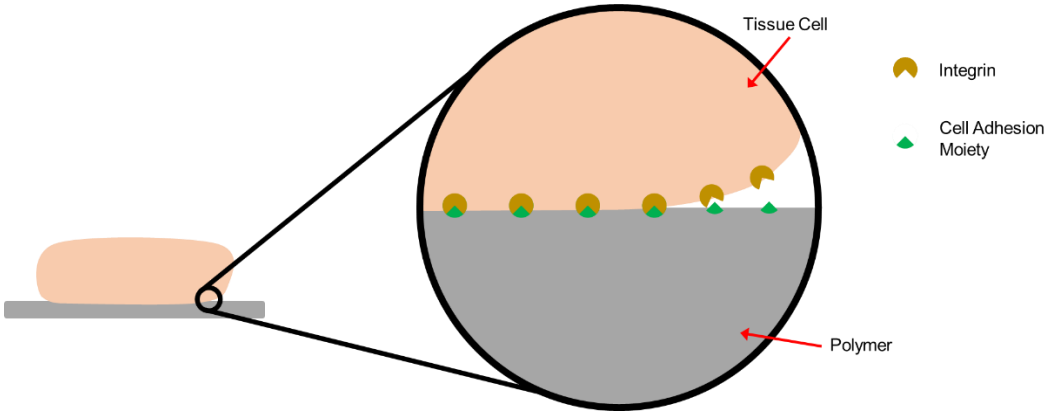

Figure 2.1 Simplified schematic diagram showing interaction between adhesion moiety modified polymer and cell integrin peptide.

Polyelectrolyte multilayer deposition relies upon the alternate adsorption of polycations and polyanions to build multi-layered materials with tuneable properties. By varying polyelectrolyte structure, pH, ionic strength, immersion and rinsing times, it is theoretically possible to produce an infinite range of architectures.[54-57] However, care should be taken in systematically altering the chemical composition of the surface as small changes in structure can result in large changes in biological activity potentially leading to cytotoxicity. Bioactivity of these multilayer materials can be accomplished *via* insertion of biocompatible peptides coupled to polyelectrolytes conserving their full biological activity[65] or embedding of the peptide within the material's structure.[66] Materials have been produced under different conditions that can be cytophobic or cytophilic. By altering the pH or ionic strength, assembly systems can result in materials with very different cell adhesion properties despite presenting comparable molecular features.[67]

Other than polyelectrolyte multilayer deposition, direct surface modification *via* plasma treatment is one way of altering the hydrophobicity of various substrates, which is known to influence cell adhesion.[58, 59] Using SO_2 plasma, oxidised sulphur species are produced that are reported to promote cell adhesion and proliferation, as compared to surfaces modified by immobilisation of diols.[60]

2.5 Mechanical Properties

Particularly for biomaterials that are to be implanted or injected into parts of the anatomy, such as the feet, where immediate load bearing capability is essential, an understanding of mechanical property requirements is essential. It is known that the mechanical properties of the material and the surrounding tissue must be compatible, *i.e*. appropriately matched, to ensure elastic transmission of mechanical loads and minimise the risk of implant failure due to remodelling, where either the implanted material or surrounding tissue deforms.[68] The mechanical compatibility also influences the probability of patient's pain and discomfort. For example, if the compression rates of the material and the surrounding tissue are poorly matched there is the possibility of slippage or shear between the two components. The mechanical properties of a material subject to deformation can be described in terms of the load-deformation or stress-strain curve, wherein the forces may be applied uniaxially or multiaxially, and in tension or compression. In the case of fat pad of the foot, cyclical compressive behaviour is of particular interest. The loading and un-loading characteristics of fat pads in the foot have been previously studied [9, 11, 18, 19, 21-24, 69], with particular reference to resistance to compression and recovery from deformation. Deformation of the fat pad is measured to determine the stiffness, presented as force applied per distance of deformation ($N.mm^{-1}$) and maximum deformation. Stress and strain are measured to determine Young's modulus, ultimate stress point and energy loss of the fat pad material.

2.5.1 Young's Modulus

Young's modulus directly applies in conditions of uniaxial stress, which can be tensile or compressive stress in one direction, and no stress in the other directions. It is effectively a measure of the resistance to deformation and is mathematically defined as the stress - strain ratio (Equation 2.1) obtained from the linear portion of the stress-strain curve (Figure 2.2).

$$Young's\ Modulus\ (E) = \frac{Stress\ (\sigma)}{Strain\ (\varepsilon)}$$

Equation 2.1 Young's Modulus equation.

Stress is measured in terms of force per unit area and strain is a measure of the corresponding deformation.

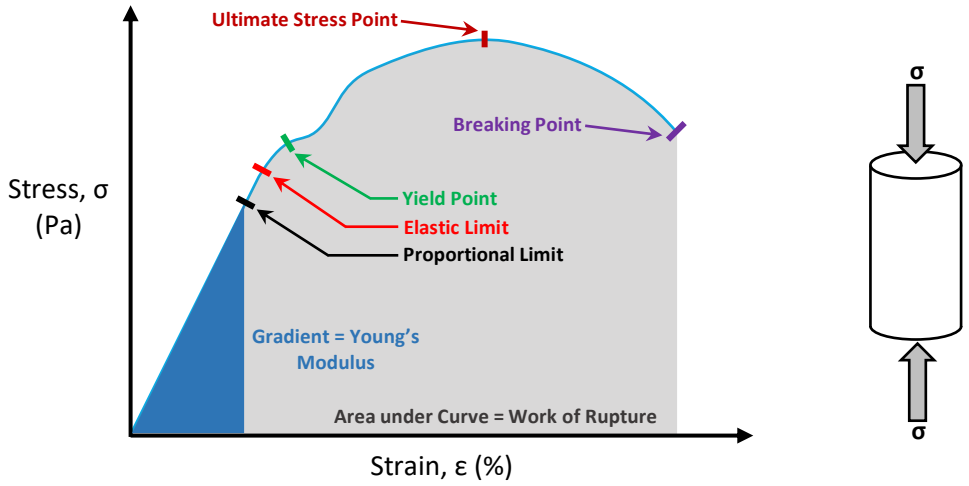

Figure 2.2 An example stress-strain curve (Left), subject to compression (Right).

Characteristic stress-strain curves are obtained for materials as represented in Figure 2.3, depending on their response to load and deformation.

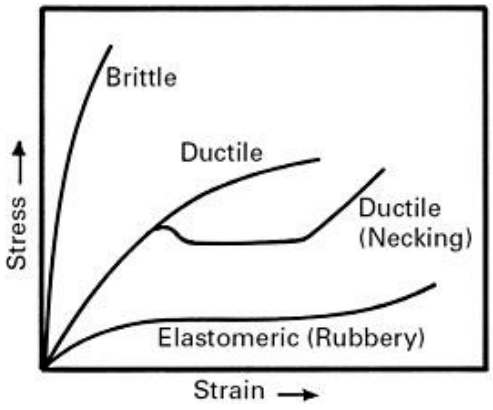

Figure 2.3 Overview of stress-strain responses for brittle, ductile and elastomeric materials [70].

It is known that Young's modulus of plantar fat pad tissue can vary greatly from patient to patient depending on patient mass, foot size (surface area) and fat pad thickness. [18, 19, 24]

Based on a phenomenological numerical model of heel region**,** a classical j-shape curve, commonly encountered for soft tissues was observed (Figure 2.4). Based on 3D numerical meso-modelling of the biomechanical behaviour of plantar fat pads in healthy and degenerative foot conditions (Figure 2.5), valuable data has been reported on the stress-strain and general deformations that are encountered under load.[71]

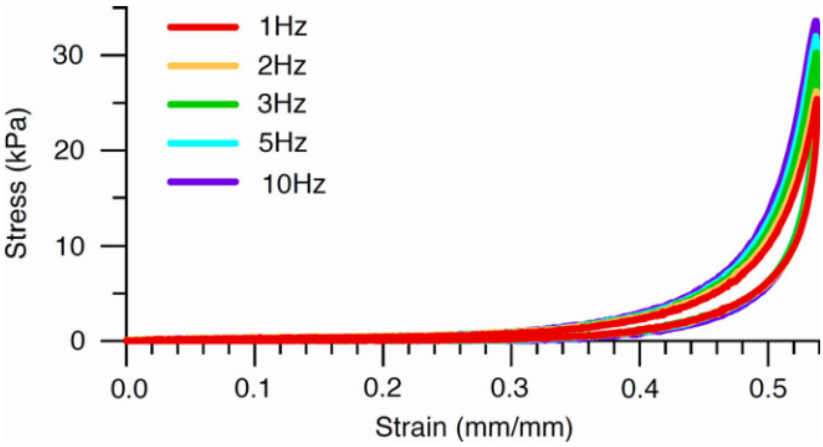

Figure 2.4 J-shaped stress-strain curve from compressive testing of toe plantar fat pads. [19]

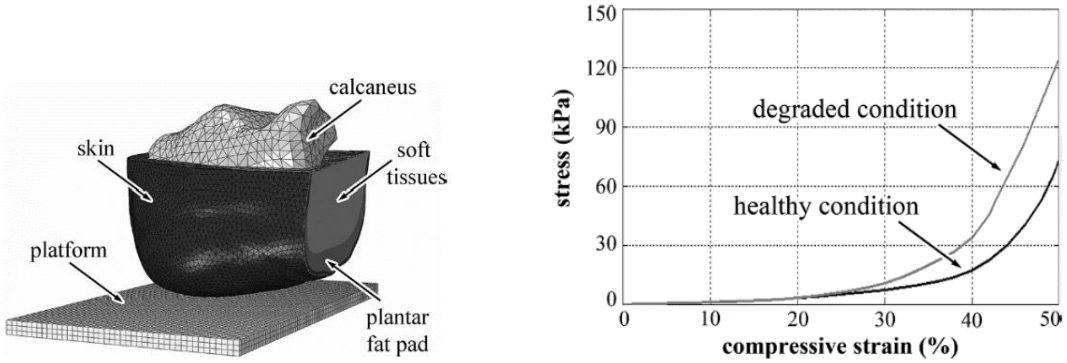

Figure 2.5 Modelling of the stress-strain response of plantar fat pads in healthy and degenerative foot conditions[71].

For the fat pad, Kassab *et al*.[20] reported an initial modulus of 105 ± 11 kPa, and then 306 ± 16 kPa at 30% strain. Pai *et al*.[19] conducted an investigation into comparing diabetic and non-diabetic patient fat pads, reporting 1147 ± 446 kPa and 593 ± 205 kPa, respectively. Ledoux *et al*.[24] reported a modulus of 750 kPa, significantly higher than the one measured by Kassab *et al*. but within the range measured by Pai *et al*. Hsu *et al*.[18] however reported an even higher modulus for healthy tissue (1140 ± 931 kPa).

2.5.2 Ultimate Stress Point

Ultimate stress point/compressive strength is the maximum load divided by the original cross-sectional area of the specimen. It is determined from the stress-strain curve, wherein the peak stress applied to a material is the compressive strength (Figure 2.2). The compressive strength of a material is the maximum amount of energy that can be stored before the material fails completely. Development of a material able to withstand the peak stresses observed in plantar soft tissue during locomotion is an important consideration. Avoidance of implant failure prevents the need for additional surgical procedures for removal of implanted material.

2.5.3 Proportional Limit

Proportional limit is the highest point at which stress is proportional to strain (Figure 2.2). The limit is the stress point at which Hooke's Law (Equation 2.2) fails to apply as a non-linear relationship between stress and strain is observed and therefore marks the end of linear elastic behaviour observed in the material.

$$\sigma = E\varepsilon$$

Equation 2.2 Hooke's Law equation.

The constant of proportionality, E, is known as Young's Modulus, and as described above (Section 2.5.1) is determined as the slope of the stress-strain curve in the linear portion.

2.5.4 Elastic Limit and Yield Point

The elastic limit of a material determines the maximum amount of stress that can be applied before the material will fail to return to its original shape (Figure 2.6).

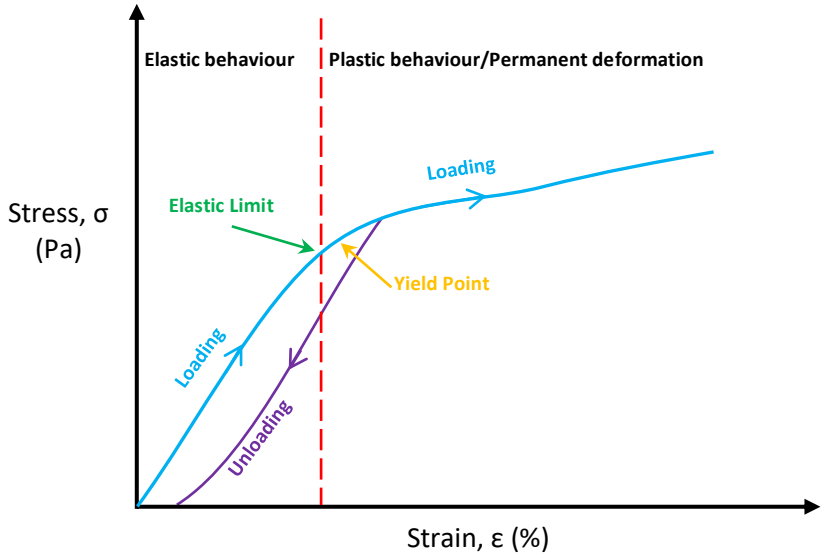

Figure 2.6 Example stress-strain curve demonstrating elastic limit and change in material behaviour. Blue represents the loading phase and purple represents unloading once the elastic limit stress threshold has been crossed.

Application of stress past the elastic limit results in the material shape changing due to plastic deformation, elasticity is no longer observed and permanent deformation occurs once loading has been removed.

The yield point is the minimum stress required to observe an arbitrary amount of plastic deformation or strain (commonly 0.2% plastic strain).[72]

2.5.5 Work of Rupture

Work of rupture or toughness is the ability of a material to absorb energy and deform before fracture,[73] determined from the area under a stress strain curve (Figure 2.7).

Mathematically defined the work of rupture is measured as energy per unit volume:

$$Toughness = \frac{Energy}{Volume} = \int_0^{\varepsilon_f} \sigma \, d\varepsilon$$

$$\varepsilon = Strain$$

$$\varepsilon_f = Strain\ at\ failure$$

$$\sigma = Stress$$

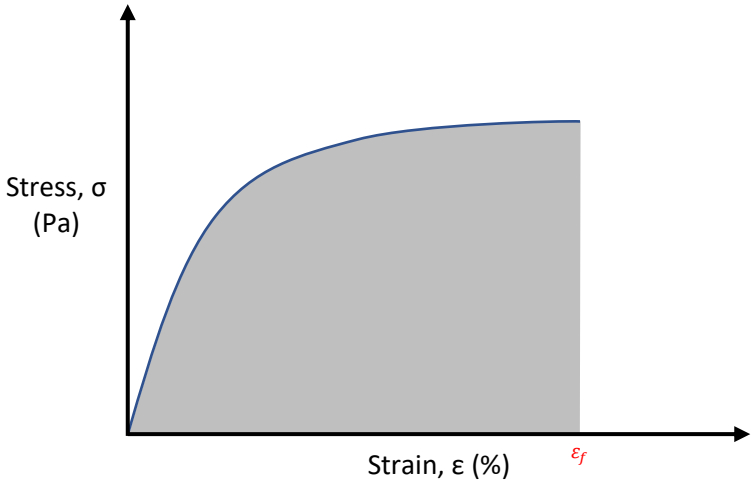

Figure 2.7 An example stress strain curve demonstrating toughness of different materials

Toughness requires a balance between strength and ductility. There are several variables that have an effect on the toughness of materials.[73] A material may possess suitable toughness properties under static loading however when undergoing dynamic testing failure may occur, generally toughness decreases as the rate of loading increases. As the temperature of materials is lowered, their ductility and toughness also decrease, resulting in brittle material behaviour – the point at which this occurs is known as the transition temperature. The notch effect is due to multiaxial

distribution of stress, the material, being unable to withstand the elastic and plastic deformation in multiple directions fractures.

2.5.6 Elasticity

Elasticity is the ability of a body to resist deformation by stress, returning to its original size and shape once the stress has been removed.[74] Elasticity in polymers is attributed to the stretching of polymer chains. When a deforming force (stress) is applied to a material, the strain does not change simultaneously, and the strain response is delayed. Similarly, when removing the deforming force, the strain response lags behind. This delay between the strain response and applied stress is called elastic hysteresis (Figure 2.8), and the area enclosed by the loading and unloading stress -strain curves is the energy dissipated due to internal friction.[75]

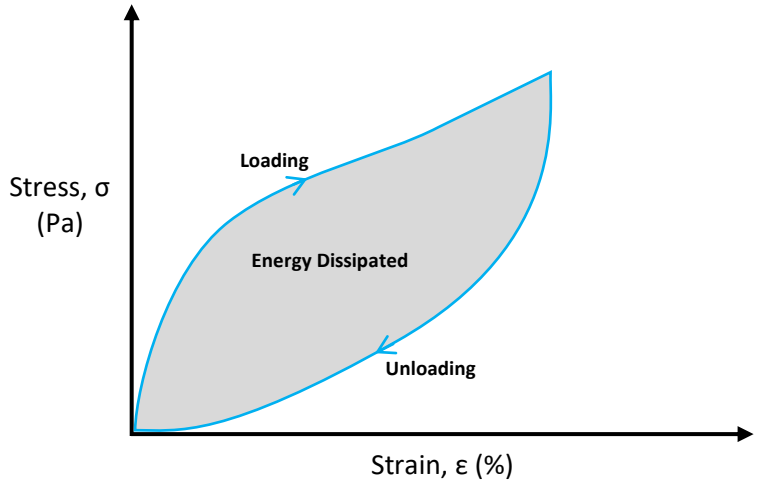

Figure 2.8 An example stress strain curve demonstrating elastic hysteresis.

After permanent deformation occurs, removal of the stress applied to a material results in a fraction of the deformation being recovered (Figure 2.9), known as the elastic recovery.[76] During the unloading cycle the curve decreases at the same gradient as the modulus of elasticity.

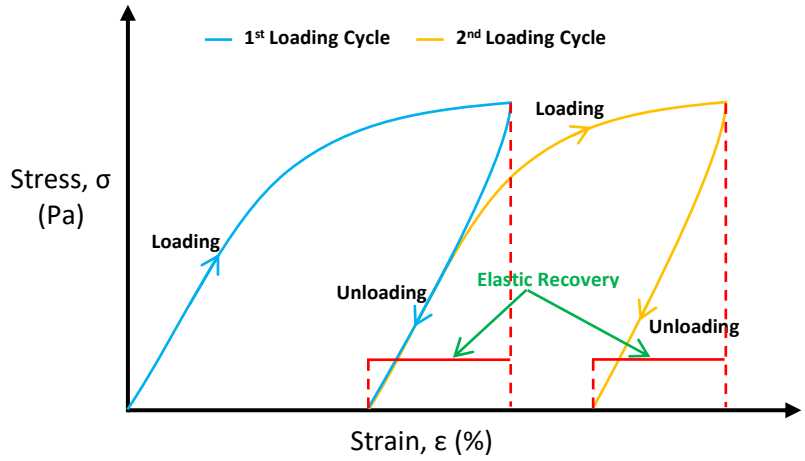

Figure 2.9 An example stress strain curve demonstrating elastic recovery under 2 different loading cycles: First cycle (Blue) and second cycle (Orange).

Application of mechanical loading after the unloading phase of the first testing cycle will yield a curve that follows a similar shape translated further along the strain axis. The second testing cycle curve will follow the linear segment of the previous cycles unloading phase. Yielding will be observed at the same stress level where unloading began in the first testing cycle.[76] A diagrammatic explanation of this is shown in Figure 2.9.

2.5.7 Fatigue

Deformation fatigue is of major importance given the foot pad replacement should provide structural support with a long implantation time. The material is subject to mechanical strain repeatedly for periods of up to 12 months[14], but must maintain its structural integrity and function, so that abrupt changes in mechanical response are avoided. Fatigue involves the weakening of a material due to repeated applied loads. It is the result of progressive and localised structural damage occurring when a material is subjected to cyclic loading. The nominal maximum stress values that lead to such damage may be considerably lower than the strength of the material, which is typically quoted as the ultimate tensile stress limit or the yield stress limit.[74]

2.6 Elastomers for Medical Devices

Given the repeated loading and unloading of the fat pad, and the typical j-shape stress-strain response of the tissue in which a small stress results in a large strain, elastomeric polymers are of particular relevance when considering potential injectable repair or regenerative materials. Elastomers or rubbers have the ability to undergo large deformation under stress combined with high elastic recovery. This type of elastic response, in cyclic loading and unloading is essential to devise a viable biomaterial capable of remaining structurally and mechanically competent. Both natural and synthetic elastomers are known for the manufacture of implantable devices, including silicones, polyurethanes, polyolefins and polydienes in varied molecular configurations.[77]

2.6.1 Physically Crosslinked Elastomers

Physically crosslinked elastomers (Figure 2.10) rely on physical interactions between the polymer chains in the form of hydrogen bonds, electrostatic interactions, or dipolar forces, resulting in crystalline and glassy regions with amorphous segments. The crystalline and glassy regions act as physical crosslinkers which provide the bulk of the mechanical strength and the amorphous segments are responsible for the materials' flexibility.[78]

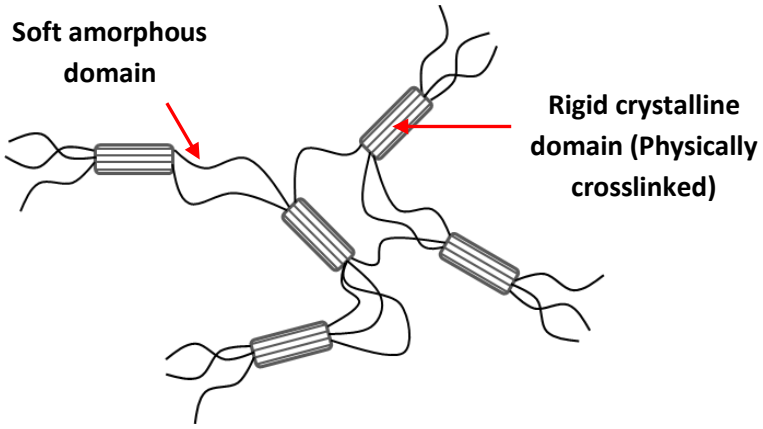

Figure 2.10 Schematic of a physically crosslinked elastomeric polymer.

2.6.1.1 Silicone Elastomers

Silicones (Figure 2.11) have found numerous applications in medical devices due to their biocompatibility and bio-durability.[79] Their hydrophobicity, low surface tension and chemical and thermal stability are the basis for their use in medical devices. Coating of needles, syringes and vials resulted in a surface which preserves blood and prevents clotting.[80] Current clinical treatment for fat pad loss involves injection of PDMS, which is the most widely used polymer in siloxane elastomers.[81] The first medical grade injectable PDMS elastomer was introduced in 1962,[10] however due to complications and lack of quality clinical data was suspended by the FDA by 1976. Other PDMS devices were still in use however, so that breast implants became available in 1962 and were implanted in 1 – 2 million women.[10] Although in widespread use, medical grade silicones are stiffer than natural plantar fat pad material, with Young's modulus of 1.4 MPa[77] compared to that of plantar fat pad tissue of 0.1 – 1.5 MPa[19, 20], with 1.5 MPa being associated with patients with increased body mass compared to average body mass patients. This is partly compensated by injecting smaller volumes *via* injection at various sites within the affected area, to re-distribute the standing forces.

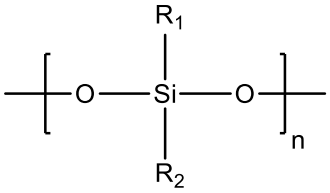

Figure 2.11 General structure of a silicone elastomer.

Long term implantation of silicones has been documented for tissue replacement as early as 1950 by Robert De Nicola, where complete replacement of a male urethra by silicone tubing was carried out with no rejection.[82] Silicone implantation has evolved greatly since 1950 with implants available for almost any part of the body however perhaps the most frequently used globally were

silicone hydrogel contact lens. Contact lenses were initially produced from glass or PMMA (Figure 2.12). However, there were inherent problems associated with the use of these as biomaterials. Their lack of oxygen permeability caused dryness and discomfort in the eye, which could manifest as corneal oedema.[83] Silicone hydrogel contact lenses solved this by allowing oxygen to permeate to the cornea preventing hypoxia.[84]

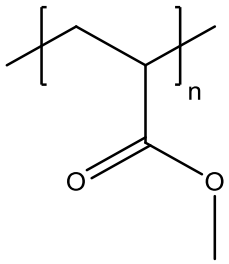

Figure 2.12 Structure of polymethylmethacrylate

While silicone is an excellent biomaterial which has provided many solutions to medical challenges, it has also been used extensively for cosmetic reasons, breast, chin and nose implants are commonly made from silicone.[77] Another limitation of silicone materials is their lack of regenerative capacity, so while mechanical function in the foot plantar may be restored for a period after implantation, there is little opportunity for tissue regeneration.

2.6.1.2 Polyurethane Elastomers

Polyurethanes (Figure 2.13) are a family of polymeric materials with large diversity of chemical compositions, mechanical properties, tissue specific interactions and biocompatibility with mechanical flexibility and moderate blood compatibility being their most prominent features.[77] Due to the sheer diversity of composition and mechanical properties, they are some of the most extensively used biomaterials in therapeutic devices,[85] as shown by their use since the 1980s in the production of durable cardiovascular devices,[77] blood bags, vascular catheters, and small calibre grafts for bypass surgery.[86] However there have been structural stability problems

associated with polyurethanes such as failed implantation of pacemaker leads and breast implant coatings[87], this has been remedied by studies into their ability to biodegrade which has allowed for the production of polyurethane biomaterials with improved stability suitable for long term implantation.[77, 87] Cytotoxicity has been an issue with some polyurethanes with the degradation process generating known carcinogenic molecules.[77]

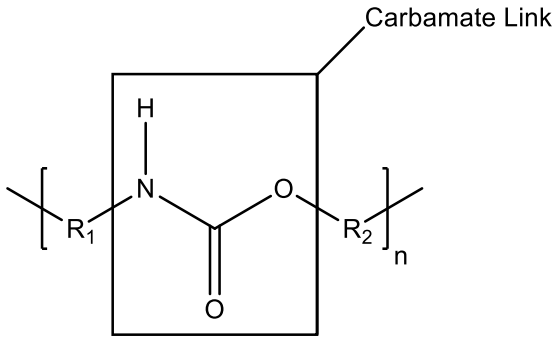

Figure 2.13 General structure of a polyurethane elastomer.

A new class of bioresorbable polyurethanes has also been developed,[88, 89] in which the balance between biodegradability and durability can be tuned depending on the intended application.[77] Early in their development, polyurethanes, specifically based on aromatic diisocyanates, were initially found to biodegrade into potentially carcinogenic by-products.[90, 91] The use of aliphatic diisocyanates has circumvented this problem, along with the beneficial properties of having better blood and tissue compatibility.[86]

Alongside their biocompatibility, polyurethanes can be designed such that their mechanical properties can be tailored for specific applications where different load bearing requirements are needed. This is achieved by varying the ratio of hard (crystalline) and soft (amorphous) components[77, 92] or by changing the structure of the reagents used.[93] The Young's modulus values of polyurethanes (of the order of 10^1 MPa[77, 94]), are close to some soft tissues, but for fat

pad tissue replacement the values are still too high to provide a mechanically biomimetic alternative.

2.6.1.3 Polyhydroxyalkanoate Elastomers

Polyhydroxyalkanoates (PHAs, Figure 2.14) are polyesters biologically produced from hydroxyl-alkanoic acids *via* various native and recombinant bacterial strains.[95, 96] These are used biologically as a carbon and energy storage medium.[97] PHAs have excellent biocompatibility, evidenced, for example, by the presence of hydroxyalkanoate poly(3-hydroxybutyrate) as a natural constituent of human blood. Furthermore, the degradation product, 3-hydroxybutyric acid is also naturally occurring in human tissue. [98] However, PHAs produced *via* bacterial fermentation can contain molecules that are known to produce an inflammatory response.[99]

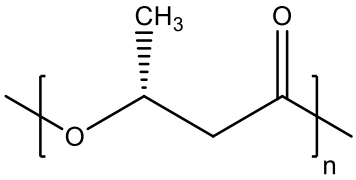

Figure 2.14 Structure of poly(3-hydroxybutyrate).

Over 150 different types of PHAs are known such that there is a large range of physical and mechanical properties available, which are modulated by the nature of the side chains in the structure. Polyhydroxyalkanoates with short side chains tend to be more crystalline and rigid than those with longer side chains.[100] The Young's modulus of PHAs covers a range from 10 MPa[101] to 3800 MPa[102]. Although much too rigid for most soft tissue applications, ligament and tendon tissue scaffolds are a promising application, with elongation at break reaching 1000% with some PHAs [102]. Due to their production *via* bacterial biosynthesis the economic cost of PHA production

is deemed unsuitable for most clinical applications, however there has been interest in developing better bacterial strains and more efficient methods of fermentation/recovery.[103]

2.6.2 Chemically Crosslinked Elastomers

Chemically crosslinked elastomers exhibit elasticity due to the chemical bonds that link different polymer chains. Covalent crosslinks can take many forms such as the reaction between multifunctional monomers (such as tri-reactive site molecules) or by connecting reactive groups located within the molecule, at the end of polymer chains or both.

When a polymer chain gains a large enough molecular weight tending to infinite it is said to have formed a gel, whereby it contains a crosslinked polymer network with branched/unbranched soluble molecules.[77] The formation of these crosslinks can be initiated thermally and *via* radiation, usually in the form of ultraviolet (UV) or visible light. Using a Steglich Esterification[104] reaction, norbornene carboxylic acid can be grafted to the polymer, introducing alkene functionality, which can be utilised with thiol functionalised molecules to further modify the polymers structure. Chemically crosslinked elastomers can be formed from natural and synthetic building blocks, often the naturally occurring elastomers have excellent biodegradability and biocompatibility.[77]

2.6.2.1 Poly(polyol sebacate) polymers

Poly(polyol sebacate) polymers are a group of polyester elastomers synthesised from a polyol (a molecule containing multiple hydroxyl groups) and sebacic acid. The properties of the material can be varied by altering the molar ratios of the polyol monomer and sebacic acid, allowing for a large range of mechanical properties to be exhibited.[105]

The elastomer is formed following a simple pathway, whereby the primary alcohols at the end of the polyol monomers react first with the carboxylic acid groups of sebacic acid, forming long

polymer chains. After this pre-polymerisation the hydroxyl groups within the polymer chains react with the carboxylic acid groups forming crosslinks between the polymer chains, eventually forming a gel. These elastomers have been shown to generally have little toxicity to biological tissues[106] with highly crosslinked variants exhibiting excellent cytocompatibility[107, 108]. However, as with other polymers, an increase in crosslink density generally leads to a material with compromised mechanical properties such as brittleness. This can however be resolved by copolymerisation.

2.6.2.1.1 Poly(glycerol sebacate)

Poly(glycerol sebacate) (PGS, Figure 2.15) is a promising elastomer in the field of regenerative medicine. Comprised of glycerol and sebacic acid, the production of this polymer is very simple and does not involve the formation of toxic by-products. Polycondensation occurs when the reagents are combined and heated. The only by-product is water, while glycerol is used as a food additive, sebacic acid is excreted through the urine naturally as a product of metabolic processes.[109]

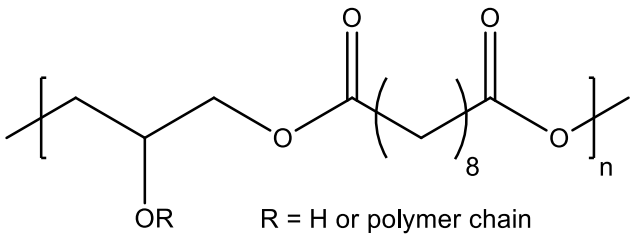

Figure 2.15 Structure of poly(glycerol sebacate).

The first stage of the polycondensation is used to produce oligomers. The second stage of the reaction is the curing stage whereby the polycondensation is continued for a selected period of time; the longer the curing time the more crosslinks are formed in the polymer structure, leading to increased rigidity. Consequently, the mechanical properties of the elastomer can be modulated by adjusting the curing time, whereby increasing the curing time is expected to lead to highly crosslinked polymers.

One potential drawback of a highly crosslinked polymer system is the consequent resistance to dissolution, making it difficult to further modify the polymer structure by for example grafting other moieties and functional molecules into the network. PGS is observed to have a Young's modulus in the range of 0.056 – 1.5 MPa and an elongation at break of 40 – 450% depending on the synthesis conditions,[110] making it ideal for soft tissue applications and for the intended use as a structural support scaffold.

2.6.2.1.2 Poly(glycerol sebacate) acrylate

Building on the attractive mechanical properties of PGS elastomers with respect to applications in tissue replacement, copolymerisation and covalent network formation provide further opportunities aiming to achieve materials with tuned physical properties. Furthermore, by exploiting the opportunities provided by photo-curing, there is potential to avoid high reaction temperatures that would otherwise be required (110°C-150°C [77]). Clearly, such high temperatures could not be tolerated *in vivo* as part of an in-situ reaction process after injection of the polymer precursors into the foot plantar.

Based on work by Nijst *et al*. [111, 112], a photo curable elastomeric variant has been synthesised, known as poly(glycerol sebacate) acrylate (PGSA). Pre-polymerisation is pursued between glycerol and sebacic acid to produce polymer chains, which are then acrylated *via* reaction between the unreacted hydroxyl groups and acrylate moiety (Figure 2.16). Finally, product exposure to UV light in the presence of a photo initiator yields the final elastomeric covalently crosslinked network product. Importantly, resulting system is biodegradable and the biodegradation profile can be adjusted by varying the molar content of acrylate derived crosslinks.[111]

Acrylation or the introduction of other forms of alkene functionality allows for the use of thiol-ene click chemistry to be utilised for selective crosslinking of the polymer chains. The advantages of using

thiol-ene click chemistry are the high yield, high rate and stereo selectivity.[113, 114] Investigations into the viability of using thiol-ene click chemistry have shown that the functional group tolerance of the reaction is excellent,[115-117] allowing for complex macromolecules to be produced with large ranges of functionality. The radical-mediated reaction can be driven/initiated either by thermoinitiators such as azobisisobutyronitrile or through photoinitiation, with the latter being preferable due to the much milder conditions and lack of explosive potential.

Thiol-ene click chemistry is especially valuable for the synthesis of dendrimers, which are valuable for biomedical and nanoengineering applications. Another exciting application of thiol-ene click chemistry is the targeted construction of localised polymer configurations on the material surface. These can be realised by photomasking, where selective exposure to a UV light source initiates subsequent thiol-ene reactions and the construction of defined polymer architectures in a targeted fashion. Introduction of acrylate groups to the PGS will allow for further modification *via* thiol-ene click chemistry, either through crosslinking between the polymer chains or by grafting functional molecules onto the structure.

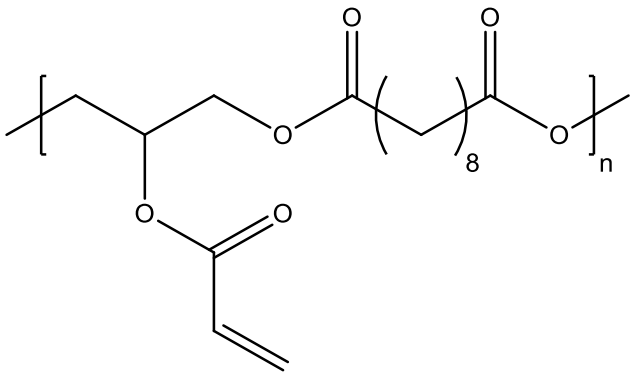

Figure 2.16 Structure of poly(glycerol sebacate) acrylate.

With PGS acrylate, other acrylated macromolecules such as polyethylene glycol (PEG)-diacrylate (a polyethylene glycol molecule functionalised with acrylate at both terminal ends) can be used as

copolymer to further tune the characteristics of resulting polymer network. e.g. mechanical strength, water swelling ratio, hydrophobicity and degradation rate.[111] Alongside the increased mechanical properties, the poly(polyol sebacate) co-polymers have been shown to promote cell growth, supporting their use as a replacement for hydrogels in regenerative medicine.[112] Furthermore the adhesive properties of poly(glycerol-*co*-sebacate) acrylate allow it to attach to tissue and resist mechanical deformations, the adhesive properties have been reported to be enhanced further by surface modification with tissue reactive oxidised dextran onto "gecko feet" nanotopographically moulded elastomers.[118]

2.6.2.1.3 Poly(diol citrate)

A novel polyester elastomer was developed by Ammer's group based upon formulation with citric acid and diol molecules.[119, 120] Citric acid is an intermediate in the tricarboxylic acid cycle in cell metabolism and is therefore biocompatible. As such, citric acid is widely used in the food industry and acts as a natural preservative. The synthesis of poly(diol citrate) is very similar to poly(polyol sebacate)s, however reaction temperatures can be as low as 37°C.[119, 120] The reaction compatibility with mild temperatures is highly desirable since it allows for polymer synthesis to occur at near-physiological conditions, avoiding the use of high, potentially toxic, temperatures to perform the polycondensation.

The Young's modulus of poly(diol citrate) is increased significantly compared to that PGS, ranging from 1.6 ± 0.05 to 13.98 ± 3.05 MPa[120] depending on the polyol used. The degradation of the materials also proved to be modulated by varying the number of methylene units present in the diol, so that an increase in the number of methylene units proved to lead to polymers with decreased degradability.

2.6.3 Protein Based Biomaterials

Proteins are organic building blocks comprised of amino acids, there are 22 naturally occurring amino acids that can be sequenced in varying orders to produce an extremely large variety of compounds that provide tissues with specific structure and function. Structural proteins maintain integrity of tissues by providing mechanical strength while functional proteins, such as enzymes, allow catalysis of biological processes.

Protein-based biomaterials are becoming a more desirable option for bio-engineering due to their biomimetic features at the molecular and microscopic scale and ability to self-assemble into mechanically competent structures. Their mechanical properties are dependent on the environment in which testing is done. For *in vivo* applications, mechanical testing of protein-based biomaterials should therefore be carried out at physiological temperature and in the hydrated state.

2.6.3.1 Collagen

Collagen is the most abundant protein present in the human body, it provides structural integrity for a large amount of tissues such as connective, cartilage and internal organs.[121] There are many different types of collagen with collagens I-V being the major types.[47] Collagen is a truly elastic protein and has been shown to be capable of reversible deformation, it also displays an extremely wide variation of Young's modulus, which makes collagen relevant for multiple applications. Unlike most synthetic polymers, collagen is susceptible to enzymatic degradation. Due to its ability to readily dissolve in acidic aqueous solutions, collagen can be processed in various material formats, such as sheets, foams, and injectables[47], making collagen customisable to the requirements of the intended application. As a major component of the extracellular matrix of biological tissues, collagen can act as a substrate for cell attachment, proliferation and differentiation, in the context of e.g. tissue engineering and wound dressing applications.[77]

The mechanical properties of collagen can vary depending on the harvesting location. The Young's modulus of collagen extracted from skin tissue can range from 2 – 46 MPa, whereas collagen deriving from human tendons has a Young's modulus of 1.2 GPa.[122] The observed variability of mechanical properties highlights the need for specificity when using elastic proteins that are harvested from natural tissues. Additionally, the enzymatic degradation of naturally derived elastic proteins raises issues with regards to their long-term functionality *in vivo*, so that chemical modification may be pursued to increase protein biostability.

2.6.3.2 Elastin

Elastin is an important component of tissues that are prone to repeated applications of strain, such as skin, lung alveoli and elastic cartilage.[123] Considering the typical stress-strain j-shaped curve of tissues, elastin is responsible for the initial low modulus region, while collagen maintains bulk structure and prevent over extension of the elastic portion of the tissue. Compared to collagen, elastin is more flexible and stable. Although elastin is regenerated at a baseline level, it remains present throughout the organisms' lifespan although decreasing in elasticity with age.[122] The biodurability of elastin is especially desirable in long term implantation.

Elastin, or rather its precursor protein tropoelastin, has the remarkable ability to self-assemble, whereby alignment of tropoelastin molecules prior to intermolecular crosslinking allows for the formation of spherical droplets.[124] Elastin's ability to self-assemble has the potential to be exploited for the development of novel bio-actuators, implantable sensors and drug delivery vehicles.[77] Elastin based networks can be prepared *via* recombinant peptide sequencing allowing for elastin mimetic materials to be synthesised[125, 126], whereby fine tuning of mechanical properties can be achieved by changing the residue identities at specific locations in the polymeric chain.[125]

Elastin is perhaps the best naturally derived elastomeric protein in terms of the lower spectrum of soft tissue engineering. With a Young's modulus ranging from 0.3 – 1 MPa[122], elastin is ideal for a large range of applications. Being the component in natural tissue that provides bulk elasticity, it exhibits a breaking strain of up to 150 %[122], and represents one of the most stable natural proteins, with a half-life of up to 70 years[77].

2.6.4 Elastomeric Composites

Elastomeric composites are especially useful for the design of hard biomaterials, whereby the inclusion of inorganic compounds into the polymer matrix can drastically increase the materials mechanical properties due to the Einstein filler effect, due to the increased crystallinity and rigidity of introduced species. Organic tissue such as bone is comprised of naturally occurring polymer and inorganic compounds, yielding a material with excellent compressive strength properties but compromised elasticity.[77]

Composite materials circumvent some of the problems associated with 'pure' elastomeric materials, whereby an increase in compressive modulus is often associated with decreased elongation at break. Another advantage in the design of composite materials is that the inclusion of the filler, such as calcium phosphate or bioactive glass, can buffer the acidic degradation products of the polymers, resulting in reduced toxic effects to surrounding cells and tissues.

2.6.4.1 Thermoplastic Rubber Based Composites

Thermoplastic based composite reinforcement results in an increase in elastic modulus and hardness due to the Einstein filler effect, *i.e*. the inorganic crystalline regions of the composite act as a crosslinker in the network providing increased structural rigidity. One of the major drawbacks of thermoplastic elastomers is their heterogeneous degradation pattern, which may lead to

unpredictable mechanical failure.[68] Therefore, substantial research efforts have focused on the development of thermoplastic composites with reliable mechanical properties and degradability.

PET(DLA-TiO_2) composites have been investigated as heart patches using a rot model, the study showed that, while the mechanical properties of the composite were superior to that of PET alone, the material rigidity promoted damage of the heart muscle *via* surface friction.[127] In comparison, PGS elastomer proved to be mechanically compatible with the surrounding tissue, and allowed to effectively prevent post-infarction hypertrophy and reduced tissue remodelling.[68]

2.6.4.2 Crosslinked Elastomer Based Composites

Crosslinked elastomer composites exhibit an increase in elastic modulus and elongation at rupture when filler reinforcement is employed. Partial replacement of the deformation matrix by rigid filler particles typically leads to increased rather than decreased stretchability. This increase in antagonistic properties is characteristic of elastomeric composites.[128]

PGS and poly(1,8-octanediol-citrate) have been composited with Bioglass®[107, 129] and hydroxyapatite[130], respectively, with both products showing improved mechanical properties relative to their homogeneous polymer systems. PGS crosslinking is affected by the type of bioceramic filler used as reinforcement, whereby introduction of acidic bioceramic fillers proved to decrease the rate of crosslinking, while basic fillers generally proved to induce the opposite effect.[77] Ionic interactions can also play a role in the crosslinking kinetics, as shown by alkaline Bioglass®, which releases metallic ions in physiological conditions. These metallic ions compete with the crosslinking esterification reaction *via* the formation of calcium dicarboxylate bridges.[107] When the composite is exposed to an aqueous solution these unstable calcium dicarboxylate bridges dissociate, resulting in a PGS elastomer with lower crosslink density than pure PGS.

The biocompatibility of bioactive glass composites can be influenced by the basic degradation of the filler material, which can help buffer the acidic degradation products of some elastomers, such as PGS. This effect has been shown to significantly decrease the cytotoxicity of resulting composite when compared to that of pure PGS elastomers.[107, 129] Other than the biocompatibility, the biodegradability can be both positively and negatively affected in bioactive glass composites.

The introduction of bioceramics into elastomers can reduce the crosslink density of the network and enhance composite's enzymatic degradability, so that reduced degradation time is required to achieve complete mechanical failure of the material. Alternatively, the filler-induced buffering effects can reduce the rate of hydrolysis of ester bonds present along the polymer backbone resulting in an increased polymer biodurability.[131, 132] Depending on which effect is more prominent, tuning of the biodegradability can be controlled by varying the proportion of filler material.

2.7 Cyanoacrylates

Cyanoacrylates (Figure 2.17) are desirable for biomedical applications due to their mechanical strength and instantaneous and rapid setting time. The 'R' group of the cyanoacrylate has a large influence on polymerisation and properties of the polymer. A decrease in the length of the side alkyl group typically results in decreased polymerisation rate and leads to polymers with increased flexibility and decreased hydrolytic degradability.[133] The polymerisation is exothermic and so heat generation could cause protein denaturation as well as local toxicity.

Cyanoacrylates degrade and form toxic by-products such as formaldehyde and cyanoacetate.[134] Shorter alkyl chain cyanoacrylates degrade faster resulting in a stronger tissue inflammatory response. On the other hand, longer alkyl chain cyanoacrylates degrade slowly, resulting in minimal build-up and prompt removal of toxic products, as well as mild inflammatory response.

Cyanoacrylates have been reported to induce tissue necrosis *in vivo*, arterial ocular lesion, occupational asthma, dermatitis, and *in vitro* cytotoxicity in either direct contact or eluate tests.[135]

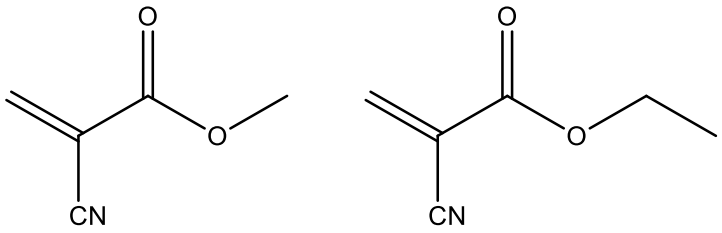

Figure 2.17 Methyl cyanoacrylate (Left) and ethyl cyanoacrylate (Right).

Integration of long alkyl chain side groups would allow for the synthesis of polymers with increased flexibility and biodurability; however, the release of formaldehyde during polymer degradation is problematic. Ethyl, n-butyl and octyl cyanoacrylates are approved by the FDA.

A study into the effects of introducing cyanoacrylates for wound closure found that the immune response matched that of typical suture closure,[136] suggesting that biocompatibility of certain cyanoacrylates is not significantly different from biomedical wound closure materials. Crosslinking of cyanoacrylate pre-polymers has also been reported as a suitable route to produce bioadhesives with excellent adhesive capability and biocompatibility,[137] whereby polymer biodegradability could be tuned by adjusting the acrylate-PEG molar ratio as well as the molecular weight of PEG. Partial pre-polymerisation can also be used to improve biocompatibility as it causes a longer chain structure.[138, 139] Preparation of water-immiscible films and coatings from poly(2-methoxyethyl acrylate) has been achieved[140]; however, the ability of the film to form inside a wound cavity that can contain a soft tissue engineering elastomeric material is unknown.

The mechanical properties of cyanoacrylates are more suited to hard tissue applications or as sealants/bioadhesives, typically the Young's modulus ranges from 50 – 1500 MPa[134]; far too high

for the intended application when their cytotoxicity issues are also considered. Although promising as surgical adhesives due to their rapid adhesion times with strong closure of wound sites.

2.8 Hydrogels for Regenerative Medicine and Medical Devices

Hydrogels consist of crosslinked hydrophilic polymer chains highly swollen with water (Figure 2.18), whereby volumetric swelling occurs due to the hydrophilicity of the polymer chains and the presence of either covalent or physical crosslinks. They have many applications such as drug delivery vehicles, wound dressings, and agricultural uses. Hydrogels are inherently weak in terms of mechanical properties, thus various approaches can be undertaken to remedy this, such as altering the crosslink density, encapsulation of particles to form a composite and fibre reinforcement[141].

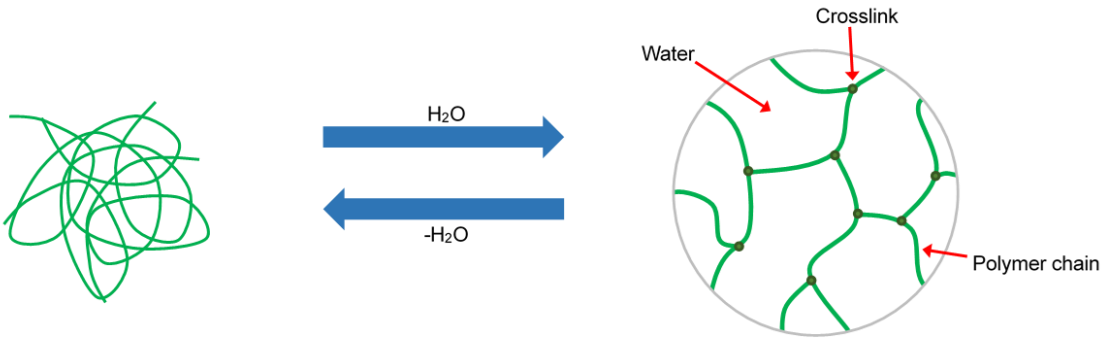

Figure 2.18 Hydrogel swelling: The collapsed polymer network (Left) swells when exposed to water forming a hydrogel (Right).

Fibre reinforcement of hydrogels is highly desirable as it produces a composite material with increased strength compared to a standard hydrogel, while maintaining other desirable properties such as hydrogel-associated loading/release capability. The materials strength properties can also be regulated in a straightforward fashion by altering the amount of fibres present in the hydrogel.[142]

Biological hydrogels found in tissues can be described as fibre reinforced hydrogels, for example, articular cartilage is comprised of a proteoglycan gel matrix and collagen fibril reinforcement;[143] the strength of articular cartilage can vary widely based upon the fibre content.[14] Another approach to customise mechanical properties in water-swollen networks is *via* the formation of double network hydrogels, which have been shown to have incredibly high strength and toughness properties.[144] Double network hydrogels are synthesised by initiating the polymerisation (and network formation) of a monomer solution swelling an existing, moderately crosslinked polymer network. Resulting products typically have a high compressive strength but have been found to have poor fatigue resistance[145]. Hydrogels with poor fatigue resistance may be problematic if intended as tissue engineering scaffold where mechanical and compressive strain are key.

2.8.1 Crosslinking

As polymer chains are linked together, crosslinking can substantially alter the physical properties of the polymer, whose mechanical behaviour can change from the one of a flowing, liquid-like polymer to the one of a solid material.

2.8.2 Crosslink Density

The crosslink density or degree of crosslinking affects a range of mechanical properties, e.g. modulus and elongation, of the hydrogel system, as the crosslink density increases the polymer chains lose their ability to move freely, resulting in a polymer network with a more rigid structure. Crosslink density also plays a part in soluble factor diffusivity and accumulation within the hydrogel. An investigation into the effects of crosslink density showed that protein accumulation increases significantly above a critical mesh size and interestingly is affected by the crosslinking mechanism.[146]

As the intended application is for a regenerative tissue replacement, these molecular characteristics should be considered. The swelling degree and elastic modulus of hydrogels are also related to the crosslink density,[147] whereby the elastic modulus tends to increase with crosslink density, whilst the volumetric swelling is inversely affected [148]. Variation in volumetric swelling will directly and significantly affect the mechanical properties of the gel since the amount of water in the network changes accordingly.

2.8.3 Encapsulation of Filler Materials in Hydrogels

Encapsulation of other materials such as fibres, particles or filling materials within polymer matrices and hydrogels can lead to marked changes in the mechanical properties of polymer nanocomposites.[149-151] Tuning the concentration of the filling materials present in the hydrogel enables mechanical properties to be modulated and for hydrogels with specific loading capacities to be produced.

The use of filler materials in hydrogel nanocomposites has been investigated for a range of different hydrogel networks and filler materials. For example, integration of cellulose nanocrystals into poly(acrylamide) has been shown to produce biomaterials that are highly extensible.[152] The composite can be considered as a double network with the covalent polymer network dominating the elastic portion of the material, whilst the stiffening effect is attributed to the adsorption of the polymer chains onto the cellulose nanocrystals surface. The composite was able to dissipate a larger amount of energy than the native polymer matrix and elastically recover shape when tensile strain to failure as high as 450% were applied.[152]

Incorporation of filler materials that are found in biological tissues are also capable of producing hydrogels with elastomeric properties;[153] PEG-hydroxyapatite nanocomposites have been produced with the attractive and beneficial property of being in an injectable format. The aqueous

prepolymer solutions can potentially be injected and photo-polymerised *in situ* using a biocompatible photoinitiator such as Irgacure 2959, resulting in a hydrogel with interconnected pore sizes from 100 to 300 nm.[153] Their mechanical properties are excellent when compared with conventional PEG hydrogels, so that material customisation can be promptly achieved by varying the hydroxyapatite content in the composite. It was also demonstrated that integration of hydroxyapatite into hydrogels improves osteoblast adhesion.[153]

2.8.4 Composite Nonwoven-Hydrogel Materials

Combining nonwoven materials with hydrogels is an emerging area of research, and provides potential to create a three-dimensional fibre matrix with high porosity encapsulated by the hydrogel and the ability to modulate or 'reinforce' mechanical properties .[154] However, most hydrogels are inherently weak, which can lead to issues when fibre reinforcement is employed, due to fibres cutting through the hydrogel causing a loss of structural integrity.[142] Such issues can be minimised by tuning the mechanical properties of the hydrogel.

The physical structure and assembly of composite materials will also affect mechanical properties. Alignment of fibrous meshes parallel to one another, orientated parallel to the direction of force application, may result in improved mechanical response due to increased load dispersion through the composite structure.

Nanofibrous reinforcement of hydrogels is a biomimetic approach, whereby man-made fibres with comparable dimensions to natural collagen fibres are dispersed in the extracellular matrix.[154] Nanofibrous nonwoven reinforcements can be produced by a variety of techniques, including splitable or fibrillating bicomponent fibres, centrifugal spinning and solution blowing, but the most common is electrospinning.[155]

Electrospinning relies on electrostatic interactions between a polymer solution and an extremely high electrostatic potential. Breaking the surface tension of the solution allows for a polymer jet to be ejected from the solution onto a suitable substrate. As the jet travels, the solvent evaporates allowing the polymer to solidify,[156, 157] so that polymer can then collected onto a substrate.[154] Electrospinning provides a simple and fast fabrication method for nanofibrous assemblies, although there are issues that limit the flexibility of the technique, for example, the poor strength of electrospun materials can make them prone to tearing when physically manipulated post-production. Additionally, the dependency on polymer solutions means that the efficacy of dopants is limited due to interactions between polymer, solvent and processing conditions, such as high temperatures.[158]

The drawbacks of electrospinning, however, are overshadowed by the prompt ability to generate composite materials with varying layers of structural organisation. Resulting structural organisation goes beyond those found in traditional fibrous scaffold assemblies, as the structure can be largely tailored to suit the intended function. Stiff nanomaterials can be incorporated into the electrospinning solution,[159] allowing for the production of polymer and ceramic-loaded nanofibres with multiple beneficial properties such as electrical conductivity, magnetism and super-hydrophobicity.[160, 161]

Nano particles and nanotubes can also be dispersed into the electrospinning polymer solution to enhance the properties of the produced fibres.[162, 163] The alignment of nanotubes in the longitudinal direction has also been achieved,[164, 165] as confirmed *via* Raman spectroscopy.[166] The ability to control the electrospun fibre orientation is also desirable, particularly in respect of modulating bulk mechanical properties. Dual component nanofibres can also be produced, provided the solution that forms the outer core is capable of being electrospun. This allows for the inner core to be made of other additives with minimal electrospinning compatibility, such as therapeutic

molecules,[167] proteins[168] and oils.[169] Loaded soluble factors can be released *via* controlled mechanisms depending on the environmental pH, temperature and enzymatic degradation of the polymer.

Reinforcement by integration of nonwoven materials to produce mechanically enhanced composites, is an attractive option in regenerative medicine. PCL fibres produced by Melt Electrospinning Writing (MEW) can be integrated into weak materials such as gelatin-methacrylamide (GelMA) and hyaluronic acid-methacrylamide (HAMA) hydrogels.[170] The extracellular matrix like structure of the gels is intended to promote cell migration and proliferation (a vital property for any material designed for regenerative medicine), while the stacked fibres which are laid in different patterns and orientations provide mechanical support. MEW is a printing technology similar to 3D printing where a fibre structure can be precisely mapped and produced, allowing for exceptional detail and thus fine tuning of mechanical properties of the composite.[170]

Figure 2.19 shows a schematic diagram of a basic setup for electrospinning, consisting of three components: A spinneret (metallic needle), high voltage power supply and a collector (grounded metallic plate).

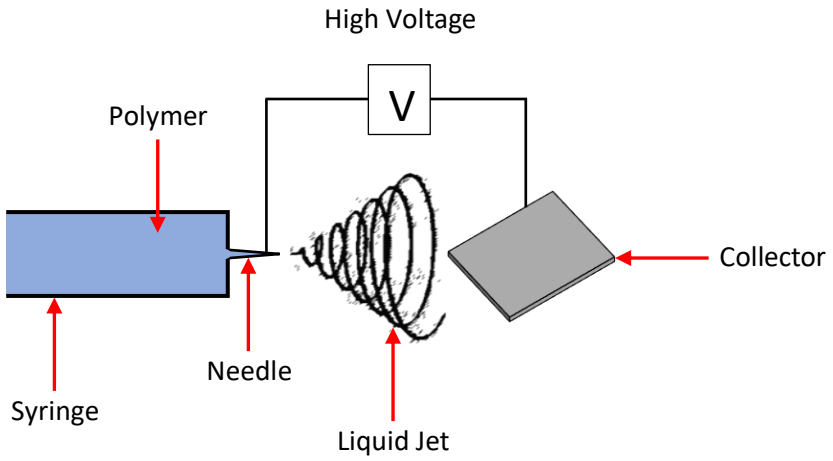

Figure 2.19 Schematic diagram of basic setup for electrospinning.

High voltage is applied to the needle and the solution droplet at the end of the needle becomes electrified resulting in charge induction across the surface of the droplet. As a result of this charge induction the droplet experiences two primary types of electrostatic interaction: repulsion between the surfaces charges and the Coulombic force exerted by the external electric field[156], these forces overcome the surface tension of the fluid. Consequently, the droplet will be distorted under these forces into a conical object known as a Taylor cone (Figure 2.20).

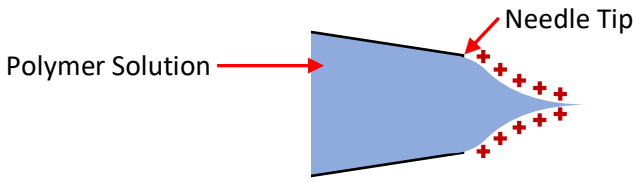

Figure 2.20 Diagram of Taylor cone, showing surface charges induced through current application.

As the strength of the electric field is increased it reaches a threshold value whereby the electrostatic forces overcome the surface tension of the polymer solution, resulting in the ejection of a liquid jet. This liquid jet then undergoes a stretching process resulting in the formation of a long, thin nanofibre with a diameter as low as tens of nanometres[156]. The jet is attracted to the collector plate and is usually deposited on the surface as a randomly orientated nonwoven mat. Droplets can be ejected from the Taylor cone however if the voltage is increased beyond the optimal range for plume formation which can result in a web of nanofibre and polymer film.

Although the equipment setup for electrospinning is relatively simple, the process involves complex mechanics. Initial inspection of a liquid jet ejection (Figure 2.21) appears to show a linear jet which then destabilises into multiple jets however, closer inspection establishes that the area of instability is a single polymer jet which is rapidly stretching and whipping[171] forming an envelope before deposition onto a collection plate. The frequency of this whipping action is so high that conventional photography is incapable of capturing it and so high-speed photography is needed.

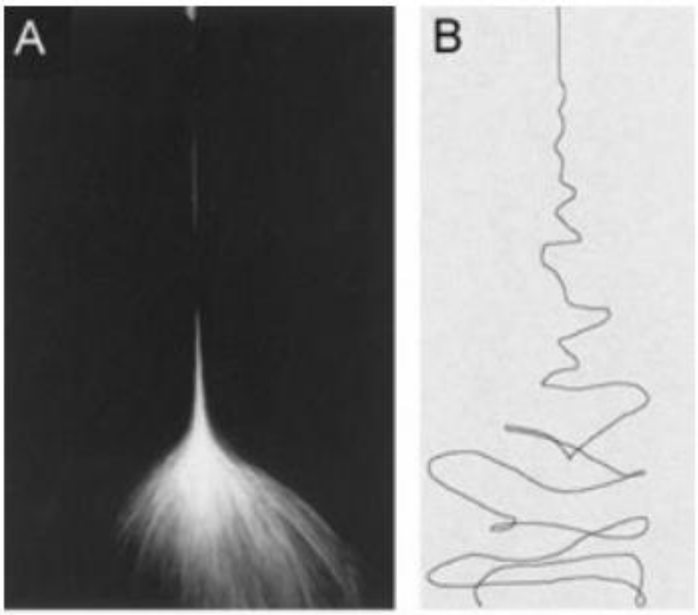

Figure 2.21 Instability region in an electrospun jet (A) with a tracer line displaying the shape of the entire instability region (B), the tracer line demonstrates the continuous fibre production. [171]

Mathematical modelling[156, 171] showed that the whipping instability is mainly caused by electrostatic interactions between the external electric field and the induced charges present on the polymer jet. The formation of ultrathin fibres is achieved by the stretching and acceleration of the jet in the instability region.

2.9 Summary

Based on the mechanical requirements of the fat pad in the foot plantar, and the requirements of a replacement material in terms of biocompatibility and the potential to promote tissue regeneration, this review has focussed on elastomeric materials capable of replacing the current clinical gold-standard material, silicone. A summary of the reviewed materials with respect to key mechanical properties is given in Table 2.1.

Table 2.1 A summary of the mechanical properties of potential alternative materials to silicone in the treatment of foot plantar defects.

Polymer Group	Polymer	Young's Modulus (MPa)	Breaking Strain (%)	References
Plantar Fat Pad Tissue		0.1 – 1.5		[18-20, 24]
Silicones	PDMS	1.4		[77]
Polyurethanes	Poly(ester-urethanes)	4.6 – 1427	291 – 726	[77, 94, 172-174]
	Poly(ether ester urethanes)			
	Lysine based polyurethanes			
PHAs	Poly(3-hydroxybutyrate)	10 – 3800	4 – 1000	[101, 102, 175]
	Poly(3-hydroxyoctanoate)			
	Poly(4-hydroxybutyrate)			
	Poly(3-hydroxybutyrate-hydroxyvalerate)			
Poly(glycerol sebacate)s	Poly(glycerol sebacate), Poly(glycerol sebacate) acrylate	0.056 – 1.5	40 – 450	[109-111]
Poly(Diol citrate)s	Poly(1,8-octanediol-*co*-citrate), Poly(1,8-octanediol-*co*-citrate-*co*-MDEA), Poly(1,6-hexanediol-*co*-citrate)	1.6 – 13.98	117 – 502	[119, 120]
Elastic Proteins	Collagen	2 – 1200	13 – 50	[77, 122, 176]
	Elastin	0.3 – 1	60 – 150	
Cyanoacrylates	Methoxyethyl cyanoacrylate, Propoxyethyl cyanoacrylate, Hexoxyethyl cyanoacrylate, Dermabond (2-octyl-cyanoacrylate)	50 – 1500		[134]

Based on the core criteria, elastomers such as polyurethanes, poly(diol citrate)s, polyhydroxyalkanoates and cyanoacrylates can be discounted on the basis of inadequate mimicking of the necessary mechanical properties, and others on the basis of cytotoxic composition (e.g. cyanoacrylates have been reported to induce tissue necrosis *in vivo*[135]), PHAs can contain

molecules that illicit an inflammatory response[99]), degradation products (e.g. cyanoacrylates degrade into formaldehyde and cyanoacetate[134]), some polyurethanes can degrade into known carcinogen molecules[77]) or elevated temperatures during processing (e.g. cyanoacrylates polymerise through an exothermic reaction which causes protein denaturation resulting in cell toxicity, some poly(diol citrate)s require curing temperatures in excess of 37°C.[119, 120]) PHAs are produced through bacterial biosynthesis, which can be expensive and involves large amounts of time, the economic factor combined with the non-biomimetic mechanical properties discount them as a viable candidate for the intended application.

By contrast, poly(glycerol sebacate) or PGS has been identified as the most attractive candidate for further development, based on its combination of biomimetic mechanical properties, biocompatibility, and the potential for photo-curing, circumventing the need for cytotoxic reactants or elevated processing temperature. Accordingly, experimental work as described in the following chapters was progressed using PGS as the primary elastomeric building block.

Chapter 3

Materials and Methods

3.1 Introduction

Having identified the potential utility of photo-curable poly(glycerol sebacate) elastomer building blocks, for the treatment of foot plantar cavity wounds, this chapter describes the chemicals, processes and methods used for the polymer synthesis, fibre manufacturing, analytical and other experimental work described in subsequent chapters. The chemical reagents utilised are summarised in Table 3.1.

Table 3.1 Chemicals used in the experimental work

Chemical	**Supplier**	**Chemical**	**Supplier**
Glycerol	Fisher Scientific	PEG_{100000}	Sigma-Aldrich
4-Dimethylaminopyridine (DMAP)	Fisher Scientific	Stannous octanoate	Sigma-Aldrich
Triethylamine	Fisher Scientific	p-Toluenesulfonic acid monohydrate	Sigma-Aldrich
N,N'-Dicyclohexylcarbodiimide (DCC)	Fisher Scientific	,2-Dimethoxy-2-phenylacetophenone	Sigma-Aldrich
5-Norbornene-2-carboxylic acid	Fisher Scientific	1,1,1,3,3,3-Hexafluoro-2-propanol	Sigma-Aldrich
Anhydrous dimethyl sulphoxide (DMSO)	Fisher Scientific	$Polycaprolactone_{80000}$	Sigma-Aldrich
chloroform-D ($CDCl_3$)	Fisher Scientific	PEG_{8000} diacrylate	Sigma-Aldrich
Sebacic Acid	Alfa Aesar	Lactic acid	Sigma-Aldrich
Dichloromethane	Sigma-Aldrich	2,2'-(Ethylenedioxy)diethanethiol	Sigma-Aldrich
Dimethyl sulphoxide (DMSO)	Sigma-Aldrich	Irgacure 2959	Sigma-Aldrich
Acryloyl chloride	Sigma-Aldrich		
poly(vinyl alcohol-*co*-ethylene)	Sigma-Aldrich		
Methanol	Sigma-Aldrich		
PEG_{1000}	Sigma-Aldrich		
PEG_{8000}	Sigma-Aldrich		

3.2 Experimental Methods

A range of analytical methods were harnessed to evaluate the PGS materials produced in this research. The methods used are explained in this section, together with sample preparation procedures.

3.2.1 Drying of Samples

Material synthesis products were dried in a Rotary Evaporator (Model number: RV 10 auto pro V) at 50 °C, 500 mbar for 1 h until the majority of solvent was removed.

Final material samples were dried in a FiStream vacuum oven (Model number: OVA031.XX3.5) at 50 – 80 °C, 200 mbar overnight to ensure complete solvent removal. Samples were covered with a fine cloth to prevent contamination during repressurising of the vacuum oven.

3.2.2 NMR Analysis

^{1}H Nuclear magnetic resonance (NMR) spectra were obtained and recorded using a Bruker AV3HD 400 for 128 scans. NMR spectra were obtained using Norell® 500 NMR tubes. MestreNova® Research Lab software was used to analyse and integrate the spectra. Samples were prepared by dissolution of 20 mg in deuterated solvent (DMSO or $CDCl_3$ depending on solubility of material) under stirring at 250 rpm.

3.2.3 FTIR Analysis

Infrared spectra were obtained on a Bruker Platinum FTIR-ATR spectrometer (Model: Alpha-P), using a diamond attenuated total reflectance (ATR) accessory with 32 total scans being completed. Bruker OPUS 7.0 software was used to analyse the recorded spectra. Samples were loaded onto the ATR

crystal in a dried state, ensuring complete coverage. Raw data was exported to excel for further analysis.

3.2.4 Microscopy

Scanning electron microscopy (SEM) micrographs were obtained using a Jeol JSM-6610LV instrument employing a 10 mm focusing lens. Micrographs were collected at accelerating voltages from 15 to 30 kV and magnification from 250 to 10000. Different accelerating voltages were used to enhance resolution of the nanofibers present in the nonwoven web. Magnification was changed to allow accurate fibre diameter and porosity measurements. Samples were prepared by cutting to 10 x 10 mm, sputter coating was employed to produce high quality micrographs.

3.2.5 Differential Scanning Calorimetry

A TA instruments Q100 was used to collect differential scanning calorimetry data and allow determination of glass transition temperature, melting, and crystallisation point of the materials. 5.5 mg of material was weighed into a hermetically sealed pan and placed into the instrument, a ramping rate of 10 °C min^{-1} was used for both heating and cooling cycles. The sample was first heated to 185 °C to remove previous thermal history, cooled to - 60 °C and then re heated to 185 °C. This allows the first heat cycle to impart a known thermal history into the material, whereby any differences observed in the second heating cycle are related to differences in the material such as molecular weight.

3.2.6 Thermogravimetric Analysis

A TA instruments Q50 thermogravimetric analyser was used to collect thermogravimetric data and allow measurement of thermal stability and composition of multicomponent materials, including

volatile content. 5.5 mg of sample material was weighed into a thermogravimetric pan and placed into the instrument. Heating of the material from room temperature (15 °C) to 500 °C.

3.2.7 Electrospinning

Electrospinning was employed in the experimental work to explore the spinning of the synthesised PGS-based polymer materials produced in this work. It is a simple and versatile fibre production method capable of producing nano and microfibres from polymer solutions containing an appropriate solvent.

3.2.7.1 Electrospinning Setup

As shown in Fig. 3.1, a syringe pump is connected to the syringe allowing for a constant, controlled rate of polymer solution to flow through the needle.

Figure 3.1 Image of electrospinning setup used for the production of nanofibre samples used in composites.

As the basic electrospinning setup is so simple, modification is also relatively easy. A grounded collection plate is required for deposition of the formed fibres, building on this principle by

incorporation of a rotating drum allows for a more uniform deposition process – avoiding fibre build-up at specific points which is a potential outcome using a static collection plate.

Many applications of nanostructures benefit from some fibre orientation, however because of the bending instability associated with the spinning jet produced through a typical electrospinning process the deposition of fibres is random. Modification of the spinning process has yielded the ability to control the fibre deposition. Some success in controlling fibre orientation has been achieved by use of a modified rotating drum,[177] Zussman and co-workers used a tapered disk as the collector resulting in the fibres being collected predominantly on the sharp edge, with their orientation being parallel to each other. Simulation of the electrostatic field revealed the field strength increased significantly at the edge of the disk, because of this increased electrostatic field the fibres were deposited in a continuous fashion when the disk was rotated at a high speed.

Split electrodes have also been used to demonstrate that physical configurations of collection plates can have a substantial effect on the orientation of electro spun nanofibre.[178, 179] Conductive strips separated by a void have been used as a collection device to produce uniaxially aligned fibres. The fibres align themselves perpendicular to the edges of the conductive strips, resulting in parallel fibre formation, this is further enhanced by the repulsion between the electrostatic charges present on the surface of the fibres. Another significant advantage of this method is the ability to conveniently and efficiently transfer the fibres to another substrate, preventing mechanical deterioration of the structure due to handling – particularly important in some applications that employ the use of hollow fibres.

3.2.8 Photo Crosslinking

Photo crosslinking experiments used a Chromato-Vue C-71 UV viewing system (4 x 15-watt 365 nm UV tubes fitted) to generate UV light. Formulations were incubated at 50 °C, with stirring at 200 rpm

to ensure homogeneity. Containment vessels during incubation were wrapped in foil to prevent light entering the solution and activating the photoinitiator prematurely. Vessels were also sealed with parafilm to prevent evaporation during the incubation period.

Chapter 4 Synthesis and Modification of Poly(glycerol sebacate)

4.1 Introduction

Following consideration of plausible elastomer systems in Chapter 2, PGS was identified as a promising candidate to replace silicone as fat pad filling material because of its chemical and physical properties. The biocompatibility of PGS is well established in the literature,[109-111] and is reflected by other groups that have sought to use the material as a starting point for the development of new biomedical devices.[180-182] This chapter focuses on the synthesis and modification of PGS, including the development of novel PGS-based polymers, with added functionality, namely the ability to be photo-crosslinked. Clinically, this is important as it provides the opportunity for the polymer to be crosslinked in-situ, following injection into the foot plantar, as well as for the mechanical properties of the polymer to be modulated at a later-stage, potentially at the bed side.

Previous investigation into the introduction of norbornene functionality[183] to PGS has been carried out, however a different approach was employed experimentally *via* the use of Steglich esterification.[184] Doing so avoided the modification of the norbornene carboxylic acid with oxalyl chloride and thus removed the risk of introducing the highly toxic molecule oxalyl chloride. Despite the potential for PGS to replace silicone as an injectable material for lost fat pad tissue, it was also important to consider other challenges such as biostability, which will govern the long-term mechanical competency following implantation.

The synthesis strategy adopted herein, was also aimed at delivery of a photo-cross linkable material. Photo-crosslinking of polymers is a highly desirable property as it allows for the material to form with the exact shape requested by the intended application. Implantation or Injection of the photo-crosslinking polymer solution into a cavity would such as those created by diabetic ulcers in the foot plantar allows for the polymer to completely fill the void formed due to tissue loss. Contact between the cavity walls and the material increases adhesion,[29] improving the chances of successful implantation.

A common method of introducing photo-crosslinking functionality is the introduction of alkene groups in the form of acrylation (Figure 4.1), although more attractive, oxygen-insensitive options are available such as the utilisation of thiol-ene click chemistry.

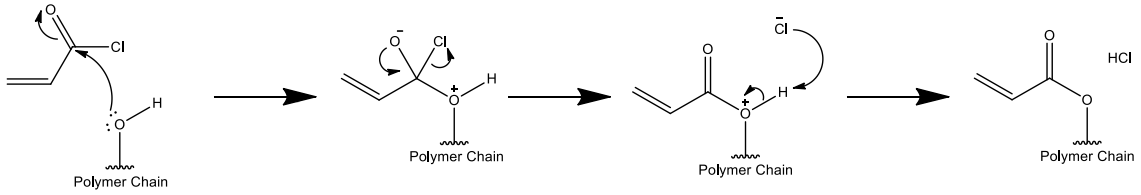

Figure 4.1 Mechanism for the acrylation of a hydroxyl containing polymer.

Introduction of alkene functionality through grafting of moieties such as norbornene allows for the photo-crosslinking reaction to occur selectively with di-thiol crosslinkers. Using a Steglich Esterification[104] reaction, norbornene carboxylic acid can be grafted to the polymer, introducing alkene functionality, which can be utilised with thiol functionalised molecules to further modify the polymers structure. The mechanism of modification is reported in Figure 4.2.

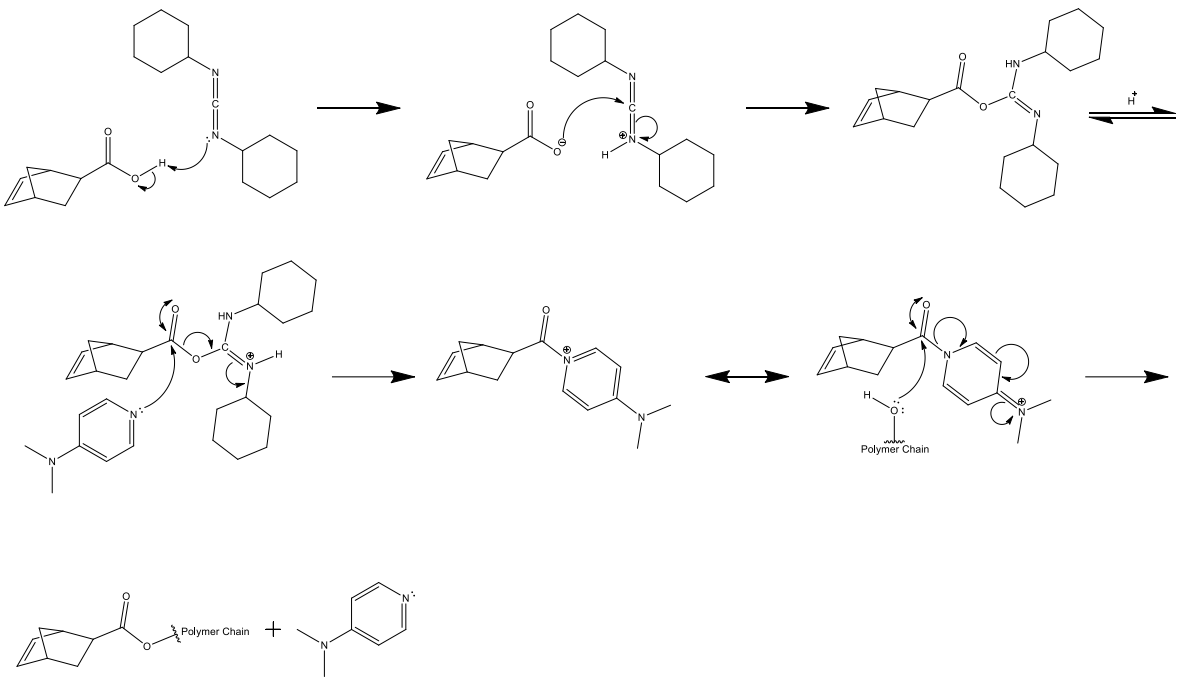

Figure 4.2 Steglich esterification mechanism for the modification of a hydroxyl containing polymer with 5-norbornene-2-carboxylic acid.

This chapter describes the materials and methods employed for the preparation of PGS and the following modifications to produce 5-Norbornene-2-carboxylic acid modified PGS and PGSA. Furthermore, this chapter describes the materials and procedures that were employed to synthesise and modify hydrophilic variants of PGS, crosslinking of these materials and the spinning of nanofibres.

4.2 Experimental

This section describes the preliminary work that was conducted based on a model polymer modification, as well as the synthesis of the PGS and PGSA. Synthesis of PGS was based on well documented and used procedures as laid out by Nijst *et al*.[111]

4.2.1 Model Polymer Modification

Owing to the restricted number of industry suppliers of the requisite polymer, a model polymer was first selected to enable the intended modification chemistry to be pre-tested. Poly(vinyl alcohol-*co*-ethylene) was selected due to the presence of hydroxyl groups on the polymeric chain and the solubility with the intended reagents. A schematic of the procedure used to prepare the materials is shown in Figure 4.3.

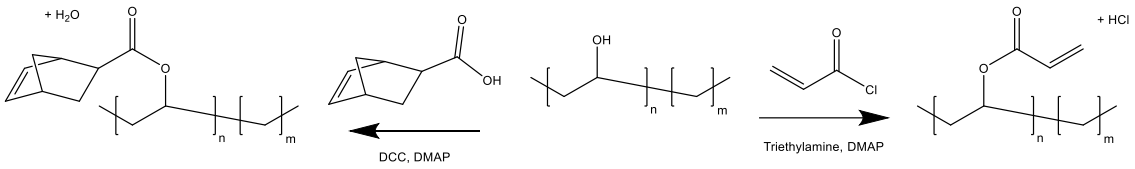

Figure 4.3 Modification reactions of poly(vinyl alcohol-*co*-ethylene).

The acrylation and steglich esterification reaction pathways can be investigated and evaluated using ^{1}H NMR analysis, allowing for confirmation of the feasibility of the intended modification routes. Upon analysis if the associated alkene proton peaks are absent then complete modification of the polymers structure with a functional moiety was successful.

4.2.1.1 Partial (20 mol. %) acrylation of Poly(vinyl alcohol-*co*-ethylene)

Introduction of acrylate functionality allows for a controllable degree of crosslinking within the polymer matrix, this is useful in biomedical applications of polymers as it allows the tuning of mechanical properties – increased crosslinking produces a more rigid molecular structure in the matrix phase. If the material can be photocured *in-situ* it can also bypass the need for surgical intervention for implantation, rather the material can be injected locally with a biocompatible photoinitiator.

The acrylation reaction procedure that was adopted was modified from previous research detailing the acrylation of PGS[111]. A round bottom flask was flame dried and charged with poly(vinyl-*co*-ethylene) (1.0 g) and anhydrous DMSO (50 mL) was added, and the stirring magnetic stirring at 350 rpm turned on.

The mixture was heated to 130°C and left stirring for 24 h. The apparatus was cooled to room temperature, and 4-dimethylaminopyridine (DMAP) (0.004 g, 0.03 mmol) was added. Following this, acryloyl chloride (0.25 g, 2.78 mmol) and triethylamine (0.28 g, 2.78 mmol) were added simultaneously.

The solution turned a dark orange colour upon addition of the acryloyl chloride, upon further addition the colour lightened to yellow. The reaction was then stirred for a further 24 h at room temperature. Deionised water (200 mL) was then added to the reaction mixture to precipitate the polymer out of solution, an excess was used for complete precipitation to increase reaction yield. Filtration using a sintered funnel (porosity grade 2) and a vacuum pump (Vacuubrand RC6) yielded a porous, sponge-like brown mass. The brown mass was washed with diethyl ether (3 x 50 mL) to remove any excess DMSO and the product collected and dried under vacuum at 50°C. ^{1}H NMR and IR analysis showed no presence of acrylate functionality (Section 4.3.1.1), another reaction was investigated with the aim of completely saturating the polymer's hydroxyl groups with acrylation reagent to introduce functionality.

4.2.1.2 Complete Acrylation of Poly(vinyl alcohol-*co*-ethylene)

An increased degree of modification with acrylate functionality potentially allows for more crosslinks to be formed, increased crosslink density will produce material with increase mechanical properties such as modulus and maximum stress.

A round bottom flask was flame dried and charged with poly(vinyl alcohol-*co*-ethylene) (1.0 g). Anhydrous DMSO (50 mL) was then added and magnetic stirring at 350 rpm was initiated. The mixture was heated to 130°C and left stirring for 24 h. The apparatus was cooled to room temperature and DMAP (0.004 g, 0.03 mmol) was added. Following this, acryloyl chloride (1.0 g, 11.11 mmol) and triethylamine (1.12 g, 11.11 mmol) were added to dropping funnels containing DMSO, upon addition of acryloyl chloride to neat DMSO a white vapour was produced. White crystals began to form around the mouth of the triethylamine funnel, addition of the reagents was continued until complete.

The reaction was then stirred for a further 24 h at room temperature. Deionised water (200 mL) was added to the reaction mixture to precipitate the polymer out of solution, an excess was used to precipitate the synthesis product completely, filtration yielded a spongey brown mass as in previous experiments (Section 4.2.1.1). The brown mass was washed with diethyl ether to remove any excess DMSO, the product collected and dried under vacuum at 50°C.

4.2.1.3 Partial (50 mol. %) Modification of Poly(vinyl alcohol-*co*-ethylene) with Norbornene Moiety

Introduction of norbornene functionality into the molecular structure potentially allows for the use of thiol-ene click chemistry to form crosslinks, this is advantageous as it avoids the use of acrylate functionality and is associated with higher reaction speeds and yields.

A round bottom flask was charged with poly(vinyl alcohol-*co*-ethylene) (0.5 g), DMSO (50 mL) was added, and the flask heated to 130°C and left stirring at 350 rpm for 24 h. The reaction vessel was cooled to room temperature, 5-Norbornene-2-carboxylic acid (0.48 g, 3.47 mmol), DCC (3.58 g, 17.36 mmol) and DMAP (0.04 g, 0.35 mmol) were added, and the reaction left to stir at 350 rpm for

24 h. Deionised water (50 mL) was added to the mixture to precipitate the product which was collected by filtration and dried in an oven.

4.2.1.4 Complete Modification of Poly(vinyl alcohol-*co*-ethylene) with Norbornene Moiety

The small alkene peaks observed in ^{1}H NMR analysis of previous experiments (Section 4.2.1.3) suggested a low grafting rate therefore, a further reaction was carried out with the intention of completely modifying all available reactive sites to increase polymer functionality.

A round bottom flask was charged with poly(vinyl alcohol-*co*-ethylene) (0.5 g), DMSO (50 mL) was added, and the flask heated to 130°C and left stirring at 350 rpm for 24 h. The reaction vessel was cooled to room temperature, 5-Norbornene-2-carboxylic acid (0.96 g, 6.94 mmol), DCC (7.15 g, 34.72 mmol) and DMAP (0.09 g, 0.70 mmol) were added, and the reaction left to stir at 350 rpm for 24 h. Deionised Water (50 mL) was added to the mixture to precipitate the product which was collected by filtration and dried in an oven.

4.2.2 Poly(glycerol sebacate) Synthesis

Given the limited number of suppliers of the PGS elastomer needed for the chemical modification experiments, the polymer was synthesised as part of the experimental work. Additionally, this had the following advantages:

- The degree of crosslinking during the curing stage of the reaction could be controlled or halted completely, allowing for the modification and functionalisation of prepolymer and partially crosslinked polymer. This was felt to be especially useful, as using the prepolymer allows for a greater degree of modification such as the introduction of functional groups necessary to enable photo-curing.

- The production of samples whereby the prepolymer could be directly cast into a mould of a specific size, to ensure a convenient format for mechanical analysis.
- An array of different materials could be produced by altering the polymerisation conditions.

4.2.2.1 Synthesis of Oligo and Poly(glycerol sebacate)

The following procedure was adapted from a protocol described by Nijst *et al*.[111], parameters for the reaction were changed to suit equipment available while still producing the desired material as confirmed by ^{1}H NMR analysis.

A round bottom flask was charged with glycerol (2.0 g, 21.74 mmol) and sebacic acid (4.39 g, 21.74 mmol). The vessel was flushed with nitrogen, heated to 130°C to and magnetic stirring turned on at 250 rpm to enable complete mixing. The vessel was then left stirring at 350 rpm, 130°C for 24 h to enable oligomer formation under vacuum (0.001 bar) (Vacuubrand RC6). After 24 h, a sample was collected for ^{1}H NMR analysis and the rest of the mixture was put under reduced vacuum (0.0005 bar) (Vacuubrand RC6) and left for a further 48 h under continuous 350 rpm stirring at 130°C. Upon reaction completion a transparent brown solid was present in the flask.

4.2.2.2 Synthesis of Oligo(glycerol sebacate) (OGS)

To solve residual solubility issues when dealing with the post polymerisation modification of PGS, separate OGS batches were synthesised simultaneously with the intention of modification *via* acrylation and coupling with 5-Norbornene-2-carboxylic acid.

In order to synthesise OGS, two round bottom flasks were charged with glycerol (3.0 g, 32.61 mmol) and sebacic acid (6.59 g, 32.61 mmol). The vessels were flushed with nitrogen and heated to 130°C and the vessels were then left magnetically stirring at 250 rpm and 130°C for 24 h to enable oligomer formation under vacuum (0.001 bar) (Vacuubrand RC6). The oligomer was collected as a clear,

viscous, free-flowing liquid, although some material was left inside the flask estimated to be 10 % of total material mass by measuring the mass of collected material and reaction vessel.

4.2.2.3 Synthesis of Poly(glycerol sebacate)

Previous experiments (Section 4.2.2.2) synthesised the linear chains of the PGS pre-polymer, OGS, as a way to avoid solubility issues. An investigation as to whether the OGS pre-polymer could undergo polymerisation to PGS after initially being halted was carried out.

OGS prepolymer (9.0 g) was heated in a round bottom flask at 130°C, under vacuum (0.0005 bar, Vacuubrand RC6) and stirring (250 rpm) for 24 h. After which, the polymer was collected as a clear viscous liquid. Heating was required to remove the polymer from the reaction vessel, material was left inside the flask which was estimated to be 20 % of total polymer mass, the increased viscosity of the material compared to OGS contributed to the decreased overall yield as it was more difficult to remove from the reaction vessel.

4.2.3 Modification of Poly(glycerol sebacate)

Introduction of norbornene or acrylate functionality allows for crosslinking of the material without the use of high temperatures required (greater than 130 °C), the intention is to produce a material that could potentially be used as a biomedical implant without the requirement of surgical intervention. Injection of a material that can be cured in a physiological environment without increasing the risk of infection to the patient is an attractive characteristic.

4.2.3.1 Modification of Poly(glycerol sebacate) with Norbornene Moiety in DMSO, PGS-Nor

Modification of PGS to introduce norbornene functionality was carried out initially in DMSO, as it is a less toxic solvent compared to other suitable solvents for the modification reaction.

PGS (1.5 g) was added to a round bottom flask, DMSO (50 mL) was added, and the vessel heated to 130°C and left stirring at 350 rpm for 24 h. Then, 5-Norbornene-2-carboxylic acid (0.72 g, 5.21 mmol), DCC (5.36 g, 26.03 mmol) and DMAP (0.06 g, 0.52 mmol) were added, and the reaction left under magnetic stirring at 350 rpm for 24 h. The mixture then produced a white precipitate, which was believed to be the DCC urea. Separation of the polymer from the DCC urea was not possible, gravity and vacuum assisted filtration were attempted but a viscous fluid was collected which was observed to contain the white precipitate dispersed throughout – the material was assumed to be a PGS-Norbornene and DCC urea mixture. ^{1}H NMR analysis was deemed unsuitable due to large scale DCC urea contamination.

4.2.3.2 Modification of Oligo(glycerol sebacate) with Norbornene Moiety in Dichloromethane, OGS-Nor

Due to the large scale DCC urea contamination of previous experiments using DMSO as a solvent (Section 4.2.3.2), and the inability to remove the DCC urea after the modification reaction was complete, a solvent change to dichloromethane (DCM) was used, as it would potentially allow separation of the DCC urea by-product due to it partially crashing out as it forms.

In order to modify the OGS, the OGS (1.0 g) was added to a round bottom flask and dichloromethane (50 mL) was added to the vessel and left magnetically stirring at 350 rpm for 30 min. After 30 min, 5-Norbornene-2-carboxylic acid (0.23 g, 1.74 mmol), DCC (1.79 g, 8.68 mmol) and DMAP (0.02 g, 0.17 mmol) were added, and the reaction left to stir for 24 h. Upon reaction completion, the flask was placed in a freezer at -20°C overnight. Upon collection after 18 h, a white precipitate was observed in the reaction vessel, vacuum assisted filtration of this material yielded a clear solution. The solution was then heated on a hot plate to yield a dark honey coloured viscous liquid.

4.2.3.3 Modification of Poly(glycerol sebacate) with Norbornene Moiety in Dichloromethane, PGS-Nor

PGS was also used as a polymer for grafting of norbornene functionality in DCM.

PGS (1.0 g) was added to a round bottom flask, dichloromethane (50 mL) was added, and the vessel magnetically stirred at 350 rpm for 30 min. After 30 min 5-Norbornene-2-carboxylic acid (0.23 g, 1.74 mmol), DCC (1.79 g, 8.68 mmol) and DMAP (0.02 g, 0.17 mmol) were added, and the reaction continued to be stirred for 24 h. Upon reaction completion the flask was placed in the freezer at -20°C overnight, after 18 h upon collection a white precipitate had formed. Filtration of the white precipitate yielded a clear solution; the solution was heated on a hot plate to yield a honey-coloured viscous liquid.

4.2.3.4 Acrylation of Oligo(glycerol sebacate)

Acrylation of OGS to introduce crosslinking functionality is advantageous as it avoids the need for high temperature curing procedures. Introduction of acrylate functionality was conducted as follows.

A flame dried round bottom flask was charged with OGS (9.0 g), anhydrous dichloromethane (100 mL) was added. DMAP (0.01 g, 0.07 mmol) was added, stirring (350 rpm) turned on and the flask cooled to 0°C. Acryloyl chloride (1.10 g, 12.18 mmol) and triethylamine (1.23 g, 12.18 mmol) were added simultaneously. The vessel was allowed to reach room temperature and the reaction stirred for a further 24 h. After 24 h the mixture was dissolved in ethyl acetate, filtered then dried at 45°C in a vacuum oven.

4.2.4 Synthesis and Modification of Poly(glycerol sebacate) with varied curing times

In addition to forming hydrogels, synthesis of PGS was also carried out to prepare material for the electrospinning of nanofibers, both with and without photocuring functionality. Reactions were carried out with differing reaction times to determine if shorter curing times gave rise to more reactive sites for grafting of photo curing functionality.

The procedure for curing time investigations was again adapted from a protocol described by Nijst *et al*[108], parameters of the reaction were maintained from previous reactions (Section 4.2.2) but the curing period after oligomer synthesis was altered.

4.2.4.1 Synthesis of Poly(glycerol sebacate) with increased curing time, PGS-L

Increasing the curing time during PGS synthesis produces a matrix with a higher degree of crosslinking, thus reducing the number of reactive sites where functional grafting can occur. The changes to the molecular structure will also have an effect on the electrospinning behaviour of the material.

A round bottom flask was charged with glycerol (15.0 g, 163.04 mmol) and sebacic acid (32.93 g, 163.04 mmol). The vessel was flushed with nitrogen, heated to 130°C and left stirring at 250 rpm, 130°C for 1 h to allow for reagent melting and mixing. Following this the reaction vessel was placed under reduced pressure and the reaction left to continue for 48 h. The material was dissolved in dichloromethane (DCM), water was removed with magnesium sulphate and the solvent removed on a rotary evaporator. The polymer was collected as a clear viscous free flowing liquid although some material was left inside the flask.

4.2.4.2 Synthesis of Poly(glycerol sebacate) with decreased curing time, PGS-S

Decreasing the curing time during PGS synthesis increases the number of reactive sites, allowing for a greater amount of grafting to occur which translates to a higher potential for photocuring behaviour. Variations in molecular structure will alter the spinning behaviour of the material, having a material with a more linear molecular structure should reduce the viscosity which can results in electrospray occurrence during electrospinning into a fibrous network.

A round bottom flask was charged with glycerol (15.0 g, 163.04 mmol) and sebacic acid (32.93 g, 163.04 mmol). The vessel was flushed with nitrogen, heated to 130°C and left stirring at 350 rpm, 130°C for 1 h to allow for reagent melting and mixing. Following this the reaction vessel was placed under reduced pressure and the reaction left to continue for 32 h. The material was dissolved in DCM, water was removed with magnesium sulphate and the solvent removed on a rotary evaporator. The polymer was collected as a clear viscous free flowing liquid although some material was left inside the flask.

4.2.4.3 Acrylation of PGS-L

Acrylation of PGS-L was performed in order to introduce photocuring functionality, to allow for the potential of curing the material *in-situ* and to avoid the use of surgical procedures during implementation.

A flame dried round bottom flask was charged with PGS-L (30.0 g), anhydrous dichloromethane (250 mL) was added. DMAP (0.11 g, 0.91 mmol) was added, magnetic stirring at 350 rpm turned on and the flask cooled to 0°C with an ice bath. Acryloyl chloride (20.54 g, 228 mmol) and triethylamine (23.05 g, 228 mmol) solutions were added simultaneously through separate dropping funnels. The vessel was allowed to reach room temperature after addition of the solution was complete and the reaction magnetically stirred at 350 rpm for a further 24 h. After 24 h the mixture was dissolved in

ethyl acetate (400 mL), vacuum assisted filtration removed the bulk of the solvent and the material washed in ethyl acetate (4 x 50 mL) then dried at 45°C in a vacuum oven. A light-yellow powder was collected.

4.2.4.4 Acrylation of PGS-S

Acrylation of the shorter curing time PGS should yield a polymer with increased potential for crosslinking, which will increase elastic modulus of the gel material produced through photo crosslinking.

A flame dried round bottom flask was charged with PGS-S (30.0 g), anhydrous dichloromethane (250 mL) was added. DMAP (0.11 g, 0.91 mmol) was added, magnetic stirring at 350 rpm turned on and the flask cooled to 0°C with an ice bath. Acryloyl chloride (20.54 g, 228 mmol) and triethylamine (23.05 g, 228 mmol) solutions were added simultaneously through separate dropping funnels. The vessel was allowed to reach room temperature after addition of the solution was complete and the reaction magnetically stirred at 350 rpm for a further 24 h. After 24 h the mixture was dissolved in ethyl acetate (400 mL), vacuum assisted filtration removed the bulk of the solvent and the material washed in ethyl acetate (4 x 50 mL) then dried at 45°C in a vacuum oven. A light-yellow powder was collected.

4.3 Results and Discussion

As a preliminary step, the acrylation and 5-Norbornene-2-carboxylic acid grafting reactions was initially carried out with poly(vinyl alcohol-*co*-ethylene) to act as a PGS model, since both polymers present hydroxyl functions that are targeted for the grafting reaction.

Following this, the synthesis and modification of PGS was conducted to produce poly(glycerol sebacate) acrylate (PGSA) and 5-Norbornene-2-carboxylic acid modified PGS as shown in Figure 4.2.

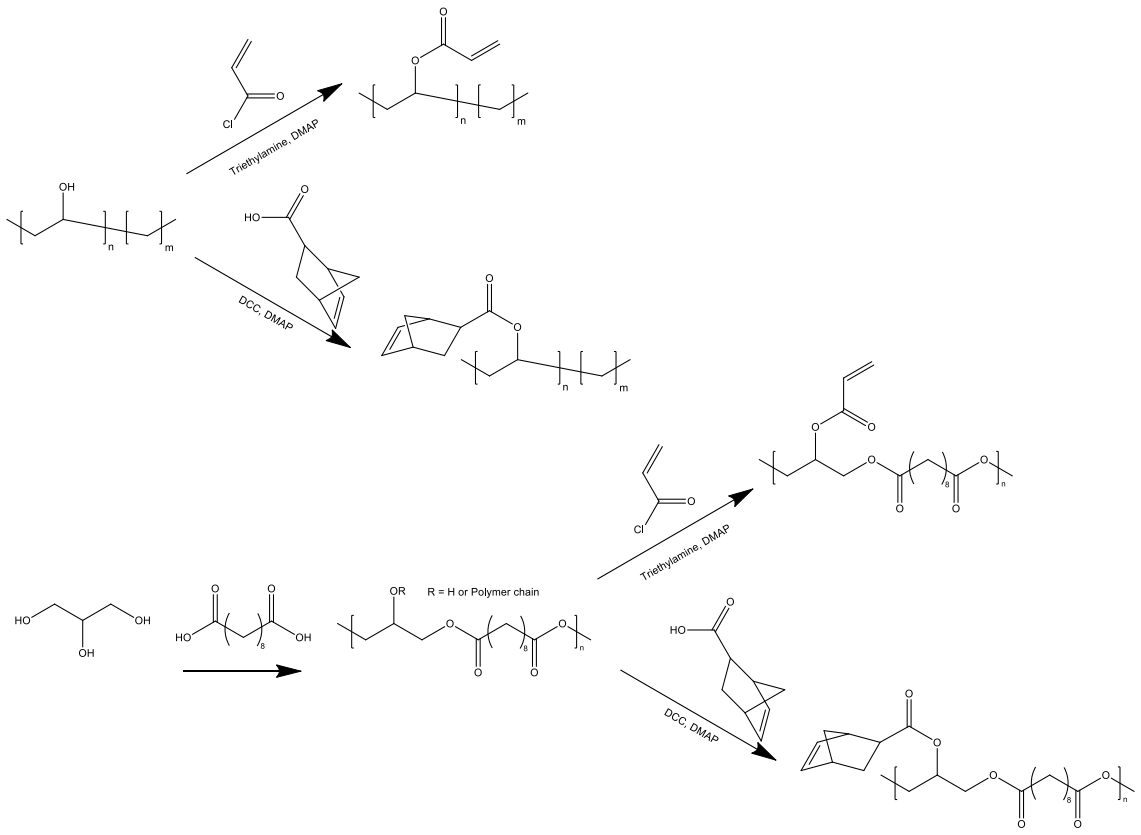

Figure 4.2 Reaction schematics for the synthesis of poly(glycerol sebacate) and the modification of poly(vinyl alcohol-*co*-ethylene) and poly(glycerol sebacate)

4.3.1 Model Polymer Modification

A model polymer was used to investigate the viability of the proposed chemical routes of modification (Figure 4.2). Poly(vinyl alcohol-*co*-ethylene) was chosen as a model polymer as the hydroxyl groups present in the structure should enable the same synthetic routes to be applied as intended for PGS and due to restrictions in PGS material supply as stated in Section 4.2.1.

4.3.1.1 Partial (20 mol. %) acrylation of Poly(vinyl alcohol-*co*-ethylene)

Preliminary reactions were carried out to reach ca. 20 mol. % functionalisation of hydroxyl functions with acrylate moieties, whereby reacted products were analysed with ^{1}H NMR.

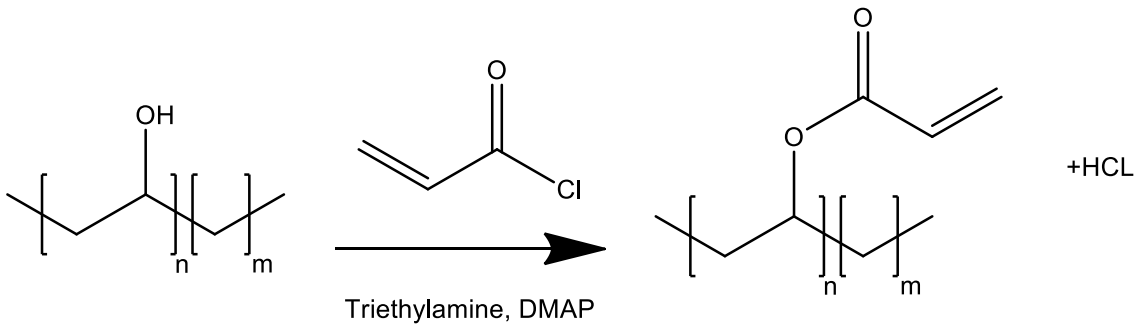

Figure 4.3 Acrylation of poly(vinyl alcohol-*co*-ethylene).

^{1}H NMR analysis (Figure 4.4, Table 4.1) showed a lack of peaks at 6 – 6.5 ppm, which is where the geminal protons would be situated if successful grafting of acrylate moiety had taken place. The infrared (IR) spectrum obtained also failed to show an absorption stretch at ~1670 cm^{-1}, which would represent an alkene (C=C). Upon addition of the acryloyl chloride, the reaction solution turned dark orange, and, following ca. 15-min magnetic stirring at 250 rpm, the solution turned light yellow – an indication of ammonium salt formation which then dissolves in the reaction solvent. A reaction yield of 74 % was obtained.

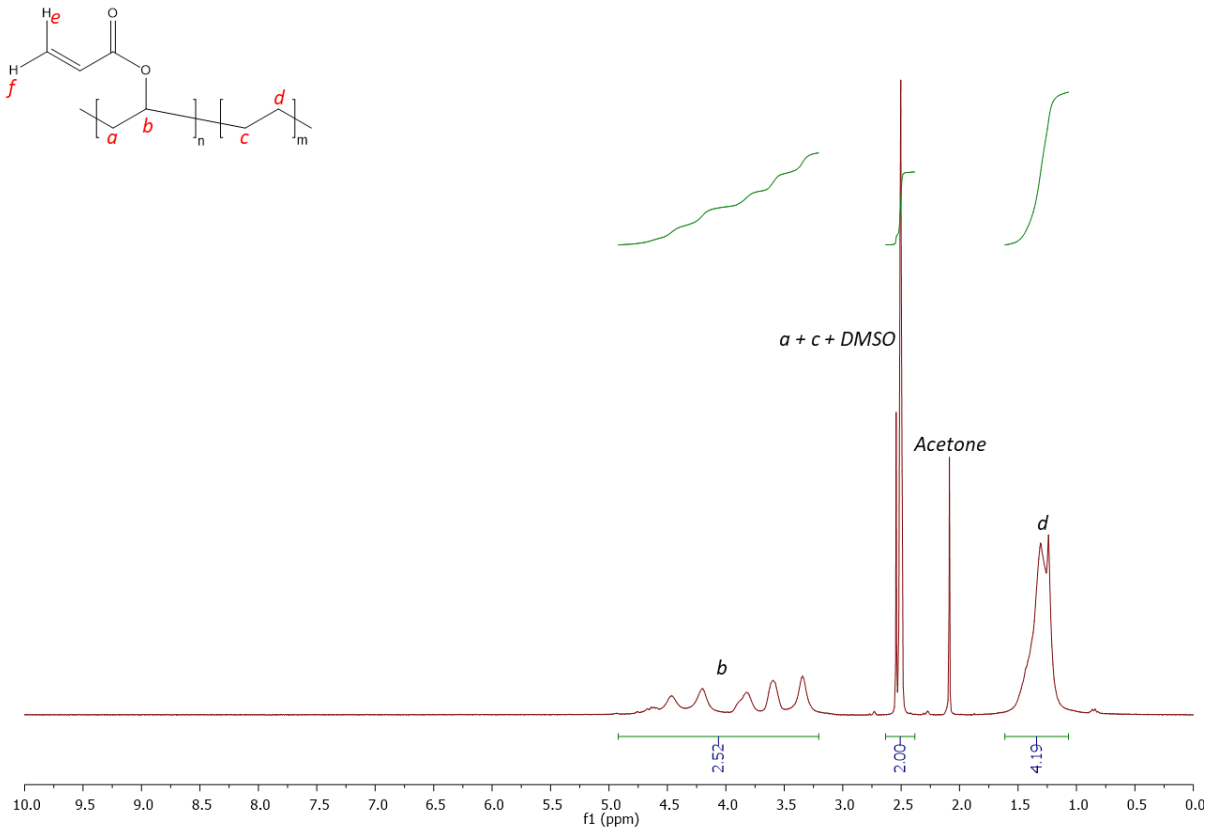

Figure 4.4 ^{1}H NMR spectrum (DMSO) of product obtained from acrylation of poly(vinyl alcohol-*co*-ethylene).

Table 4.1 ^{1}H NMR data of product obtained from acrylation of poly(vinyl alcohol-*co*-ethylene).

^{1}H NMR (300 MHz)			
δ (ppm)	**Multiplet**	**J Frequency (Hz)**	**Protons**
4.55	d	51.3	9
4.01	d	114.1	17
3.47	d	74.9	26
2.51	dd	7.5, 5.9	47
1.81	d	168.2	9
1.27	d	20.2	100

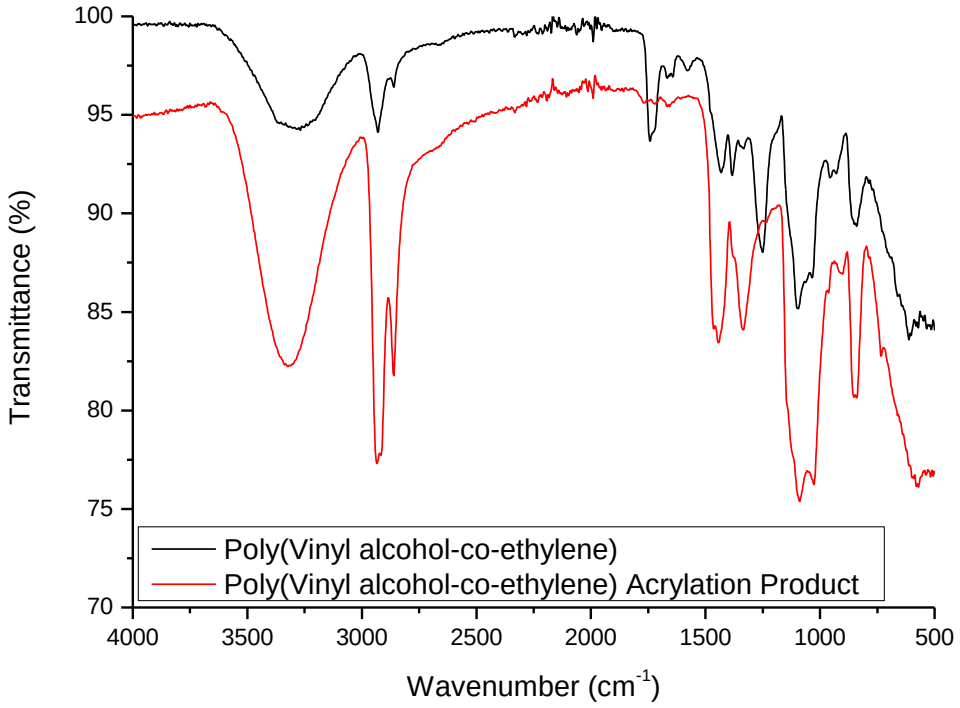

Figure 4.5 IR Spectrum of partially acrylated poly(vinyl alcohol-*co*-ethylene), a lack of peaks associated with acrylate functionality showed functionalisation was not successful.

As the ^{1}H NMR (Figure 4.4, Table 4.1) and IR spectrum (Figure 4.5) did not show the peaks relating to the alkene group of the acrylate functional group, another attempt was made, with the aim of completely saturating the polymer's hydroxyl groups with acrylation reagent.

4.3.1.2 Complete Acrylation of Poly(vinyl alcohol-*co*-ethylene)

The acrylation reaction (Section 4.3.1.1) was repeated, however alterations were made to the reaction protocol. The acryloyl chloride and triethylamine were added slowly from a dropping funnel, a solution of the reagents in anhydrous DMSO was to be made up in the funnels and added dropwise. Upon addition of the acryloyl chloride to the dropping funnel containing DMSO a white vapour was produced, whilst the reaction was continued; upon release of the acryloyl chloride solution into the reaction vessel, white crystals began to form around the mouth of the

triethylamine solution dropping funnel. From these observations, it appeared that the acryloyl chloride was interacting/reacting with the DMSO, to form what can be assumed to be HCl vapour. The HCl vapour can be expected to react with triethylamine, to form a salt in the form of white crystals, which will dissolve into solution, adding a yellow hue to the solution. A decrease in yield was observed, 65 %, which implies that a large amount of acryloyl chloride was left unused or reacted with the DMSO instead of the polymer.

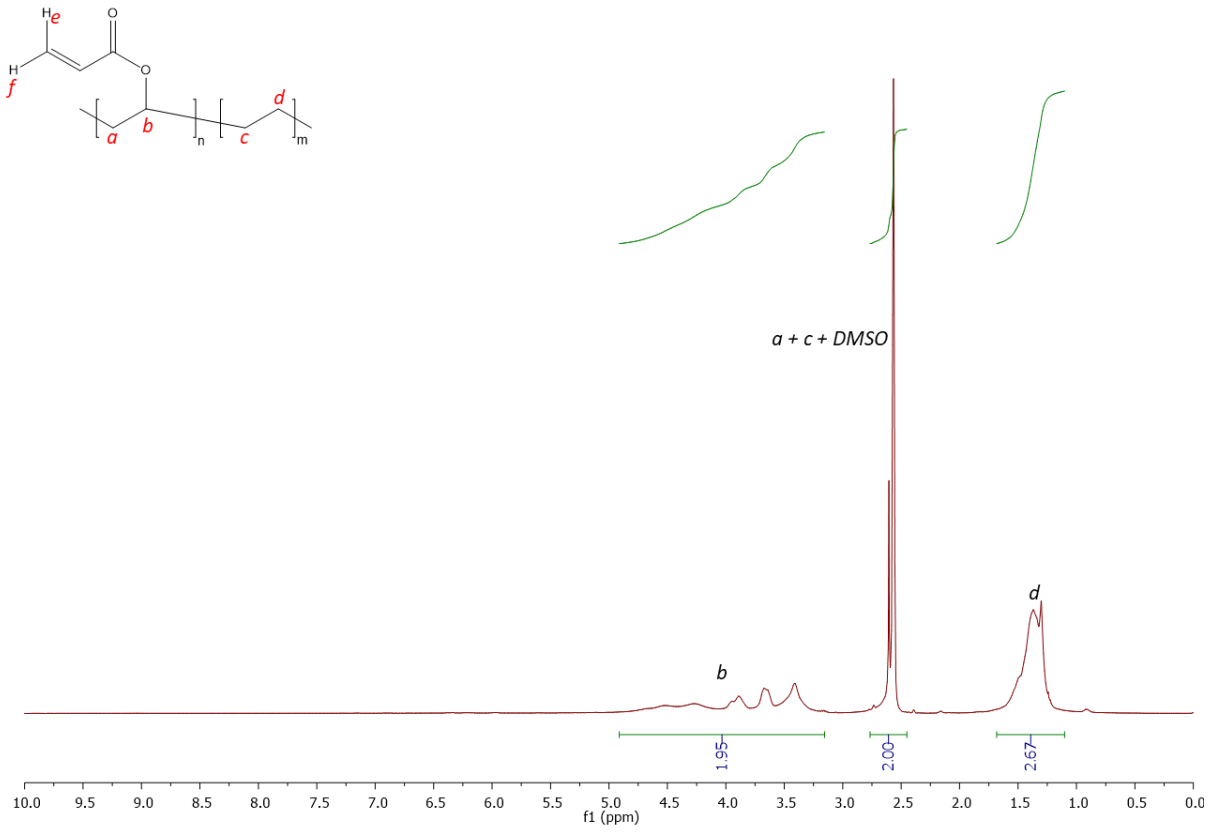

Figure 4.6 ^{1}H NMR spectrum (DMSO) of product obtained from complete acrylation of poly(vinyl alcohol-*co*-ethylene).

Table 4.2 ^{1}H NMR data of product obtained from complete acrylation of poly(vinyl alcohol-*co*-ethylene).

^{1}H NMR (300 MHz)			
δ (ppm)	**Multiplet**	**J Frequency (Hz)**	**Protons**
4.39	d	100.9	17
3.66	d	11.7	13
3.43	m	-	23
2.59	d	15.7	114
1.43	d	44.8	110
1.26	d	23.2	100

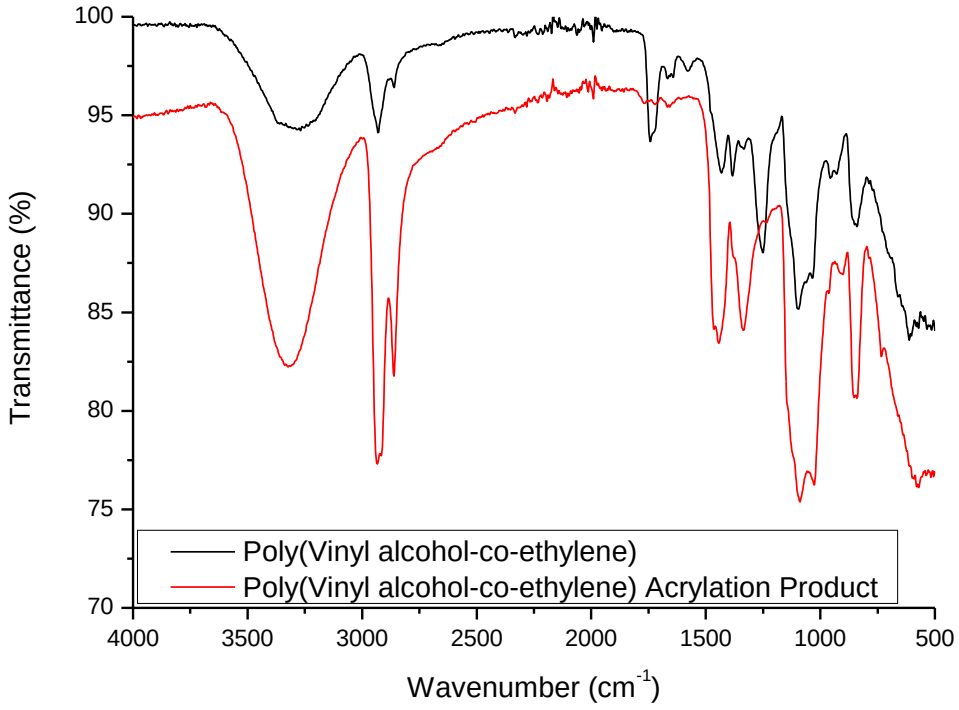

Figure 4.7 IR Spectrum of partially acrylated poly(vinyl alcohol-*co*-ethylene), a lack of peaks associated with acrylate functionality showed functionalisation was not successful.

^{1}H NMR (Figure 4.6, Table 4.2) and IR analysis (Figure 4.7) once again showed that no peaks or absorption stretch was present relating to the alkene groups. As there was a solvent reaction with

the acrylation reagent, and the only solvent applicable for dissolving the polymer was DMSO, the modification route relating to this polymer was deemed non-viable.

4.3.1.3 Partial (50 mol. %) Modification of Poly(vinyl alcohol-*co*-ethylene) with Norbornene Moiety

Steglich esterification is a modification technique using hydroxyl containing molecules and carboxylic acids. The procedure was based on those detailed by Steglich *et al*.[104]. Further to the acrylation reaction, the functionalisation reaction of hydroxyl groups with norbornene was pursued with Poly(vinyl alcohol-*co*-ethylene) as model compound.

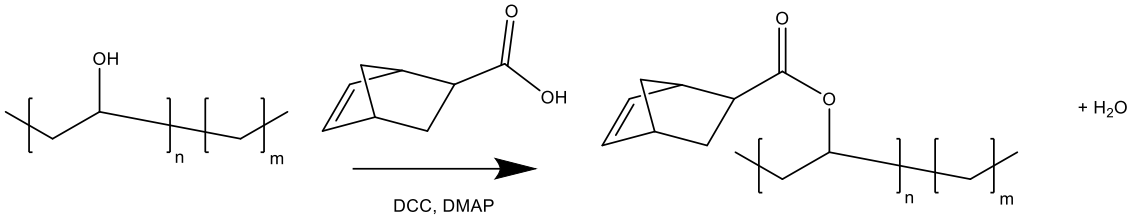

Figure 4.8 Modification of poly(vinyl alcohol-*co*-ethylene) with 5-Norbornene-2-carboxylic acid.

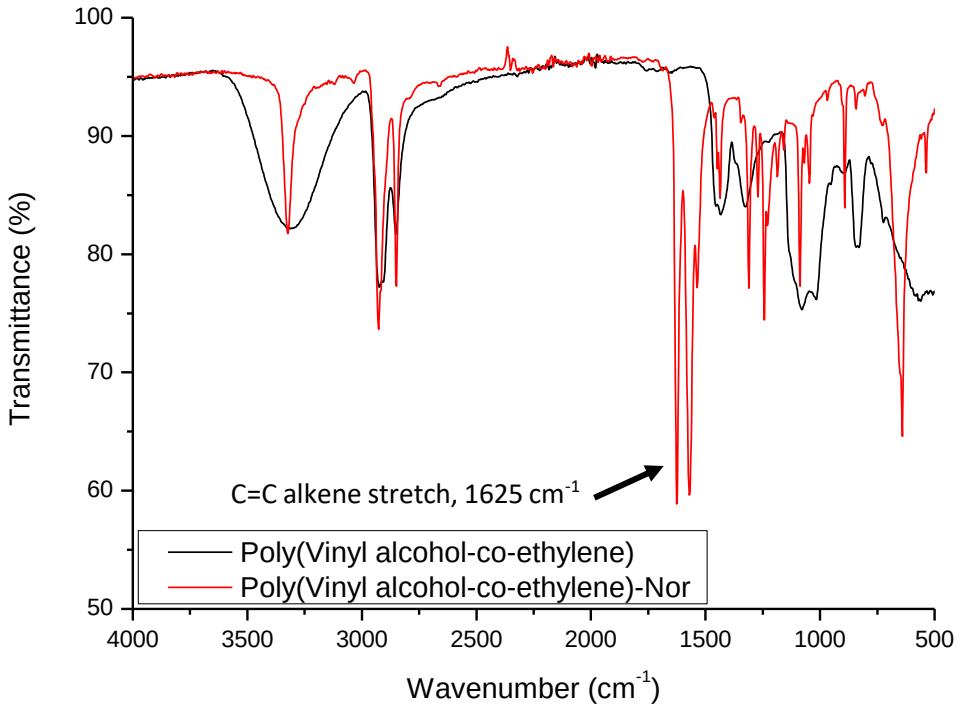

Figure 4.9 IR Spectrum of partially norbornene modified poly(vinyl alcohol-*co*-ethylene), the two peaks present at 1625 cm^{-1} show that norbornene was successfully grafted to the polymer structure.

Modification of poly(vinyl alcohol-*co*-ethylene) was attempted *via* a hydroxyl function-initiated coupling reaction, resulting in the formation of an ester. ^{1}H NMR analysis (Figure 4.6) showed small peaks at 6.08 and 5.80 ppm, which corresponded to the alkene carbons present in the norbornene moiety. The two peaks were found as the reagent used was a mixture of endo and exo isomers and so there were two proton environments present in the molecule resulting in different peaks on the ^{1}H NMR spectrum. An absorption stretch at ~1625 cm^{-1} in the infrared spectrum (Figure 4.9) relating to an alkene (C=C) group also confirmed the presence of the norbornene moiety.

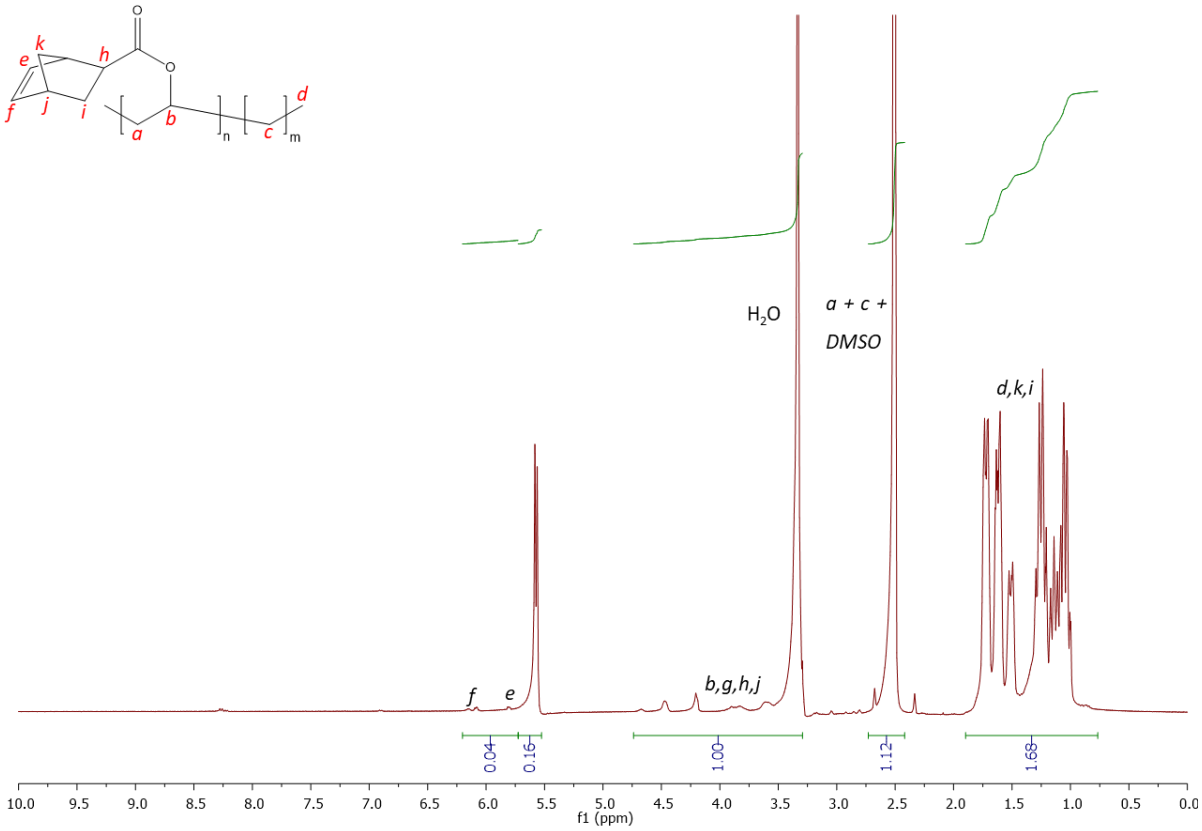

Figure 4.6. ^{1}H NMR spectrum (DMSO) of product obtained from norbornene modification of poly(vinyl alcohol-*co*-ethylene).

The product obtained (1.27 g) related to a 139 % yield for the reaction, which is due to the presence of DCC urea, which is extremely difficult to remove. The removal was made more difficult by the solvent, as the polymer and urea were both soluble in DMSO. The small alkene peaks observed in ^{1}H NMR analysis suggest a low grafting rate therefore, a further reaction was carried out with the intention of completely modifying all available reactive sites to increase polymer functionality.

4.3.1.4 Complete Modification Poly(vinyl alcohol-*co*-ethylene) with Norbornene Moiety

The norbornene-induced modification of poly(vinyl alcohol-*co*-ethylene) (Section 4.3.1.3) was repeated to obtain a higher grafting rate. An excess of 5-Norbornene-2-carboxylic acid was used with the intention of complete hydroxyl saturation.

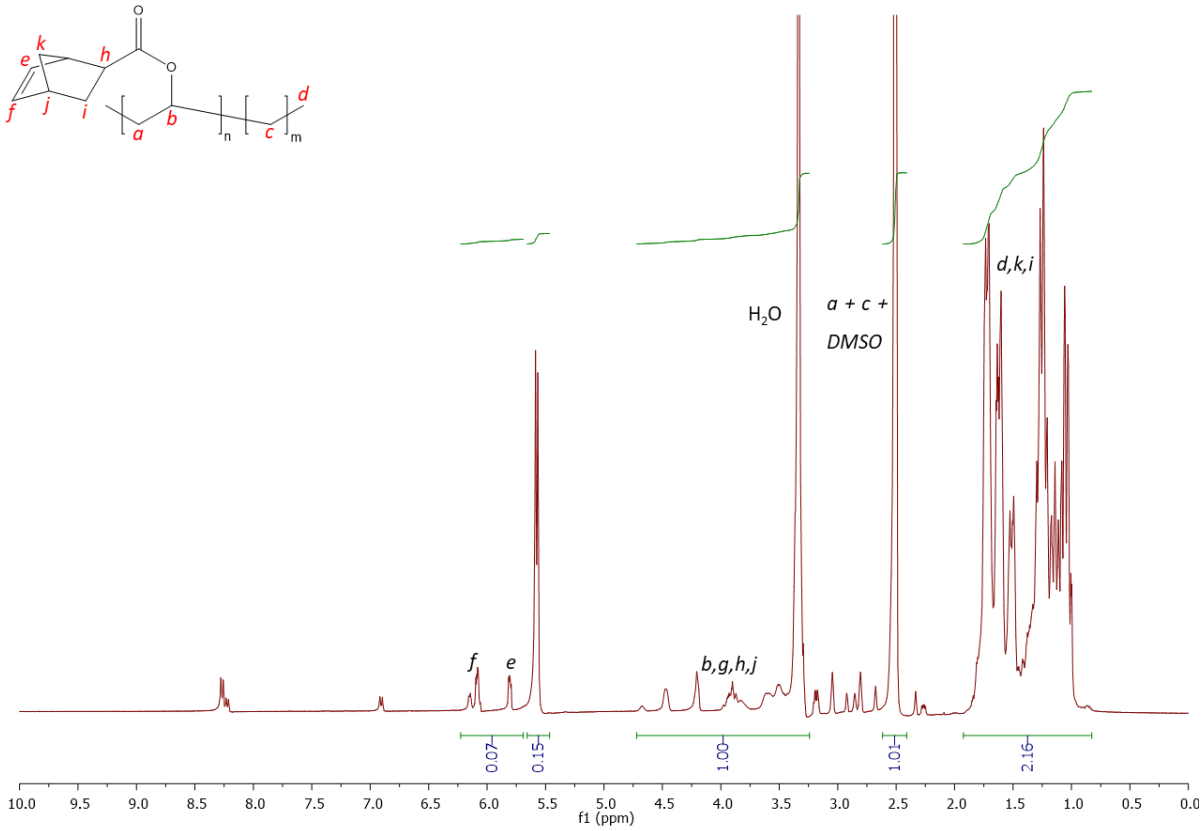

Figure 4.10 ^{1}H NMR spectrum (DMSO) of product obtained from norbornene modification of poly(vinyl alcohol-*co*-ethylene).

The ^{1}H NMR spectrum (Figure 4.10) clearly showed an increase in alkene protons present, which can only arise from the norbornene moiety. The integration value of these peaks increased from 0.04 to 0.07.

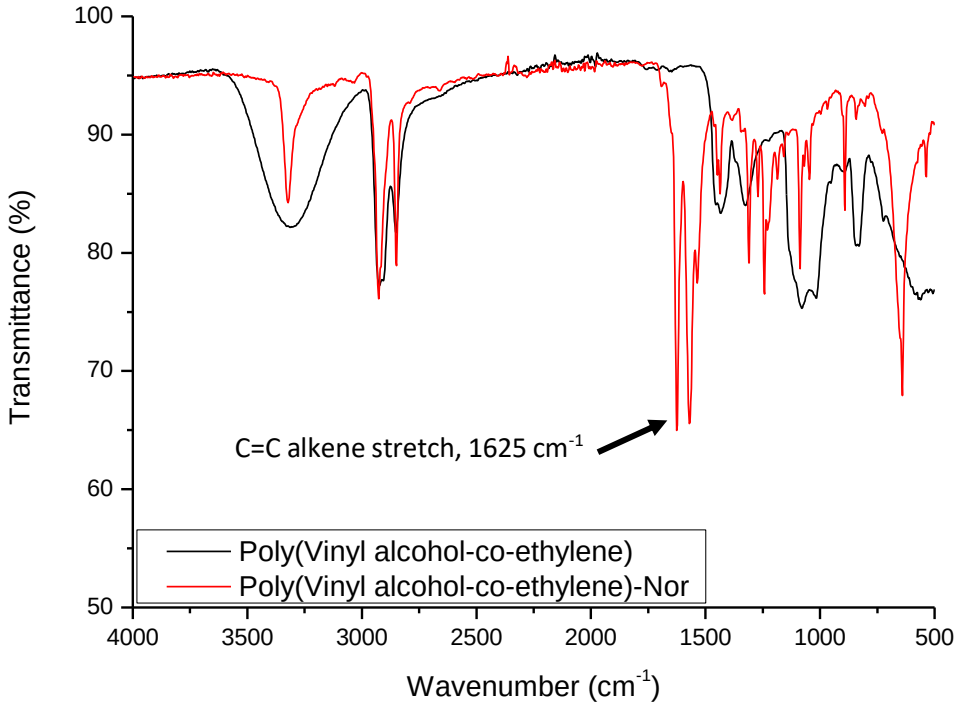

Figure 4.11 Infrared spectrum of product obtained from norbornene modification of poly(vinyl alcohol-*co*-ethylene).

The product obtained (1.87 g) related to a 140 % yield for the reaction, which again means the presence of DCC urea in the product. The IR spectrum (Figure 4.11) again showed the alkene (C=C) absorption stretch at ~1625 cm^{-1} and a change in the absorption at ~3300 cm^{-1} from a broad stretch to a sharp stretch, which is indicative of a change from alcohol hydroxyl groups to carboxylic acid hydroxyl groups. The successful norbornene modification of the model polymer poly(vinyl alcohol-*co*-ethylene) allows for the possibility of modifying the PGS derivatives in a similar fashion, introducing the potential for alternative curing functionality through a thiol reaction.

4.3.2 Poly(glycerol sebacate) Synthesis and Modification

In performing an in-house synthesis of PGS, the initial chemical pathway testing was intended to be carried out on a polymer synthesised to a high purity.

4.3.2.1 Synthesis of Poly(glycerol sebacate)

Synthesis of PGS was based on well documented and used procedures as laid out by Nijst *et al*.[111]. PGS was initially synthesised with an intended 100% yield of polycondensation reaction, for this the curing stage was left for 48 h. The product obtained was highly insoluble. An ^{1}H NMR sample was left dissolving overnight and it appeared only trace amounts were in solution. The structure of the PGS was confirmed by the ^{1}H NMR spectrum (Figure 4.13).

Figure 4.12 Poly(glycerol sebacate).

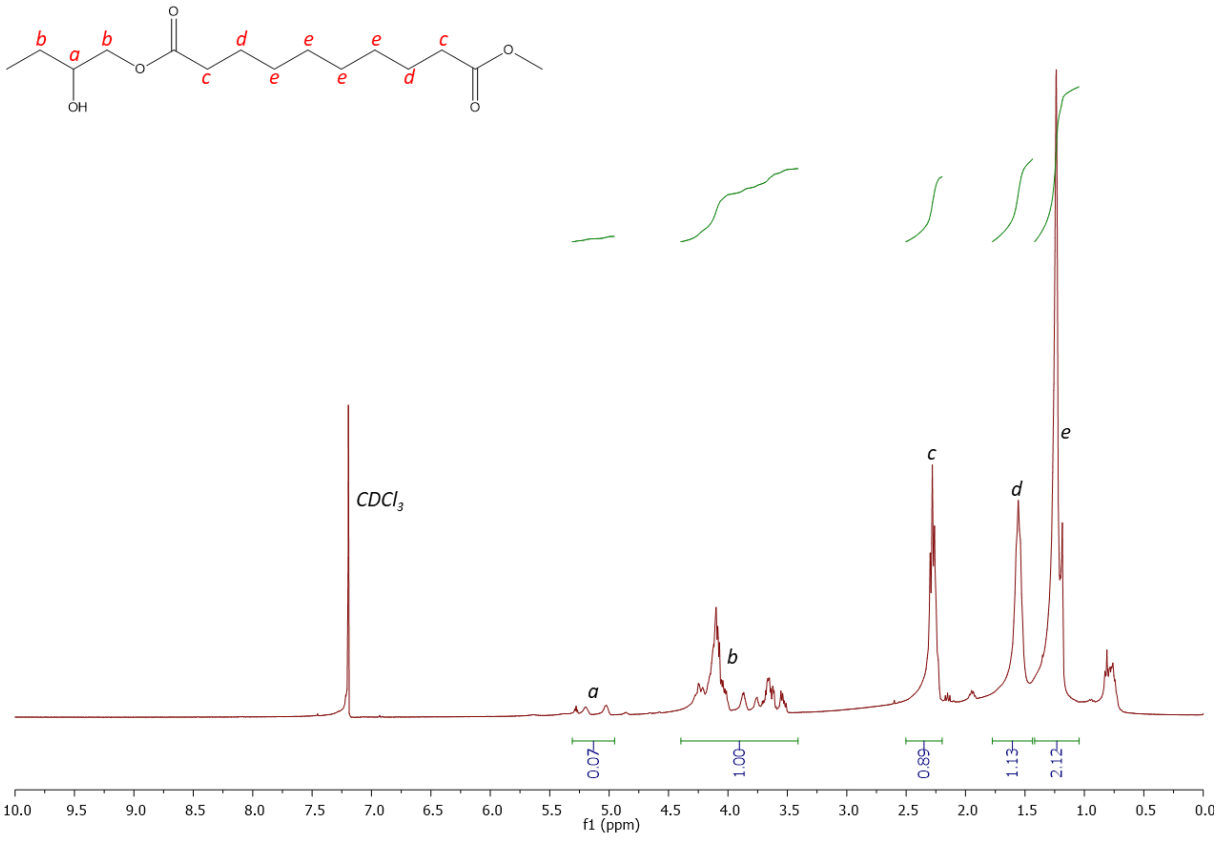

Figure 4.13 ^{1}H NMR spectrum ($CDCL_3$) of poly(glycerol sebacate).

The polymer obtained was very elastic and transparent although over time it (24 h) appeared to become cloudy and discoloured (Figure 4.12), possibly due to the polymer crystallising as it cooled.

4.3.2.2 Modification of Poly(glycerol sebacate) with Norbornene Moiety in DMSO

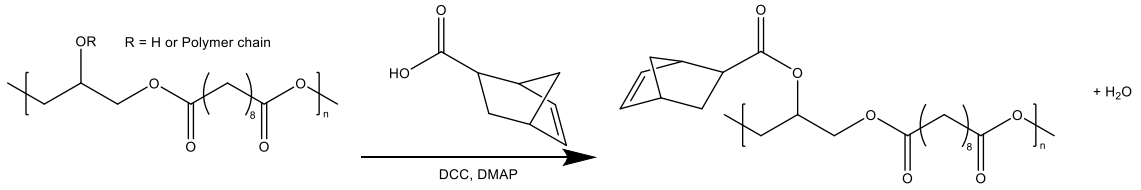

Figure 4.14 Modification of poly(glycerol sebacate) with 5-Norbornene-2-carboxylic acid.

The same protocol that was used to modify poly(vinyl alcohol-*co*-ethylene) (Sections 4.3.1.3 & 4.3.1.4) was applied for the norbornene-induced modification of PGS. Upon reaction completion,

the reaction solution was found to have a white precipitate suspended in it; filtration of the mixture failed to separate the polymer from the white precipitate believed to be the DCC urea. The polymer also appeared to be only slightly soluble in DMSO, as, when filtration was carried out, the polymer maintained its initial shape (the polymer particles were still intact, with only slight changes to their shape). This would suggest that the polymer had swollen upon heating and stirring in the DMSO and became transparent in the solution, giving the appearance of dissolution. ^{1}H NMR and IR analysis were deemed unsuitable due to DCC urea contamination.

4.3.2.3 OGS Prepolymer Synthesis

Solubility issues when attempting to modify PGS necessitated the synthesis of OGS batches intended for both acrylation and coupling with 5-Norbornene-2-carboxylic acid. The synthesis of the less crosslinked material avoids the insolubility properties of the polymer while allowing for a higher degree of modification.

4.3.2.4 Synthesis of Oligo(glycerol sebacate)

One of the OGS batches was cured for 24 h rather than 48 h in an attempt to produce PGS with enhanced solubility. This was to enable comparison of the difference in modification reactions between the material in its oligomer and polymer forms.

4.3.2.5 Modification of Oligo(glycerol sebacate) with Norbornene Moiety

To avoid solubility issues with dissolution of the PGS, the solvent was changed from DMSO used in the previous protocol (Section 4.3.1.3 and Section 4.3.1.4) to dichloromethane. This solvent change also had the additional benefit of allowing major bulk removal of the DCC urea more easily. Once the reactions were completed, the flask was placed in the freezer, which caused the DCC urea to

precipitate out as a white suspension. Filtration of this mixture allowed for the polymer to be kept in solution, so that a very viscous honey coloured material was obtained (Figure 4.15).

IR: 3300 cm^{-1} (-O-H), 2900 cm^{-1} (-C-H), 2100 cm^{-1} (-N=C=N), 1625 cm^{-1} (-C=C)

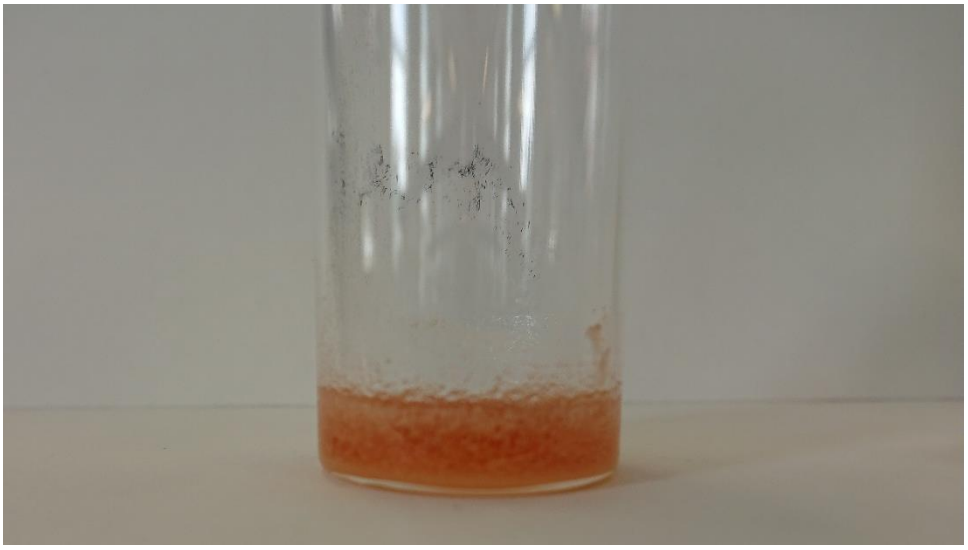

Figure 4.15 5-Norbornene-2-carboxylic acid modified oligo(glycerol sebacate).

Table 4.3 ^{1}H NMR data of 5-Norbornene-2-carboxylic acid modified oligo(glycerol sebacate).

^{1}H NMR (400 MHz)			
δ (ppm)	**Multiplet**	**J Frequency (Hz)**	**Protons**
6.10	m	-	15
5.90	m	-	8
5.17	m	-	13
4.37-3.31	m	-	96
2.23	m	-	63
1.95-1.11	m	-	516

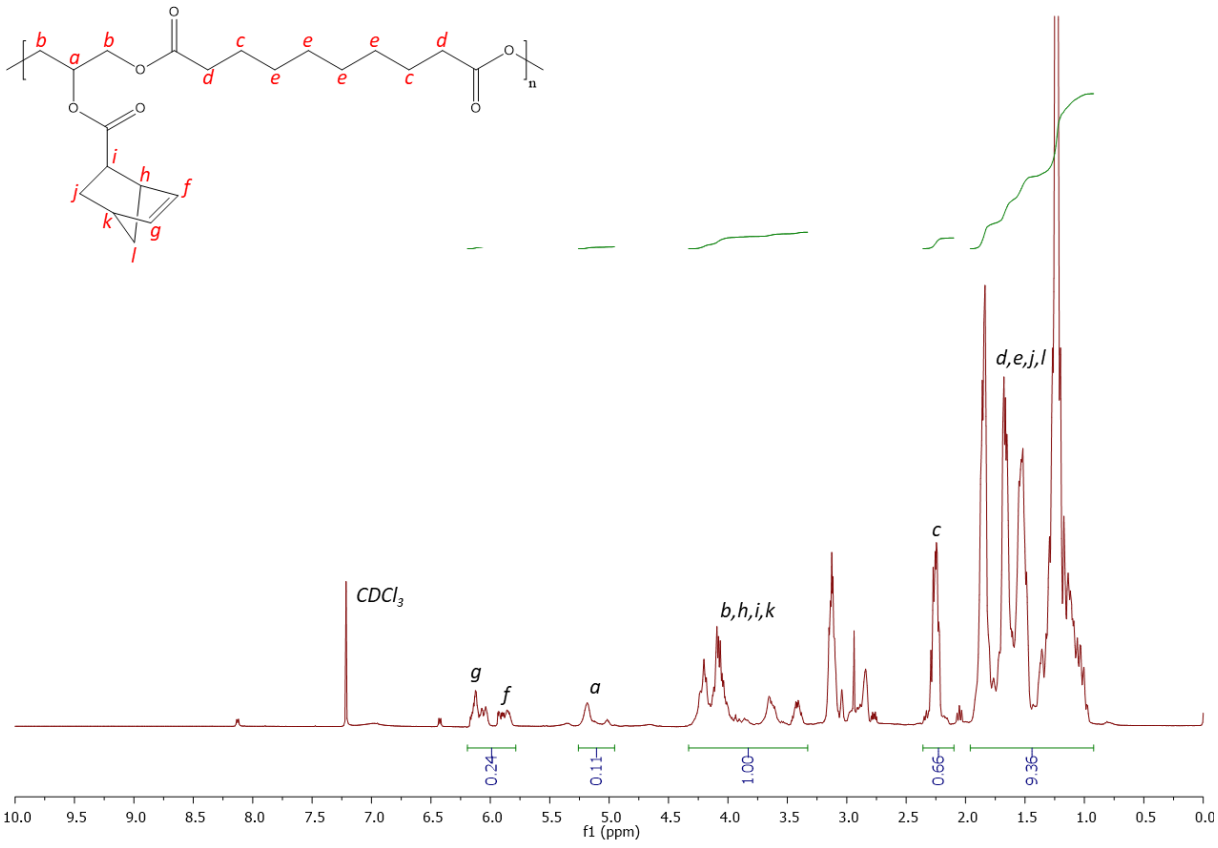

Figure 4.16 ^{1}H NMR spectrum ($CDCL_3$) of 5-Norbornene-2-carboxylic acid modified oligo(glycerol sebacate).

The ^{1}H NMR spectrum (Figure 4.16, Table 4.3) showed the two peaks (6.10 and 5.90 ppm), relating to the geminal protons of the norbornene moiety, confirming that grafting was successful. The IR spectrum also confirms the presence of an alkene bond with an absorption stretch at 1625 cm^{-1}, although it also includes an absorption stretch at 2100 cm^{-1} which is indicative of a carbodiimide being present – the DCC urea is extremely difficult to remove from the product; this raises the question of whether a different synthetic route is more viable or simply a change of coupling reagent would be practical.

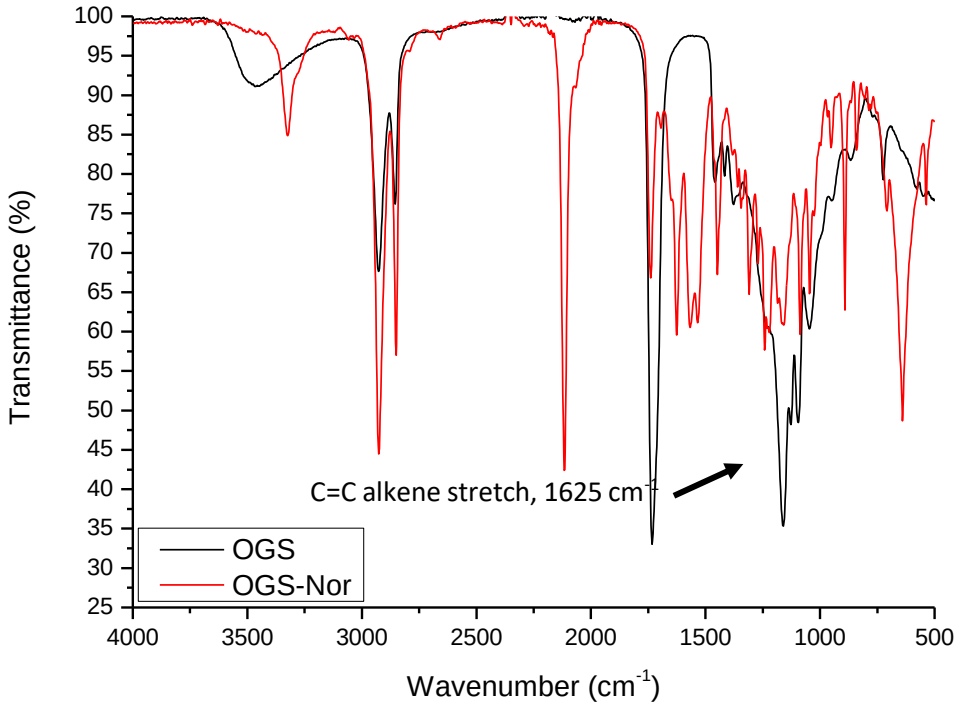

Figure 4.17 Infrared spectrum of norbornene modified oligo(glycerol sebacate), large DCC and DCC urea contamination produces a complex fingerprint region, but alkene functionality can be observed at 1625 cm^{-1}.

As the IR spectrum (Figure 4.17) confirmed that either DCC, or its urea was present in the end product, the outlying peaks on the ^{1}H NMR spectrum ranging from 3.25 – 2.75 ppm are likely to be related to the carbodiimide molecule. The yield obtained (1.79 g), which relates to a yield of 148 % further confirmed the presence of the DCC urea being present in the product. Dialysis may be an effective method of separating the product from the DCC urea, a different synthetic route or change in coupling reagent may also be required.

4.3.2.6 Modification of Poly(glycerol sebacate) with Norbornene Moiety

The reaction protocol of previous norbornene modification (Section 4.2.3.2) was reproduced for the 24 h cured PGS. The product obtained (Figure 4.18) was more viscous than the modified oligomer and took a longer amount of time to dissolve into ^{1}H NMR solvent.

Figure 4.18 5-Norbornene-2-carboxylic acid modified poly(glycerol sebacate).

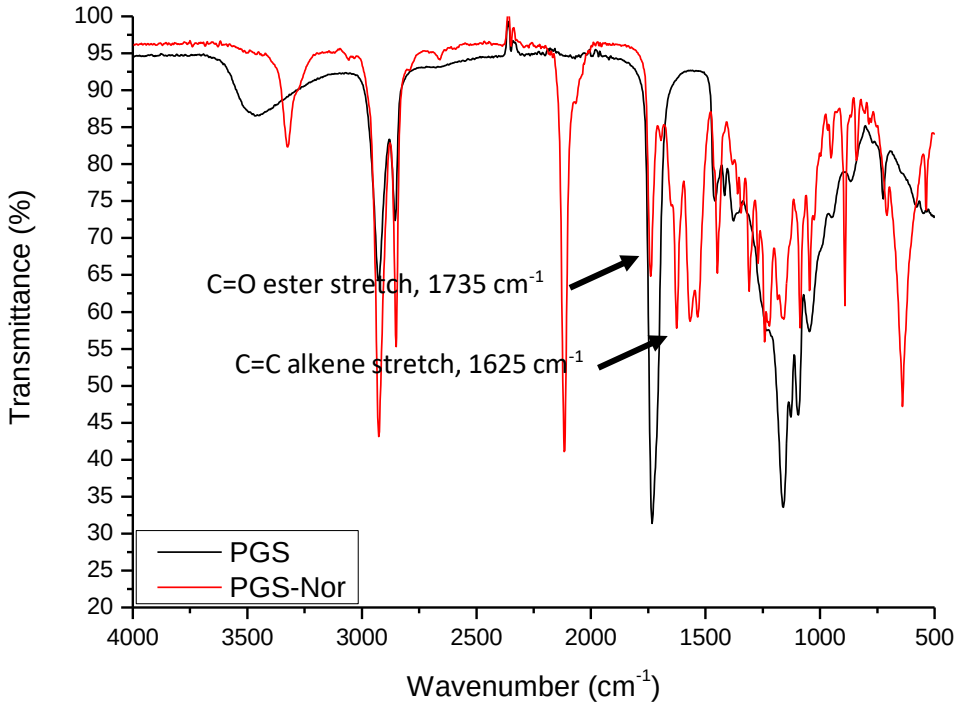

Figure 4.19 Infrared spectrum of norbornene modified poly(glycerol sebacate), large DCC and DCC urea contamination produces a complex fingerprint region, but alkene functionality can be observed at 1625 cm^{-1} and ester functionality can additionally be observed at 1735 1625 cm^{-1}.

As with the modified oligomer, the ^{1}H NMR spectrum (Figure 4.20, Table 4.4) showed peaks (6.10 and 5.90 ppm) relating to the geminal protons confirming that modification was successful. The infrared (IR) spectrum (Figure 4.19) also confirmed that grafting of the norbornene moiety was successful due to the absorption stretches at 1735 and 1625 cm^{-1}. Similarly, to the previous reaction product (Section 4.2.3.2), an absorption stretch at 2100 cm^{-1} was still observed, which is indicative of a carbodiimide being present, as confirmed again by the outlying peaks from 3.25 – 2.75 ppm in the ^{1}H NMR spectrum.

Table 4.4 ^{1}H NMR data of 5-Norbornene-2-carboxylic acid modified poly(glycerol sebacate) – 24 h cured.

^{1}H NMR (400 MHz)			
δ (ppm)	**Multiplet**	**J Frequency (Hz)**	**Protons**
6.1	m	-	16
5.9	m	-	8
5.16	m	-	15
4.35-3.32	m	-	85
2.22	m	-	57
1.94-1.11	m	-	498

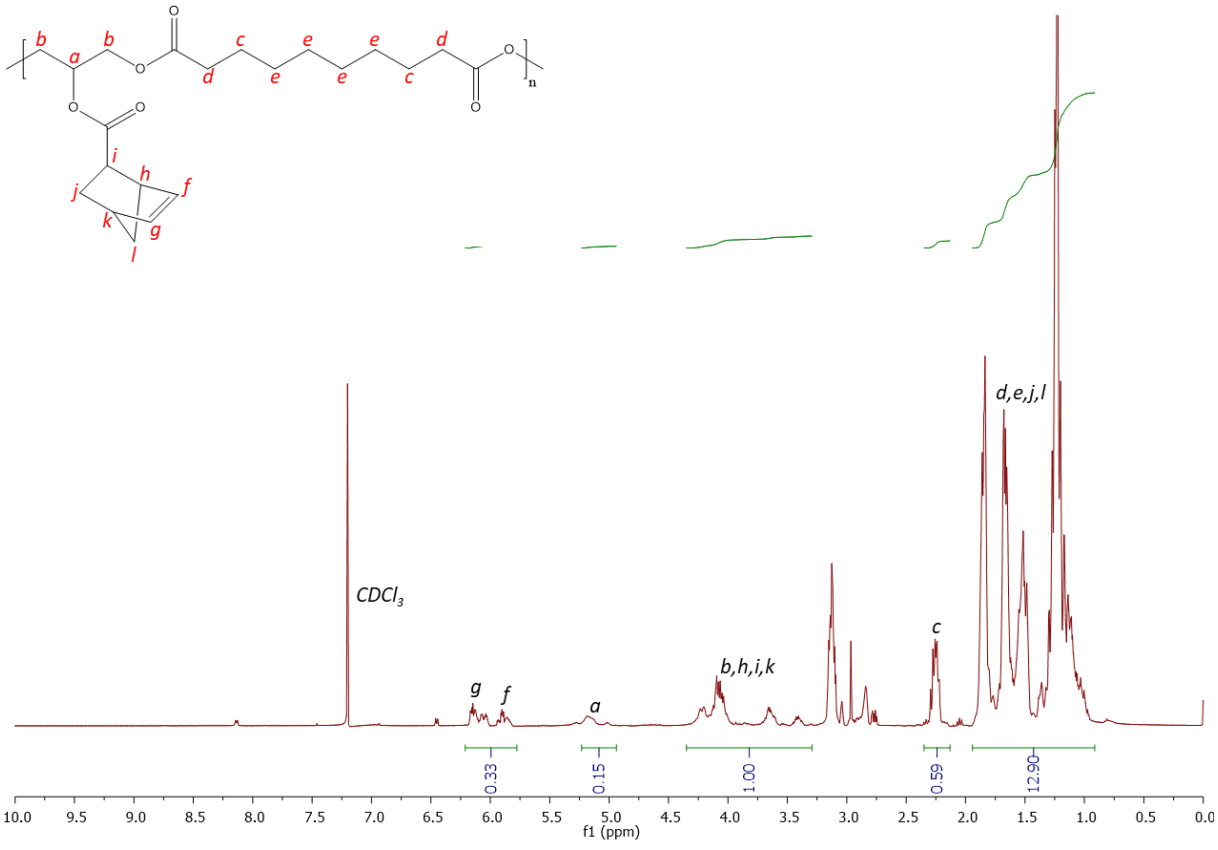

Figure 4.20 ^{1}H NMR spectrum ($CDCL_3$) of 5-Norbornene-2-carboxylic acid modified poly(glycerol sebacate) – 24 h cured.

The yield obtained (1.85 g), which relates to a yield of 153 %, further confirms the presence of the DCC urea being present in the product. Ultimately, either a different synthetic route should therefore be considered or, a change of coupling reagent or purification by dialysis.

4.3.2.7 Acrylation of Oligo(glycerol sebacate)

Acrylation to form a photocurable polymer (Figure 4.21) is highly desirable, as avoiding the high temperatures required to crosslink PGS would enable it to be crosslinked quickly *in situ*, potentially at the bedside in a clinical setting. To avoid solubility and solvent interactions, the solvent was changed from DMSO to dichloromethane. This enabled quick dissolution of the oligomer and other reagents. In contrast to the acrylation of poly(vinyl alcohol-*co*-ethylene), there was no colour changes upon addition of the acryloyl chloride.

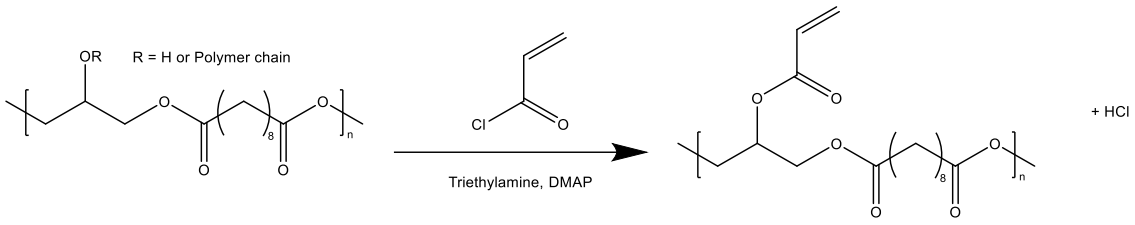

Figure 4.21 Acrylation of poly(glycerol sebacate).

From the ^{1}H NMR spectrum (Figure 4.22), it was observed that three peaks relating to the alkene group were present at 6.39, 6.10 and 5.85 ppm, confirming that the acrylation was successful. Three peaks were present due to the three different proton environments of the alkene group (Figure 4.23).

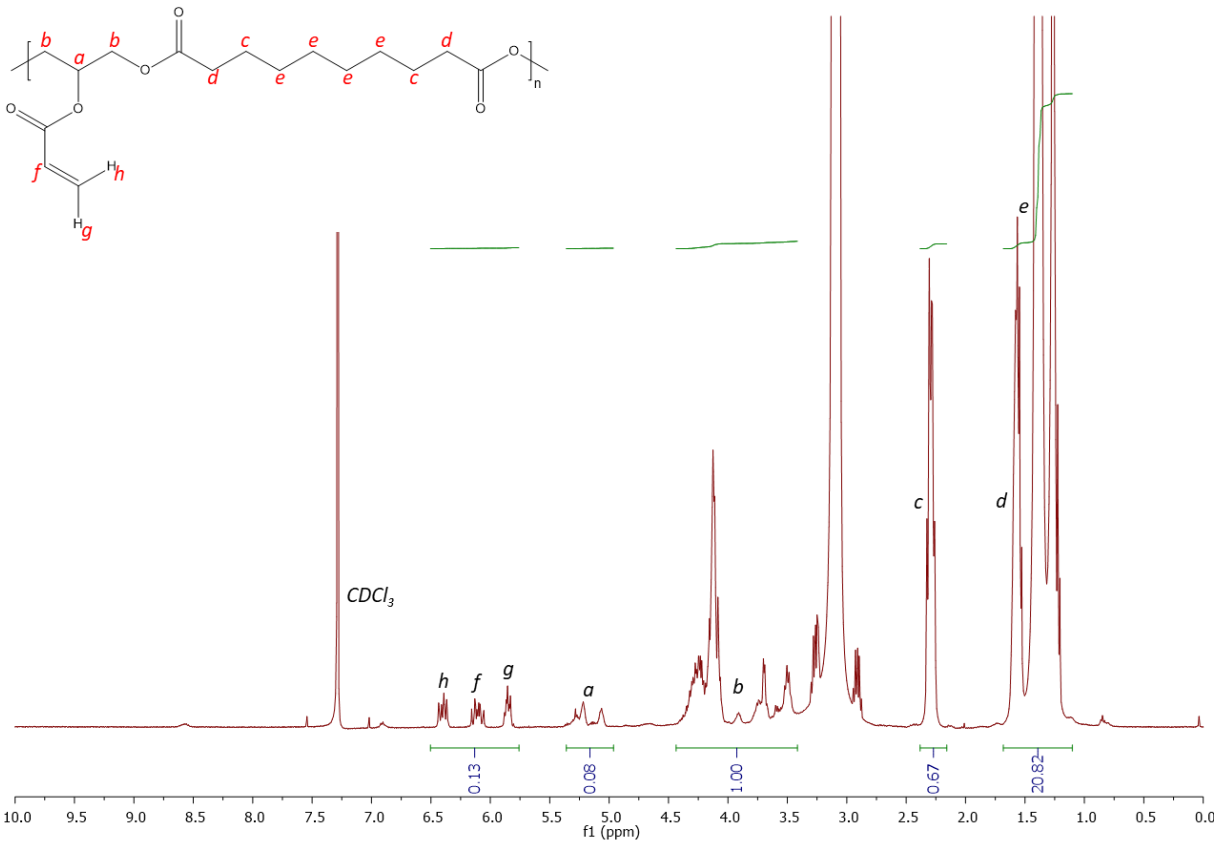

Figure 4.22 ^{1}H NMR spectrum ($CDCL_3$) of acrylated poly(glycerol sebacate) prepolymer.

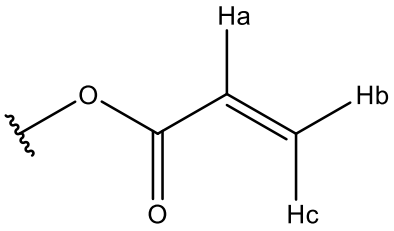

Ha = 6.10 ppm
Hb = 5.85 ppm
Hc = 6.39 ppm

Figure 4.23 Diagram of the different proton environments and their respective peaks in an acrylate functional group.

The yield obtained of 1.85 g related to a yield of 21 %, this is much lower than expected as acrylate reactions usually generate a moderate to high yield. A suggested reason for this low yield is excessive washing to remove the acryloyl chloride, triethylamine and DMAP.

4.3.3 Synthesis and Modification of poly(glycerol sebacate) with Varied Curing Times

4.3.3.1 Synthesis of PGS with Increased Curing Time, PGS-L

The same procedure was used as in the previous synthesis of PGS (Section 4.3.2.1) and as with the different cure times in the PGSLP syntheses the reaction time was varied, as the glycerol is present in the synthesis of PGS from the start the reaction and there is no period solely for crosslinking the reaction was left 24 h from start to finish. Acrylation was intended so the material underwent an $MgSO_4$ drying step in preparation, to remove any water residue from the material and prevent the formation of by-products during the acrylation process.

^{1}H NMR analysis (Figure 4.24) confirmed the correct material had been synthesised, the ability to dissolve the material in solvent was also an indication that maximum crosslinking had not occurred.

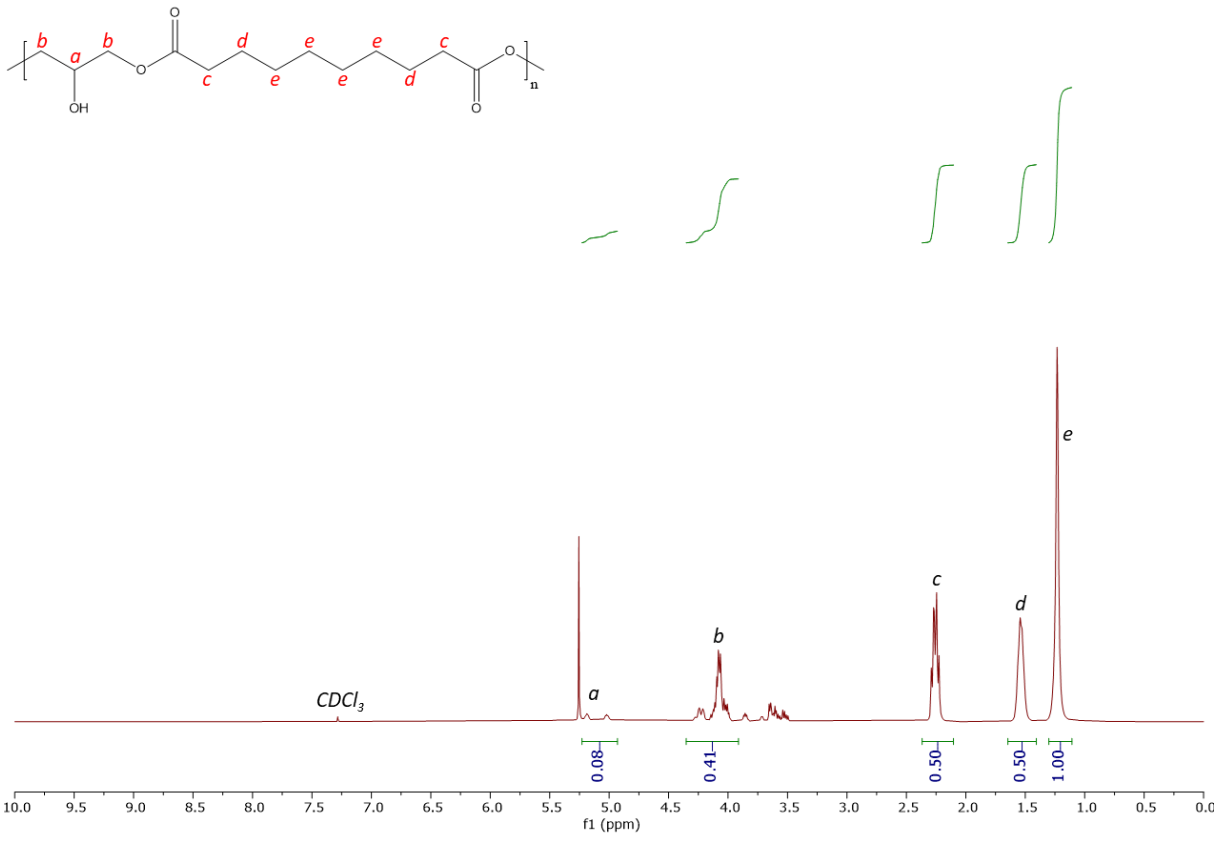

Figure 4.24 ^{1}H NMR spectrum ($CDCL_3$) of PGS-L.

A yield of 82 % was obtained as a clear viscous free flowing fluid.

4.3.3.2 Synthesis of PGS with Shorter Curing Time, PGS-S

The reaction time for the shorter derivative was reduced from 24 h to 18 h, with the aim of increasing the number of reactive sites available for grafting. Acrylation was also intended for this polymer and so, an $MgSO_4$ drying step was used in preparation.

^{1}H NMR analysis (Figure 4.25) confirmed the intended polymer material had been successfully synthesised, but its ability to dissolve in solvent was also an indication that maximum crosslinking had not occurred.

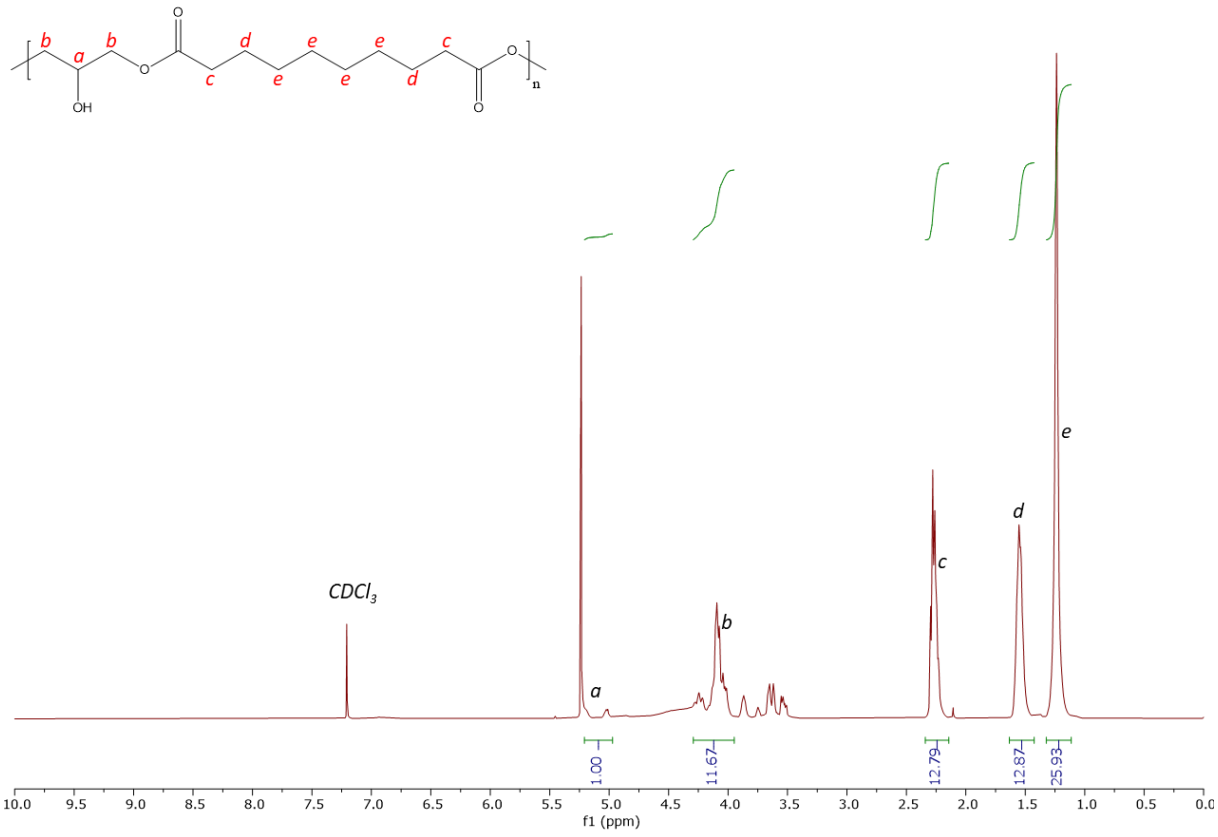

Figure 4.25 ^{1}H NMR spectrum ($CDCL_3$) of PGS-S.

A yield of 83 % was obtained as a clear viscous free flowing fluid.

4.3.3.3 Acrylation of PGS-L

From the ^{1}H NMR spectrum (Figure 4.26), it was observed that 3 peaks relating to the alkene group were present at 6.39, 6.10 and 5.85 ppm, confirming that the acrylation was successful.

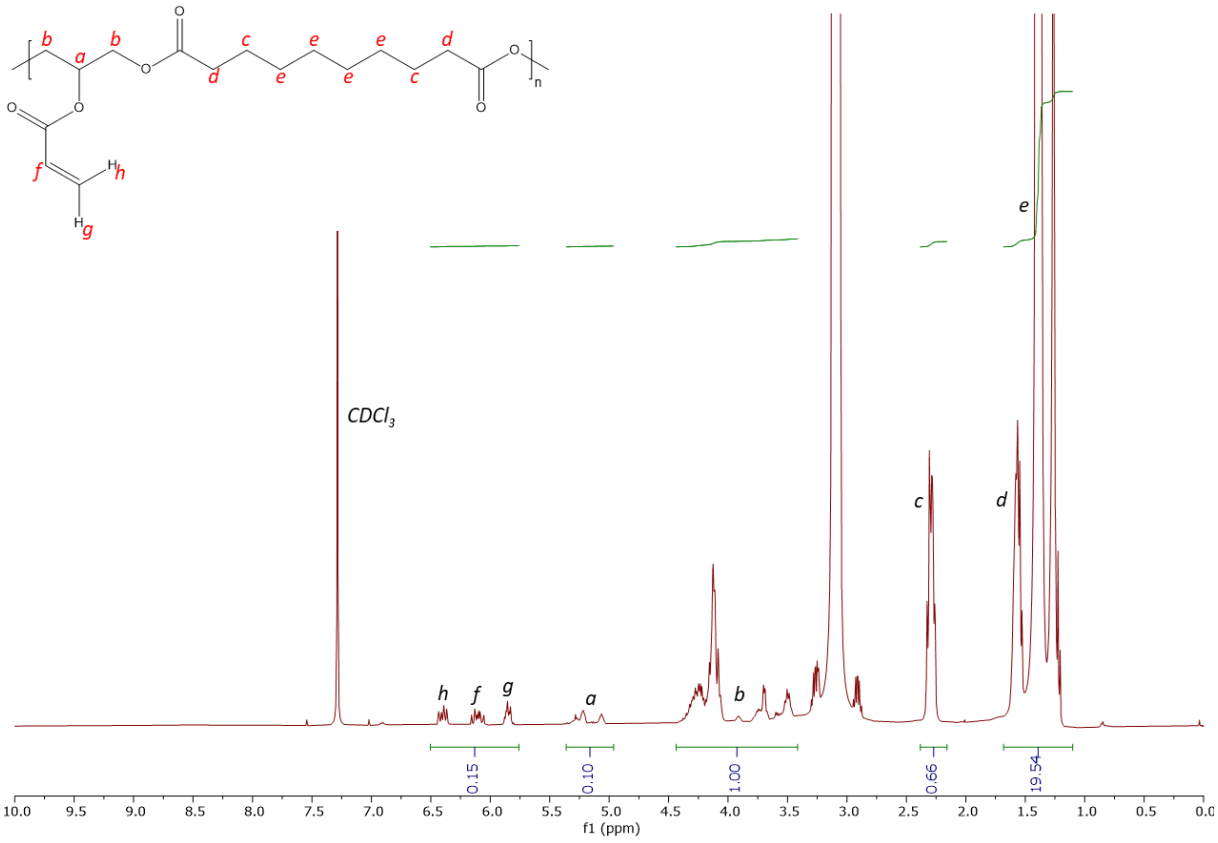

Figure 4.26 ^{1}H NMR spectrum ($CDCL_3$) of PGSA-L.

A yield of 71 % was obtained, which is consistent with previous acrylation procedures of PGS (Section 4.3.2.7).

4.3.3.4 Acrylation of PGS-S

From the ^{1}H NMR spectrum (Figure 4.27), it was observed that 3 peaks relating to the alkene group are present at 6.39, 6.10 and 5.85 ppm, confirming that the acrylation was successful.

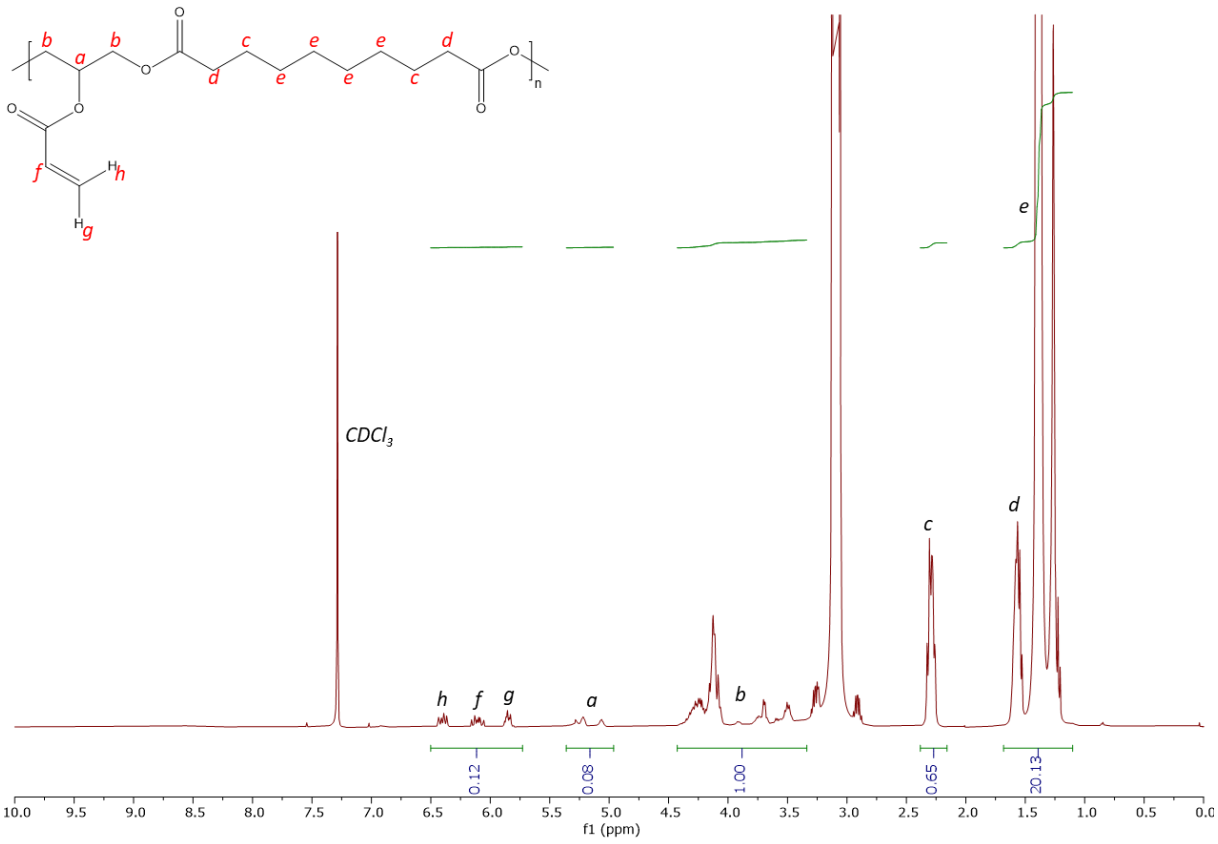

Figure 4.27 ^{1}H NMR spectrum ($CDCL_3$) of PGSA-S.

A yield of 69 % was obtained, which is consistent with previous acrylation procedures[111] of PGS however, a decrease in yield was not expected as the intention of decreasing the curing time was to increase the grafting rate of the acrylate functionality. A possibility is that the solvent used in the shorter curing time reaction contained a higher amount of water, which caused a loss of acryloyl chloride through the formation of acrylic acid. Another possibility is a temperature differential between the two reactions which could have decreased the yield if the temperature for the shorter curing time PGS was higher due to the exothermic nature of the reaction.

4.4 Summary

The synthesis and modification reactions revealed that grafting of norbornene moieties, such as 5-Norbornene-2-carboxylic acid, to oligo and poly(glycerol sebacate) can be achieved using coupling

agents such as DCC. DCC was chosen as the coupling reagent due to the solubility of the polymer, PGS is insoluble in water and therefore a more commonly used coupling reagent combination of 1-Ethyl-3-(3’-dimethylaminopropyl)carbodiimide and N-hydroxysuccinimide would not be applicable. Although there are some issues with removing the DCC urea from the reaction mixture, the synthetic route is a viable option that can be built upon to include other moieties and functional molecules.

The acrylation of PGS is also a viable route enabling circumvention of the need to cure at high temperatures, for extended periods of time. Although the photocuring of PGSA needs to be carried out and tested to confirm its feasibility, there is strong evidence to suggest that it may be the more desirable option (with respect to PGS norbornene) for the intended application of the biomaterial. Although in this case the homo-polymerisation of acrylates should be considered, pH- rather than light-induced thiol-ene click chemistry could be pursued for the formation of the covalent thiol-ene network.

The synthesis of PGS using this route was found to be practical, and the lack of solvent and harmful chemicals means that scale up for biomedical applications should be feasible. Another additional benefit of using oligo/poly(glycerol sebacate) as a starting point for further testing is that most modification reactions can be done in a one-pot synthesis style, whereby the polycondensation reaction is halted either after prepolymer formation or after a set curing period. In this respect, 24 h seems to be a convenient end-of-reaction time point, as it allows for the polymer to still be free-flowing following application of heat and is soluble in dichloromethane.

Chapter 5

Preparation of Water Soluble Poly(glycerol sebacate) Based Materials

5.1 Introduction

In order to produce a water soluble (potentially injectable) form of the PGS material it was further modified to increase hydrophilicity. The purpose was to create a Poly(glycerol sebacate)-based polymer with potential for direct implantation or injection into the foot plantar, without the need for dissolution in organic solvents. A further aim was to provide materials with photo-crosslinking capability, to enable mechanical properties of the elastomer to be modulated. This chapter details the experimental approaches that were pursued for synthesis of the new materials:

- Copolymerisation of poly(glycerol sebacate) with lactic acid and PEG, forming poly(glycerol sebacate-*co*-lactic acid-*co*-polyethylene glycol) (PGSLP)
- Modification of PGSLP derivatives with a norbornene moiety to introduce photo crosslinking functionality
- Acrylation of PGSLP derivatives to provide photo crosslinking functionality

The synthesis procedures used were modified from a paper detailing the synthesis of such polymers[183].

5.2 Experimental

5.2.1 Increasing the hydrophilicity of Poly(glycerol sebacate) based materials.

Integration of polyethylene glycol and lactic acid into the polymer would be expected to markedly increase hydrophilicity, allowing the Poly(glycerol sebacate)-based polymer to be dissolved as an aqueous formulation, the synthesis procedure was modified from a paper detailing the synthesis of such polymers[185]. Further modification of this polymer would allow for crosslinking functionality to be introduced, allowing for a material with the potential to be injected into a cavity and gelled *in situ* through the use of an aqueous formulation. Use of this newly functionalised material as a reinforcement phase in an elastomeric composite would provide good phase interactions, ensuring the composites structural integrity.

5.2.1.1 Synthesis of Poly(glycerol sebacate-*co*-lactic acid-*co*-polyethylene glycol$_{1000}$) (PGSLP$_{1000}$)

A water-soluble derivative of PGS was prepared by copolymerisation with PEG_{1000} and lactic acid.

A round bottom flask was charged with sebacic acid (1.10 g, 5.43 mmol), lactic acid (7.83 g, 86.96 mmol) and PEG (Mw 1000, 2.72 g, 2.71 mmol). The vessel was flushed with nitrogen, magnetic stirring at 350 rpm turned on and heated to 120°C, once the temperature reached 120°C vacuum (0.001 bar) was applied and stirring was continued for 4 h. Stannous octanoate, $Sn(oct)_2$ (2.20 g, 5.43 mmol) and p-Toluenesulfonic acid monohydrate, $TSA.H_2O$ (1.03 g, 5.43 mmol) were added, vacuum (0.001 bar) was reapplied, and the temperature was increased to 180°C. The reaction was then continued for 24 h. Glycerol (0.50 g, 5.43 mmol) was then added, and the reaction continued for a further 2 h under reduced vacuum (0.0005 bar). The material produced was a clear viscous fluid.

5.2.1.2 Modification of $PGSLP_{1000}$ with Norbornene Moiety, $PGSLP_{1000}$-Nor 1

Introduction of norbornene functionality was again investigated as a way of introducing photo-sensitive functionality and allow an alternate crosslinking route to thermal curing. The procedure was repeated from previous experiments with grafting norbornene functionality to PGS (Section 4.3.2.6).

$PGSLP_{1000}$ (1.0 g) was added to a round bottom flask, dichloromethane (50 mL) was added and the vessel left stirring at 350 rpm for 30 min. 5-Norbornene-2-carboxylic acid (0.12 g, 0.89 mmol), DCC (0.92 g, 4.47 mmol) and DMAP (0.01 g, 0.089 mmol) were added and the reaction left to magnetically stir at 350 rpm for 24 h. Deionised water (100 mL) was added to crash unreacted DCC and DCC urea by-products, the mixture was then vacuum filtered, and the DCM and water layers separated. Further water extraction to increase yield of collected polymer was carried out, the water layers were collected and combined and thus reduced on a rotary evaporator and dried yielding a brown viscous fluid.

5.2.1.3 Modification of $PGSLP_{1000}$ with Norbornene Moiety, $PGSLP_{1000}$-Nor 2

To remove as much unreacted DCC and DCC urea by-products the procedure was changed to include an overnight chilling period to crash as much DCC urea out of solution as possible and to allow vacuum filtration to remove as much DCC urea as possible.

$PGSLP_{1000}$ (1.0 g) was added to a round bottom flask, dichloromethane (50 mL) was added, and the vessel left magnetically stirring at 350 rpm for 30 min. 5-Norbornene-2-carboxylic acid (0.12 g, 0.89 mmol), DCC (0.92 g, 4.47 mmol) and DMAP (0.01 g, 0.089 mmol) were added, and the reaction left to stir on a magnetic stirrer at 350 rpm for 24 h. The reaction mixture was then left in the freezer at -20°C overnight, upon collection 18 h later a white precipitate had formed. Vacuum filtration of the white precipitate yielded a clear solution. Deionised water (100 mL) was added to crash further

unreacted DCC and DCC urea by-products, the mixture was then vacuum filtered, and the DCM and water layers separated. Further water extraction to increase yield of collected polymer was carried out, the water layers were collected and combined and thus reduced on a rotary evaporator to yield a honey-coloured viscous liquid.

5.2.1.4 Acrylation of $PGSLP_{1000}$, $PGSLP_{1000}A$

Acrylate functionality enables photo crosslinking and is an effective method of introducing photosensitivity due to high yields and quick reaction rates. Acrylation of PGSLP to form poly(glycerol sebacate-*co*-lactic acid-*co*-polyethylene glycol) Acrylate (PGSLPA) uses the same experimental procedure as described in Section 4.2.3.4 for the acrylation of PGS.

$PGSLP_{1000}$ (2.0 g) and DMAP (0.02 g, 0.17 mmol) was added to a flame dried round bottom flask, the flask sealed and flushed with N_2. Anhydrous dichloromethane (100 mL) was added to the flask and the magnetic stirring turned on at 350 rpm, the flask was then cooled in an ice bath to 0 °C. Acryloyl chloride (0.06 g, 0.71 mmol) and triethylamine (0.07 g, 0.71 mmol) were added dropwise simultaneously with dropping funnels and the reaction left stirring at 350 rpm for 24 h. The reaction mixture was then dissolved in ethyl acetate and vacuum filtered to yield an off-white powder.

5.2.2 Synthesis and Modification of Increased Glycerol and Sebacic Acid Content, $PGSLP_{1000}$

5.2.2.1 Synthesis of Increased Glycerol Content PGSLP, PG^SLP_{1000}

The intent of increasing glycerol content was to produce a material with a higher degree of potential crosslinking, an increased number of reactive sites present through an increase in the triol glycerol means that a highly crosslinked network can be formed through the grafting of a larger number of photosensitive moieties to the structure.

A round bottom flask was charged with sebacic acid (2.20 g, 10.87 mmol), lactic acid (11.74 g, 130.43 mmol) and PEG (Mw 1000, 4.53 g, 4.53 mmol). The vessel was flushed with nitrogen, magnetic stirring at 350 rpm turned on and heated to 120°C, once the temperature reached 120°C, vacuum (0.001 bar) was applied and stirring was continued for 4 h. Stannous octanoate, $Sn(oct)_2$ (3.67 g, 9.06 mmol) and p-Toluenesulfonic acid monohydrate, $TSA.H_2O$ (1.72 g, 9.06 mmol) were added, vacuum (0.001 bar) was reapplied, and the temperature was increased to 180°C. The reaction was then continued for 24 h. Glycerol (10.0 g, 108.70 mmol) was then added, and the reaction continued for a further 2 h under reduced vacuum (0.0005 bar). The material produced was a clear viscous fluid.

5.2.2.2 Synthesis of Increased Glycerol and Sebacic Acid Content PGSLP, $PG^S^LP_{1000}$

Glycerol and sebacic acid content were increased 10-fold with the primary intent of increasing the number of reactive sites on the polymers molecular structure while also extending the chain length of the polymer, extending the network, and providing longer linear portions between the glycerol branching points to determine the effect on viscosity and modification efficacy.

A round bottom flask was charged with sebacic acid (10.98 g, 54.34 mmol), lactic acid (5.87 g, 65.21 mmol) and PEG (Mw 1000, 2.26 g, 2.26 mmol). The vessel was flushed with nitrogen, magnetic stirring at 350 rpm turned on and heated to 120°C, once the temperature reached 120°C vacuum (0.001 bar) was applied and stirring was continued for 4 h. Stannous octanoate, $Sn(oct)_2$ (1.83 g, 4.53 mmol) and p-Toluenesulfonic acid monohydrate, $TSA.H_2O$ (0.86 g, 4.53 mmol) were added, vacuum (0.001 bar) was reapplied, and the temperature was increased to 180°C. The reaction was then continued for 24 h under vacuum (0.001 bar). Glycerol (5.0 g, 104.35 mmol) was then added, and the reaction continued for a further 2 h under reduced vacuum (0.0005 bar). The material

produced was a viscous fluid, with crystalline particulate agglomerations in. Dialysing the material in deionised water removed the crystallised agglomerates yielding a viscous fluid.

5.2.2.3 Modification of PG^SLP$_{1000}$ with Norbornene Moiety, PG^SLP$_{1000}$-Nor

Modification of the increased glycerol content PGSLP was carried out to determine how the increased number of potential reactive sites within the polymer structure translated to successful grafting. The procedure for norbornene modification was replicated from previous reactions (Section 5.2.1.3).

PG^SLP$_{1000}$ (1.0 g) was added to a round bottom flask, dichloromethane (50 mL) was added, and the vessel left to stir on a magnetic stirrer at 350 rpm for 30 min. 5-Norbornene-2-carboxylic acid (0.60 g, 4.34 mmol), DCC (2.68 g, 13.01 mmol) and DMAP (0.05 g, 0.43 mmol) were added, and the reaction left to stir for 24 h. The reaction mixture was then left in the freezer at -20°C overnight, following collection after 18 h a white precipitate had formed. Vacuum filtration of the white precipitate yielded a clear solution. Deionised water (100 mL) was added to crash further unreacted DCC and DCC urea by-products, the mixture was then vacuum filtered, and the DCM and water layers separated. Further water extraction to increase yield of collected polymer was carried out, the water layers were collected and combined and thus reduced using a rotary evaporator to yield a viscous liquid.

5.2.2.4 Modification of PG^S^LP$_{1000}$ with Norbornene Moiety, PG^S^LP$_{1000}$-Nor

Norbornene modification was carried out on the increased glycerol and sebacic acid content material to determine the effectiveness of increasing the potential number of reactive sites, and linear chain length on modification success. The procedure for norbornene modification was replicated from previous reactions (Section 5.2.1.3).

PG^S^LP_{1000} (1.0 g) was added to a round bottom flask, dichloromethane (50 mL) was added, and the vessel left stirring at 350 rpm for 30 min. 5-Norbornene-2-carboxylic acid (0.60 g, 4.34 mmol), DCC (2.68 g, 13.01 mmol) and DMAP (0.05 g, 0.43 mmol) were added, and the reaction left to magnetically stir at 350 rpm for 24 h. The reaction mixture was then left in the freezer at -20°C overnight, upon removal a white precipitate had formed. Vacuum filtration of the white precipitate yielded a clear solution. Deionised water (100 mL) was added to crash further unreacted DCC and DCC urea by-products, the mixture was then vacuum filtered, and the DCM and water layers separated. Further water extraction to increase yield of collected polymer was carried out, the water layers were collected, combined, and reduced using a rotary evaporator to yield a viscous liquid.

5.2.2.5 Acrylation of PG^SLP_{1000}, PG^SLP_{1000}A

Similar to the norbornene modification investigations, acrylation of the increased glycerol content materials to determine the effectiveness of increasing potential reactive sites was carried out. The intent was to produce a material with a high degree of acrylate functionality and therefore a high degree of photo-sensitive functionality which would translate into a material with highly tuneable mechanical properties.

PG^SLP_{1000} (2.0 g) and DMAP (0.02 g, 0.17 mmol) was added to a flame dried round bottom flask, the flask sealed and flushed with N_2. Anhydrous dichloromethane (100 mL) was added to the flask and the magnetic stirrer at 350 rpm turned on, the flask was then cooled in an ice bath to 0 °C. Once the reaction mixture was cooled to 0 °C acryloyl chloride (1.56g, 17.35 mmol) and triethylamine (1.75 g, 17.35 mmol) were added dropwise simultaneously using dropping funnels and the reaction left stirring for 24 h. The reaction mixture was then dissolved in ethyl acetate and filtered to yield an off-white powder, the powder was washed with ethyl acetate (4 x 50 mL) and dried in a vacuum oven at 40 °C.

5.2.2.6 Acrylation of PG^S^LP$_{1000}$, PG^S^LP$_{1000}$A

Acrylation of the increased glycerol and sebacic acid content material was intended to produce a highly functional photo-curing material, with the increased linear chain length allowing for the potential use as a dope carrier in implant applications.

PG^S^LP$_{1000}$ (4.0 g) and DMAP (0.04 g, 0.34 mmol) was added to a flame dried round bottom flask, the flask sealed and flushed with N_2. Anhydrous dichloromethane (100 mL) was added to the flask and the magnetic stirring at 350 rpm turned on, the flask was then cooled in an ice bath to 0 °C. Once the reaction was cooled, acryloyl chloride (2.34g, 26.02 mmol) and triethylamine (2.63 g, 26.02 mmol) were added dropwise simultaneously with dropping funnels and the reaction left stirring for 24 h. The reaction mixture was then dissolved in ethyl acetate and filtered to yield an off-white powder. The powder was washed with ethyl acetate (4 x 50 mL) and dried in a vacuum oven at 40 °C.

5.2.3 Synthesis of Increased PEG Chain Length poly(glycerol sebacate-*co*-lactic acid-*co*-polyethylene glycol$_x$) (PGSLP$_x$)

Due to the difficulty in gel formation and the intended use of the polymers in electrospinning of nanofibres, an increase in the molecular weight of the PEG component was deemed desirable. Increasing the PEG chain length will potentially improve the gelation behaviour of the polymer and increasing the molecular weight increases the chances the polymer can be successfully electro spun.

5.2.3.1 Synthesis of Increased PEG Chain Length PGSLP (PGSLP$_{100000}$)

A high chain length PEG, PEG$_{100000}$, was used to increase the chain length of the polymer material. This was intended to increase the spacing between grafting sites for photo crosslinking functionality and thus air in the production of gels.

A round bottom flask was charged with sebacic acid (11.0 g, 54.35 mmol), lactic acid (14.67 g, 163.04 mmol) and PEG (Mw 100000, 67.93 g, 0.68 mmol). The vessel was flushed with nitrogen, magnetic stirring at 350 rpm turned on and heated to 120°C.

Upon heating the mixture, the PEG_{100000} formed an extremely viscous mass in the flask, the stirring was no longer functional, and the reaction abandoned as the conditions required for reaction could not be met. Instead, a lower molecular weight PEG, PEG_{8000} was used. Differing reactions times were also used in the curing stage to determine if shorter curing times leave more reactive sites for grafting of photo curing functionality as issues had occurred when trying to form gels with other derivatives.

5.2.3.2 Synthesis of Increased PEG Chain Length PGSLP With Increased Curing Time ($PGSLP_{8000}L$)

An increased chain length PEG was intended to allow for better gelation behaviour while also enabling the production of nanofibers through an electrospinning procedure. Synthesis of the $PGSLP_{8000}L$ followed the same procedure as with all PGSLP syntheses, the only difference being the length of the curing period, this is the length of time the reaction is continued for after the introduction of glycerol into the mixture, this curing time was varied to determine the effect of internal thermo-crosslinking on the efficacy of modification. The polymer undergoes crosslinking between the linear chains in this curing period, variation of this curing period should theoretically provide a way to influence the degree to which it internally crosslinks and thus allow for control on the number of reactive sites capable of grafting functionality to. $PGSLP_{8000}L$ was left in the curing period for 8 h before the reaction stopped. This material was intended to be acrylated after synthesis and so the polymer was dissolved in DCM at the end of reaction and dried with $MgSO_4$, the solvent was then removed on a rotary evaporator. The $MgSO_4$ is used to remove the by-product

of the polycondensation so that addition of acryloyl chloride doesn't result in the formation of acrylic acid.

A round bottom flask was charged with sebacic acid (11.0 g, 54.35 mmol), lactic acid (14.67 g, 163.04 mmol) and PEG (Mw 8000, 10.87 g, 1.36 mmol). The vessel was flushed with nitrogen, 350 rpm magnetic stirring turned on and heated to 120°C, once the temperature reached 120°C vacuum (0.001 bar) was applied and stirring was continued for 4 h. Stannous octanoate, Sn(oct)2 (1.1 g, 2.72 mmol) and p-Toluenesulfonic acid monohydrate, TSA.H2O (0.52 g, 2.72 mmol) were added, vacuum (0.001 bar) was reapplied, and the temperature was increased to 180°C. The reaction was then continued for 24 h. Glycerol (5.0 g, 54.35 mmol) was then added, and the reaction continued for a further 8 h under reduced vacuum (0.0005 bar). The material produced was a clear viscous fluid. The material was dissolved in DCM, water removed with magnesium sulphate (5 g) and the solvent removed on a rotary evaporator. The material was collected as a viscous brown fluid, that was left for 24 h in vacuum oven at 40 °C.

5.2.3.3 Synthesis of Increased PEG Chain Length PGSLP with Shorter Curing Time ($PGSLP_{8000}S$)

Increasing the chain length of the polymer material while also decreasing curing time was intended to increase the spacing between the reactive sites where photo crosslinking functional groups would be grafted, while also providing a greater degree of photo crosslinking potential due to a higher content of functionality. This would allow for a material with increased chain length and increased crosslink density, which would potentially allow for production of a gel with improved elastic modulus.

A round bottom flask was charged with sebacic acid (11.0 g, 54.35 mmol), lactic acid (14.67 g, 163.04 mmol) and PEG (Mw 8000, 10.87 g, 1.36 mmol). The vessel was flushed with nitrogen, 350 rpm

magnetic stirring turned on and heated to 120°C, once the temperature reached 120°C vacuum (0.001 bar) was applied and stirring was continued for 4 h. Stannous octanoate, Sn(oct)2 (1.1 g, 2.72 mmol) and p-Toluenesulfonic acid monohydrate, TSA.H2O (0.52 g, 2.72 mmol) were added, vacuum (0.001 bar) was reapplied, and the temperature was increased to 180°C. The reaction was then continued for 24 h. Glycerol (5.0 g, 54.35 mmol) was then added, and the reaction continued for a further 2 h under reduced vacuum (0.0005 bar). The material produced was a viscous fluid. The material was dissolved in DCM, water removed with magnesium sulphate (5 g) and the solvent removed on a rotary evaporator. T The material was collected as a viscous brown fluid, that was left for 24 h in vacuum oven at 40 °C.

5.2.3.4 Acrylation of Increased PEG Chain Length $PGSLP_{8000}L$, $PGSLP_{8000}AL$

Acrylation introduces photo crosslinking functionality, combined with the increased chain length would allow for stable gel formation by exposing the material to UV radiation in a suitable solvent system.

$PGSLP_{8000}L$ (35.0 g) and DMAP (1.66 g, 13.59 mmol) was added to a flame dried round bottom flask, the flask sealed and flushed with N_2. Anhydrous dichloromethane (150 mL) was added to the flask and the magnetic stirrer turned on at 350 rpm, the flask was then cooled in an ice bath to 0 °C. Acryloyl chloride (24.46g, 271.74 mmol) and triethylamine (27.45 g, 271.74 mmol) were added dropwise simultaneously using dropping funnels and the reaction left stirring for 24 h.

The reaction mixture was poured in ethyl acetate to facilitate the crashing out of the polymer however no precipitate formation occurred. The mixture was placed on a rotary evaporator to remove all the solvent, the polymer mass formed after solvent removal was then dissolved in dichloromethane and poured into n-pentane, resulting in a mass of polymer settling in the bottom of the flask. The solvent mixture was decanted off, the polymer dissolved in dichloromethane and

placed on a rotary evaporator. Upon drying the material appeared to have solid particulates embedded within the structure, the mixture was dissolved in deionised H_2O and dialysed over a period of 3 days with regular water changes. The polymer solution was then dried on a rotary evaporator yielding a viscous brown fluid.

5.2.3.5 Acrylation of Increased PEG Chain Length $PGSLP_{8000}AS$

Acrylation of the increased chain length polymer with decreased curing time would introduce a higher photo crosslinking functional group content. This would potentially produce a material with increased crosslink density when compared to the one produced in Section 5.2.3.4, which would increase the elastic modulus of the cured material.

$PGSLP_{8000}S$ (35.0 g) and DMAP (1.66 g, 13.59 mmol) was added to a flame dried round bottom flask, the flask sealed and flushed with N_2. Anhydrous dichloromethane (150 mL) was added to the flask and the magnetic stirring turned on at 350 rpm, the flask was then cooled in an ice bath to °C. Acryloyl chloride (24.46g, 271.74 mmol) and triethylamine (27.45 g, 271.74 mmol) were added dropwise simultaneously using dropping funnels and the reaction left stirring for 24 h.

The reaction mixture was poured in ethyl acetate to facilitate the crashing out of the polymer however again no precipitate formation occurred. The mixture was placed on a rotary evaporator to remove all the solvent, the polymer mass then dissolved in dichloromethane and poured into n-pentane, resulting in a mass of polymer settling in the bottom of the flask. The solvent mixture was decanted off, the polymer dissolved in dichloromethane and placed on a rotary evaporator. Solid particulates were again present in the mixture, the mixture was dissolved in deionised H_2O and dialysed over a period of 3 days with regular water changes. The polymer solution was then dried on a rotary evaporator yielding a viscous brown fluid.

5.3 Results and Discussion

5.3.1 Synthesis of Poly(glycerol sebacate-*co*-lactic acid-*co*-polyethylene glycol$_{1000}$) (PGSLP$_{1000}$)

As with PGS, synthesis of PGSLP (Figure 5.1) involves a polycondensation reaction, however catalysts are required to ensure the reaction rate is acceptable for production of suitable masses of polymer. In these experiments, Stannous octanoate and p-Toluenesulfonic acid monohydrate were added to reduce the reaction time. The product obtained was a viscous, clear, or milky white fluid similar to that of OGS; this indicates that curing had not taken place, which is optimal as little to no thermo-curing is highly advantageous when grafting of functional moieties is intended. The yield theoretically should be 100 %, however due to the viscous nature of the material removal from the reaction vessel decreases this yield.

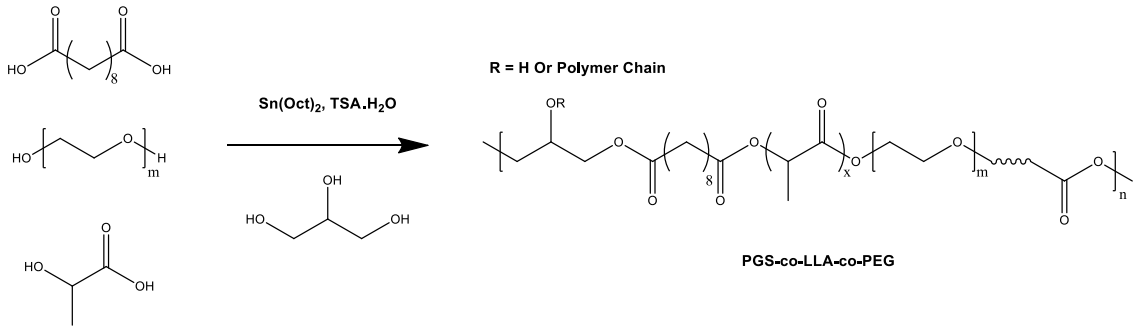

Figure 5.1 Synthesis of PGSLP.

^{1}H NMR analysis (Figure 5.2, Table 5.1) confirmed the target polymer structure had been achieved with reference to the literature[185] and to predicted ^{1}H NMR spectra for the structure. The inclusion of catalysts in the reaction procedure does mean that some peaks are masked slightly, but positive interpretation of the structure was still possible.

Table 5.1 ^{1}H NMR data of PGSLP$_{1000}$.

^{1}H NMR (400 MHz)			
δ (ppm)	**Multiplet**	**J Frequency (Hz)**	**Protons**
5.48-4.93	m	-	3
4.46-4.15	m	-	5
3.68	d	20.6	11
2.42-2.26	m	-	1
1.73-1.38	m	-	13
1.31	s	-	3

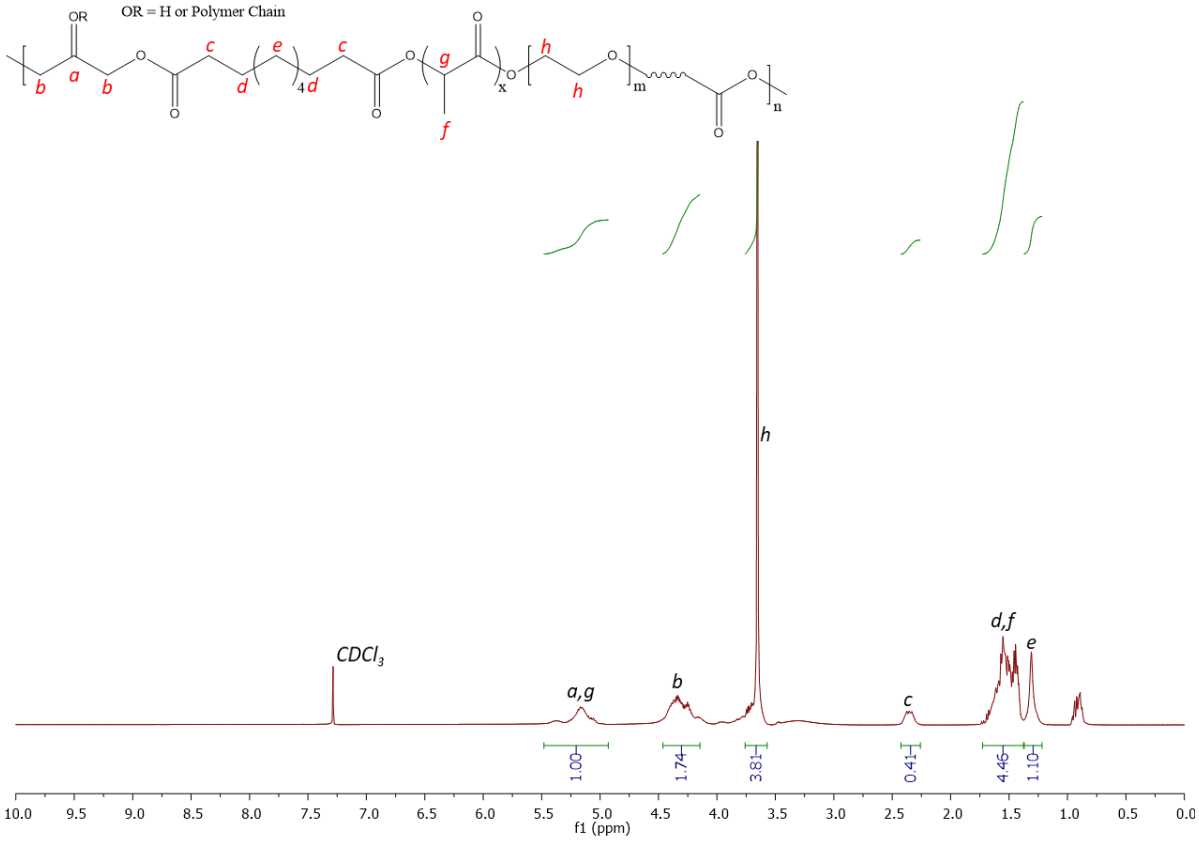

Figure 5.2 ^{1}H NMR spectrum ($CDCL_3$) of $PGSLP_{1000}$.

A yield of 70 % was obtained, which is similar to that previous PGS syntheses (Section 4.3.2.1). A yield of near 100 % was likely obtained however due to the viscous nature of the polymer removal from the reaction vessel is difficult.

5.3.2 Modification of $PGSLP_{1000}$ with Norbornene Moiety, $PGSLP_{1000}$-Nor 1

The same protocol that was used to modify OGS and PGS previously (Sections 4.3.2.5 and 4.3.2.6) was applied to modification of PGSLP (Figure 5.3).

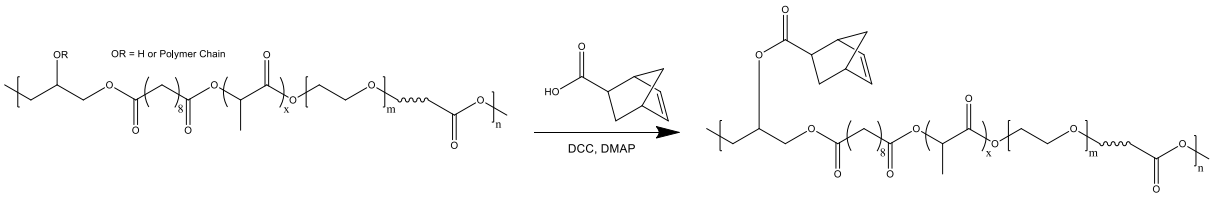

Figure 5.3 Modification of PGSLP with 5-Norbornene-2-carboxylic acid.

Upon reaction completion the resulting material was a brown viscous fluid, ^{1}H NMR analysis (Figure 5.4) of the material showed the presence of the peaks at 6.10 and 5.90 ppm associated with the alkene bond of the norbornene moiety however contamination of DCC and associated by-products is evident by the messy nature of the spectrum and lack of resolution in peaks.

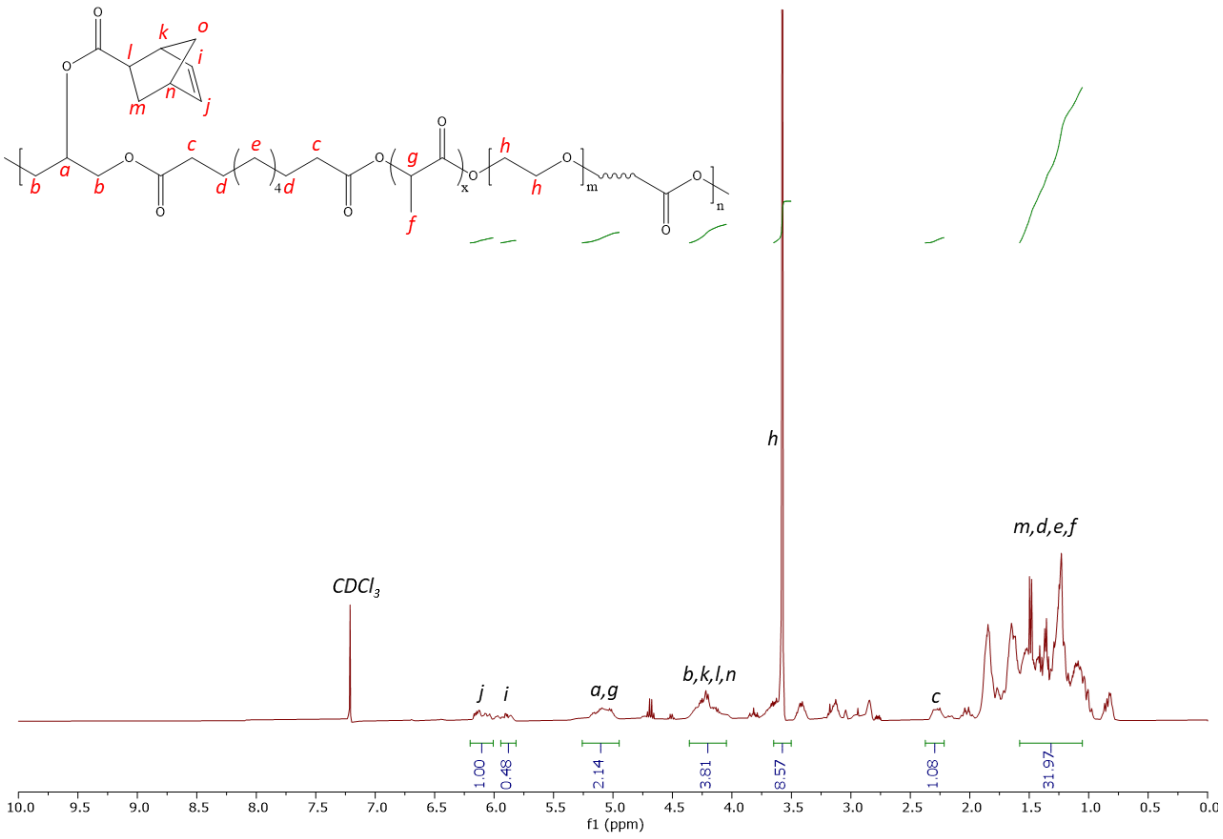

Figure 5.4 ^{1}H NMR spectrum ($CDCL_3$) of $PGSLP_{1000}$-Nor 1.

The yield of 67 % also indicates that a lot of polymer was lost during filtration, this could be due to the presence of DCC in solution causing the polymer to crash out due to interactions between these species.

5.3.3 Modification of $PGSLP_{1000}$ with Norbornene Moiety, $PGSLP_{1000}$-Nor 2

Modification of $PGSLP_{1000}$ was attempted again this time with an extended chilling period in a freezer at -20°C; this was to encourage as much DCC and associated by-products to crash out of solution; allowing them to be removed by filtration. The product was again collected as a brown viscous fluid.

^{1}H NMR analysis (Figure 5.5) showed a marked decrease in DCC and by-product contamination and the peaks at 6.10 and 5.90 ppm associated with the alkene bond of the norbornene moiety are

present, thus confirming that the extended chilling period is an efficient way to remove DCC and associated by-products. However, as can be seen from the ^{1}H NMR spectrum, there is still large-scale contamination as can be seen by the large grouping of peaks from 2.00 – 1.00 ppm.

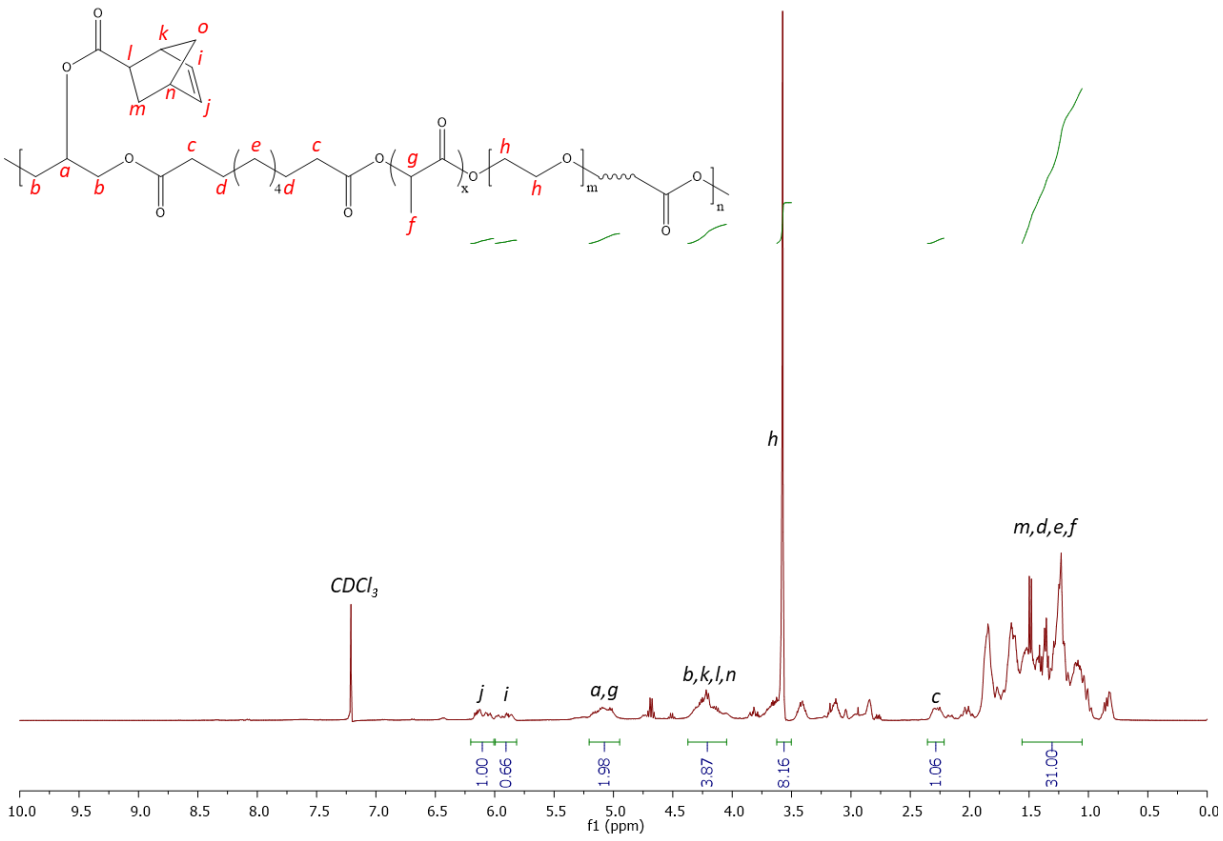

Figure 5.5 ^{1}H NMR spectrum ($CDCL_3$) of PGSLP1000-Nor 2.

A yield of 57% was achieved which suggests, along with the ^{1}H NMR analysis, that the true yield of modified polymer was much higher than the previous experiment (Section 5.3.2). Furthermore, due to the molecular weight of the polymer the use of dialysis to remove by-products is an option if purification is required; however, due to the nature of these being investigatory experiments to determine crosslinking behaviour, this was not deemed necessary.

5.3.4 Acrylation of $PGSLP_{1000}$, $PGSLP_{1000}A$

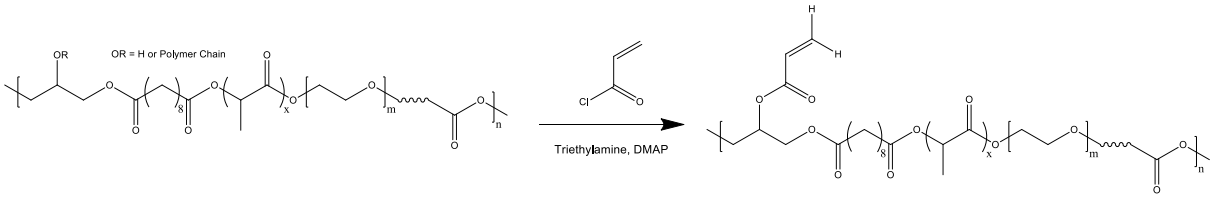

Figure 5.6 Acrylation of PGSLP.

The acrylation of $PGSLP_{1000}$ (Figure 5.6) to introduce photo crosslinking functionality used the same protocol as for the acrylation of OGS. Upon addition of the acryloyl chloride the solution gained a mild yellow hue, with small volumes of vapour formation. After the reaction had been left for 24 h the reaction mixture was poured into ethyl acetate forming a white precipitate. The precipitate was filtered, collected, and dried to yield an off-white powder.

From the ^{1}H NMR analysis (Figure 5.7) the peaks associated with the alkene groups are present at 6.40, 6.10 and 5.85 ppm, confirming that the acylation was successful.

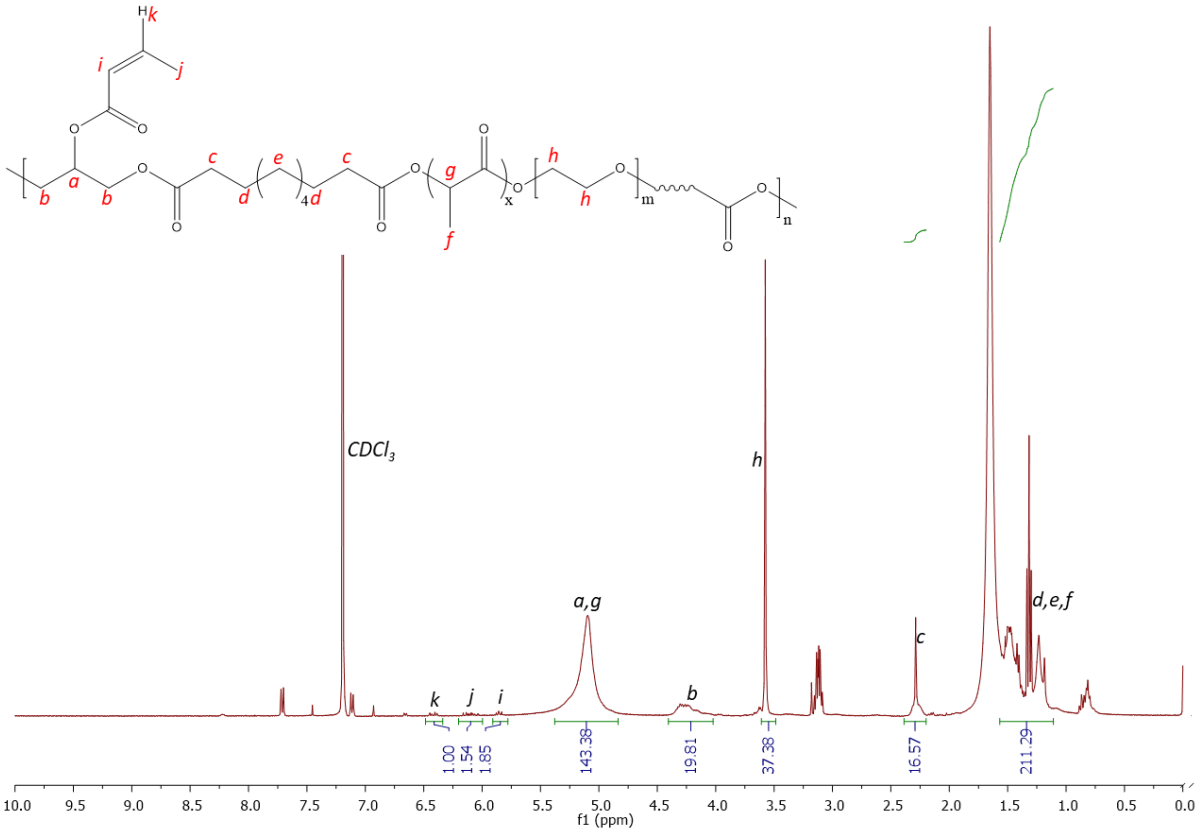

Figure 5.7 ^{1}H NMR spectrum ($CDCL_3$) of $PGSLP_{1000}A$.

The yield obtained of 88% was much higher than anticipated, it was expected that material loss due to solubility issues would decrease the overall yield.

5.3.5 Synthesis and Modification of Increased Glycerol and Sebacic Acid Content, PG^S^LP$_{1000}$

The introduction of a reducing agent to combat disulphide bond formation and the large increase to crosslinker presence did not result in successful crosslinking, the decision was made to increase the glycerol content of the synthesised polymer and therefore introduce more reactive sites capable of modification and introduction of functionality. Additional polymers were also synthesised with increased glycerol and sebacic acid content.

5.3.5.1 Synthesis of Increased Glycerol Content PGSLP, PG^SLP$_{1000}$

An increased glycerol content PGSLP was synthesised with the same reaction procedure used previously (Section 5.2.1.1), a 10-fold increase in glycerol content by moles was the only modification to the reaction.

^{1}H NMR analysis (Figure 5.8) confirmed that the reaction was successful, and the target material synthesised. The material was slightly less viscous that its reduced glycerol content derivative, but this was to be expected due to the increased glycerol content.

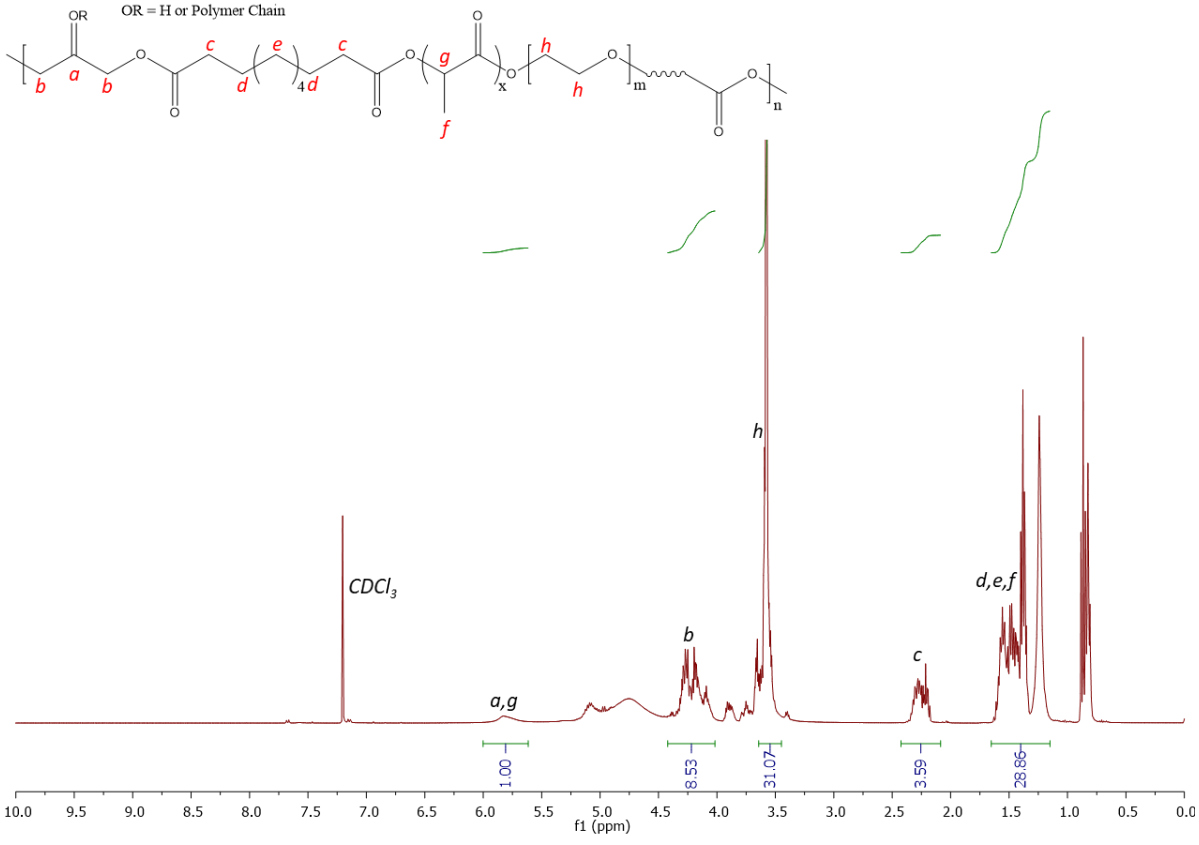

Figure 5.8 ^{1}H NMR spectrum ($CDCL_3$) of PG^SLP$_{1000}$.

The material was noticeably easier to remove from the reaction vessel and a yield of 90 % was obtained, significantly higher than the yield for the initial PGSLP synthesised.

5.3.5.2 Synthesis of Increased Glycerol and Sebacic Acid Content PGSLP, PG^S^LP$_{1000}$

A secondary batch of polymer was also synthesised with an increased glycerol and sebacic acid content, this was intended to increase chain length and provide a larger amount of potential modification sites.

^{1}H NMR analysis (Figure 5.9) confirmed that the reaction was successful, and the target material synthesised. The material was more viscous than previous iterations of the polymer, with the sample having to be heated thoroughly for removal from the reaction vessel.

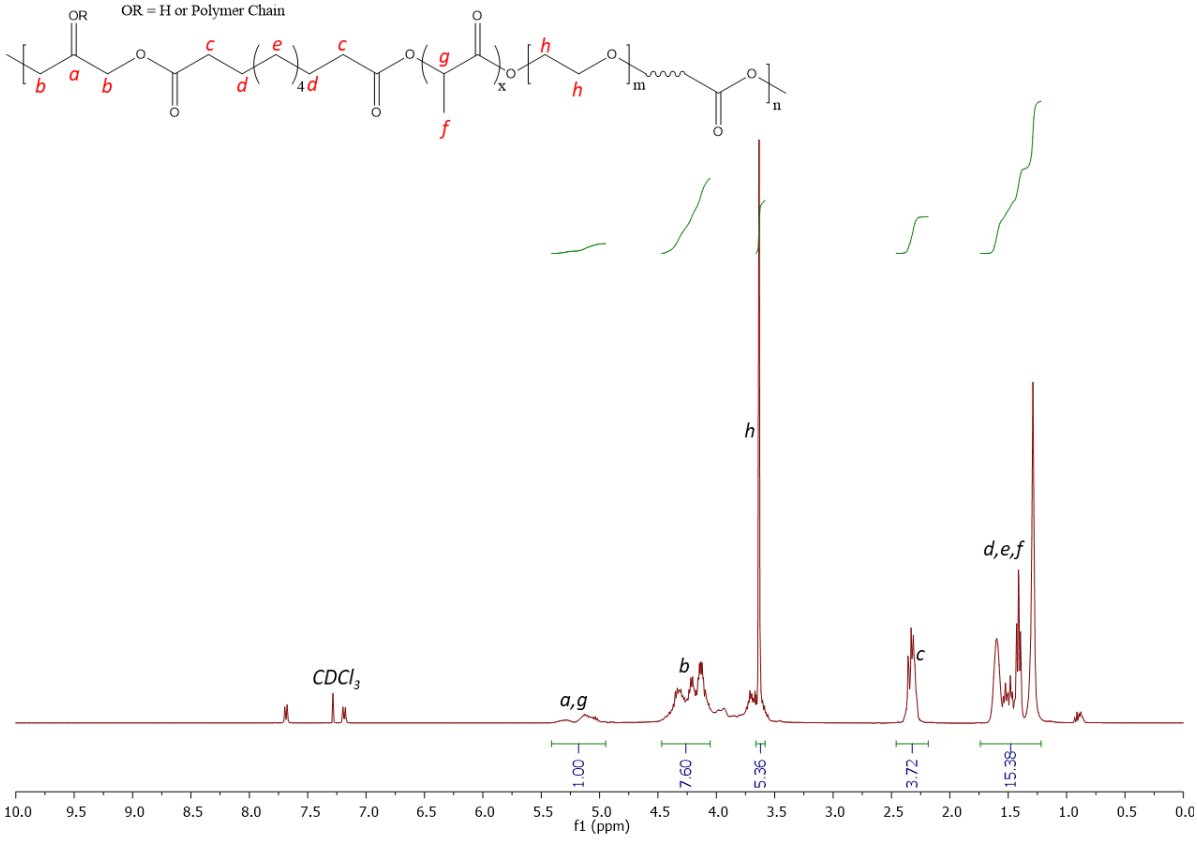

Figure 5.9 ^{1}H NMR spectrum ($CDCL_3$) of PG^S^LP$_{1000}$.

The yield obtained of 63 % is testament to the viscosity of the material, as removing it from the reaction vessel required the flask to be left with the material dripping into a suitable container over a period of h, with heating regularly being applied.

5.3.5.3 Modification of PG^SLP$_{1000}$ with Norbornene Moiety, PG^SLP$_{1000}$-Nor

The modification of the increased glycerol PGSLP followed the same procedure as the modification of PGSLP$_{1000}$-Nor 2, this includes the extended chilling period to aid in DCC by-product removal.

^{1}H NMR analysis (Figure 5.10) showed the presence of peaks at 6.10 and 5.90 ppm associated with the alkene bond of the norbornene moiety, as can be seen from the ^{1}H NMR spectrum there is still large-scale contamination by DCC, and its associated by-products as can be seen by the peaks present throughout the spectrum. As has been stated earlier, dialysis could be used for purification of the polymer when biological testing is required.

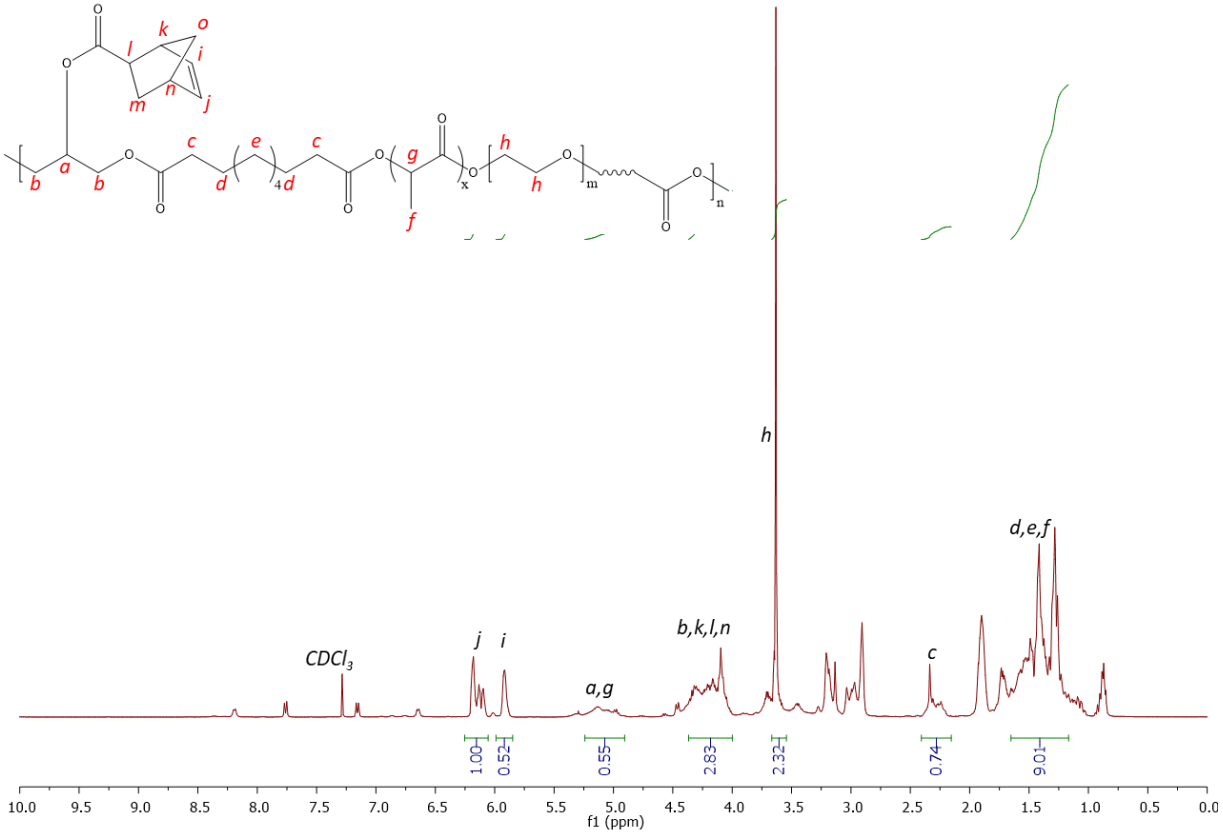

Figure 5.10 ^{1}H NMR spectrum ($CDCL_3$) of PG^SLP$_{1000}$-Nor.

A yield of 49 % was obtained, this lower yield than expected could be due to the changes to the polymeric structure, the inclusion of increased glycerol content may have changed the solubility of the material making it more difficult to isolate in filtration steps.

5.3.5.4 Modification of PG^S^LP$_{1000}$ with Norbornene Moiety, PG^S^LP$_{1000}$-Nor

Modification of the increased glycerol and sebacic acid content PGSLP proceeded *via* the procedure used previously for the increased glycerol content derivative (Section 5.3.5.1).

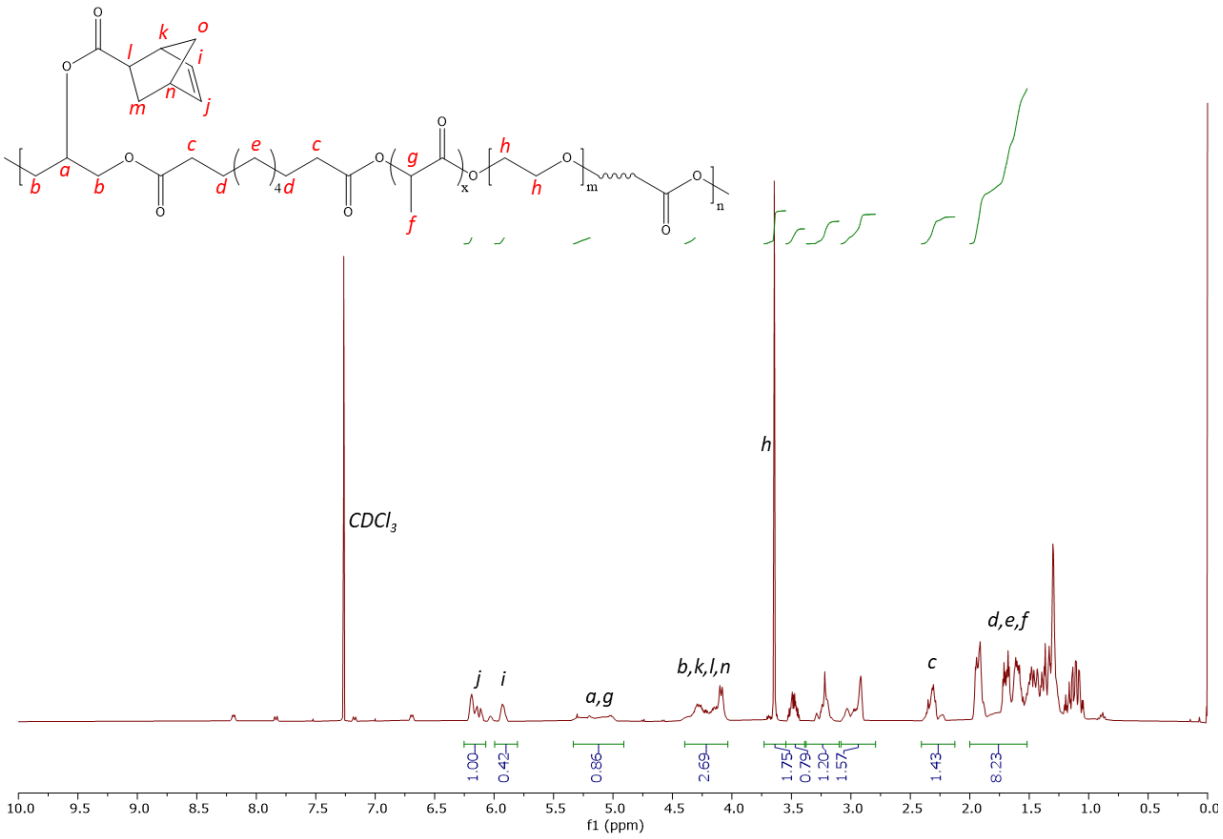

Figure 5.11 ^{1}H NMR spectrum ($CDCL_3$) of PG^S^LP$_{1000}$-Nor.

A yield of 48 % was obtained, this was again lower than anticipated but could be due to the changes to the polymeric structure by the inclusion of increased glycerol and sebacic acid content causing a solubility change resulting in isolation during filtration being poor.

5.3.5.5 Acrylation of PG^SLP$_{1000}$, PG^SLP$_{1000}$A

The procedure for acrylation of increased glycerol content PGSLP is identical to that of PGSLP but with an increased amount of acryloyl chloride and triethylamine, to account for the increased reactive sites in the polymer structure. Upon addition of the acryloyl chloride a slight yellow was observed in the solution with small volumes of vapour being released. After the reaction had been left for 24 h the solution had turned an opaquer yellow. Precipitation in ethyl acetate followed by filtration and drying yielded an off-white powder.

From the ^{1}H NMR analysis (Figure 5.12), the peaks associated with the alkene groups are present at 6.40, 6.10 and 5.85 ppm, confirming that the acrylation was successful.

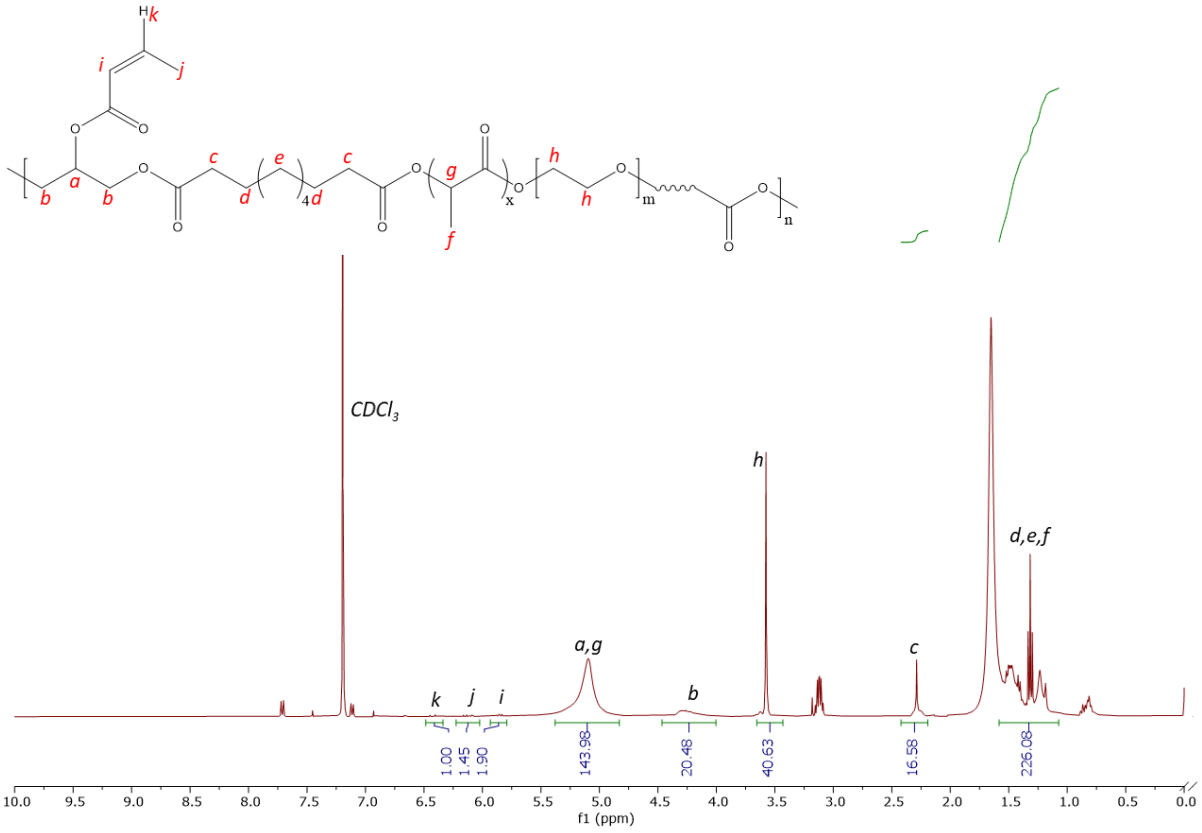

Figure 5.12 ^{1}H NMR spectrum ($CDCL_3$) of PG^SLP$_{1000}$A.

A yield of 66 % was obtained, which is lower than previous PGSLP derivative reactions however this could be due to the change in molecular structure due to the increased glycerol content causing a change in solubility behaviour.

5.3.5.6 Acrylation of PG^S^LP$_{1000}$, PG^S^LP$_{1000}$A

The same procedure of acrylation was used as for the increased glycerol content PGSLP.

Upon addition of the acryloyl chloride a slight yellow was observed in the solution with small volumes of vapour being released. After the reaction had been left for 24 h the solution had turned an opaquer yellow. Precipitation in ethyl acetate followed by filtration and drying yielded an off-white powder.

From the ^{1}H NMR analysis (Figure 5.13) the peaks associated with the alkene groups are present at 6.40, 6.10 and 5.85 ppm, confirming that the acylation was successful.

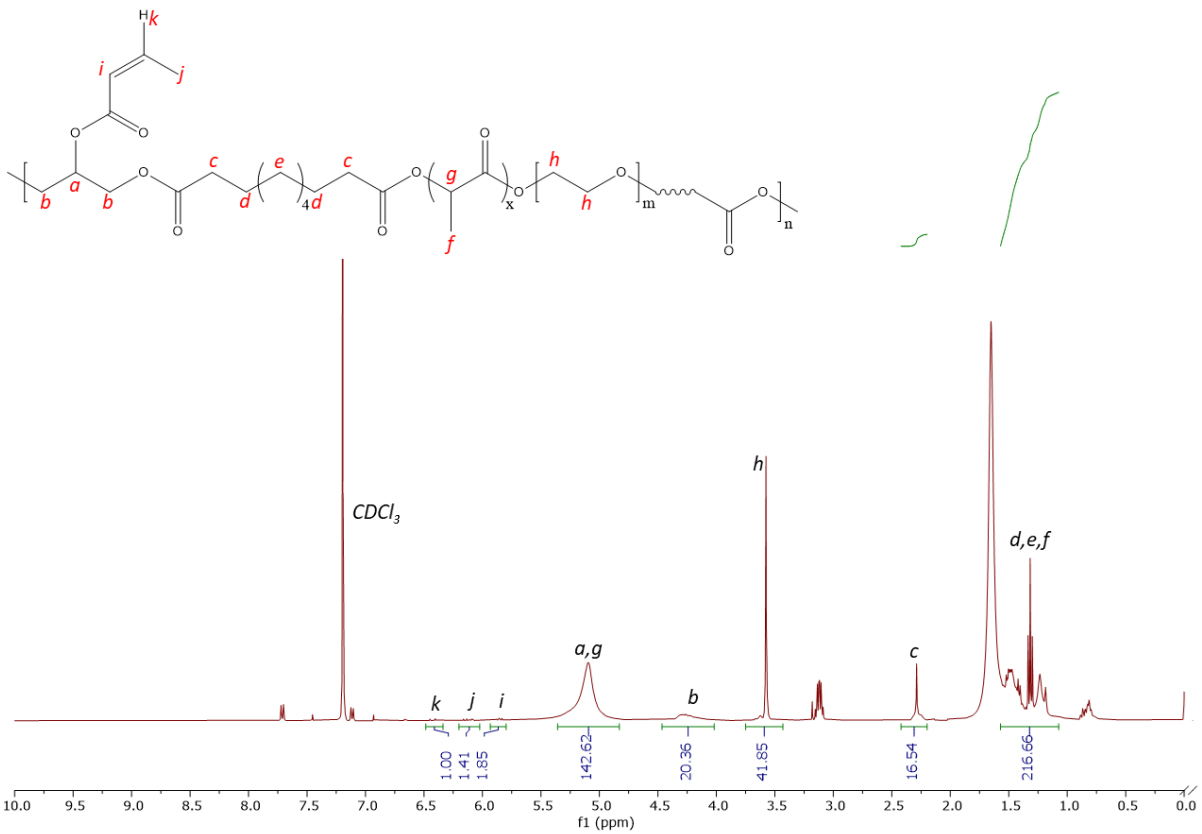

Figure 5.13 ^{1}H NMR spectrum ($CDCL_3$) of PG^S^LP_{1000}A.

A yield of 87 % was obtained which is much higher when compared to that of the increased glycerol content derivative, this difference could imply the ratio between glycerol and sebacic acid components within the material can regulate the solubility behaviour and thus allow for a degree of control over post synthesis modification reaction yields.

5.3.6 Synthesis of Increased PEG Chain Length poly(glycerol sebacate-*co*-lactic acid-*co*-polyethylene glycol$_x$) (PGSLP$_x$)

As the intention was to form the materials into a fibre reinforcement phase used in the composite, the integration of a high molecular weight PEG molecule into the polymeric structure was attractive for methods that involve the spinning of fibres, aiming to generate fibre-forming molecular entanglements between polymer chains. The inclusion of a higher molecular weight PEG was also attractive in gel formation, as an increase in chain length should facilitate the synthesis of covalent bonds and the formation of gels with larger spaces capable of being occupied by fibre reinforcement phases.

5.3.6.1 Synthesis of Increased PEG Chain Length PGSLP (PGSLP$_{100000}$)

A 100,000 Mw PEG was attempted to be integrated into the polymeric structure however, upon application of heat and stirring for the initial mixing step of the polycondensation it was observed that the PEG had melted into an extremely viscous mass in the reaction vessel. The stirring was no longer functional and thus the reaction was abandoned. Without stirring the reaction could not mix properly, meaning that polycondensation would occur between the physical boundaries of the different reagents and that synthesis of a homogenous polymer would be impossible. A PEG molecular of molecular weight 8000 was selected, as it matched the molecular weight of the PEG diacrylate (PEGDA) used in photo crosslinking experiments and would melt appropriately allowing for suitable reaction conditions.

5.3.6.2 Synthesis of Increased PEG Chain Length PGSLP with Increased Curing Time ($PGSLP_{8000}L$)

^1H NMR analysis (Figure 5.14) showed the correct material had been synthesised by comparison of the ^1H NMR structure to literature and predicted ^1H NMR spectrums. Solubility testing with water showed the material to dissolve meaning the material had retained its hydrophilic properties. The inclusion of catalysts in the reaction procedure does mean that some peaks are perhaps masked slightly but the ability to interpret the structure is still present.

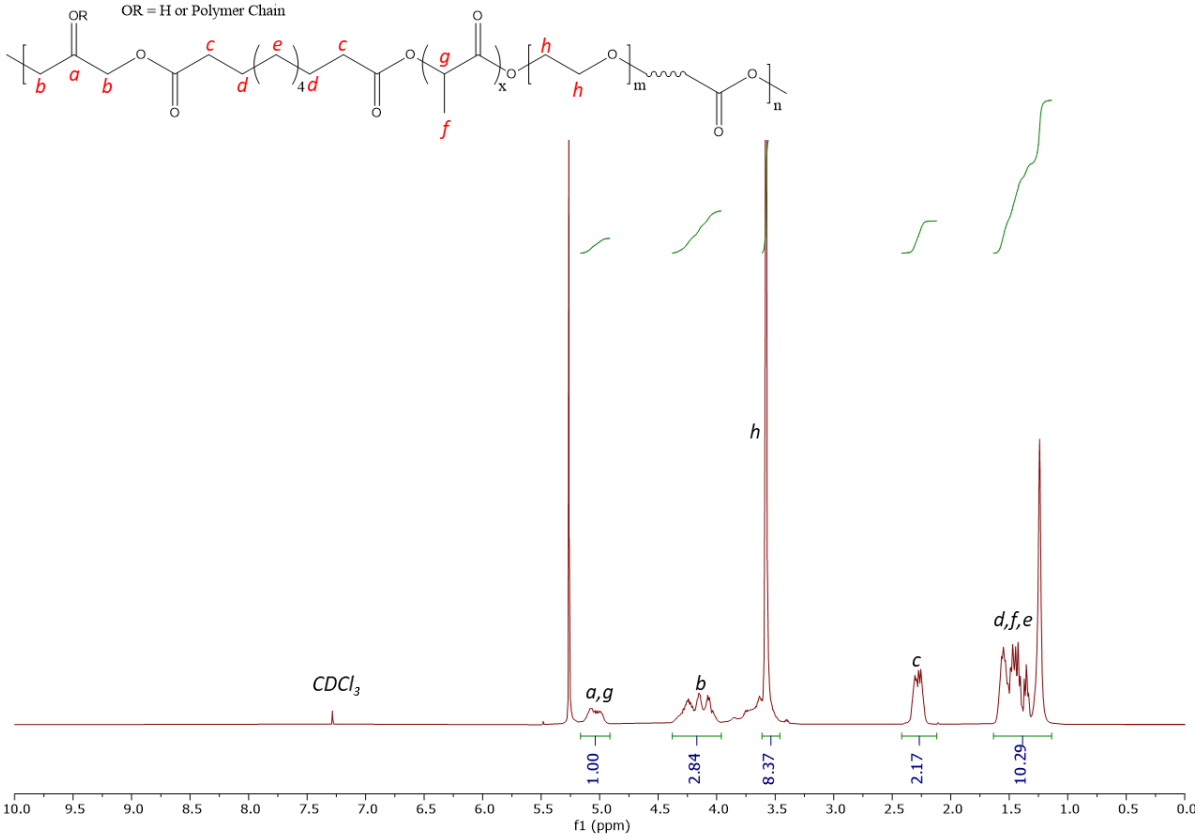

Figure 5.14 ^1H NMR spectrum ($CDCL_3$) of $PGSLP_{8000}L$.

A yield of 90 % was obtained with the material being a viscous fluid, a near 100% yield was obtained however due to the viscous nature of the product complete removal from the reaction flask was deemed unnecessary.

5.3.6.3 Synthesis of Increased PEG Chain Length PGSLP with Shorter Curing Time ($PGSLP_{8000}S$)

Synthesis of $PGSLP_{8000}S$ was the same as $PGSLP_{8000}L$; however, the curing period was 2 h. This polymer was also to be acrylated and so the $MgSO_4$ drying step was employed.

^1H NMR analysis (Figure 5.15) by comparison of structures to predicted and literature values showed the correct material had again been synthesised successfully. The material dissolved in water and so was hydrophilic

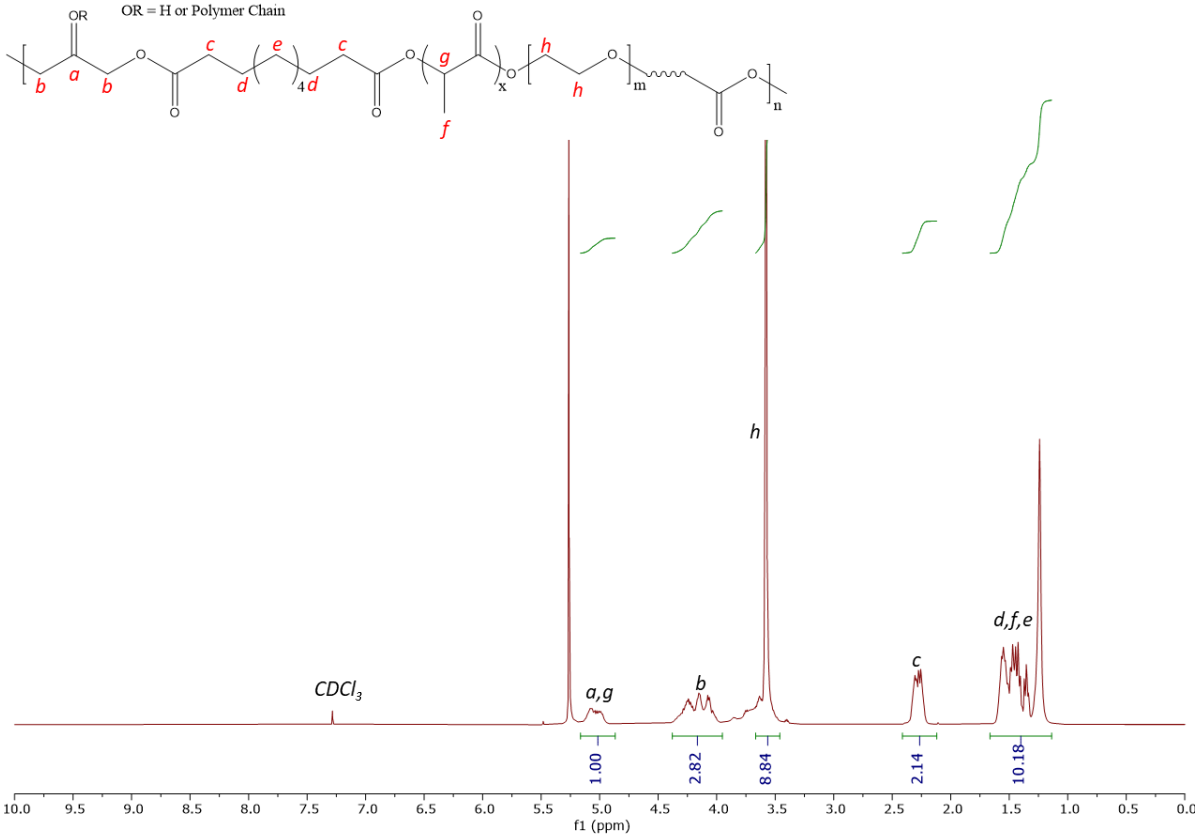

Figure 5.15 ^1H NMR spectrum ($CDCL_3$) of $PGSLP_{8000}S$.

A yield of 89 % was obtained with the material being a viscous fluid, again an estimated 100 % yield was obtained however material is left in the reaction vessel due to difficulty of removal.

5.3.6.4 Acrylation of Increased PEG Chain Length $PGSLP_{8000}L$, $PGSLP_{8000}AL$

Acrylation of $PGSLP_{8000}L$ followed previous procedures (5.3.4). Upon pouring the polymer into ethyl acetate no precipitation occurred, this could be due to the increased PEG chain length. The mixture was placed on a rotary evaporator and the solvent removed. The material was dissolved again in DCM and poured into n-pentane to facilitate precipitation however instead of a powder precipitate forming a mass of polymer was present at the bottom of the flask. The increased PEG chain length could have caused a solubility change in the polymer, which decreased the clear precipitation and prevented the product being collected as a powder. The remaining solvent was decanted off and the polymer dried however the polymer appeared to have solid particulate crystals embedded within the mass. The mass was then dissolved in deionised H_2O and dialysed in batches over a period of 3 days with frequent changing of the deionised water. The dialysed polymer batches were combined and dried on a rotary evaporator yielding a thick brown viscous fluid.

^1H NMR analysis (Figure 5.16) confirmed that successful grafting of alkene functionality onto the structure by the presence of peaks at 6.36, 6.06 and 5.82 ppm.

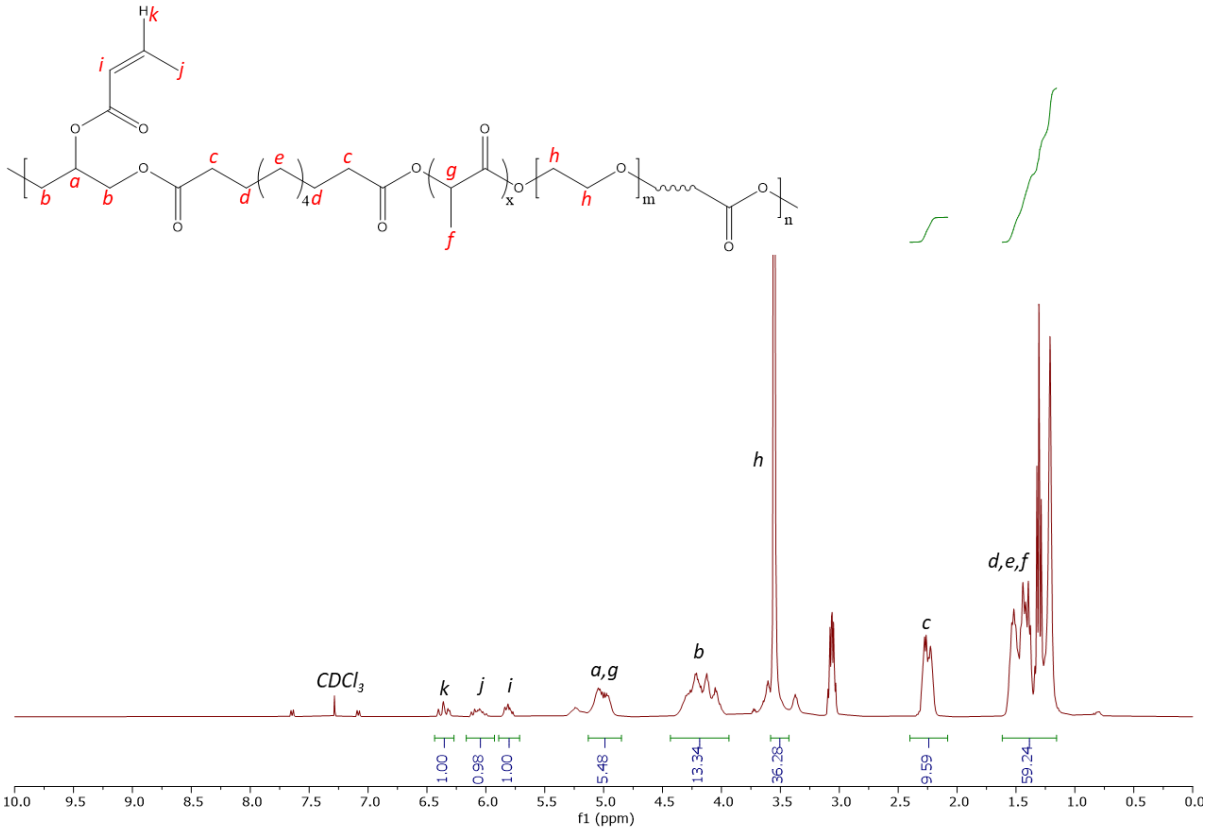

Figure 5.16 ^{1}H NMR spectrum ($CDCL_3$) of $PGSLP_{8000}AL$.

A yield of 52% was obtained which is lower than previous acrylation reactions (Section 5.3.4); this could be due to the product being in a different form to previously carried out acrylations likely due to the change in PEG chain length. The viscous product will have a decreased yield due to material retention in the reaction vessel.

5.3.6.5 Acrylation of Increased PEG Chain Length $PGSLP_{8000}S$, $PGSLP_{8000}AS$

Acrylation of $PGSLP_{8000}S$ followed previous procedures (Section 5.2.1.4). Like $PGSLP_{8000}AL$ pouring the polymer into ethyl acetate yielded no precipitate. The mixture was placed on a rotary evaporator and the solvent removed. Purification of the material using previously stated procedures again yielded a thick brown viscous fluid.

^{1}H NMR analysis (Figure 5.17) confirmed that successful grafting of alkene functionality onto the structure by the presence of peaks at 6.36, 6.06 and 5.82 ppm.

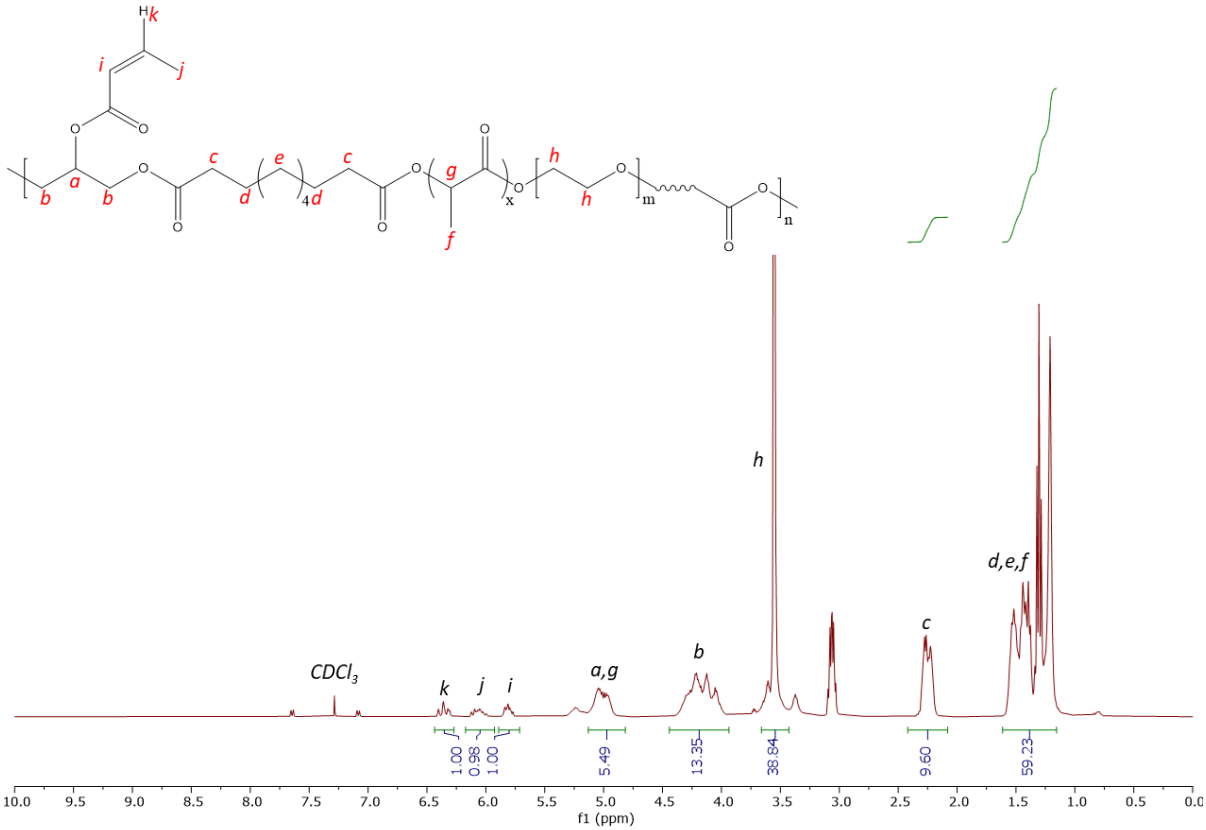

Figure 5.17 ^{1}H NMR spectrum ($CDCL_3$) of $PGSLP_{8000}AS$.

A yield of 53% was obtained which is similar to the yield obtained when acrylating $PGSLP_{8000}L$, which implies that the increased chain length and thus altered form for the polymer decreases yield. The viscous product will have a decreased yield due to material retention in the reaction vessel.

5.4 Summary

The experimental results obtained from the synthesis and modification reactions revealed that grafting of norbornene moieties, such as 5-Norbornene-2-carboxylic acid, to varying chain lengths of PGSLP is possible by utilisation of coupling agents such as DCC. Using methods of grafting such as

steglich esterification is highly desirable as it avoids the use of acid chloride moieties, which in this case would risk introducing highly toxic compounds such as oxalyl chloride (used to form the acid chloride) into the polymer during modification. Although there were some issues with removing the DCC urea formed, the synthetic route was shown to be a viable option for modification of PGS and building upon this synthetic route to include other moieties and functional molecules is a viable option. Improvements to the method could involve purification by dialysis. Introduction of norbornene functionality potentially allows for the exploitation of thiol-ene click chemistry, crosslinking *via* thiol-ene click chemistry with a di-thiol crosslinker was investigated and no successful gelation took place. Other thiol-ene click functional molecules could be investigated as it could be the norbornene functional group currently grafted to the polymeric structure that is not a viable option for photo crosslinking.

The acrylation of PGSLP has also been shown to be a suitable method for introducing alkene functionality and therefore photo curing capability, which circumvents the need for high temperatures and extended time periods required for curing of the PGSLP base material.

The synthesis of PGSLP is simple, cheap, and safe. The solvent free conditions and absence of harmful chemicals means that scale up to produce large bulk quantities of the polymer should not be an issue. As the polymerisation reaction only involves the polymer constituents with water as a by-product, one pot synthesis for further modification is another additional benefit. The polycondensation reaction can be altered in effective run time, specifically in the curing period for the synthesis of PGSLP; this allows some control over the degree of internal crosslinking within the polymer produced and the degree to which the material can be modified by grafting functionality to the exposed reactive sites.

The mechanical properties of PGSLP could be altered simply by changing the time of curing during polycondensation, whereby increasing this curing time significantly increases the rigidity of the material. Further modification of mechanical properties can be achieved by grafting functional molecules such as acrylate or norbornene moieties, introducing the capability of photocuring chemistry further increases the degree to which tuning of the mechanical properties is possible. The grafting rate, crosslinker structure and fibre reinforcement phase also allow further fine tuning.

The aim of producing a water-soluble elastomer capable of photocuring was achieved by the increase in PEG chain length and grafting of photocuring functionality. $PGSLP_{8000}AS$ and $PGSLP_{8000}AL$ were both synthesised successfully, ^{1}H NMR analysis showed the peaks relating to acrylate groups are present and therefore photocuring functionality has successfully been introduced to the water-soluble elastomer. Homogenous aqueous solutions can be achieved using elevated temperature incubation procedures, following this incubation period, the polymers remain in solution when cooled which allows for crosslinking reactions to take place at room temperature.

Chapter 6

Electrospinning of PGS and PGSLP Nanofibres

6.1 Introduction

Conceivably, the mixing of nanofibers with hydrogel could provide the basis for improved structural support through enhancement of compressive strength, with the potential for materials to be photo-crosslinked *in-situ*. Therefore, with a view to combining PGS-based hydrogels with nanofibers, the feasibility of electrospinning PGSLP was explored for the first time. Electrospinning is a well-known technique for the production of fibres with sub-micron scale dimensions. It was also reasoned that the inclusion of photocuring functionality in the PGSA and PGSLP materials could also present opportunities to modulate bulk properties by inducing crosslinking functionality between the fibres and the hydrogel.

6.2 Experimental

The electrospinning of PGSLP and PGSLPA have not been previously investigated as a way of producing a nonwoven web. PGSA has previously been spun using PEG, gelatin and PCL as a carrier polymer.[186] For this reason, appropriate solvent solutions and spinning conditions needed to be developed for successful electrospinning of PGSLP and PGSLP derivatives.

6.2.1 Electrospinning of PGS Based Materials and PCL_{80000}

Preliminary experiments revealed that electrospinning of 100% PGSA or PGSLP was not feasible, and therefore each was commixed with polycaprolactone (PCL), which is a known fibre-forming, biocompatible, and bioresorbable material.

6.2.1.1 Electrospinning of $PGSLP_{1000}$ and PCL_{80000}

Given the lack of previous studies on the electrospinning of PGSLP, appropriate conditions to support effective electrospinning needed to be established. A solution of 5 wt % $PGSLP_{1000}$ and 5 wt % polycaprolactone$_{80000}$ (PCL_{80000}) was prepared in 1,1,1,3,3,3-Hexafluoro-2-propanol (HFIP), and the solution was then transferred to a glass syringe and placed inside the electrospinning apparatus. The experiment was conducted with a 18G needle. The needle tip to collector distance was set at 20 cm (which is within the range normally used to spin other polymers), and spinning was attempted at 20 kV, with a flow rate of the syringe pump adjusted to 1 mL h^{-1}. The polymer solution did not form a jet under these conditions and no fibre collection was observed on the charged plate.

The procedure was repeated with the distance being progressively changed from 10 – 25 cm, and voltage varied between 10 – 25 kV, but again no jet could be formed consistent with fibre collection.

6.2.1.2 Electrospinning of $PGSLP_{8000}$ and PCL_{80000}

A further set of experiments were conducted using PGSLP with a higher molecular weight.

A solution of 5 wt % $PGSLP_{8000}$ and 5 wt % PCL_{80000} was formulated in HFIP, the solution transferred to a glass syringe and placed inside the electrospinning apparatus. A charged plate with distance to an 18G needle tip of 20 cm was secured in place, the needle tip was then charged with 20 kV and the flow rate of the syringe pump adjusted to 1 mL h^{-1}. The syringe pump was activated and jets of $PGSLP_{8000}$-PCL_{80000} were directed towards the charged collection plate. A nonwoven web formed on the collection plate readily. The procedure was repeated with a needle tip to collector distance of 15 cm and web formation was again observed. Reducing the voltage to 15 kV also resulted in uniform web formation.

6.2.1.3 Electrospinning of $PGSLP_{8000}$

In attempt to produce 100 % PGSLP fibres, a solution of 10 wt % $PGSLP_{8000}$ was prepared in HFIP, and the solution transferred to a glass syringe and placed inside the electrospinning apparatus. A 18G needle tip to collector distance of 20 cm was used, with an operating voltage of 20 kV and a flow rate of 1 mL h^{-1}. Only partial jet formation was observed, and even after 30 min, no nonwoven web formation was observed. Modulation of the operating voltage, tip to collector distance, and flow rate from 15 to 20 kV, 5 to 25 cm, and 0.5 to 2 mL h^{-1} respectively did not yield any fibrous deposition.

6.2.1.4 Electrospinning of $PGSLP_{8000}$ and gelatin

As an alternative to poly(ε–caprolactone) (PCL) as a fibre forming carrier material, gelatin was evaluated. The gelatin was commixed with the PGSLP in an effort to produce electrospun fibres.

A solution of 5 wt % $PGSLP_{8000}$ and 5 wt % gelatin was made up in HFIP, the solution transferred to a glass syringe and placed inside the electrospinning apparatus. A charged plate with distance to an 18G needle tip of 20 cm was secured in place, the needle tip was then charged with 20 kV and the flow rate of the syringe pump adjusted to 1 mL h^{-1}. The syringe pump was activated, and jets of $PGSLP_{8000}$-Gelatin were directed towards the charged collection plate. A nonwoven web formed on the collection plate, but intermittent electrospraying occurred, with droplets being observed that combined with the nonwoven web. This suggested that molecular chain entanglement in the polymer was insufficient to form a stable process, necessary to consistently form fibres. However, increasing the voltage to 25 kV improved spinning stability.

A challenge that was observed with spinning of PGSLP and gelatin was gel formation in the needle tip, which caused intermittent blockages. Gelling was also observed within the syringe, causing

increased back pressure at the syringe pump. This was mitigated by reducing the volume of spinning solution held in the syringe, and therefore the residence time prior to extrusion.

6.2.1.5 Electrospinning of $PGSLP_{8000}AL$ and PCL_{80000}

A photo crosslinking functionalised PGSLP derivative was also investigated for its potential to form nanofibre *via* electrospinning.

A solution of 5 wt % $PGSLP_{8000}AL$ and 5 wt % PCL_{80000} was made up in HFIP, the solution transferred to a glass syringe and placed inside the electrospinning apparatus. A charged plate with distance to an 18G needle tip of 20 cm was secured in place, the needle tip was then charged with 20 kV and the flow rate of the syringe pump adjusted to 1 mL h^{-1}. The syringe pump was activated and jets of $PGSLP_{8000}AL$-PCL_{80000} were directed towards the charged collection plate.

The flow rate of the syringe pump was then increased incrementally by 0.25 mL h^{-1}, the material successfully spun at 1.25 mL h^{-1} however at 1.5 mL h^{-1} spraying was observed, increasing the voltage to 25 kV reduced spraying significantly, improving spinning stability and allowing a uniform nonwoven web to be collected.

6.2.1.6 Electrospinning of Increased Glycerol and Sebacic Acid Derivatives

The feasibility of electrospinning the increased Glycerol and Sebacic Acid derivatives (PG^SLP, PGS^LP, PG^S^LP) was also studied.

Solutions of PGSLP derivatives were formulated in HFIP, ranging from 1 – 15 wt % of PGSLP derivative and 5 wt % PCL_{80000}. The spinning solution was transferred to a glass syringe and placed inside the electrospinning apparatus. Using an 18G needle, a needle tip to collector distance of 10 – 25 cm, voltages ranging from 10 – 25 kV and flow rate adjusted from 0.5 – 1.5 mL h^{-1} spinning experiments were conducted. Partial jet formation was observed, and nonwoven webs were obtained.

6.2.1.7 Electrospinning of DMPA Photoinitiator Doped PGSA and PCL_{80000}

It was reasoned that inclusion of a photoinitiator molecule in the spinning solution would potentially enable curing post spinning, increasing the mechanical strength of the material. 2,2-Dimethoxy-2-phenylacetophenone (DMPA) was chosen as it is readily soluble in HFIP.

A solution of 5 wt % PGSA, 5 wt % PCL and 0.2 wt % DMPA was used, with an 18G needle and a needle tip to collector distance of 20 cm. Spinning at 20 kV voltage with a flow rate or 1 mL min^{-1} led to the production of a nonwoven web.

6.2.1.8 Electrospinning of DMPA Photoinitiator Doped $PGSLP_{8000}AL$ and PCL_{80000}

Inclusion of a photoinitiator into PGSLPA fibres provided the potential for photocuring between the fibre and PGSLPA hydrogel phases when subsequently formed into a composite structure. It was reasoned that photocuring functionality in each phase could lead to enhanced mechanical properties. DMPA was chosen as it is readily soluble in HFIP.

A solution of 5 wt % PGSLPA, 5 wt % PCL and 0.2 wt % DMPA was used, with an 18G needle operating with a needle tip to collector distance of 20 cm, 20 kV voltage, and a flow rate or 1 mL min^{-1}. Under these conditions a nonwoven web was successfully formed.

6.2.1.9 Characterisation and Testing

As the spinning solutions were viscous liquids, characterisation by differential scanning calorimetry (DSC) and thermogravimetric analysis (TGA) were problematic due to the nature of the polymers constituents. These techniques require materials to be heated, which in this case causes polymerisation – a polycondensation reaction, which has water as a by-product. This can affect the results obtained in the analysis. DSC relies on the heat energy used to increase temperature, water can influence this heat energy and produce erroneous results. TGA relies on mass measurements,

which are affected when the water produced is removed as a result of heating. Therefore, the thermoanalytical techniques were used on the final electrospun nonwoven webs, given their much higher thermal stability (compared to the spinning solutions).

Tensile testing was also carried out to determine the Young's modulus, stress at break and cyclic loading to determine the hysteresis response of the materials produced. The latter of course is related to the elasticity of the material.

6.2.1.9.1 Differential Scanning Calorimetry

Differential scanning calorimetry was used to determine the thermal transitions of the polymers synthesised. A TA instruments Q100 was used in the process. The method for DSC analysis was to heat the polymer to 185 °C, cool to -60 °C and then a second heating cycle to 185 °C again. The ramping rate for these heating and cooling cycles was 10 °C min^{-1}. Sample measurements were collected in triplicate to reduce the effect of sample variability.

6.2.1.9.2 Thermogravimetric Analysis

TGA was used to determine the thermal stability of the polymers synthesised. The polymers in their post synthesis state could not be analysed due to the large amounts of water vapour released upon heating. Clearly, evaporation of the water through boiling and the associated water vapour, would lead to large inaccuracies in the mass measurements however the electrospun samples could be analysed as they were thermally stable relative to the unmixed polymers.

A TA instruments Q50 was used in the process. The method for TGA analysis was to heat the materials from room temperature to 500 °C at a rate of 5 °C min^{-1} to collect a full TGA profile. Sample measurements were collected in triplicate to reduce the effect of sample variability.

6.2.1.9.3 Tensile Testing

Uniaxial tensile testing was used to assess the mechanical strength of the nonwoven webs. As the synthesised polymers could not be spun without a fibre-forming carrier polymer, PCL was used as it provided an efficient carrier material. Therefore, the presence of the PCL polymer component was expected to be a large factor in determining overall bulk mechanical properties of the webs.

All tensile testing was conducted on a James Heal, Titan Universal Strength Tester in tensile testing configuration with a 100N load cell. Jaw separation was calibrated to 30 mm and checked manually using Preciva FRDM730002 Verniers. 1 mm/min extension rate was applied in all nonwoven testing. Sample measurements were done in triplicate to allow for an average to be calculated and reduce the effect of sample variability. Electrospun nonwoven webs were conditioned at 20.0 °C and 65 % relative humidity.

Electrospun nonwoven webs were cut into 25 mm strips and assembled onto templates (Figure 6.1) using double sided adhesive tape as anchor points, the effective testing length of these samples was 30 x 25 mm strips. Once assembled the collection plate was removed from the sample. Often due to the high adhesion properties of the nonwoven web, the material would either tear or delaminate thus destroying or compromising the sample.

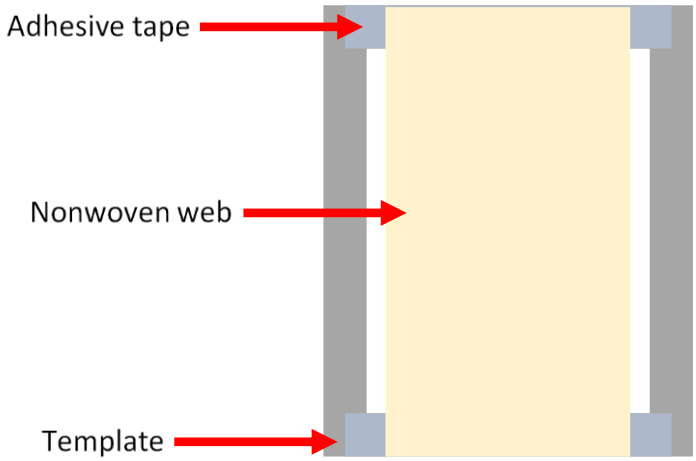

Figure 6.1 Tensile testing template assembly used for the electrospun samples

The tensile data was normalised to account for differences in the areal densities of the samples being tested, which allows for clearer comparison of the stress-strain curves.

Samples that contained photo crosslinking functionality and thus doped with a photoinitiator were crosslinked by placing them in a Chromato-Vue C-71 UV viewing system (4 x 15-watt 365 nm UV tubes fitted) for 2 h with the electrospun web facing upwards, this was to ensure that complete crosslinking occurred.

Wet tensile testing was also carried out whereby the sample was wet out prior to placing in the testing apparatus. The sample was wet out by using a syringe and dropping 2 mL of deionised water along the length of the electrospun webs, this ensured complete wetting where applicable. The materials capable of water absorption were fully saturated and the excess was removed by gently placing both faces onto an absorbent towel.

6.2.1.9.4 Elastic Recovery

Elastic recovery was used to determine the hysteresis response of the nonwoven substrates. This is important due to the intended application of the material; cyclic strain recovery behaviour is key to having an implant with long longevity. Although the intended application requires compressive

strength, the profile of tensile hysteresis for the nonwoven webs intended for use as a fibre reinforcement phase is useful as it allows for understanding of the deformation behaviour of the fibre reinforcement phase.

All elastic recovery testing was conducted on a James Heal, Titan Universal Strength Tester in tensile testing configuration with a 100N load cell. Jaw separation was calibrated to 30 mm and checked manually using Preciva FRDM730002 Verniers. 1 mm/min extension rate was applied in all nonwoven testing. Sample measurements were collected in triplicate to reduce the effect of sample variability. Similar to tensile to failure testing (Section 6.2.1.9.3) the testing data was normalised to eliminate the effect of variations in areal density.

Previously collected tensile to break data (Section 6.2.1.9.3 and 6.3.9.3) was used to determine strain limits for the cycling of the nonwoven webs for elastic recovery testing, a strain limit of 50 % was selected as it allowed for direct comparisons between all the nonwoven samples. Cycling of the material 5 times was deemed suitable due to observations made during initial testing. The materials equilibrated into a repeating stress-strain relationship after the loading portion of cycle 1. Additional cycles were conducted to establish if further degradation of the stress-strain behaviour occurred following the first cycle. DMPA photoinitiator doped nonwoven webs were also tested before and after curing to determine the change in the elastic recovery due to increased crosslink density within the structure. Curing of the webs was done as previously described in Section 6.2.1.9.3.

6.2.1.9.5 Contact Angle Measurements

Contact angle measurements were performed to determine the hydrophilicity of the electrospun nonwoven samples by manual measurement. A level surface was prepared by using a bubble leveller and a nonwoven sample was attached flush with the surface, this was achieved by taping or pinning the nonwoven web without stretching or deforming the structure. A transfer pipette (1 mL) was

used to drop a single droplet of deionised water onto the surface, equating to 0.05 mL of fluid volume, 5 s of equilibration time was used to allow any potential wetting to occur before capturing an image. Images were captured using a macro lens with a Samsung S10 Lite camera in macro image collection mode (5 MP, F2.4). Three images were collected for each samples, allowing for determination of an average and to reduce the effect of sample variability. DMPA photoinitiator doped nonwoven webs were also tested before and after curing to determine the change in hydrophilic behaviour. Curing of the webs was done as previously described in Section 6.2.1.9.3.

ImageJ image processing software was used to determine the angle of the droplet relative to the flat surface. Angles over 90 ° mean there is negligible wetting, and the sample is hydrophobic, angles below 90 ° mean the sample is hydrophilic.

6.2.1.9.6 Degradation Studies

The stability and degradation rate of materials in biological conditions is important as it directly affects clinical efficacy and the treatment frequency, *i.e*. the intervals required between patient treatments. Implanted materials can only provide structural support if their mechanical properties are appropriately matched to the conditions of the defect size, and the degradation rate is appropriately engineered. This balance is also important to allow tissue regeneration, as well as to avoid the risk of infection by repeated treatments.

Submersion of the material in simulated body fluid (phosphate buffer solution, or PBS) is a common approach for evaluating the stability and degradation of experimental samples.[187] Herein, electrospun samples were individually immersed in PBS for a period of 8 weeks to determine the stability in a physiological setting, methodology was based on degradation studies of other electrospun nonwoven substrates.[187] The buffer solution was prepared in deionised water with a concentration of 0.01 M phosphate buffer, 0.0027 M potassium chloride and 0.137 m sodium

chloride with a pH of 7.4 at 25 °C. Measurements were done in triplicate to allow determination of an average and to reduce the effect of material variability. Samples were submersed in separate vials containing PBS to reduce the possibility of agitation causing material abrasion due to friction between samples. DMPA photoinitiator doped nonwoven webs were also tested before and after curing to determine the change in the degradation behaviour due to increased crosslink density within the structure. Curing of the webs was done as previously described in Section 6.2.1.9.3.

To determine the rate of degradation, samples were cut to equal dimensions (10 x 30 mm), the initial mass of the samples was measured, and then re-measured at 1-week intervals, to provide a degradation rate, *via* quantification of the residual mass. All mass measurements were obtained using oven dried samples (dried at 50 °C for 24 h, in a Binder ED56 Series static oven).

6.2.1.9.7 Swelling Degree

The swelling of polymer materials is a useful metric for determining its potential absorbent capacity and drug loading capacity (if intended as a drug delivery vehicle). There is also the potential for an implanted material to swell into an irregularly shaped wound cavity, providing better contact and between the material and the physiological surface. Swelling ratio is a direct measure of water absorption which will also have a direct impact on mechanical properties.

Swelling measurements were made on the electrospun webs and based on methodologies described by Jia *et al*,[185] whereby samples were measured before submersion in PBS, and then allowed to equilibrate before weighing again. The buffer solution was prepared with a concentration of 0.01 M phosphate buffer, 0.0027 M potassium chloride and 0.137 m sodium chloride with a pH of 7.4 at 25 °C. Measurements were done in triplicate to allow determination of an average and to reduce the effect of material variability. DMPA photoinitiator doped nonwoven webs were also tested before and after curing to determine the change in the swelling behaviour due to increased

crosslink density within the structure. Curing of the webs was done as previously described in Section 6.2.1.9.3.

$$Swelling\ Degree\ (\%) = \frac{W_i - W_s}{W_i} \times 100$$

Equation 6.1 Swelling degree equation

Degree of swelling was calculated using

$Swelling\ Degree\ (\%) = \frac{W_i - W_s}{W_i} \times 100$

Equation 6.1, where W_i is initial mass and W_s is swollen mass. Equilibration of the sample was achieved by measuring the mass of the sample in 1 h increments until no mass change was observed.

6.2.1.9.8 Porosity And Fibre Diameter

Porosity is a measure of the void volume within the bulk structure and can be measured by image analysis of SEM images. Porosity is a useful indicator of the potential for tissue growth into a porous structure, as well as potential for cell proliferation and nutrient diffusion. The porosity of the electrospun nonwovens before and after immersion in PBS buffer solution was measured to understand how degradation might be linked to changes In porosity. The samples were submerged in PBS for 8 weeks prior to determining the residual porosity. The buffer solution was prepared with a concentration of 0.01 M phosphate buffer, 0.0027 M potassium chloride and 0.137 m sodium chloride with a pH of 7.4 at 25 °C. Three measurements were taken for porosity, allowing for determination of an average.

ImageJ image analysis software was used to calculate porosity from SEM micrographs. Micrographs were taken from 1500x magnification at 25 kV, the image was then transferred to ImageJ, transformed to a black and white (binary) image and the contrast altered until a clear distinction between fibre and void space was observed. ImageJ analysis was then deployed to calculate the relative solid and void areas, to enable porosity (%) to be determined.

Fibre diameter of electrospun webs can affect solid surface area and pore size distribution, which in a clinical setting can also have a direct effect on cell seeding and proliferation. Fibre diameter was measured (n = 50 per sample) before and after immersion into a PBS buffer solution for 8 weeks. The buffer solution was prepared with a concentration of 0.01 M phosphate buffer, 0.0027 M potassium chloride and 0.137 m sodium chloride with a pH of 7.4 at 25 °C.

Following dimensional calibration, image analysis software (ImageJ) was used to calculate fibre diameter from SEM micrographs, with n=100 fibre being measured per sample. Micrographs were taken from 1500x magnification at 25 kV.

DMPA photoinitiator doped nonwoven webs were also tested with and without curing to determine the change in the porosity and fibre diameter after immersion. Curing of the webs was done as previously described in Section 6.2.1.9.3.

6.3 Results and Discussion

The PGS-based materials produced in this work were intended to act both as elastomeric hydrogel materials, as well as materials for making electrospun fibres for use as a reinforcement phase in a composite. There is a dearth of previous studies dealing with the electrospinning of PGS materials, and this work provided an opportunity to develop an improved understanding of the conditions required for stable electrospinning and the production of defect free electrospun fibre webs.

Furthermore, this work was novel because of the PGSLP photocuring functionality that was synthesised, such that the feasibility of producing photo-curable PGSLP fibres was explored whose physical properties could be further modulated post-electrospinning by a subsequent photo-curing step. To overcome the difficulties of spinning 100% PGSLP, it was commixed with PCL. The electrospinning of PCL is well documented and the polymer is FDA approved and has been studied extensively for its use in biomedical applications[188].

6.3.1 Electrospinning of $PGSLP_{1000}$ and PCL_{80000}

To enable fibres to be produced using PGSLP, commixing with a carrier polymer such as PCL was necessary, but it was unknown how molecular chain length might affect spinnability. It was found that the spinning of $PGSLP_{1000}$ with PCL_{80000} was problematic, most likely because of insufficient molecular chain entanglement during electrospinning. No fibre formation was observed even with modulation of the spinning parameters.

6.3.2 Electrospinning of $PGSLP_{8000}$ and PCL_{80000}

Insufficient molecular chain length was tackled by increasing the PEG chain length during synthesis. Increasing the PEG chain length from 1000 to 8000 and use of diacrylate PEG with a molecular weight of 8000 was implemented to determine the effect on spinnability. A spinning solution of 5 % wt/w of $PGSLP_{8000}$ and 5 % wt/w PCL_{80000} was prepared in HFIP, and the solution transferred to a glass syringe and placed inside the electrospinning apparatus. Formation of a Taylor cone, liquid jets of fibrous web formation on the collector were observed (Figure 6.2).

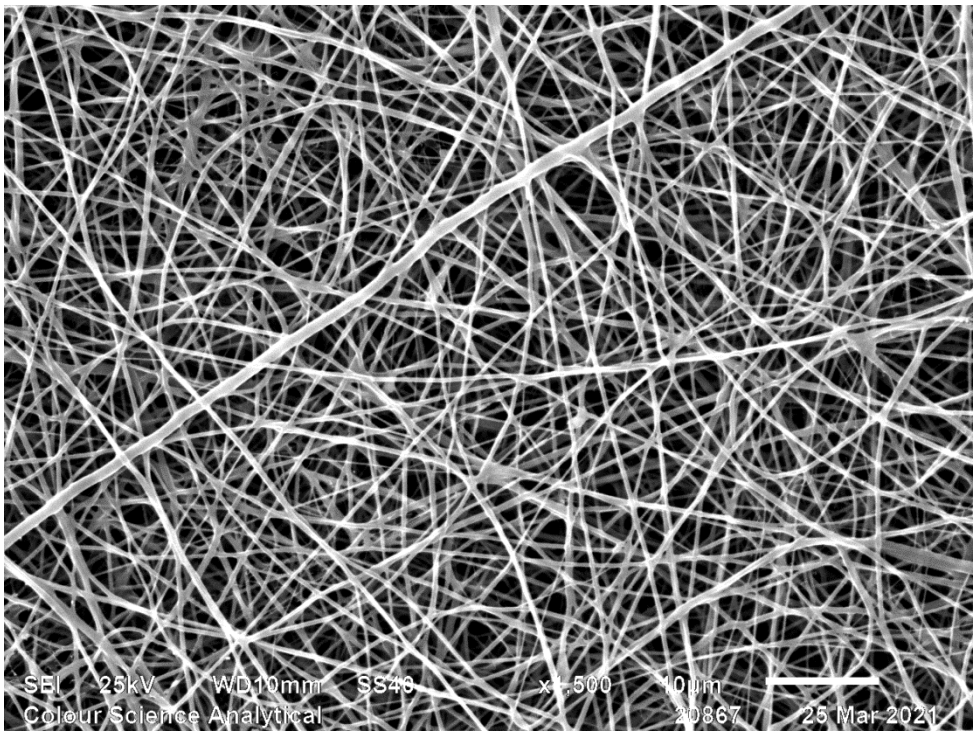

Figure 6.2 SEM micrograph of electrospun $PGSLP_{8000}$ / PCL_{80000} fibres.

Intermittently, web formation occurred between the needle tip and collection plate, such that it interfered with the deposition of fibres on the collector. Progressively increasing the tip to collector distance up to 15 cm was found to be the optimum distance and allowed more uniform material deposition and ultimately resulted in stable fibre deposition.

6.3.3 Electrospinning of $PGSLP_{8000}$

It was instructive to determine if 100% PGSLP fibres could be produced from the higher molecular weight PGSLP material (PEG component increased from 1000 to 8000 g mol^{-1} during synthesis). To determine the feasibility, a solution of 5 % wt/w $PGSLP_{8000}$ in HFIP was electrospun using a needle tip to collector distance of 20 cm and a voltage of 20 kV. Continuous liquid jet formation was difficult to establish, although sporadic jet formation was observed. Alterations to the operating voltage, tip to collector distance and flow rate from 15 to 20 kV, 5 to 25 cm, and 0.5 to 2 mL h^{-1} respectively did not allow for stable jet formation. No fibrous web formation could be obtained, but PGSLP films

would be produced, suggesting insufficient molecular chain length entanglement to support electrospinning. The deposited PGSLP film was highly adhesive and could be freely moved around on the collection plate. Therefore, PGSLP fibres could not be formed without a carrier polymer such as PCL. SEM image analysis (Figure 6.3) revealed no fibrous structure and confirmed that a film had been produced.

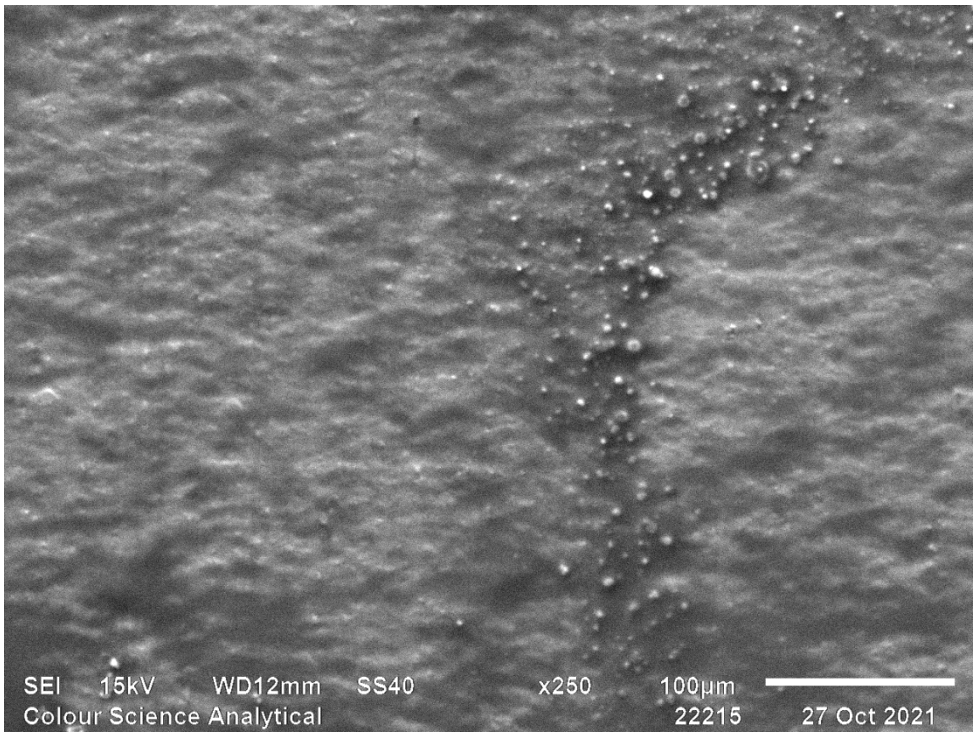

Figure 6.3 SEM micrograph of electrospun $PGSLP_{8000}$.

There may still be potential applications for the film, e.g., as a wound dressing layer however, curing of unmodified PGSLP polymer requires curing at temperatures in excess of 150°C with a reduced pressure environment. Photo-curable PGSLP is more attractive as a clinical material because of the potential to photo-cure the material *in situ* after it has been conformed to the unique shape of the wound site.

6.3.4 Electrospinning of $PGSLP_{8000}$ and gelatin

As reported in Sections 6.2.1.3 and 6.3.3, the spinning of PGSLP without a carrier polymer commixed in the spinning solution resulted in film formation. While PCL has been found to act as an effective carrier, the use of gelatin (derived from collagen) was also explored due to its relatively low cost and biocompatibility. The different mechanical properties of carrier polymers (compared to PGSLP) also present opportunities to tune bulk properties further.

A solution of 5 % wt/w $PGSLP_{8000}$ and 5 % wt/w gelatin was prepared in HFIP solvent and used for initial electrospinning experiments using the spinning conditions reported in Section 6.2.1.4. The formation of a white fibrous web was observed on the collection plate, with spinning solution being ejected from the needle tip during electrospinning. On closer inspection droplet deposition due to electrospraying was found to be occurring. The needle tip to collector distance and voltage were altered incrementally up to 20 cm, and a voltage of 25 kV, which were found to represent optimal processing conditions. Electrospraying of the solution was markedly decreased as the increased voltage but was not entirely eliminated.

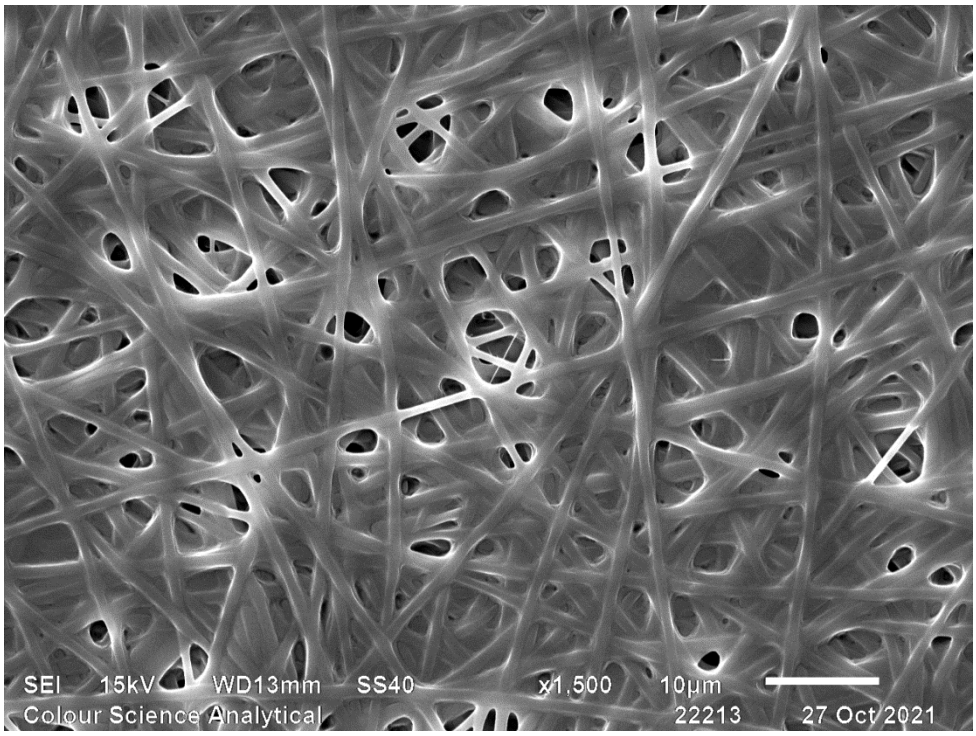

Figure 6.4 SEM micrograph of electrospun $PGSLP_{8000}$ / gelatin fibres.

SEM image analysis (Figure 6.4) showed a fibrous structure however, fibre melding was observed at the edges of fibres, possibly as a result of residual solvent being present following fibre formation, and differences in the solidification rates of the commixed PGSLP and gelatin components during spinning.

6.3.5 Electrospinning of $PGSLP_{8000}AL$ and PCL_{80000}

The introduction of photo crosslinking functionality to polymers can be advantageous, especially in the case of PGSLP where the alternative curing approaches using chemical reagents, requires potentially cytotoxic chemistry.

5 % wt/w $PGSLP_{8000}AL$ and 5 % wt/w PCL_{80000} in HFIP were used in an electrospinning environment, with the experimental parameters described in Section 6.2.1.5. The first objective was to determine the viability of spinning the modified material with a carrier, if this was successful then further

investigation into the efficacy of the photo crosslinking functionality was to be undertaken – If the photo sensitive functionality is exposed when used with a carrier material, then the use of this material as a fibre reinforcement phase is beneficial. This is due to the adhesion between materials of the same nature, mainly the bulk and fibre reinforcement phase but also due to the ability to reinforce the composite not only through the addition of a reinforcement phase but to crosslink the reinforcement phase to the bulk of the composite, forming covalent bonds between them and increasing the mechanical properties greatly.

Upon activation of the spinning equipment continuous jets of material were observed being ejected to the collection plate, a white nonwoven web was deposited onto the surface of the collection plate. For the purpose of increasing the rate of sample production, the flow rate of the syringe pump used was increased incrementally to determine the maximum flow rate that could be used with the specific formulation used in this experiment. The flow rate was increased to a maximum of 1.5 mL h^{-1} where there was a significant increase in spraying of solution onto the collection plate, increasing the voltage to 25 kV reduced spraying significantly allowing for more uniform deposition of material.

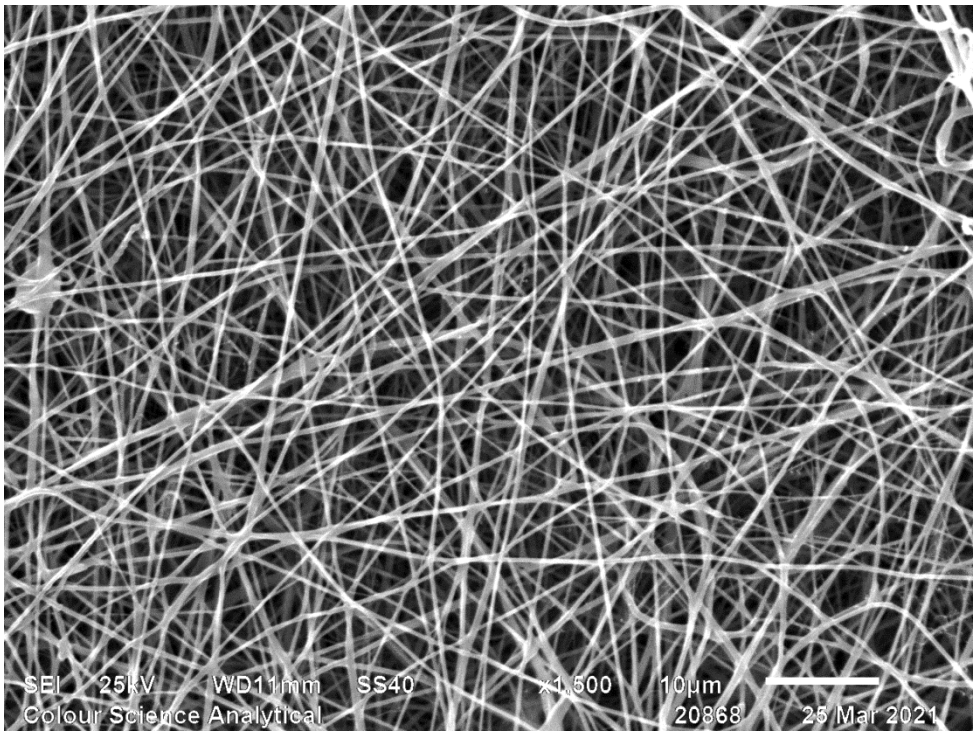

Figure 6.5 SEM micrograph of electro-spun $PGSLP_{8000}AL$ / PCL_{80000} fibres.

SEM image analysis (Figure 6.5) showed a fibrous matrix had been produced, as can be observed from the micrograph there are some droplet formations within the nanofibrous structure, produced during the electrospinning due to electrospraying.

6.3.6 Electrospinning of Increased Glycerol and Sebacic Acid Derivatives

Increased Glycerol and Sebacic acid derivatives were spun to test whether the acrylation procedure would be necessary, if successfully spun the materials would then be modified with photosensitive functionality in the hopes of providing a more active photosensitive material. The increased number of reactive sites would allow for greater grafting of the acrylate groups resulting in a material that would more readily crosslink. However, upon spinning the quality of the nonwoven web produced was poor, there was considerable spraying and agglomeration of polymer beads.

6.3.7 Electrospinning of DMPA Photoinitiator Doped PGSA and PCL_{80000}

Inclusion of photo crosslinking functionality was shown to be successful, further development involved inclusion of a photoinitiator which would enable the fibrous network to be cured post spinning and would enable improved crosslinking interactions between the gel phase and the fibre reinforcement phase.

5 % wt/w PGSA, 5 % wt/w PCL_{80000} and 0.2 % wt/w DMPA in HFIP were used in an electrospinning experiment, using the parameters described in Section 6.2.1.7. The objective was to determine the viability of spinning PGSA with a photoinitiator present in the formulation, allowing for post spinning curing. Upon activation of the spinning equipment continuous jets of material were observed being ejected to the collection plate, a white fibrous web was deposited onto the surface of the collection plate.

Successful spinning of DMPA doped PGSA and PCL solution showed that inclusion of a photoinitiator is possible, allowing for investigations into post spinning curing. The introduction of photo crosslinking functionality to materials is always advantageous, especially in the case of PGSLP where the curing requires harsh conditions.

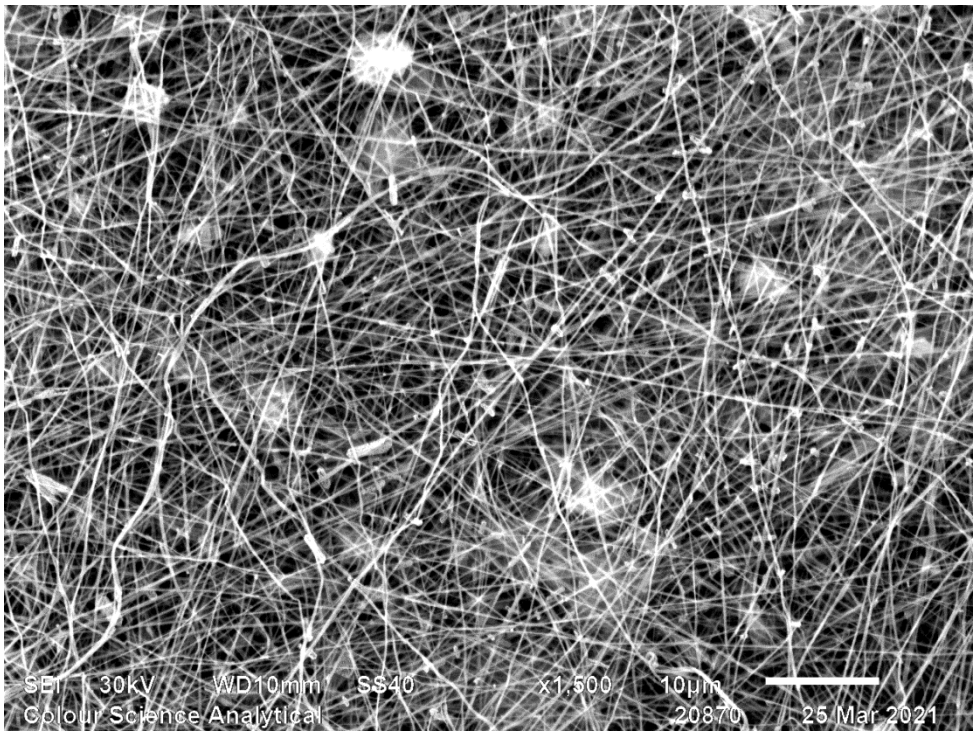

Figure 6.6 SEM micrograph of DMPA doped PGSA / PCL_{80000} electrospun fibres. Large visual defects suggest the presence of crystalline DMPA in the nanofibrous network.

SEM image analysis (Figure 6.6) showed a nanofibrous network had been formed, the presence of large crystalline structures within the fibre network micrograph suggests that DMPA was successfully incorporated into the structure with large agglomerations of crystalline DMPA forming in the spinning process.

6.3.8 Electrospinning of DMPA Photoinitiator Doped $PGSLP_{8000}AL$ and PCL_{80000}

5 % wt/w $PGSLP_{8000}AL$, 5 % wt/w PCL_{80000} and 0.2 % wt/w DMPA in HFIP were used in an electrospinning experiment, with the parameters described in Section 6.2.1.8. The objective was to determine the viability of spinning PGSLPA with a photoinitiator present in the formulation, allowing for post spinning curing and the potential for increased surface bonding in the composite formation. Upon activation of the spinning equipment continuous jets of material were observed being ejected to the collection plate, a white fibrous web was deposited onto the surface of the collection plate.

Successful spinning of DMPA doped PGSLPA and PCL solution showed that inclusion of a photoinitiator is possible.

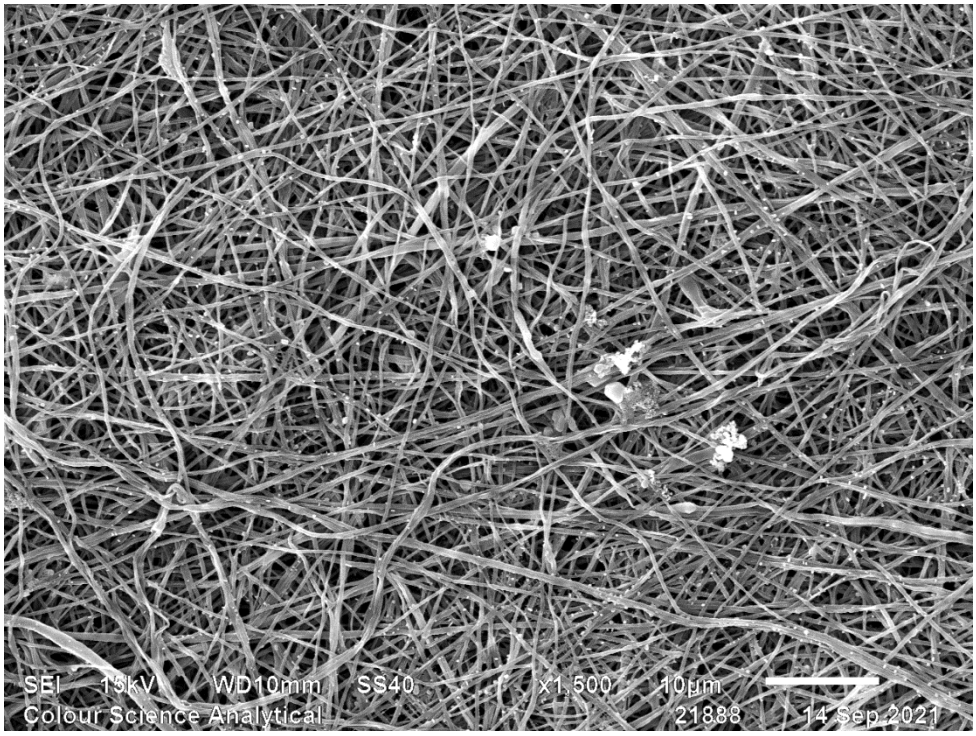

Figure 6.7 SEM micrograph of DMPA doped $PGSLP_{8000}AL$ / PCL_{80000} electrospun fibres. Large visual defects suggest the presence of crystalline DMPA in the nanofibrous network.

SEM image analysis (Figure 6.7) showed a nanofibrous network had been formed, the presence of large crystalline structures within the fibre network micrograph suggests that DMPA was successfully incorporated into the structure with large agglomerations of crystalline DMPA forming in the spinning process which is similar to other DMPA doped electrospun nonwoven webs produced previously (Section 6.3.7)

6.3.9 Characterisation and Testing

6.3.9.1 Differential Scanning Calorimetry

From the DSC cooling analysis (Figure 6.8) it can be seen that the electrospun nonwoven web exhibit a characteristic peak at 30 – 40 °C, this is consistent with the crystallisation temperature of PCL. PGS exhibits a crystallisation peak at -15 – -20 °C indicating a semi-crystalline molecular structure, however PGSLP shows no crystallisation peak indicating an amorphous structure.

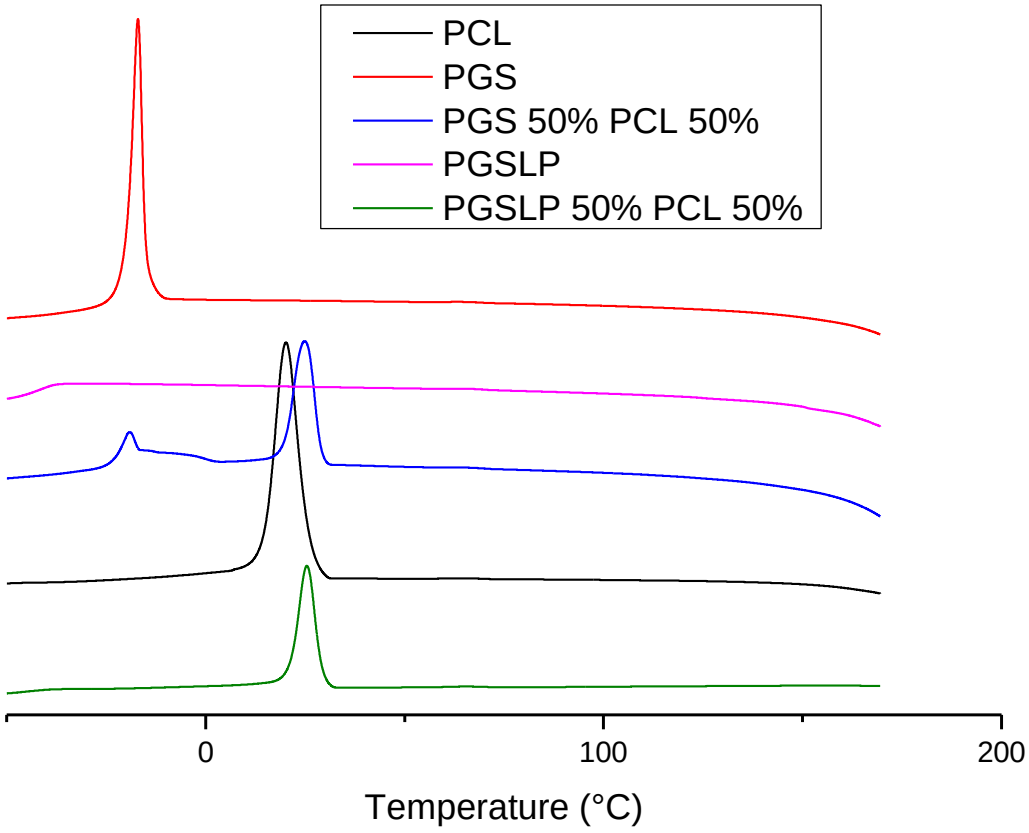

Figure 6.8 Differential scanning calorimetry curves of electrospun nonwoven webs and synthesis products.

The semi-crystalline structure of PGS isn't expected and indicates that the polymer is partially crosslinked, this is likely due to the first heating cycle of the DSC analysis, where the temperature of polymerisation is achieved. The glass transition temperature of PGSLP is -33.4 °C, having a glass transition temperature below 0 °C is indicative of the polymer behaving in an elastomeric fashion at physiological conditions.

6.3.9.2 Thermogravimetric Analysis

As can be seen from the TGA analysis (

Figure 6.9) PGS is a more stable polymer derivative compared to PGSLP, this is primarily due to the larger degree of crosslinking present in the PGS derivative. The large PEG chains present in PGSLP increase the linear chain length, decreasing the crosslink density and thus decreasing the stability of the polymer.

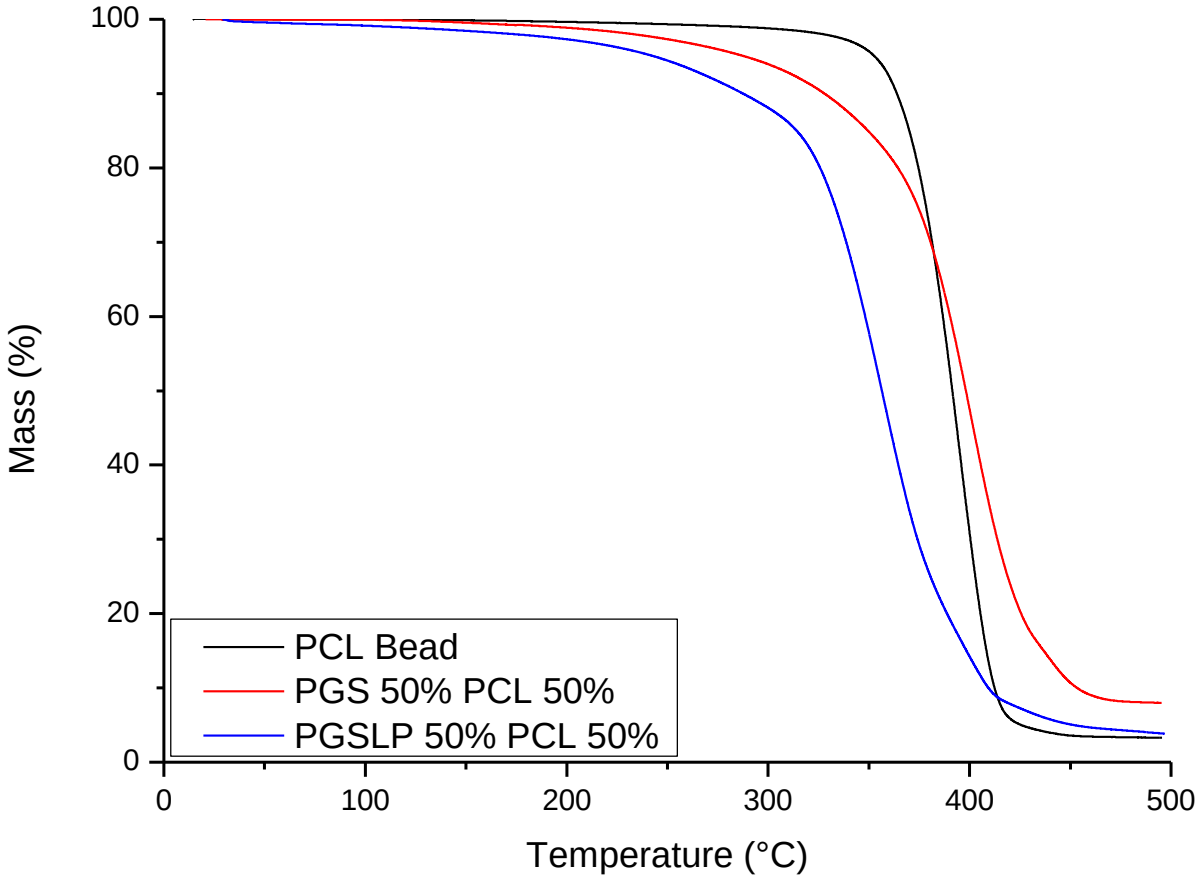

Figure 6.9 Thermogravimetric analysis of a PCL bead and electrospun nonwoven webs containing PCL either with PGS or PGSLP.

PGSLP also showed a greater content of volatile molecules which is likely explained by its hydrophilic properties which will cause it to absorb a greater amount of water from the surrounding environment.

6.3.9.3 Tensile Testing

PGS and PGSLP are both a crosslinked polyester network, with glycerol being the key crosslink enabling functional component. This makes tuning the mechanical properties of the material easier primarily due to the nature of being able to control how rigid the molecular structure is. Unmodified polymer is crosslinked by continuing the polycondensation reaction used in synthesis, leaving the polymer to react for longer produces a higher crosslink density, if the reaction is left to continue to completion a thermally cured elastomeric material is produced.

Due to the potential application of being used as a biomedical implant, different curing functionality is advantageous as it bypasses the need for high temperatures. These high temperatures are efficient at producing a material that could be implanted, but this would require surgery that increases the risk of infection in sometimes immunocompromised individuals. Photosensitive functionality was introduced by grafting of alkene functionality through the acrylation of the molecular structure. While this process uses hazardous chemicals, the potential to avoid surgery is highly desirable and the modified material can be purified to remove the risk of any adverse effects.

As the measurements for each sample type were done in triplicate, determination of an average was used to reduce variability within the data, and allow for a more representative stress-strain curve to be obtained and used in comparisons.

Although the intended application for the nonwoven webs is a structural reinforcement phase within the composite structure, the tensile testing results are still valuable due to the nature of orientation of the nonwoven webs. Application of force perpendicular to the orientation of the reinforcement phase, allows for tenacity to be a factor in the final mechanical properties of the composite material; dispersing the strain through the material evenly and allowing for greater load bearing.

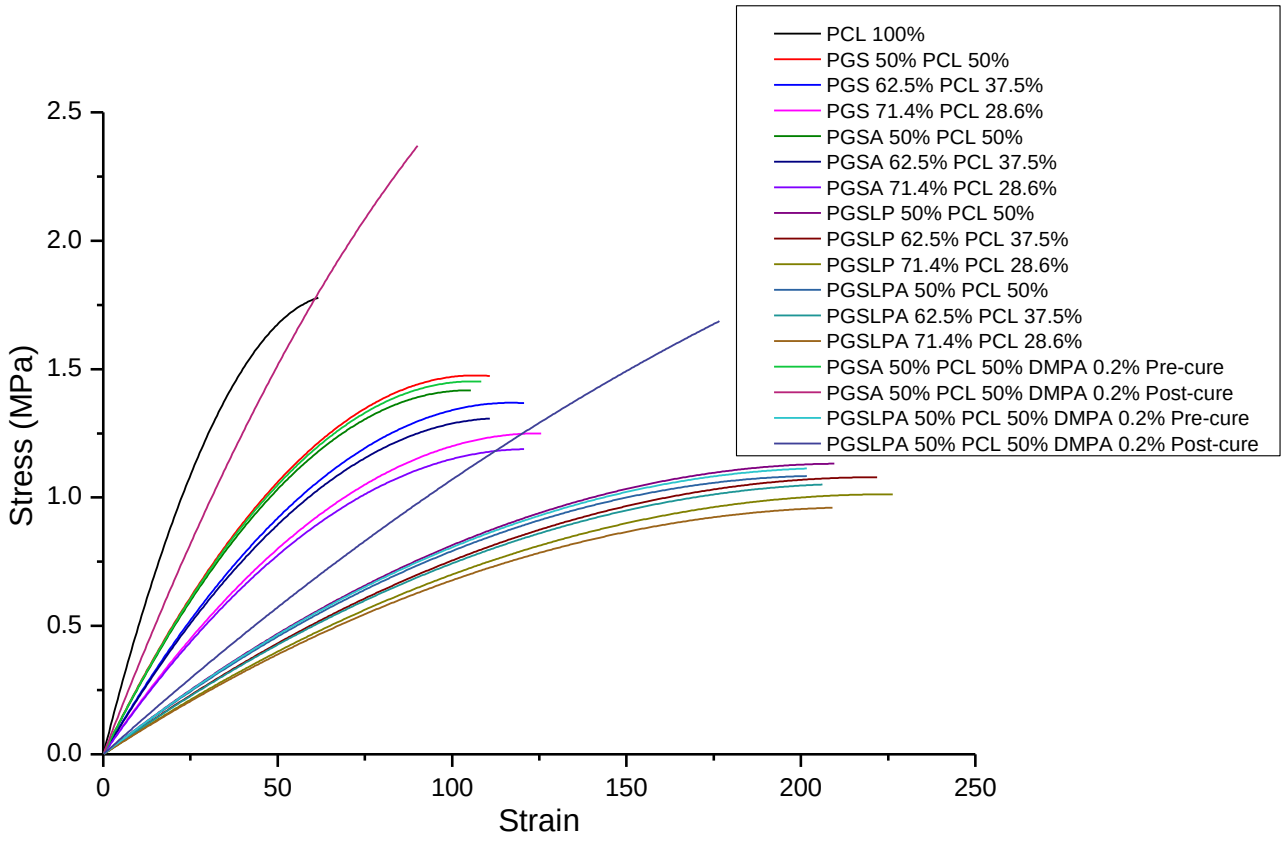

Figure 6.10 Dry tensile stress-strain curves of nonwoven webs.

The tensile stress-strain curves (Figure 6.10) show the partial elastomeric response of the nonwoven electrospun nonwoven webs, the nonlinear shape of the curves of PGS and PGSLP mixtures is indicative of an elastomeric response.

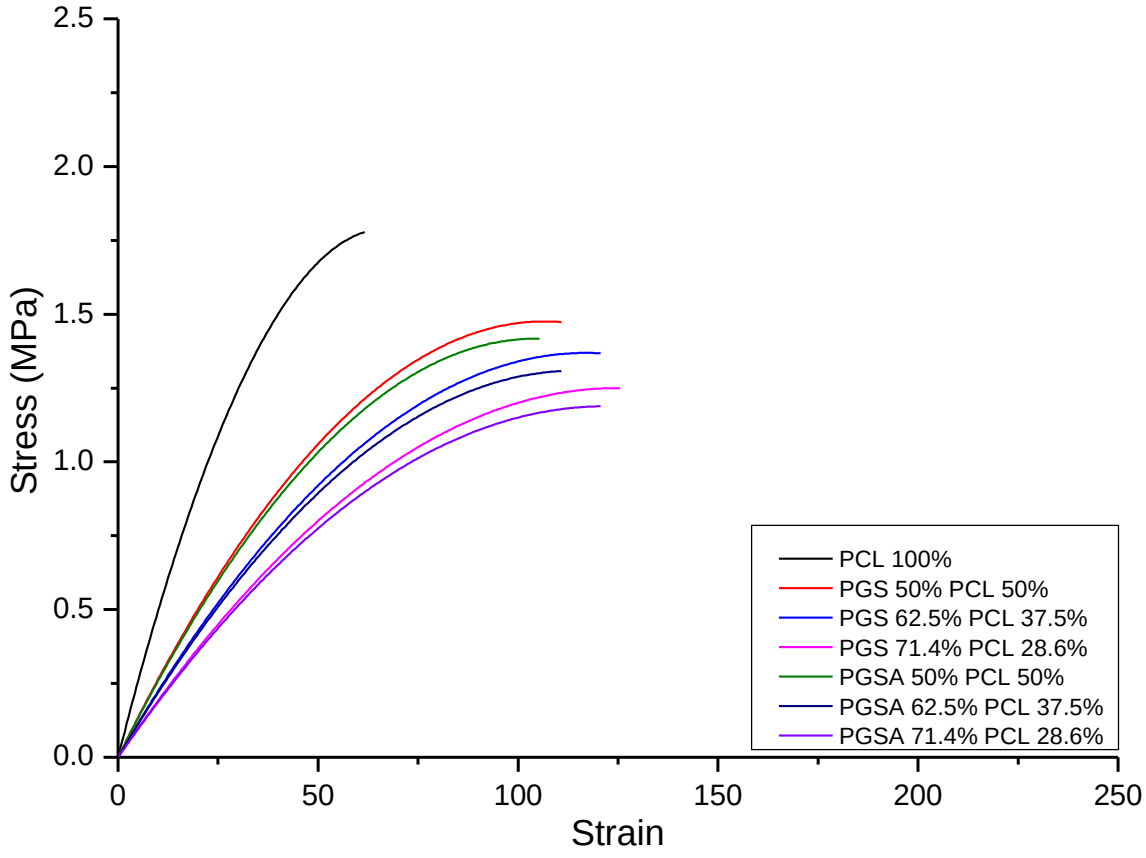

Figure 6.11 Dry tensile stress-strain curves of PGS/PGSA based nonwoven webs.

Figure 6.11 shows the dry tensile stress-strain curves of PGS and PGSA containing nonwoven webs. As can be seen from the figure the inclusion of PGS and PGSA into the nonwoven web produces a more elastomeric response than that of pure PCL, however no true elastomeric curve is observed – this is primarily because of the requirement of PCL as a carrier fibre. A blend of both materials mechanical properties is shown. Another variable that is likely affecting the mechanical properties is the physical properties of the nonwoven webs, the adhesion properties of the materials make it hard to handle and test efficiently with large amounts being destroyed or mechanically compromised simply due to handling and transfer to template assemblies.

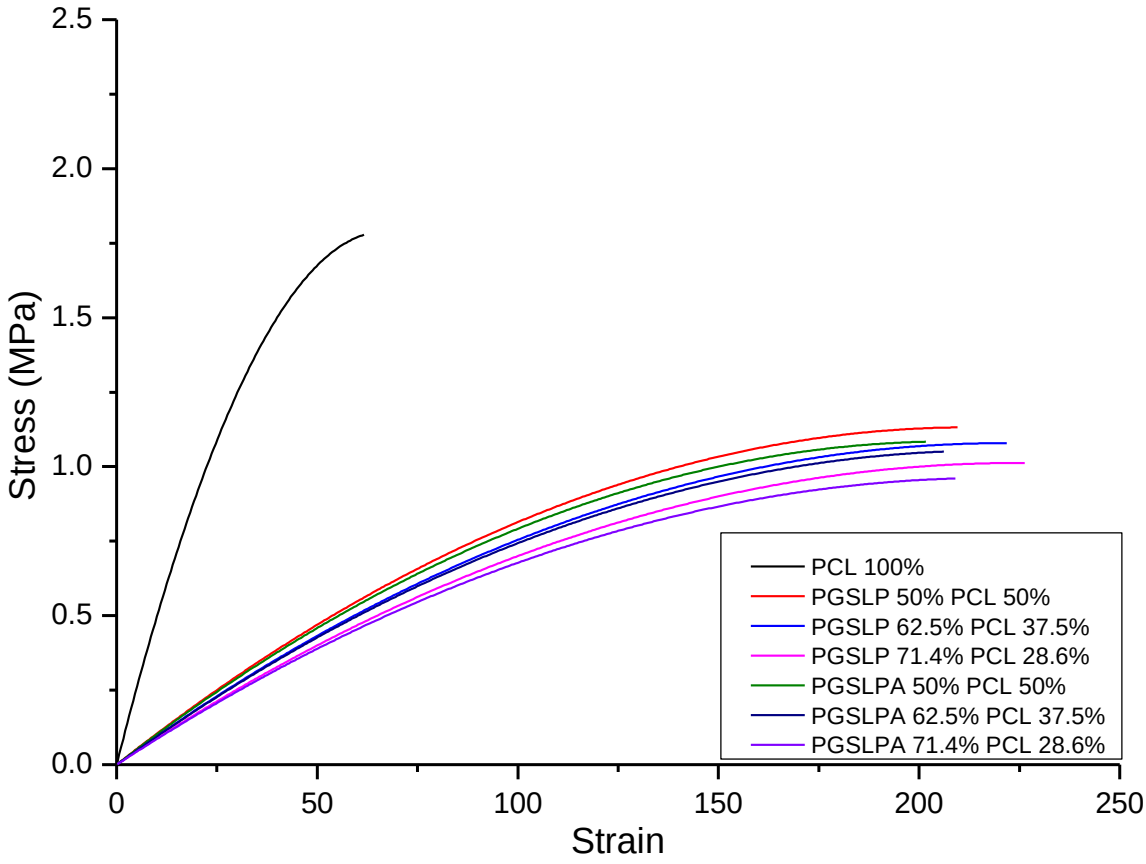

Figure 6.12 Dry tensile stress-strain curves of PGSLP/PGSLPA based nonwoven webs.

Figure 6.12 shows the stress-strain curves of PGSLP and PGSLPA containing nonwoven webs. These materials exhibit a larger maximum strain but a lower maximum stress, this is in part due to the makeup, PGSLP contains large PEG blocks in its mechanical structure which reduces crosslink density and yields a weaker web but a higher maximum extension. Again, a mix of both PGSLP and PCL mechanical properties is shown, with no true elastomeric response. Similar to the PGS derivatives the adhesion properties of the material make it hard to handle and test efficiently, sample destruction during separation from the collection area is common and transfer to testing

assemblies' results in distorted sample dimensions.

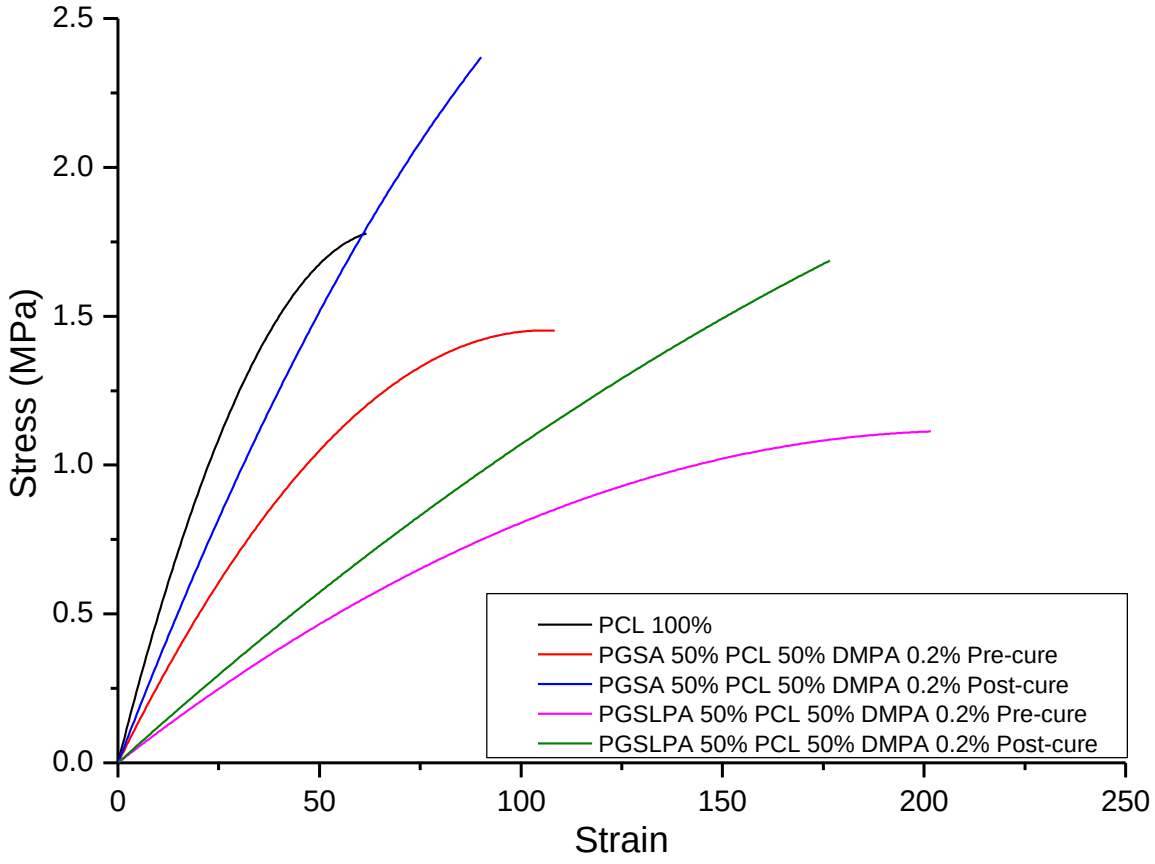

Figure 6.13 Dry tensile stress-strain curves of DMPA photoinitiator doped nonwoven webs.

Figure 6.13 shows the stress-strain curves of nonwoven webs where the spinning solution was doped with DMPA, a photoinitiator molecule. The inclusion of the photoinitiator molecule was to test if post spinning curing was possible and effective as a means of increasing the mechanical strength of the material. The stress-strain curves show a clear increase in mechanical strength, far surpassing that of a pure PCL nonwoven web however there is a decrease in the elastomeric response. The nonwoven web behaves in a much more rigid manner.

Wet tensile testing allows the mechanical properties of the material to investigated when saturation has occurred. This is important for biomaterials as it allows for an understanding of how the mechanical properties change when in a physiological environment.

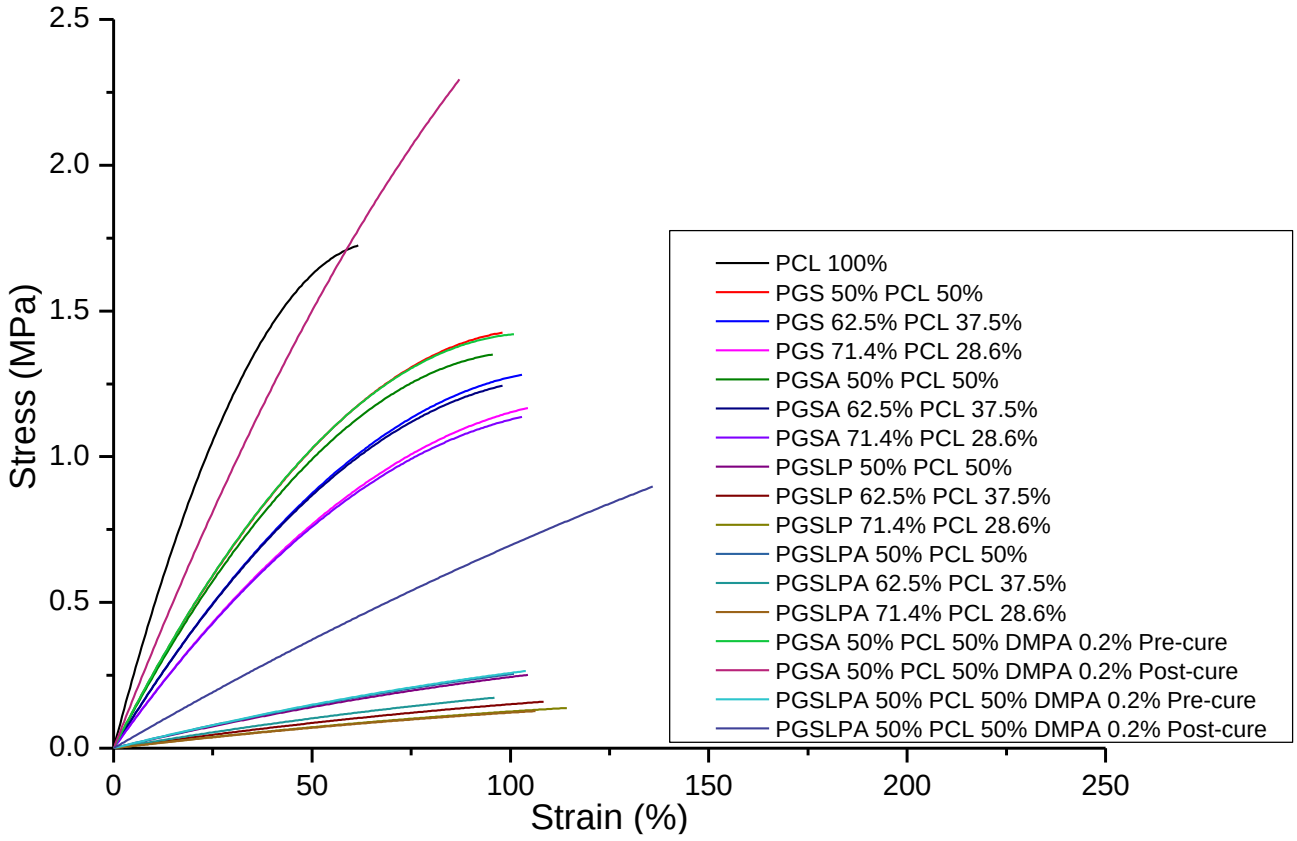

Figure 6.14 Wet tensile stress-strain curves of nonwoven webs.

Figure 6.14 shows the wet tensile stress-strain curves for appropriately saturated nonwoven webs, as can be seen from comparison with Figure 6.10 there is a significant decrease in maximum stress in the PGSLP derivatives, with a much smaller decrease in the PGS derivatives. This is due to the highly hydrophilic nature of the PGSLP derivatives, the material absorbs a much higher volumes of water (

Figure 6.32) which causes a decrease in maximum stress and strain.

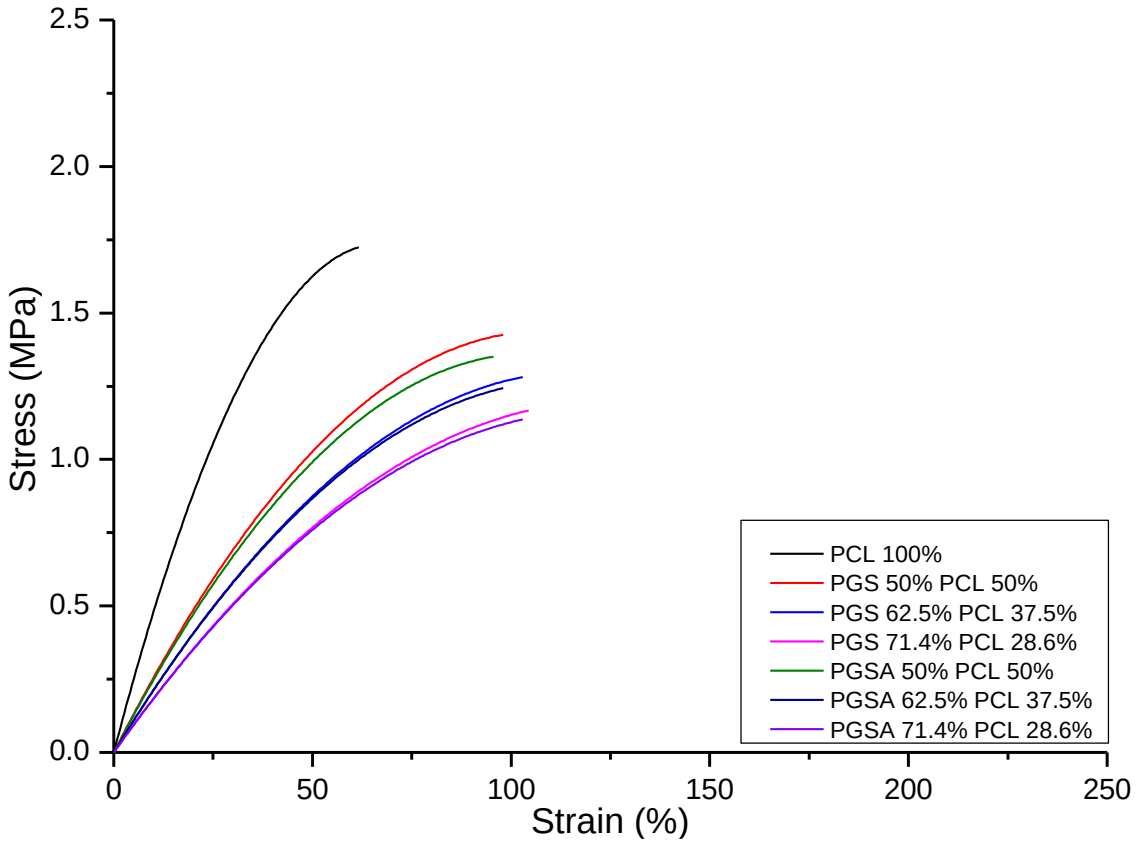

Figure 6.15 Wet tensile stress-strain curves of PGS/PGSA based webs.

Figure 6.15 shows the wet tensile stress-strain curves of the PGS and PGSA webs, due to the slight hydrophobic nature of the material and thus the relatively lower water absorption capacity the decrease in maximum stress and strain is smaller when compared to PGSLP derivatives.

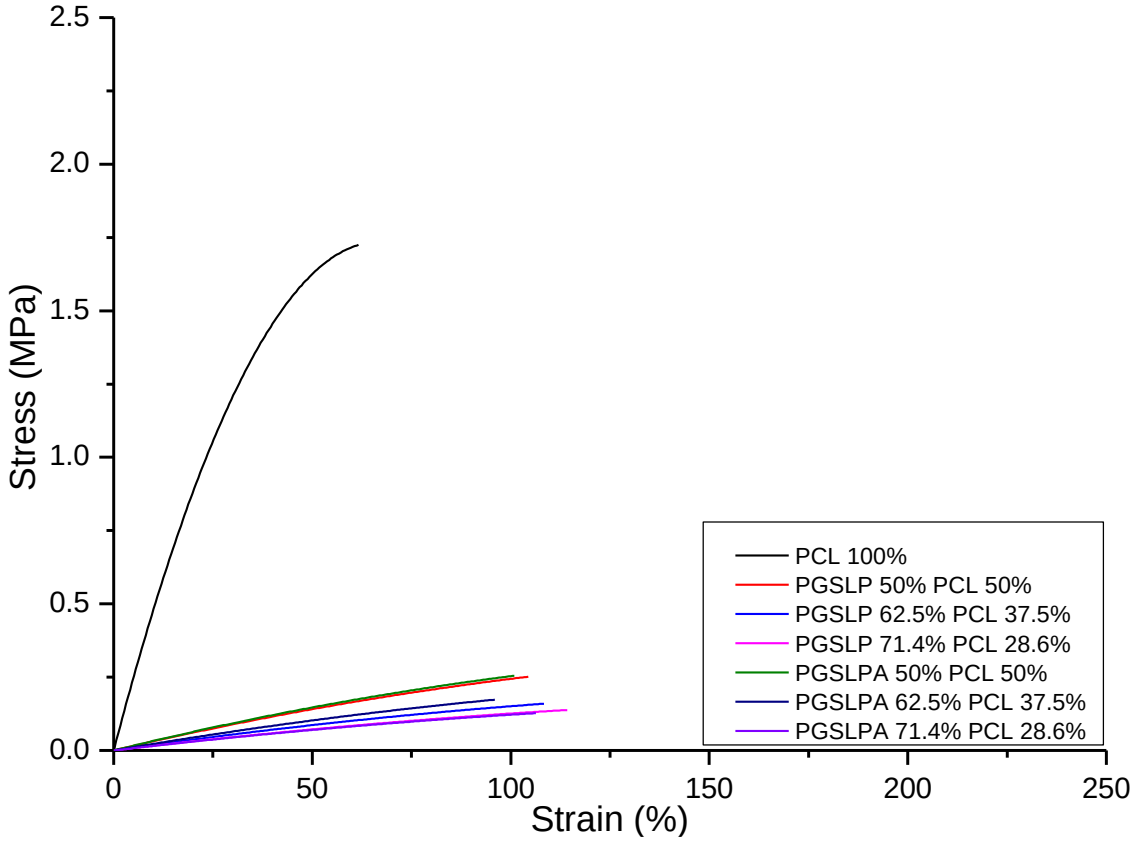

Figure 6.16 Wet tensile stress-strain curves of PGLP/PGSLPA based webs.

Figure 6.16 shows the wet tensile stress-strain curves of the PGSLP and PGSLPA derivatives, with marked decreases in the maximum stress and strain. The material is highly hydrophobic, wetting out completely and instantly which significantly decreases the mechanical properties.

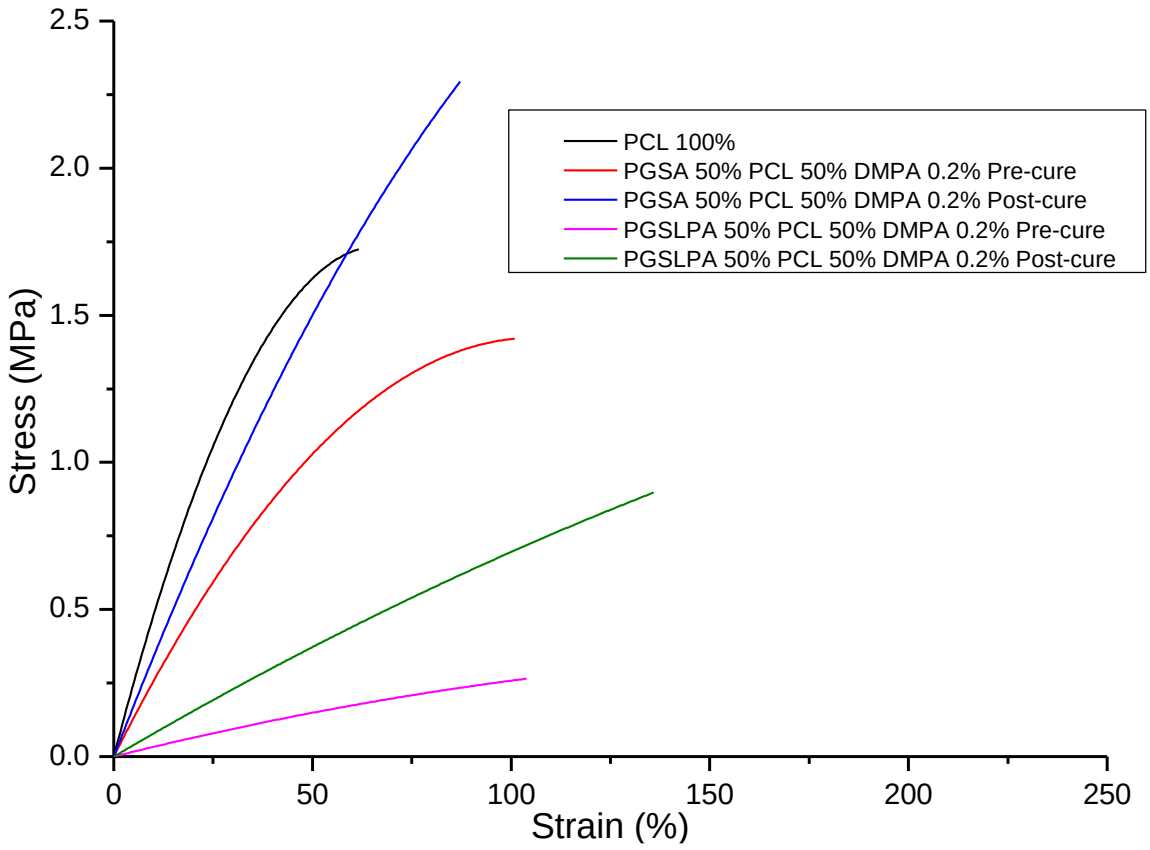

Figure 6.17 Wet tensile stress-strain curves of DMPA photoinitiator doped nonwoven webs.

Figure 6.17 shows the wet tensile stress-strain curves of the DMPA doped nonwoven webs before and after curing. Post curing the materials exhibit a much more linear profile which is indicative of a loss of elastic properties due to the increase in crosslink density, the maximum stress and strain is also significantly increased further confirming the crosslink density has increased.

Table 6.1 Maximum strain (%) and maximum stress (MPa) of dry tensile testing samples. Elastic modulus derived from the initial curve portion to a 40 % strain limit.

Sample	Maximum Strain (%)	Maximum Stress (MPa)	E (MPa)	Eσ (MPa)
PCL 100%	62	1.8	0.037	0.003
PGS 50% PCL 50%	111	1.5	0.023	0.002
PGS 62.5% PCL 37.5%	121	1.4	0.019	0.003
PGS 71.4% PCL 28.6%	126	1.2	0.017	0.004
PGSA 50% PCL 50%	105	1.4	0.022	0.003
PGSA 62.5% PCL 37.5%	111	1.3	0.019	0.005
PGSA 71.4% PCL 28.6%	121	1.2	0.016	0.005
PGSLP 50% PCL 50%	210	1.1	0.010	0.003
PGSLP 62.5% PCL 37.5%	222	1.1	0.009	0.007
PGSLP 71.4% PCL 28.6%	226	1.0	0.008	0.004
PGSLPA 50% PCL 50%	202	1.1	0.009	0.005
PGSLPA 62.5% PCL 37.5%	206	1.1	0.009	0.003
PGSLPA 71.4% PCL 28.6%	209	1.0	0.008	0.002
PGSA 50% PCL 50% DMPA 0.2% Pre-cure	108	1.5	0.022	0.003
PGSA 50% PCL 50% DMPA 0.2% Post-cure	90	2.4	0.031	0.002
PGSLPA 50% PCL 50% DMPA 0.2% Pre-cure	202	1.1	0.010	0.006
PGSLPA 50% PCL 50% DMPA 0.2% Post-cure	177	1.7	0.012	0.003

Table 6.1 shows the dry tensile testing maximum strain, maximum stress, and elastic modulus values for the electrospun nonwoven webs. PCL has the highest elastic modulus of 0.037, PGS derivatives have a modulus in the range of 0.016 – 0.023 MPa and PGSLP derivatives have a significantly decreased modulus range of 0.008 – 0.01 MPa.

Post curing the modulus of PGSA and PGSLPA increased to 0.031 and 0.012 respectively, which translates to increases of 40.6 % and 21.4 %. These increases are related to the crosslink density, PGSLPA has a lower potential for crosslink density due to the increased molecular chain length because of the inclusion of a PEG with Mw 8000.

Table 6.2 Maximum strain (%) and maximum stress (MPa) of wet tensile testing samples. Elastic modulus derived from the initial curve portion to a 40 % strain limit.

Sample	Maximum Strain (%)	Maximum Stress (MPa)	E (MPa)	Eσ (MPa)
PCL 100%	62	1.7	0.036	0.002
PGS 50% PCL 50%	98	1.4	0.022	0.002
PGS 62.5% PCL 37.5%	103	1.3	0.018	0.004
PGS 71.4% PCL 28.6%	104	1.2	0.016	0.005
PGSA 50% PCL 50%	96	1.4	0.021	0.003
PGSA 62.5% PCL 37.5%	98	1.2	0.018	0.005
PGSA 71.4% PCL 28.6%	103	1.1	0.016	0.005
PGSLP 50% PCL 50%	104	0.3	0.003	0.003
PGSLP 62.5% PCL 37.5%	108	0.2	0.002	0.001
PGSLP 71.4% PCL 28.6%	226	1.0	0.001	0.0006
PGSLPA 50% PCL 50%	101	0.3	0.003	0.001
PGSLPA 62.5% PCL 37.5%	96	0.2	0.002	0.001
PGSLPA 71.4% PCL 28.6%	209	1.0	0.001	0.0003
PGSA 50% PCL 50% DMPA 0.2% Pre-cure	101	1.4	0.022	0.003
PGSA 50% PCL 50% DMPA 0.2% Post-cure	87	2.3	0.031	0.002
PGSLPA 50% PCL 50% DMPA 0.2% Pre-cure	104	0.3	0.003	0.001
PGSLPA 50% PCL 50% DMPA 0.2% Post-cure	136	0.9	0.008	0.001

Table 6.2 shows the wet tensile testing maximum strain, maximum stress, and elastic modulus values for the electrospun nonwoven webs. PCL has the highest elastic modulus of 0.036, PGS derivatives have a modulus in the range of 0.016 – 0.022 MPa and PGSLP derivatives have a significantly decreased modulus range of 0.001 – 0.003 MPa.

Post curing the modulus of PGSA and PGSLPA increased from 0.022 and 0.03 to 0.031 and 0.08 respectively, which translates to increases of 42.0 % and 46.5 %. The increase in PGSLPA modulus is significantly higher in the wet samples compared to the dry due to the decreased water absorption.

Table 6.3 Work of rupture of dry tensile testing samples. Work of rupture derived from the area underneath stress-strain curves.

Sample	Work of Rupture
PCL 100%	70.45727
PGS 50% PCL 50%	111.0529
PGS 62.5% PCL 37.5%	111.7115
PGS 71.4% PCL 28.6%	104.821
PGSA 50% PCL 50%	100.0023
PGSA 62.5% PCL 37.5%	95.07267
PGSA 71.4% PCL 28.6%	95.04226
PGSLP 50% PCL 50%	156.9614
PGSLP 62.5% PCL 37.5%	159.7356
PGSLP 71.4% PCL 28.6%	153.1839
PGSLPA 50% PCL 50%	143.5115
PGSLPA 62.5% PCL 37.5%	140.4111
PGSLPA 71.4% PCL 28.6%	130.8729
PGSA 50% PCL 50% DMPA 0.2% Pre-cure	106.1294
PGSA 50% PCL 50% DMPA 0.2% Post-cure	118.9768
PGSLPA 50% PCL 50% DMPA 0.2% Pre-cure	146.4411
PGSLPA 50% PCL 50% DMPA 0.2% Post-cure	162.7826

Table 6.3 shows the work of rupture of electrospun nonwoven webs that were tested in a dry condition. Work of rupture is defined as the energy needed to break a specimen. PGSLP containing nonwoven webs exhibited far higher work of rupture values when compared to PCL and PGS containing webs. While PGSLP webs exhibits a lower maximum stress than PCL and PGS webs, the material absorbs a greater amount of energy due to its elastic properties.

6.3.9.4 Elastic Recovery

Fatigue testing of the nonwoven webs allows determination the elastic behaviour when an external force is applied and then removed in cycles. If the force applied causes deformation into the plastic region the material will exhibit permanent deformation, the recovery from the maximum force is elastic recovery.

Deformation cycles were only conducted 5 times as all materials exhibited equilibration after the loading phase of the first cycle. Further cycles were conducted to determine if further degradation of the stress-strain relationship occurred after cycle 1.

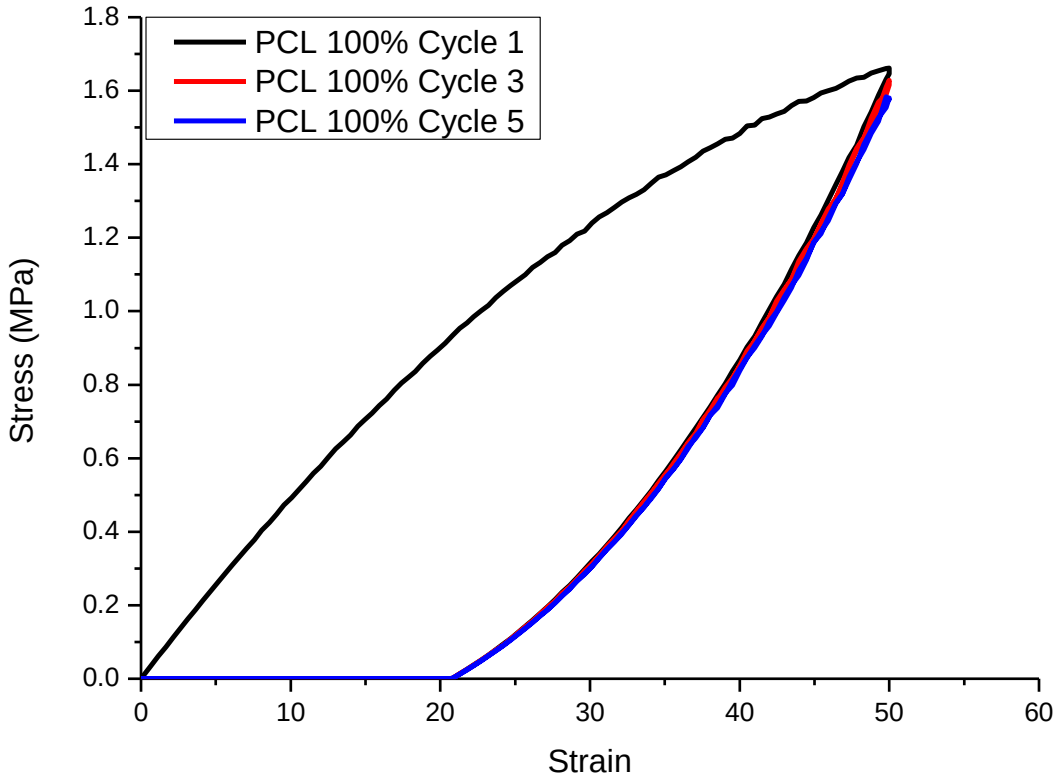

Figure 6.18 Cyclic tensile stress-strain curves of cycles 1, 3 and 5 for 100 % PCL nonwoven webs.

Figure 6.18 shows the hysteresis responses of 100 % PCL electrospun nonwoven webs. This was used to compare other nonwoven samples with different formulations to, as PCL was used as a carrier material in all samples. As in the tensile to failure testing (Figure 6.10) 100 % PCL shows much greater stress-strain response than other samples. Elastic strain recovery can be determined from the hysteresis response to be 29.2 ± 0.4 %.

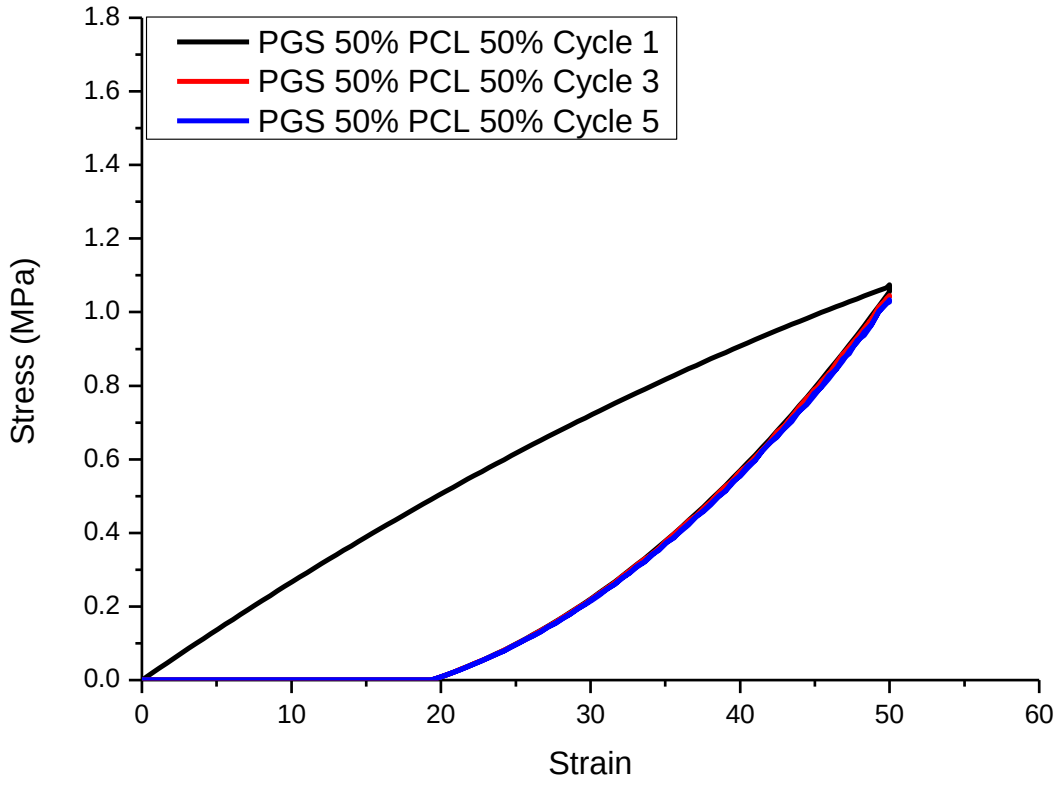

Figure 6.19 Cyclic tensile stress-strain curves of cycles 1, 3 and 5 for 50 % PGS/PCL based nonwoven webs.

Figure 6.19 shows the hysteresis responses of 50 % PGS/50 % PCL based nonwoven webs. The stress response is markedly decreased compared to 100 % PCL (Figure 6.18), as was previously shown in Section 6.3.9.3, however the general trend in hysteresis response is similar to that of the 100 % PCL sample. After the initial loading phase of cycle 1, the material exhibits an equilibrated stress-strain response for subsequent cycles that closely follows the relaxation phase of cycle 1. This is likely due to the structural makeup of the nonwoven sample, as the PGS material is blended with PCL, the nonwoven web exhibits similar properties to PCL. The resultant stress-strain response is decreased but elastic strain recovery has increased slightly to 30.7 ± 0.4 %.

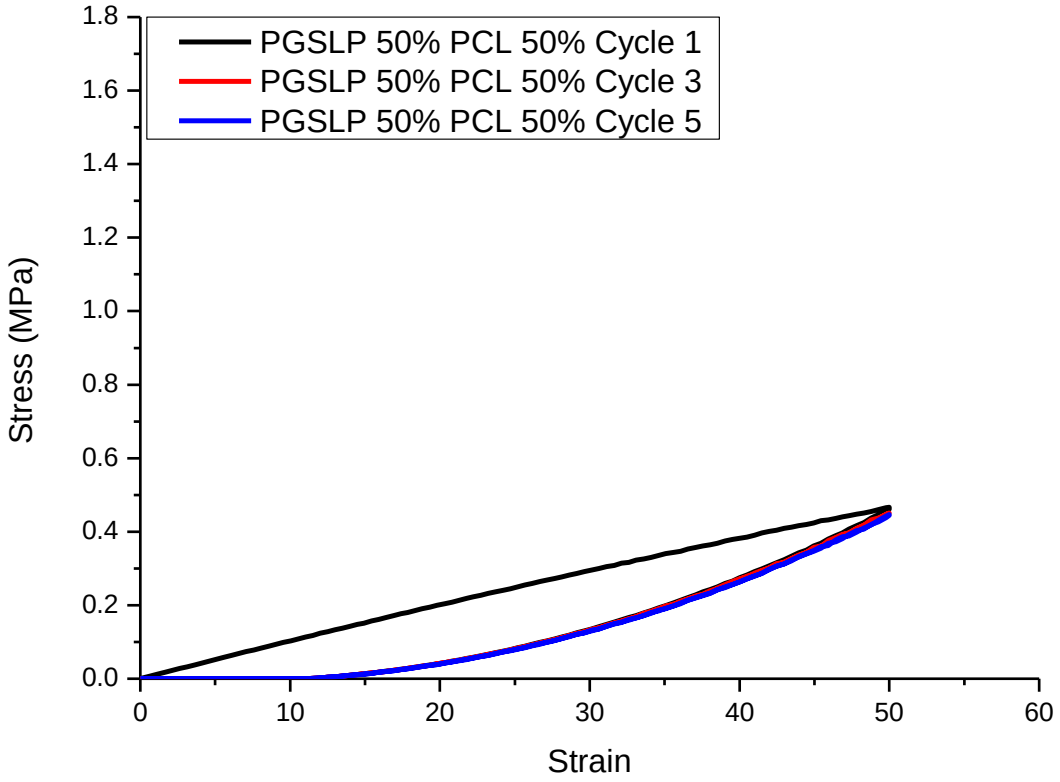

Figure 6.20 Cyclic tensile stress-strain curves of cycles 1, 3 and 5 for 50 % PGSLP/PCL based nonwoven webs.

Figure 6.20 shows the hysteresis responses of 50 % PGSLP/50 % PCL based nonwoven webs. The stress response is markedly decreased compared to 100 % PCL (Figure 6.18) and 50 % PGS/50 % PCL (Figure 6.19) based nonwoven webs, as was previously shown in Section 6.3.9.3. The same trend applies to the hysteresis response as had previously been observed in 100 % PCL and the 50 % PGS based nonwoven webs (Figure 6.18 and Figure 6.19). After the initial loading phase of cycle 1, the material exhibits an equilibrated stress-strain response for subsequent cycles that closely follows the relaxation phase of cycle 1. This is again likely due to the structural makeup of the nonwoven sample. The resultant stress-strain response is decreased but elastic strain recovery has increased to 38.5 ± 0.4 %.

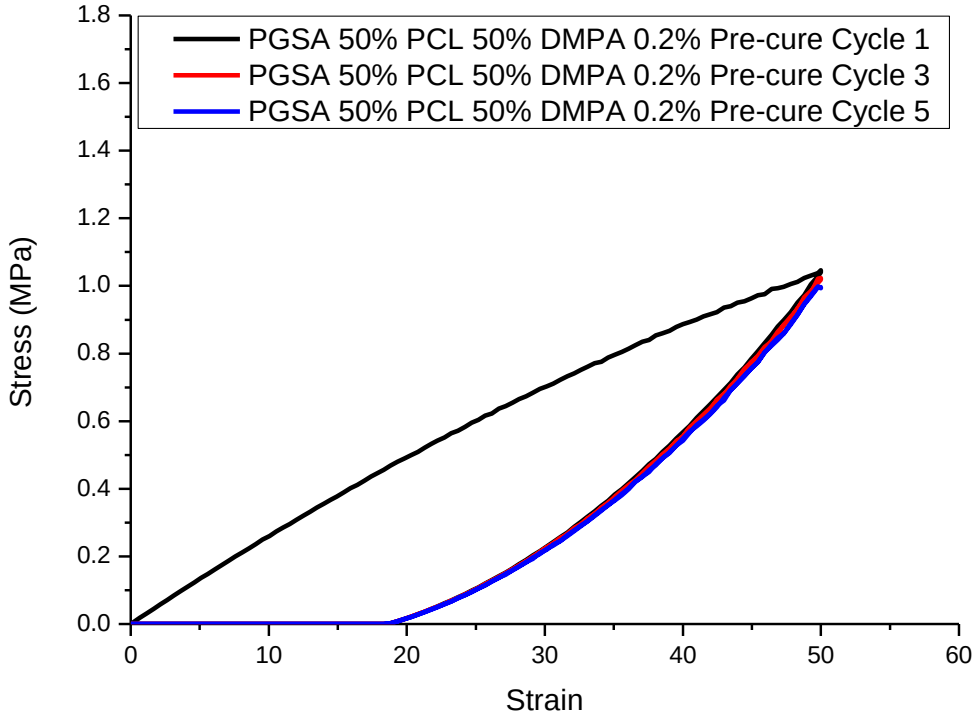

Figure 6.21 Cyclic tensile stress-strain curves of cycles 1, 3 and 5 for uncured 50 % PGSA/PCL based DMPA photoinitiator doped nonwoven webs.

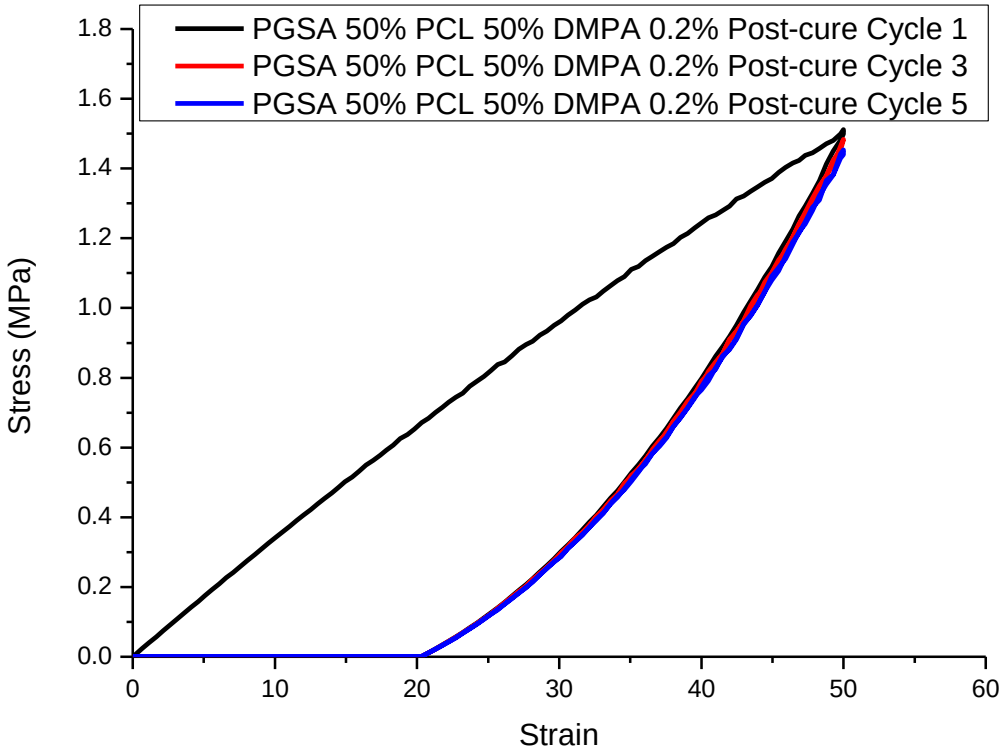

Figure 6.22 Cyclic tensile stress-strain curves of cycles 1, 3 and 5 for cured 50 % PGSA/PCL based DMPA photoinitiator doped nonwoven webs.

Figure 6.21 and Figure 6.22 show the hysteresis responses in cycles 1, 3 and 5 of 50 % PGSA/PCL based DMPA photoinitiator doped nonwoven webs before and after curing. As shown in previous tensile testing (Section 6.3.9.3) there is an increase stress response for samples post curing however, the same trend of equilibration after the first loading cycle is observed. A decrease of 1.5 % in elastic strain recovery is observed between the uncured and cured samples from 31.2 ± 0.5 to 29.7 ± 0.4 % respectively. This is likely due to the increased crosslink density, meaning the material shows less elastic behaviour and so upon deformation there is less relaxation to the original structure.

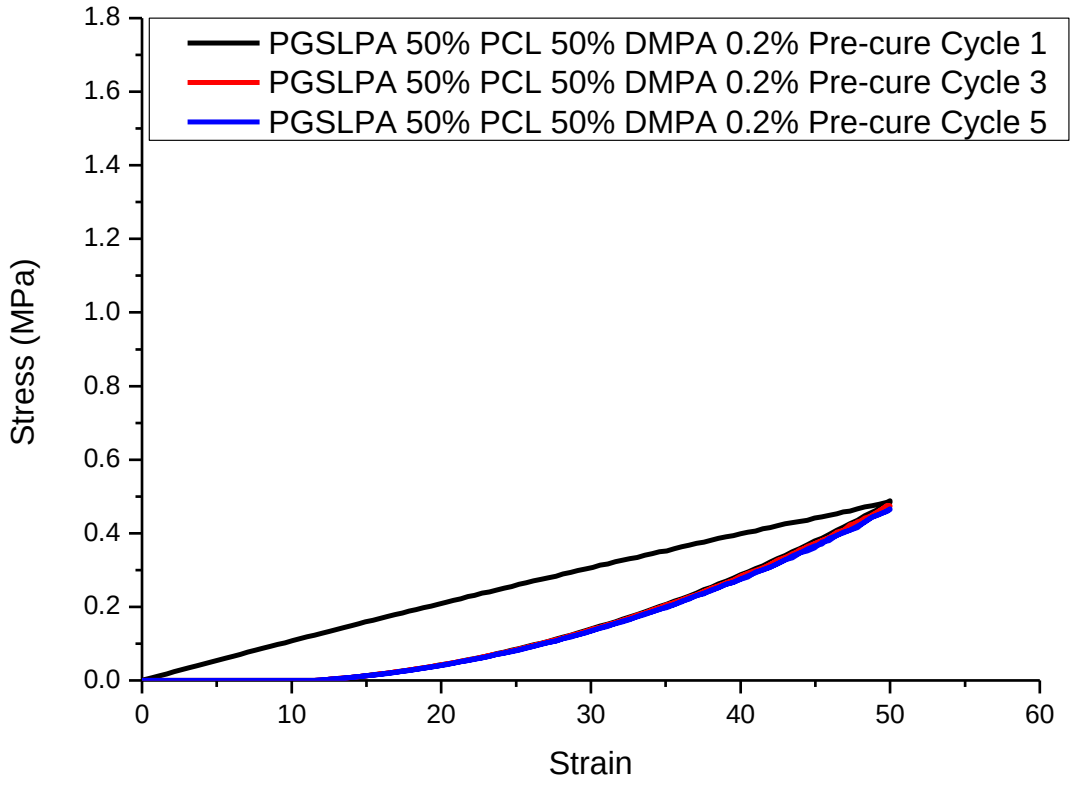

Figure 6.23 Cyclic tensile stress-strain curves of cycles 1, 3 and 5 for uncured 50 % PGSLPA/PCL based DMPA photoinitiator doped nonwoven webs.

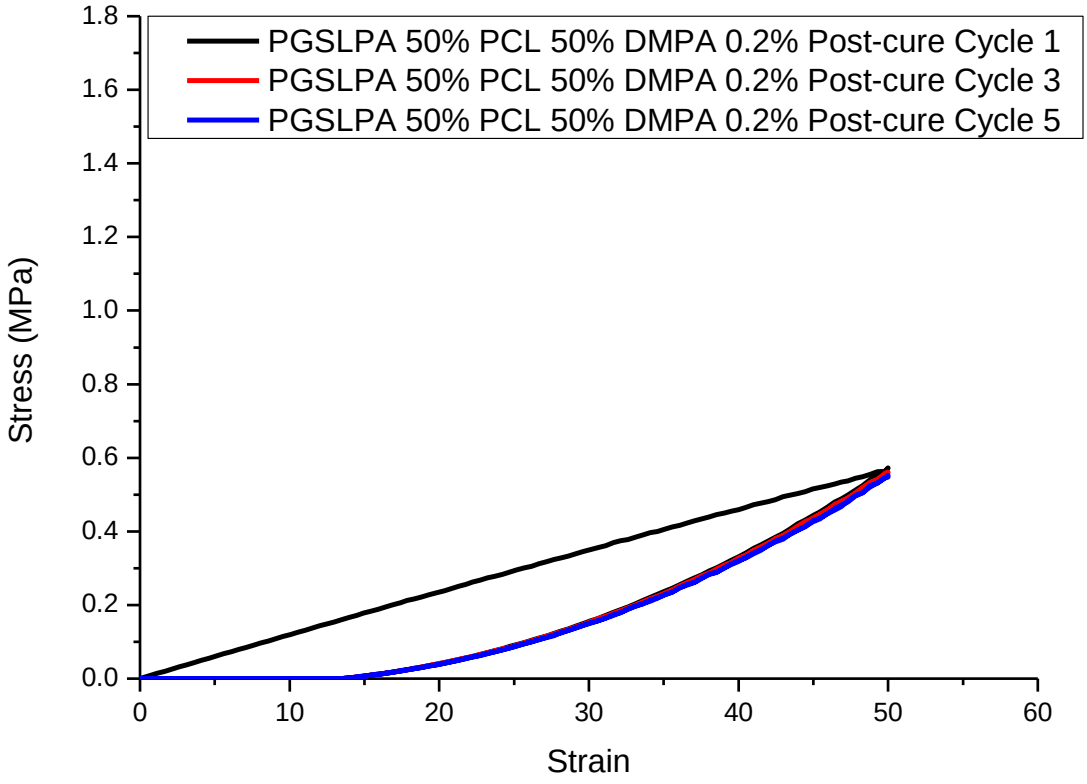

Figure 6.24 Cyclic tensile stress-strain curves of cycles 1, 3 and 5 for cured 50 % PGSLPA/PCL based DMPA photoinitiator doped nonwoven webs.

Figure 6.23 and Figure 6.24 show the hysteresis responses in cycles 1, 3 and 5 of 50 % PGSLPA/PCL based DMPA photoinitiator doped nonwoven webs before and after curing. As shown in previous tensile testing (Section 6.3.9.3) there is an increase stress response for samples post curing however, the same trend of equilibration is observed as with other samples. A decrease of 2.5 % in elastic strain recovery is observed between the uncured and cured samples from 38.0 ± 0.4 to 35.5 ± 0.4 % respectively. This is again likely due to the increased crosslink density, meaning the material shows less elastic behaviour and so less relaxation to original structure upon unloading.

Table 6.4 Energy dissipation values for cycle 1 of nonwoven web tensile fatigue testing.

Nonwoven Web	Energy Dissipated
PCL 100%	30.4
PGS 50% PCL 50%	16.6
PGSLP 50% PCL 50%	5.5
PGSA 50% PCL 50% DMPA 0.2% Pre-cure	15.8
PGSA 50% PCL 50% DMPA 0.2% Post-cure	21.7
PGSLPA 50% PCL 50% DMPA 0.2% Pre-cure	5.7
PGSLPA 50% PCL 50% DMPA 0.2% Post-cure	6.6

The hysteresis responses show that the PCL content of the nonwoven webs dictates the deformation behaviour of the material. The general trend of permanent deformation after the first loading cycle is present in all the stress-strain responses, with the stress increasing relative to what material is blended with the PCL in the nonwoven web. Inclusion of material with photo crosslinking functionality such as PGSA and PGSLPA enables an increase in the stress response by curing the material, this could provide an effective means of modulating the ultimate stress and modulus properties of the produced nonwoven web. Increasing the photo crosslinking potential within the structure and then curing for different lengths of time could allow control the potential increase in ultimate stress.

Determination of the energy of dissipation for the samples in cycle 1 (Table 6.4) showed that PCL was capable of dissipating a far larger amount of energy than the other nonwoven web samples at a fixed strain deformation, this is due to the greater stress-strain response PCL exhibits compared to other nonwoven webs. Photo crosslinking of the DMPA photoinitiator doped nonwoven webs produced increased energy dissipation, with PGSA/PCL and PGSLPA/PCL based materials showing increases of 37.4 % and 20.1 % respectively which is a similar increase observed in tensile maximum stress (Section 6.3.9.3).

6.3.9.5 Contact Angle Measurements

Hydrophilicity of materials is important for biomedical applications as it improves adhesion and cell proliferation. A material that is intended to act as a structural support composite and allow the body to regenerate lost tissue relies on the degree to which it enables the patients tissue to integrate with its structure, this ultimately determines the efficacy of the implant.

Table 6.5 Table of contact angle measurements and standard deviations.

Nonwoven web	**Θμ**	**σ**
PCL 100	125.48	1.28
PGS 50% PCL 50%	68.93	1.56
PGS 62.5% PCL 37.5%	59.66	0.70
PGS 71.4% PCL 28.6%	55.97	0.52
PGSA 50% PCL 50%	69.79	0.67
PGSA 62.5% PCL 37.5%	59.06	1.67
PGSA 71.4% PCL 28.6%	55.97	0.52
PGSLP 50% PCL 50%	0.00	0.00
PGSLP 62.5% PCL 37.5%	0.00	0.00
PGSLP 71.4% PCL 28.6%	0.00	0.00
PGSLPA 50% PCL 50%	0.00	0.00
PGSLPA 62.5% PCL 37.5%	0.00	0.00
PGSLPA 71.4% PCL 28.6%	0.00	0.00
PGSA 50% PCL 50% DMPA 0.2%	70.53	1.39
PGSLPA 50% PCL 50% DMPA 0.2%	0.00	0.00
PGSA 50% PCL 50% DMPA 0.2% Cured	87.18	3.46
PGSLPA 50% PCL 50% DMPA 0.2% Cured	0.00	0.00

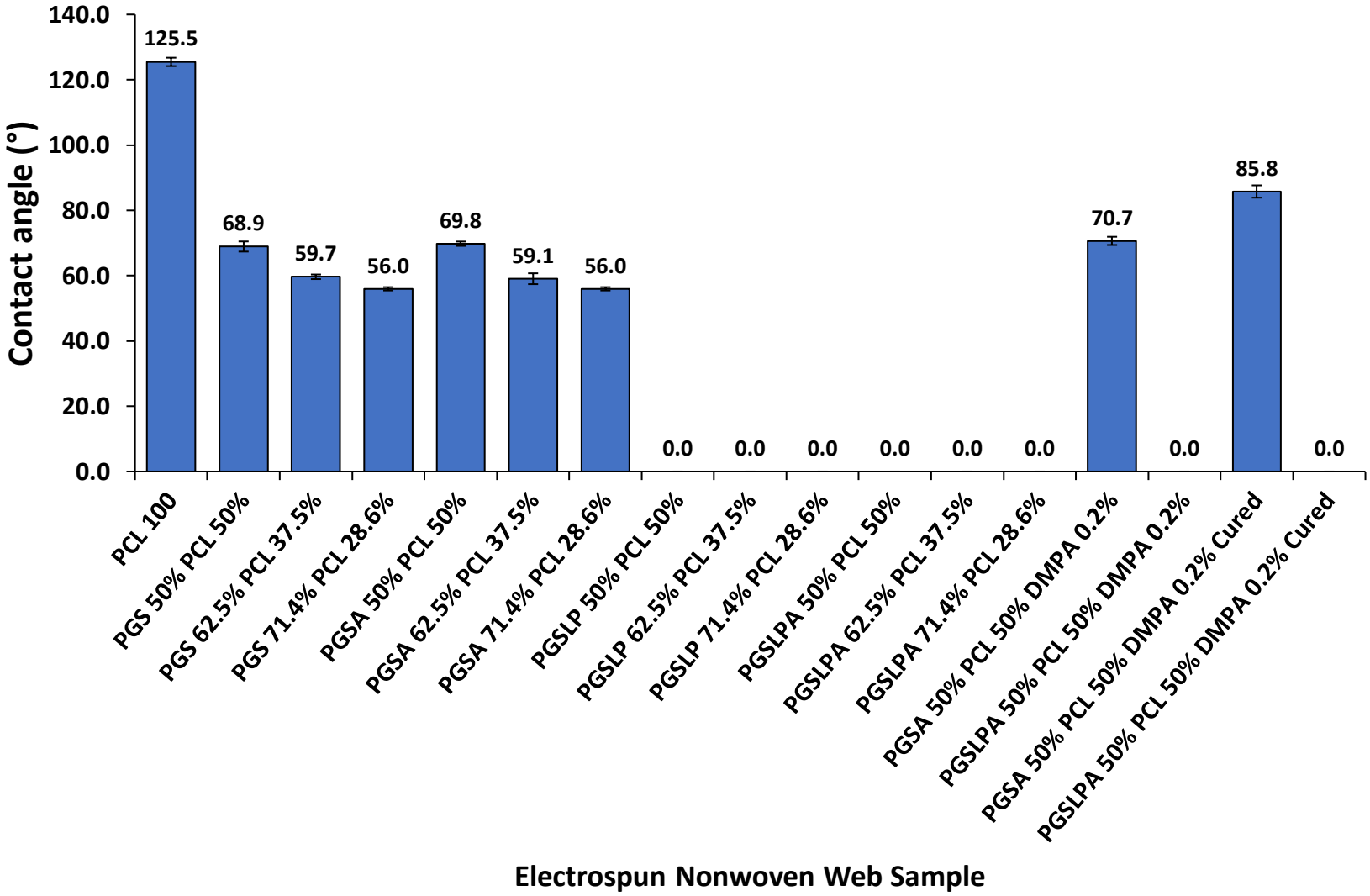

Figure 6.25 Contact angle measurements of nonwoven webs.

The contact angle measurements (Table 6.5 and Figure 6.25) show that PGSLP was successful in being a hydrophilic derivative of PGS, with the nonwoven webs wetting out instantly and thus having a contact angle of 0. In trends seen in both PGS and PGSA containing nonwoven webs, an increase in their content imparted increased hydrophilic behaviour to the structure. This is expected as reducing the PCL content, which is a much more hydrophobic material than PGS and PGSA, reduces the overall hydrophobic nature of the material.

Photo crosslinking functionality was also investigated for its effects on hydrophilicity, whereby DMPA photoinitiator doped PGSA and PGSLPA nonwoven webs were tested before and after curing. PGSA based nonwoven webs experienced an increase in contact angle after photo crosslinking from 70.4 to 84.9 °, this is due to the increased crosslink density. PGSLPA retained its exceptional hydrophilic behaviour after photo crosslinking, retaining a contact angle of 0 °.

The contact angle measurements demonstrate that the novel PGSLP based derivates have excellent hydrophilic behaviour, this is characterised by them wetting instantly with a contact angle unable to be measured. This hydrophilic behaviour is advantageous in biomedical implant application, as it allows for good surface interactions between the material and biological tissue, which creates good adhesion and ensures implant performance. Another advantage of this hydrophilic behaviour means that inclusion of the nonwoven webs into a hydrogel composite as a fibre reinforcement phase allows for good interfacing interactions with the bulk amorphous phase, allowing for a composite material with good structural integrity as there is adhesion interaction between the phases.

6.3.9.6 Degradation Studies

Degradation of polymers is influenced by their molecular structure, PGS and PGSLP contain ester bonds which are susceptible to hydrolysis. The *in vitro* degradation behaviour of PGS and PGSLP

nonwoven webs was determined by individually incubating strips in PBS buffer solution (pH 7.4, 25 °C).

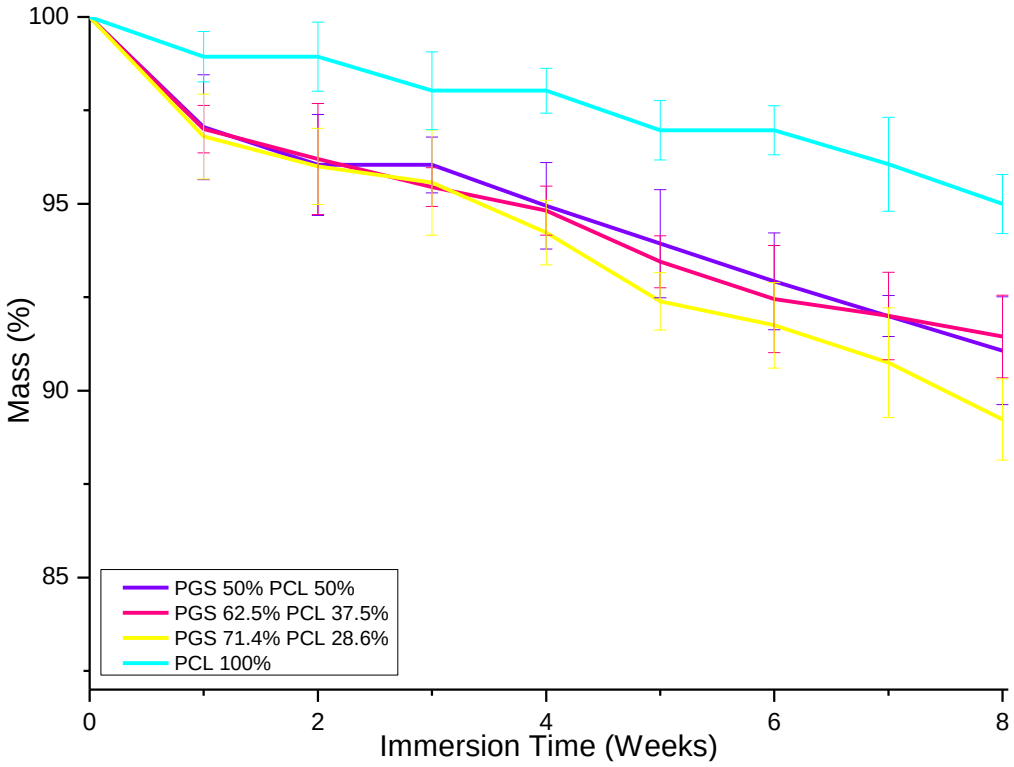

Figure 6.26 Degradation profile of PGS based nonwoven webs submerged in PBS buffer solution. 100 % PCL included as a control comparison sample.

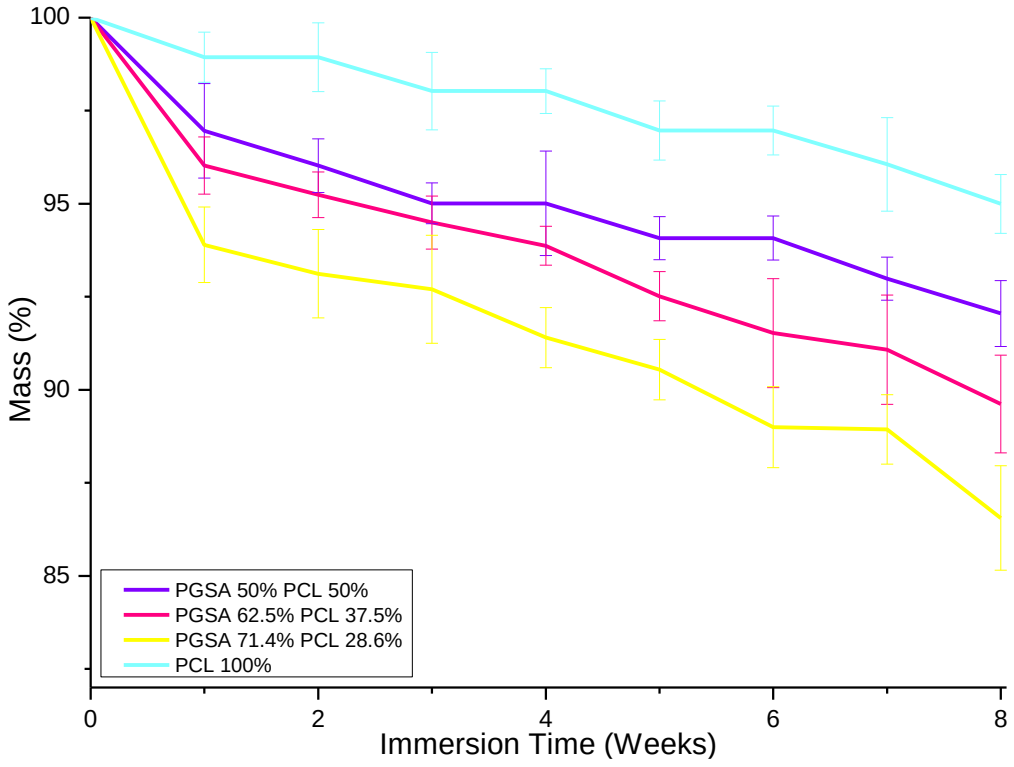

Figure 6.27 Degradation profile of PGSA based nonwoven webs submerged in PBS buffer solution. 100 % PCL included as a control comparison sample.

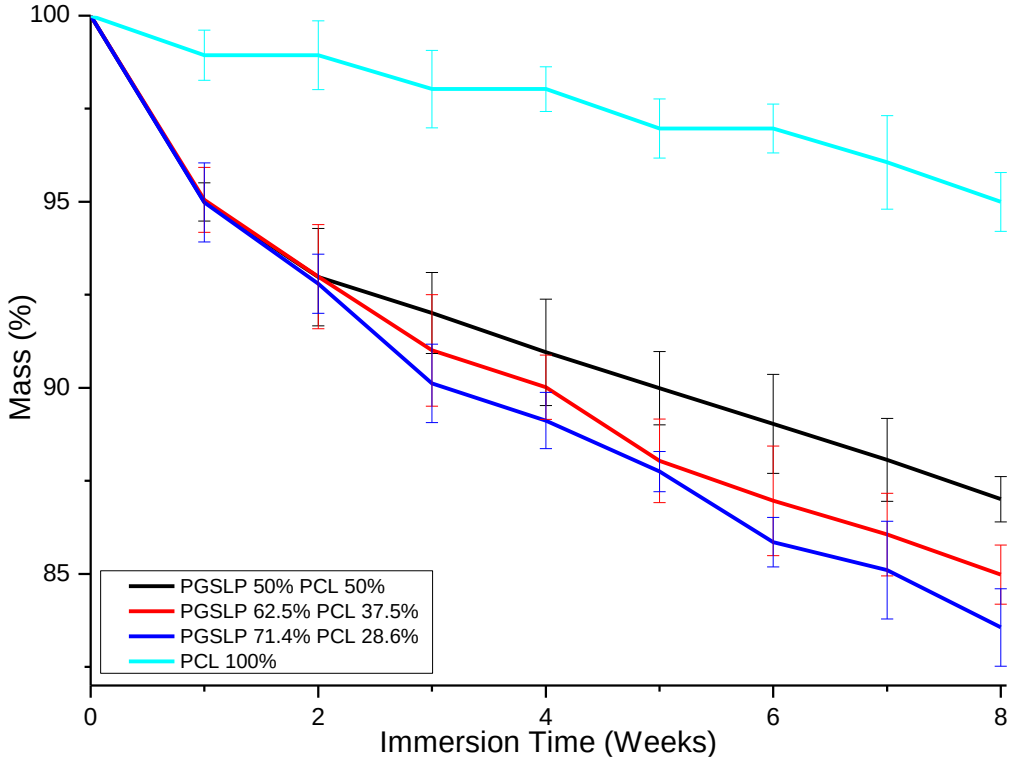

Figure 6.28 Degradation profile of PGSLP based nonwoven webs submerged in PBS buffer solution. 100 % PCL included as a control comparison sample.

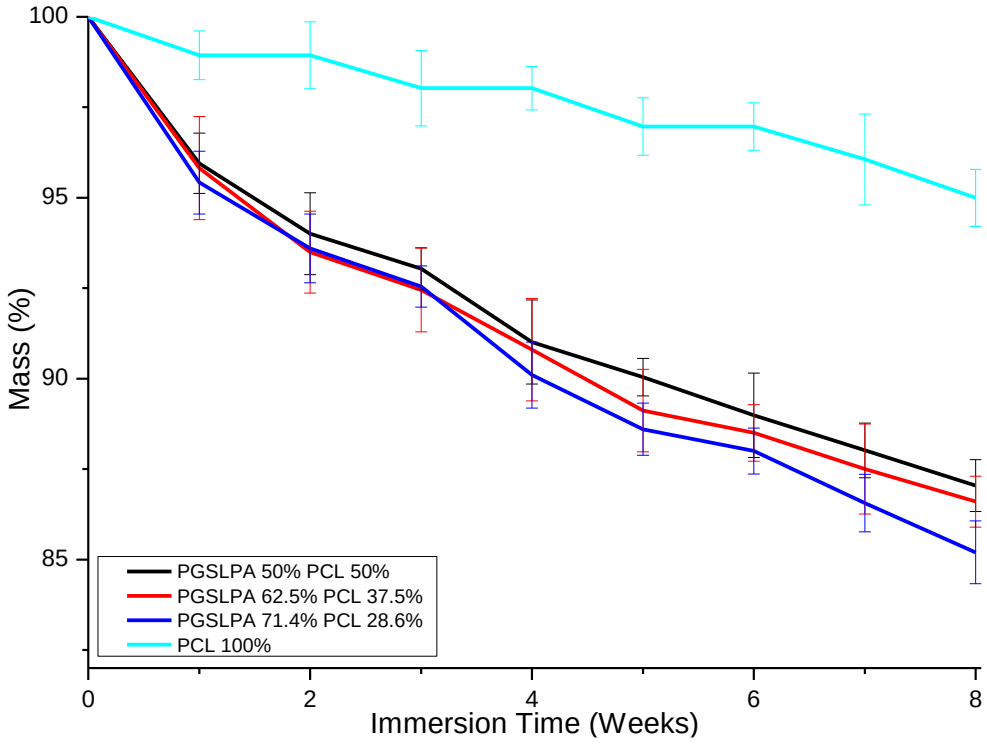

Figure 6.29 Degradation profile of PGSLPA based nonwoven webs submerged in PBS buffer solution. 100 % PCL included as a control comparison sample.

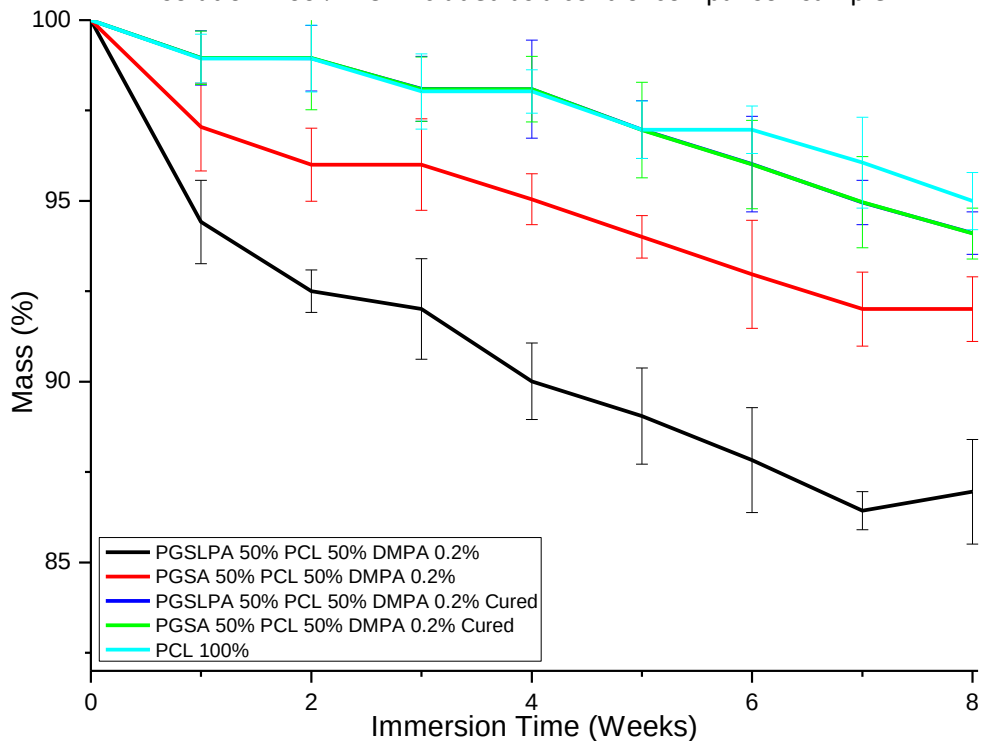

Figure 6.30 Degradation profile of DMPA doped PGSA and PGSLPA based nonwoven webs submerged in PBS buffer solution, before and after photocuring. 100 % PCL included as a control comparison sample.

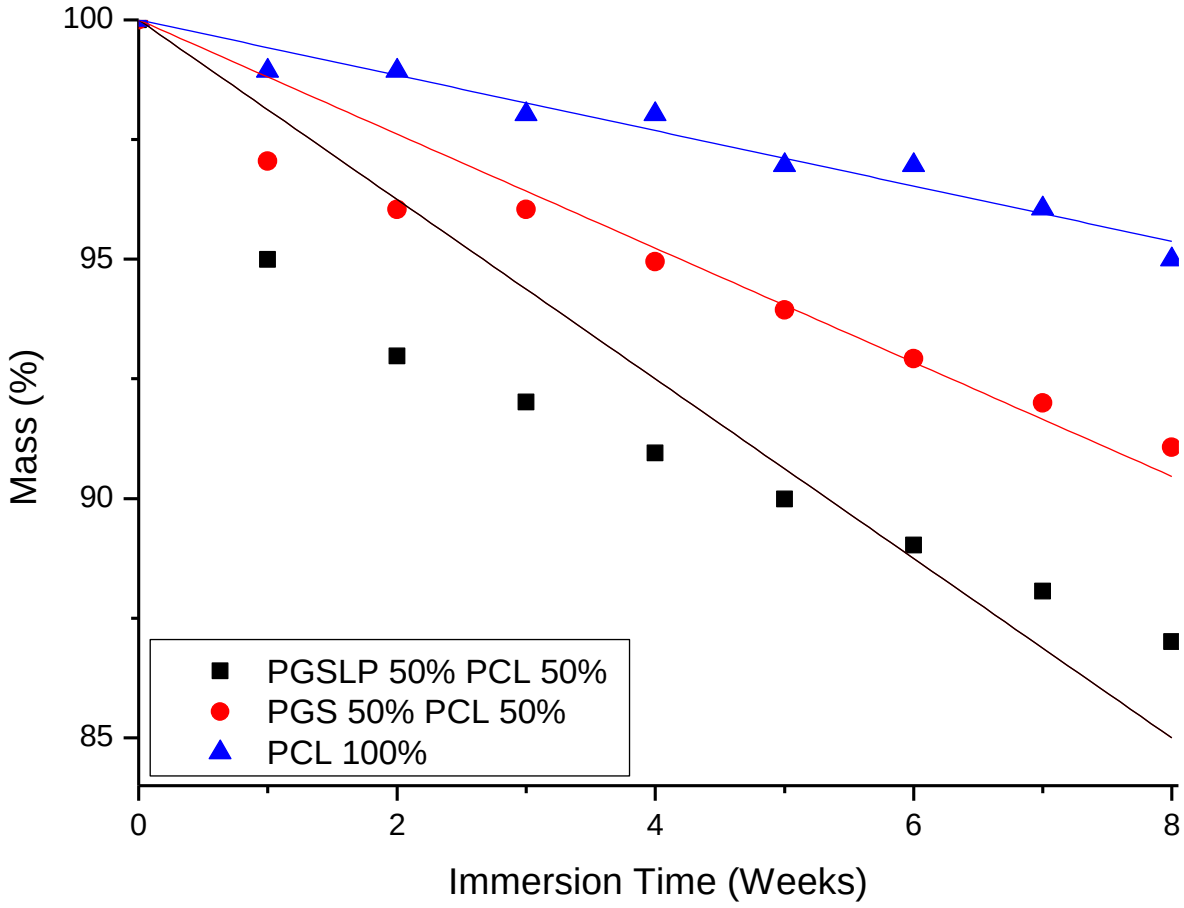

Figure 6.31 Linear fit plots for PGS, PGSLP and PCL based nonwoven webs.

Degradation profiles of the PGS, PGSLP, and DMPA doped electrospun webs (Figure 6.26 to Figure 6.30) showed that the PGSLP derivates degraded faster than PGS derivates and that as the PGSLP and PGS component of the materials was increased, the rate of degradation increased, this is due to there being a large number of crosslinks present in the molecular structure of PGS which increases its stability.

Increasing the content of PGSLP in nonwoven webs by 43% increases degradation by 5.4% over 8 weeks however increasing the percentage of PGS in webs by an equal amount only increases degradation by 1.8%. This further solidifies that the decreased crosslink density of PGSLP results in

a less stable polymer structure however the benefit is the ability to dissolve the material into an aqueous solution that can be injected instead of being cured and implanted requiring surgery.

Figure 6.31 shows the degradation profiles for 50 % PGSLP 50 % PCL, 50 % PGS 50 % PCL and 100 % PCL nonwoven webs, with linear fitting applied. The linear nature of the degradation also indicates that the erosion is principally surface rather than bulk driven, in line with the hydrophilicity of the chemical system. The materials were observed to be soft and sticky upon removal from the PBS buffer solution.

6.3.9.7 Swelling Degree

The swelling ratio of the polymers was calculated after submersion in PBS buffer solution after equilibration had been achieved. Equilibration for PCL and PGS derivatives took 6 h, equilibration for PGSLP derivatives was achieved after 1 h.

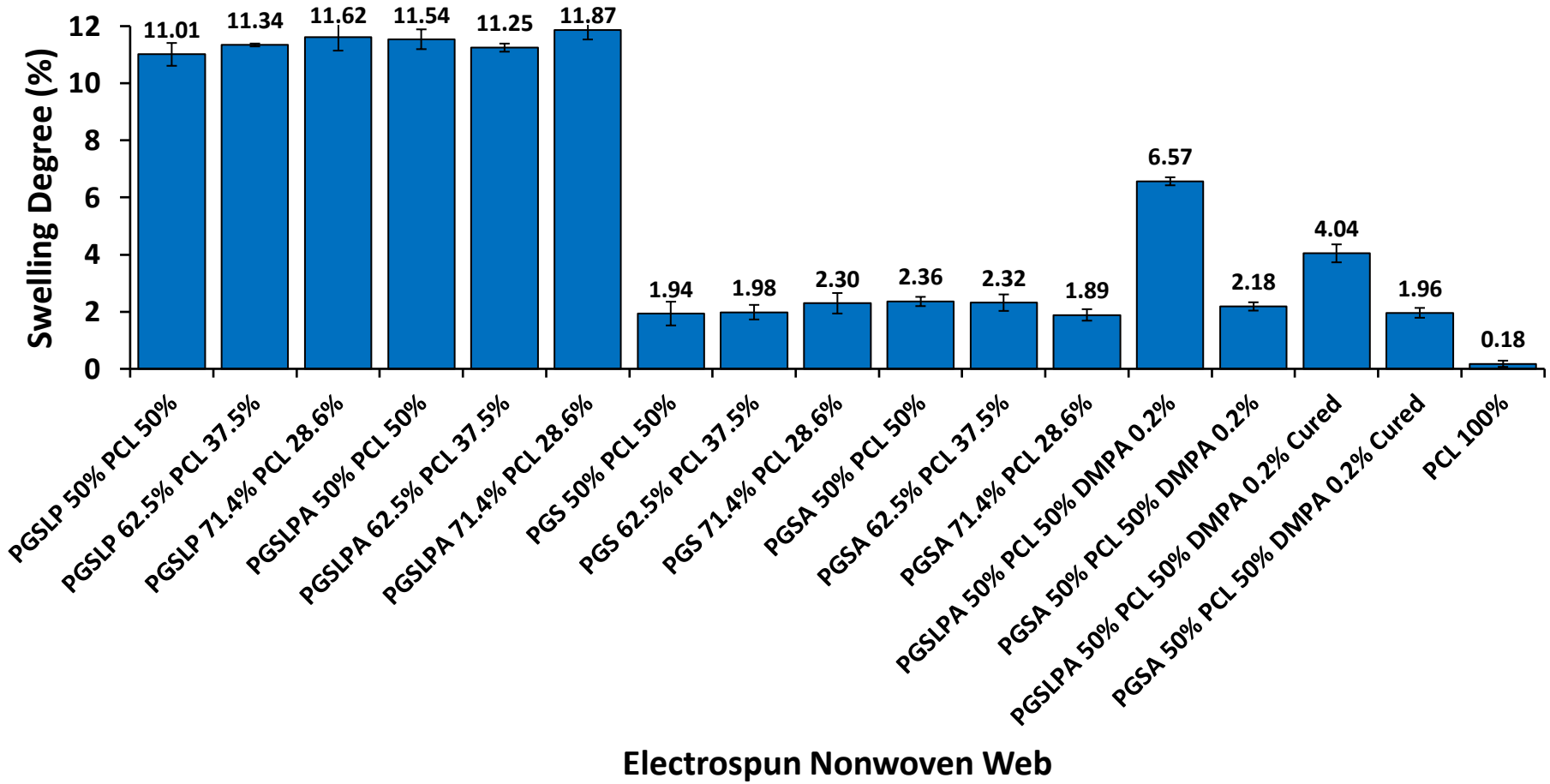

Figure 6.32 Swelling degree of the electrospun nonwoven webs when submerged in PBS buffer solution.

Figure 6.32 shows the swelling degree of the electrospun nonwoven webs. A significant increase in swelling degree between PGSLP and PGS derivatives was observed with all formulations showing a 500% increase in swelling degree when compared to PGS, this is because the hydrophilicity and decreased crosslink density of the PGSLP derivatives allows for a larger liquid absorption capacity. Inclusion of DMPA in the electrospun nonwoven web decreased swelling degree significantly in the PGSLPA nonwoven web, crosslinking of this material further decreased the swelling degree which is due to the increased crosslink density, which reduces hydrophilicity and liquid absorption capacity.

PGS derivatives exhibited increased swelling degree when compared to 100% PCL, with the crosslinked DMPA doped form showing a decrease in swelling degree.

6.3.9.8 Porosity and Fibre Diameter

Porosity of the material was measured before and after immersion into a PBS buffer solution. The change in porosity of the material post immersion for 8 weeks gives an indication of how degradation behaviour affects void space, which has a direct impact on cell penetration, proliferation, and the regenerative properties of the material.

Table 6.6 Porosity measurements before and after immersion of nonwoven webs in PBS buffer solution for 8 weeks.

Sample	Porosity Pre-Immersion (%)	Porosity Post-Immersion (%)	Δ%
PCL 100%	15.1	16.2	1.1
PGSLP 50% PCL 50%	14.3	17.0	2.7
PGSLPA 50% PCL 50%	8.3	12.2	3.9
PGS 50% PCL 50%	14.1	15.2	1.1
PGSA 50% PCL 50%	7.6	9.9	2.4
PGSLPA 50% PCL 50% DMPA 0.2%	10.5	15.9	5.4
PGSA 50% PCL 50% DMPA 0.2%	7.5	8.2	0.7
PGSLPA 50% PCL 50% DMPA 0.2% Cured	10.4	13.6	3.2
PGSA 50% PCL 50% DMPA 0.2% Cured	8.2	9.1	0.9

Table 6.6 shows that porosity increases when incubated in PBS buffer solution, degradation of the material increased void space over 8 weeks. This will have a detrimental effect on the mechanical properties but will increase the potential for cell penetration and proliferation over time, which could provide a benefit for tissue regeneration.

Surface properties such as porosity have a direct effect on the contact angle of nonwoven substrates. Due to the highly hydrophilic behaviour exhibited by PGSLP based materials, a contact angle of 0 ° is taken as the measurement (Figure 6.25,Table 6.5), as complete and instant wetting is observed. In the case of PGS based materials, an increase in porosity results in a slightly increased contact angle measurement, which could be caused by the increased swelling degree resulting in a more closed structure and allowing less fluid permeation.

DMPA doped nonwoven webs were tested with and without photo curing, when photo curing was conducted the increase in porosity was decreased due to the increased crosslink density and therefore increased material stability.

6.3.9.8.1 Fibre Diameter Analysis

Fibre diameter distributions were collected pre-immersion for comparison with samples immersed for 8 weeks in PBS buffer solution. Fibre diameter affects the mechanical properties of the nanofibrous nonwoven web, as a larger diameter fibre is more resistant to bending which can alter the properties of a composite structure where they are used as a fibre reinforcement phase.

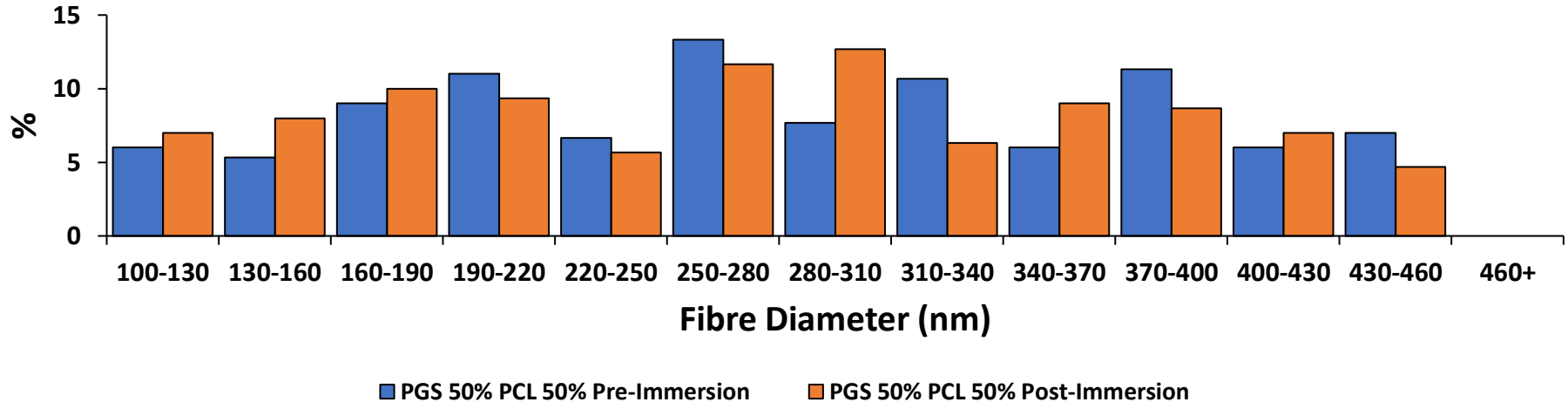

Figure 6.33 Fibre diameter distribution of PGS 50% PCL 50% electrospun nonwoven web before and after incubation in a PBS buffer solution.

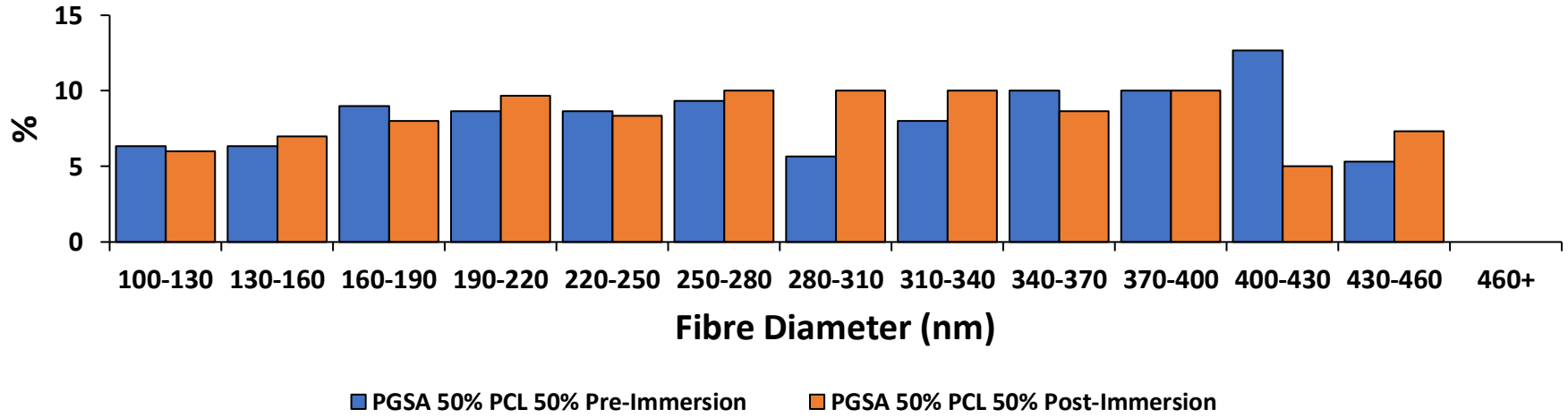

Figure 6.34 Fibre diameter distribution of PGSA 50% PCL 50% electrospun nonwoven web before and after incubation in a PBS buffer solution.

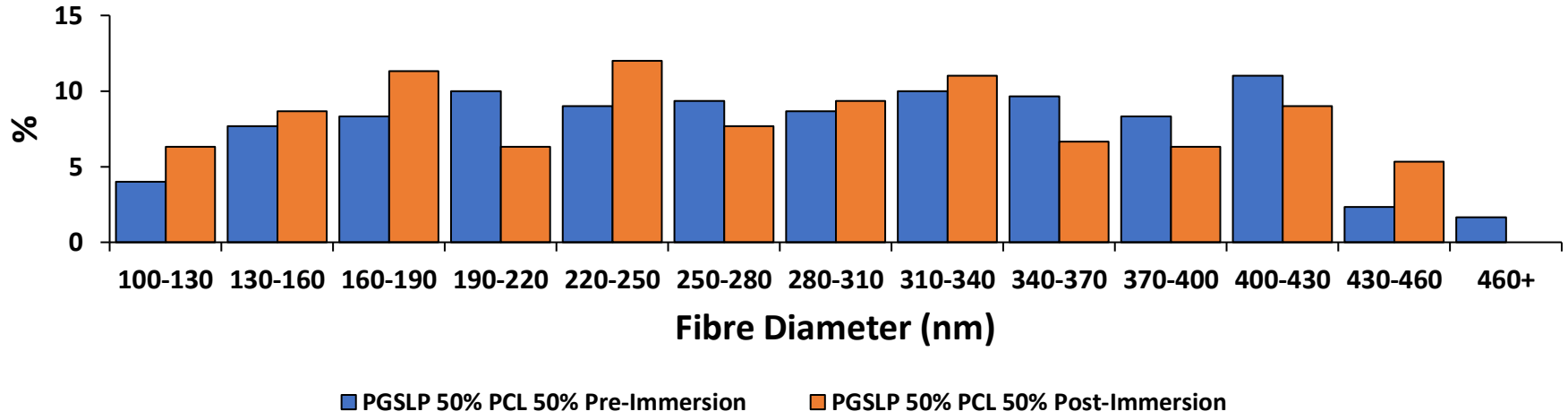

Figure 6.35 Fibre diameter distribution of PGSLP 50% PCL 50% electrospun nonwoven web before and after incubation in a PBS buffer solution.

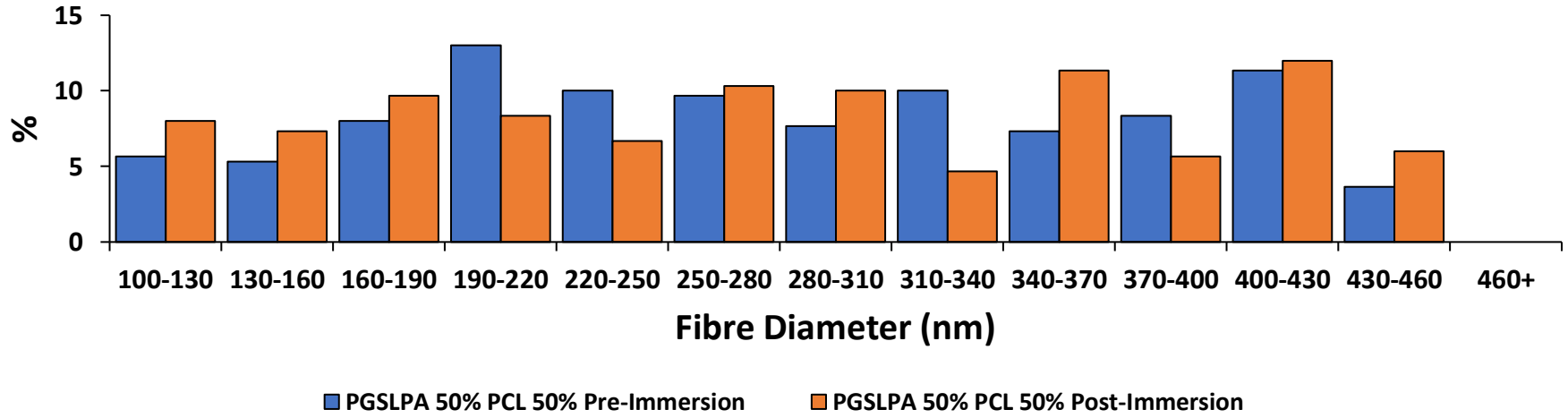

Figure 6.36 Fibre diameter distribution of PGSLPA 50% PCL 50% electrospun nonwoven web before and after incubation in a PBS buffer solution.

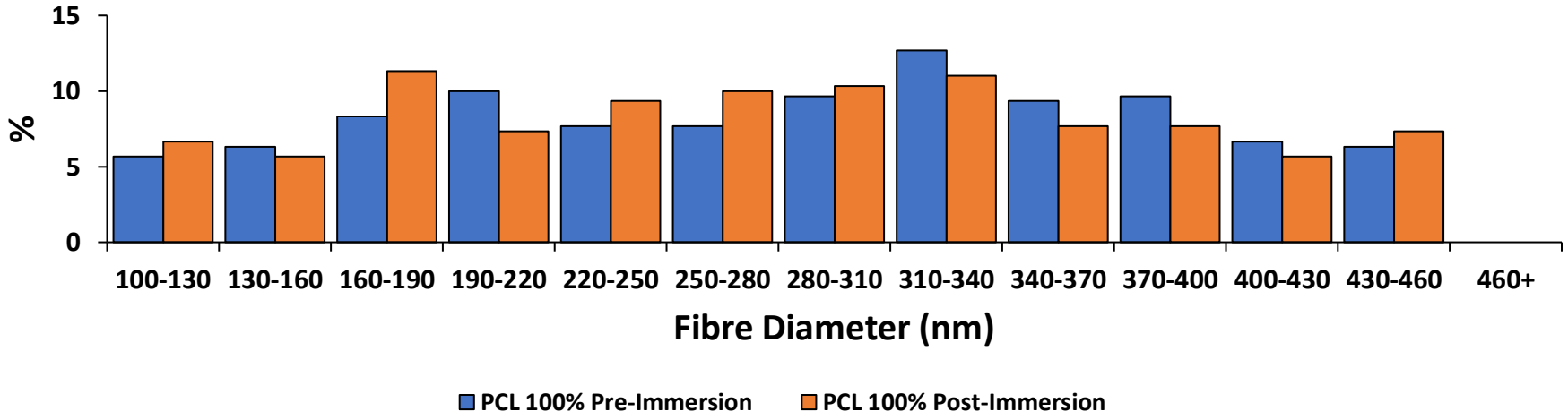

Figure 6.37 Fibre diameter distribution of PCL100% electrospun nonwoven web before and after incubation in a PBS buffer solution.

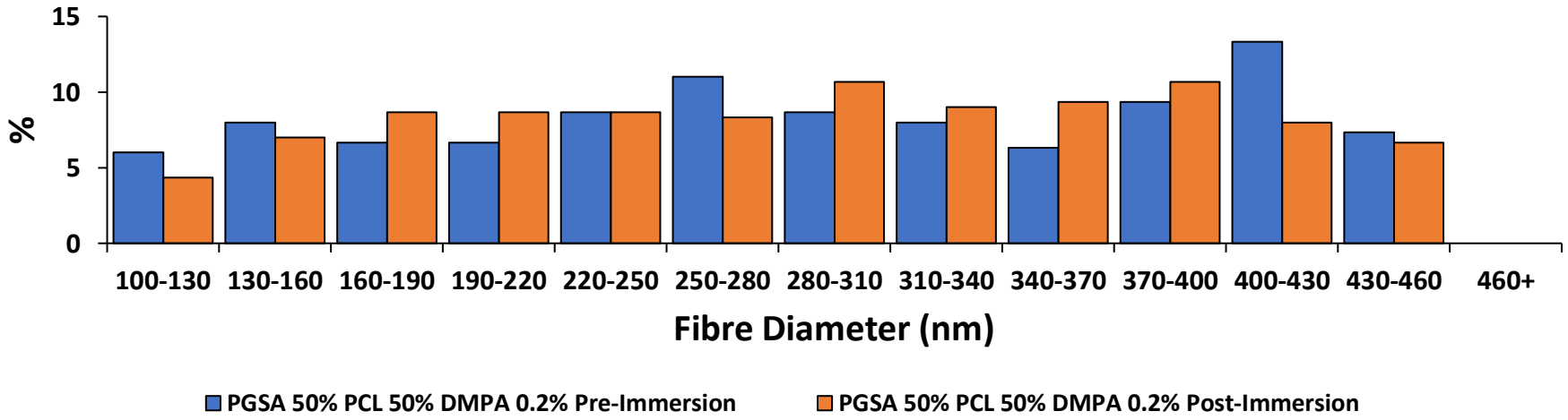

Figure 6.38 Fibre diameter distribution of PGSA 50% PCL 50% DMPA 0.2% electrospun nonwoven web before and after incubation in a PBS buffer solution.

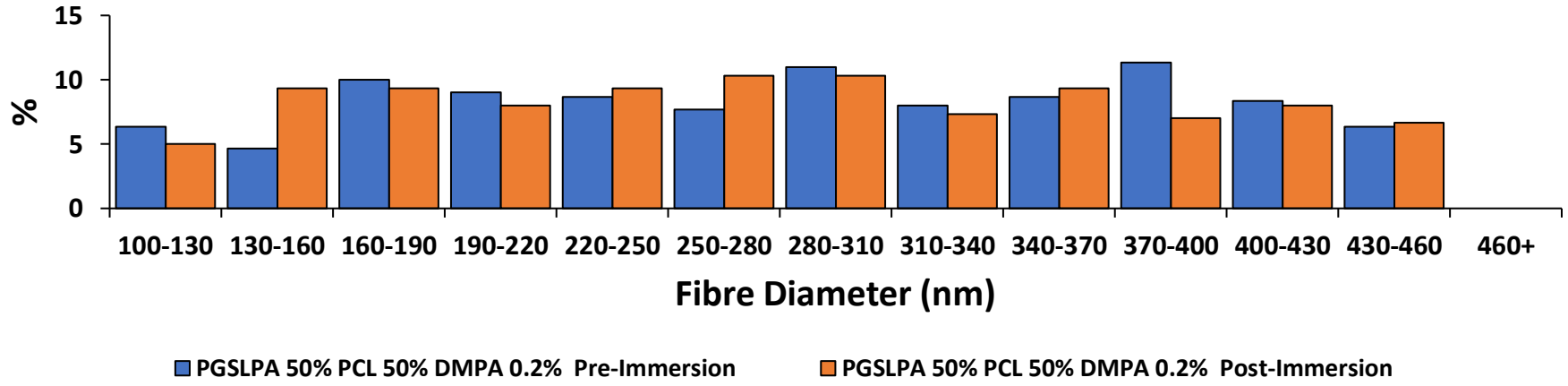

Figure 6.39 Fibre diameter distribution of PGSLPA 50% PCL 50% DMPA 0.2% electrospun nonwoven web before and after incubation in a PBS buffer solution.

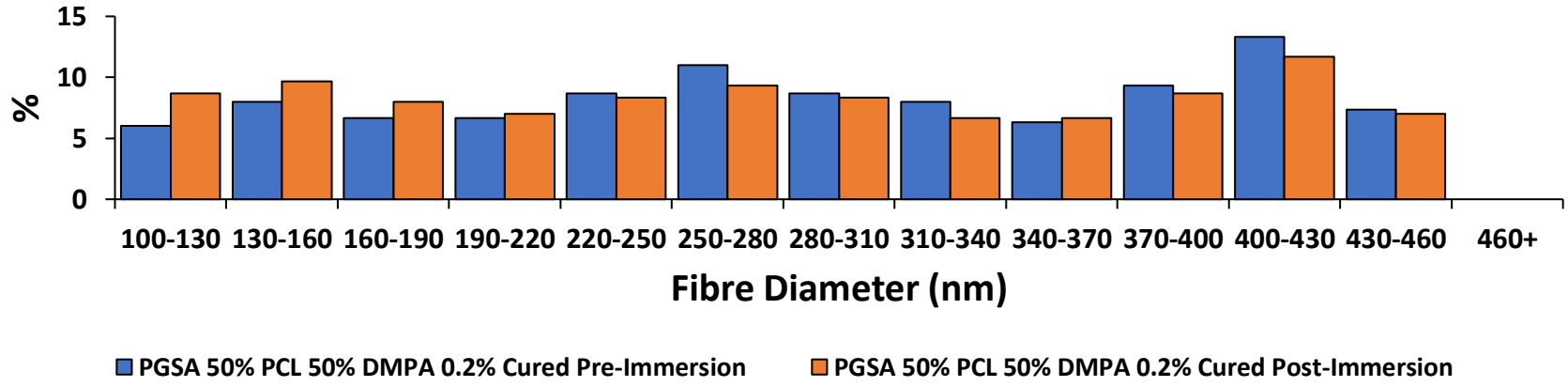

Figure 6.40 Fibre diameter distribution of PGSA 50% PCL 50% DMPA 0.2% cured electrospun nonwoven web before and after incubation in a PBS buffer solution.

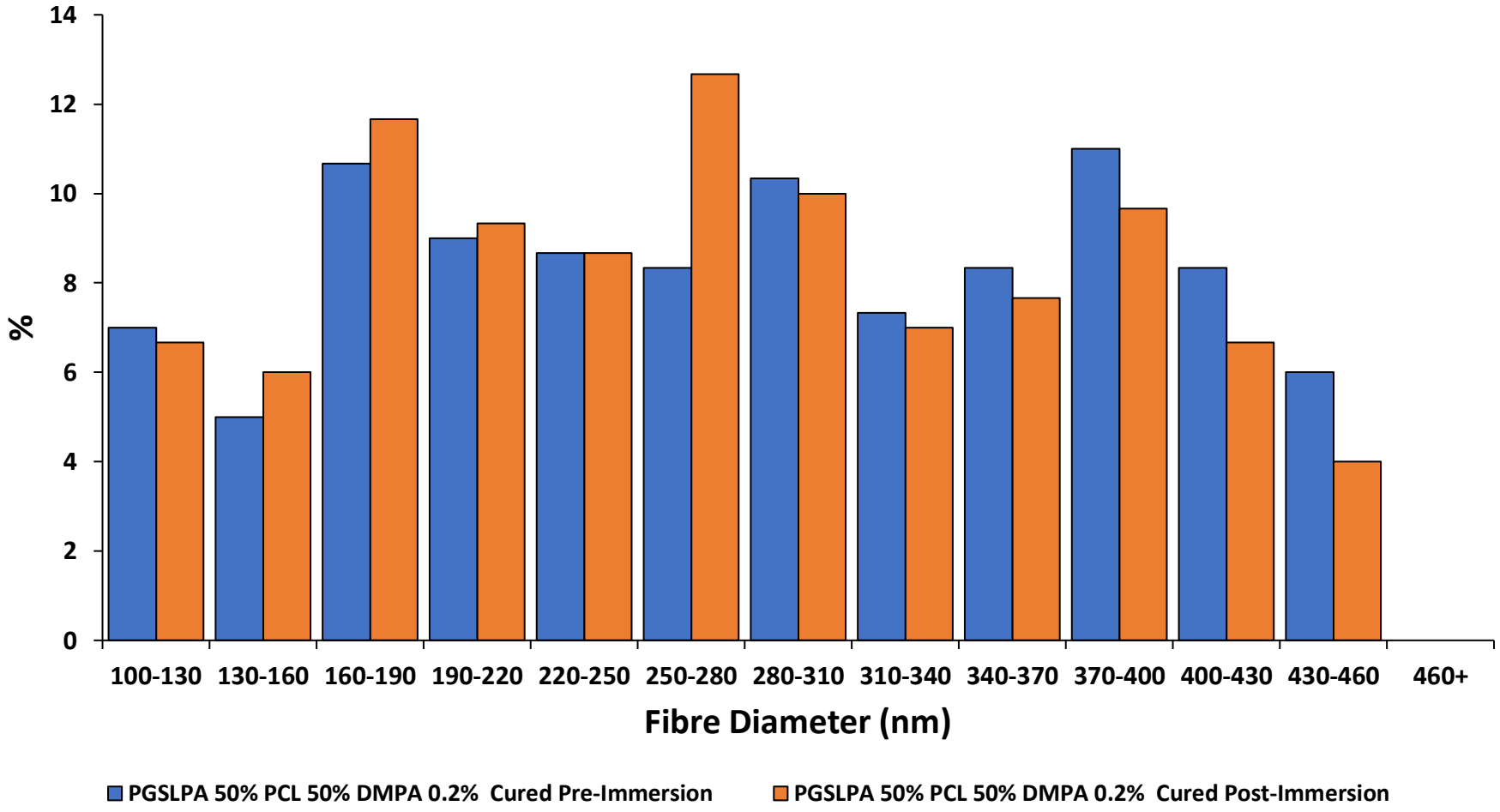

Figure 6.41 Fibre diameter distribution of PGSLPA 50% PCL 50% DMPA 0.2% cured electrospun nonwoven web before and after incubation in a PBS buffer solution.

Figure 6.33 to Figure 6.41 show the fibre diameter distributions of electrospun nonwoven webs before and after incubation in a PBS buffer solution.

Table 6.7 Mean fibre diameters of electrospun nonwoven webs before and after incubation for 8 weeks in a PBS buffer solution.

Sample	Pre-immersion		Post-immersion	
	Mean Diameter (nm)	σ (nm)	Mean Diameter (nm)	σ (nm)
PCL 100%	279.56	93.955	277.87365	91.2
PGSLP 50% PCL 50%	288.84	93.765	279.3483	94.905
PGSLPA 50% PCL 50%	281.88	90.725	273.6063	90.345
PGS 50% PCL 50%	287.1	92.91	281.358	90.345
PGSA 50% PCL 50%	283.62	93.195	278.1999	90.63
PGSLPA 50% PCL 50% DMPA 0.2%	282.75	90.82	274.4676	91.295
PGSA 50% PCL 50% DMPA 0.2%	287.68	91.485	281.9322	92.815
PGSLPA 50% PCL 50% DMPA 0.2% Cured	281.01	91.485	278.487	91.865
PGSA 50% PCL 50% DMPA 0.2% Cured	283.91	92.055	281.6451	91.865

Post-immersion fibre diameters are decreased in all samples however, although there is no statistical significance ($P>0.05$).

6.4 Summary

Forming electrospun fibres from PGSLPA and derivative materials was found to be feasible assuming a carrier polymer is commixed in a HFIP spinning solution. The introduction of a photocuring agent into the spinning solution before fibre formation was also successfully accomplished, such that both fibres and hydrogels could be produced with photocuring capabilities.

Tensile testing of the nonwoven webs showed that PGSLP derivatives are significantly weaker than PGS, which is to be expected when increasing molecular chain length by inclusion of a relatively high molecular weight PEG component. The modification of the polymer structure through inclusion of

a photoinitiator such as DMPA allows for curing after fibre formation, increasing the fibre modulus and strength, but decreasing the elastic response of the material.

The nonwoven webs also showed excellent hydrophilic behaviour, with all PGSLP derivatives instantly wetting out. This is especially beneficial in the context of a physiological setting, as hydrophilic behaviour enables surface adhesion between biological tissue and the polymer. The degree of swelling in PGSLP is also significantly increased when compared to PGS derivatives. The electrospun PGSLP webs showed up to a 500 % increase in swelling, due to the increased chain length and hydrophilicity.

Porosity and fibre diameter measurements also showed that PGSLPA webs when doped with a suitable photoinitiator (DMPA) have a reduced degradation rate compared to PGSLP, therefore tailoring of the degradation rate through alteration of the crosslink density is feasible.

Successful spinning of sub-micron PGSLPA fibres with photocuring functionality provides interesting opportunities for its use in clinical applications, the material demonstrated excellent adhesion and hydrophilicity behaviour, and the capability to tune mechanical, degradation and hydrophilic properties through alterations to the formulation and crosslink density allows for the material to be changed to specific needs.

Chapter 7

Composite PGSLPA Nanofibre-Hydrogel Formation

7.1 Introduction

This chapter explores the combination of PGS-based nanofibres and PGS-based hydrogel polymer in a composite structure, and the associated bulk material mechanical properties. The purpose was to determine the feasibility of combining the two components, and the extent to which mechanical properties are affected. Such fibre-hydrogel composites containing PGS-based polymers have not been previously manufactured or evaluated, but they may have potential applications as foot plantar filling materials, particularly if the presence of fibres allows modulation of bulk mechanical properties.

7.2 Fibre reinforcement

Fibre reinforcement of polymers (Figure 7.1) is a highly desirable and promising method of improving the physical and mechanical properties of polymer networks. Fibre reinforced composites are present in nature such as cartilage, a collagen fibre-reinforced proteoglycan gel with relevant mechanical properties.[189] Natural fibre reinforcement is frequently found in human tissue where a soft extracellular matrix comprised of tissue specific cells has interpenetrating proteins organised into fibrils.[190] These tissues have remarkable mechanical properties; consequently inspiration should be taken from such networks to inform the design of new multifunctional systems for regenerative medicine. Elastin, fibrin and collagen are extremely common throughout the human body each providing different strength properties; elastin and fibrin provide tissue resiliency while collagen provides robust tensile properties.[154]

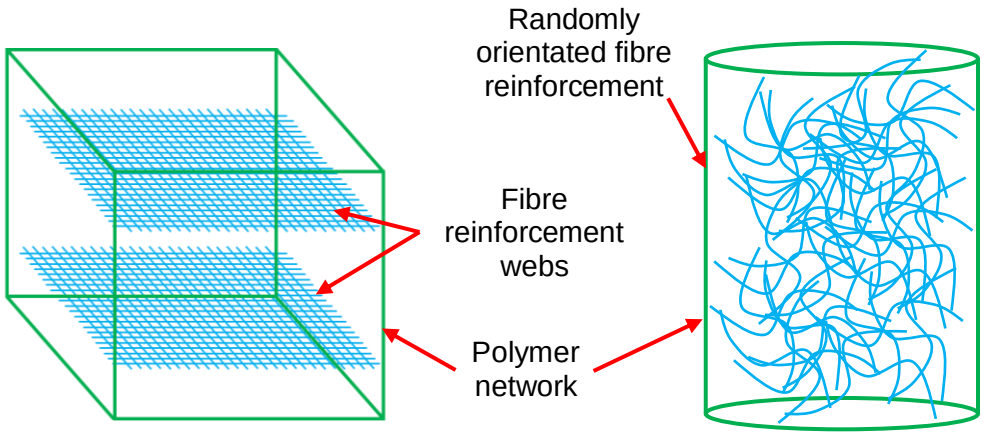

Figure 7.1 Schematic diagram of a fibre reinforced composite materials.

The mechanical properties of fibre-reinforced composites are affected by the fibre orientation, fibre dimension and volume fraction; therefore, by adjusting these parameters, the mechanical properties can be tuned to be more closely biomimetic to the tissues relating to the intended application.[191-193]

Fibre orientation is also an important factor when regeneration of native tissue is intended, since orientation affects the way in which cells grow. Cells grown on aligned fibre arrangements were found to adopt an elongated morphology to match the orientation of the fibre, whereas randomly orientated fibre results in randomly oriented cells with polygonal morphology. [192] The mechanical properties of composites can be greatly affected by orientation of fibres used for reinforcement. Elastic modulus, yield strength and ultimate stress increase with fibre reinforcement although more so with aligned orientations [192], differences in directional orientation in aligned composites (aligned in different directions) also affects mechanical properties although this is related directly to the axis of stress application[194]. Aligned fibre reinforced composites are therefore inherently anisotropic, whereby their mechanical properties will heavily depend on how stress is applied, specifically in what direction in relation to the direction of fibre reinforcement. Randomly oriented

fibre reinforced composites will therefore have no preferential stress directions and will be capable of distributing forces in a uniform manner regardless of stress direction application.

Volume fraction of fibres is also shown to improve the elastic modulus and yield strength of resulting composite material [195, 196]. Typically, the amount of fibre present in a composite directly relates to the mechanical properties. When the fibre fraction is too high, a decrease in strength of the composite is observed due to a lack of adequate space for the polymer matrix to properly surround and adhere to the fibres.[197] Therefore the fibre fraction should be carefully controlled to allow sufficient space between fibres, so that there is uniform load transfer between the polymer matrix and fibre reinforcement network.[198] At low fibre volume fractions the matrix phase (the polymer or bulk material) constitutes the major load bearing component, once the stress applied to the composite reaches the fracture point of the matrix phase the composite will fail.[199] The load will then transfer to the fibres which at such a low volume fraction will exhibit a large increase in stress, resulting in failure, known as matrix controlled fracture. For most composites reinforced with fibre the bulk of the mechanical stress is withstood by the fibre phase[74], stress applied to the point of fibre fracture and thus composite failure is termed fibre controlled fracture.

The dimensions of the fibres present in the composite material also affects the mechanical properties. Fibre length and diameter have direct effects on the mechanical properties, due to the different extent of fibre interaction with the surrounding polymer matrix[74]. Load transmittance between the surrounding polymer network and fibre is dependent on the interfacial bond between the two phases.

7.3 Experimental

Acrylated materials provide an effective means of forming crosslinks, allowing for the modification of biomaterials to introduce photo crosslinking functionality which can be utilised in the formation

of gels. Thiol-ene click reactions are an alternative to introducing photo crosslinking functionality. A click reaction satisfies certain characteristics; modularity; insensitivity to solvent parameters and oxygen; high chemical yields; stereospecificity and a thermodynamic driving force which favours a single reaction product[200]. These reaction characteristics provide an attractive alternative to acrylation procedures, which are solvent and oxygen sensitive, producing acrylic acid as a by-product and gelation can occur if reaction temperature is not controlled.

Norbornene photo crosslinking functionality was introduced (Sections 5.2.1.2 and 5.2.1.3) to PGSLP and PGS derivatives *via* a steglich esterification procedure. DCC and DMAP were used as coupling reagents to graft a norbornene carboxylic acid to the molecular structure at hydroxyl functional reactive sites. Following this a bi-terminated thiol, 2,2'-(Ethylenedioxy)diethanethiol and photoinitiator, Irgacure 2959, were used with and without a reducing agent in a photo crosslinking experiment. Standard protocol employed for all formulations and investigations is detailed in Section 3.2.8.

7.3.1 Thiol-ene Click Photo Crosslinking of $PGSLP_{1000}$-Nor

Photo-crosslinking of $PGSLP_{1000}$-Nor with a dithiol PEG crosslinker was attempted (Figure 7.2), thiol-ene click chemistry would be particularly attractive due to its high reaction speed and high reaction yields.

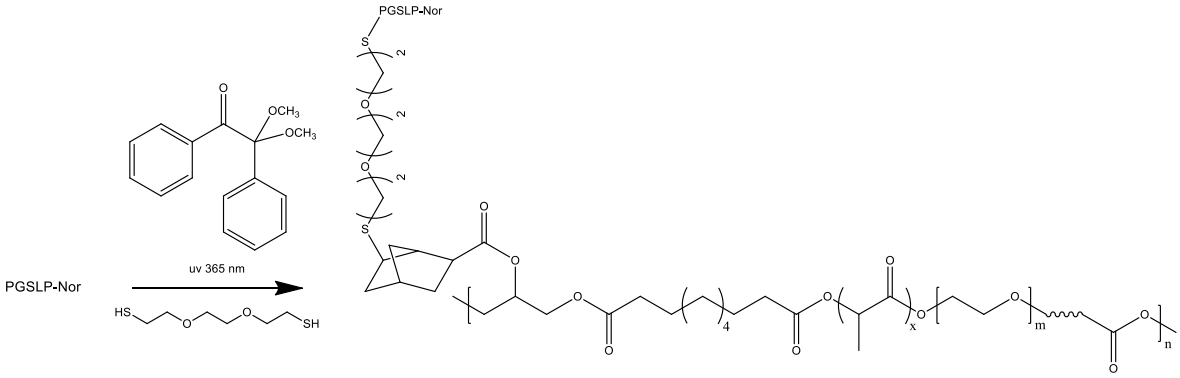

Figure 7.2 Photocrosslinking of PGSLP-Nor, using 2,2'-(Ethylenedioxy)diethanethiol as a crosslinker and DMPA as a photoinitiator.

Herein, a procedure was developed to explore the feasibility of PGSLP click-photo-crosslinking.

7.3.1.1 Thiol-ene Click Photo Crosslinking of $PGSLP_{1000}$-Nor 1

Norbornene functionalised $PGSLP_{1000}$ was investigated for its photo crosslinking and gel formation potential. As the material was water soluble a solvent compatible photoinitiator, Irgacure 2959, was used.

A solution of $PGSLP_{1000}$-Nor 1, 2,2'-(Ethylenedioxy)diethanethiol and Irgacure 2959 was made up in deionised H_2O with wt % of 10, 2 and 1 respectively. A second vial was made up of the same formulation without the Irgacure 2959 to be used as a control. These mixtures were then incubated in a shaker-water bath at 60°C for 2 h. The vials were then exposed to UV light over a period of 60 min. No change in viscosity was observed however a slight colour change from a clear solution to a 'milky' fluid was observed. The same procedure was repeated with an increased dithiol wt % of 6 %, again no change in viscosity was observed but an opaque 'milky' fluid was produced. The increased dithiol wt % procedure was repeated with the solvent being changed to methanol, no changes were observed in either the viscosity or colour.

7.3.1.2 Thiol-ene Click Photo Crosslinking of $PGSLP_{1000}$-Nor 2

A different batch of $PGSLP_{1000}$-Nor was used to investigate if grafting rate was too low in the initial batch of material used (Section 7.3.1.1) and was the reason for no gel formation occurring. A solution of $PGSLP_{1000}$-Nor 2, 2,2'-(Ethylenedioxy)diethanethiol and Irgacure 2959 was made up in deionised H_2O with wt % of 10, 2 and 1 respectively. A second vial was made up of the same formulation without the Irgacure 2959 to be used as a control. These mixtures were then incubated in a shaker-water bath at 60°C for 2 h. The vials were then exposed to UV light over a period of 60

min. No change in viscosity was observed however a slight colour change from a clear solution to a 'milky' fluid was observed suggesting thiol oxidation. The same procedure was repeated with an increased dithiol wt % of 6 %, again no change in viscosity was observed but an opaque 'milky' fluid was produced. The increased dithiol wt % procedure was repeated with the solvent being changed to methanol, no changes were observed in either the viscosity or colour. The lack of colour change when changing the solvent from deionised water to methanol reinforces thiol oxidation as the reason for the white colouration of the formulation.

7.3.1.3 Thiol-ene Click Photo Crosslinking of $PGSLP_{1000}$-Nor with Reducing Agent

A reducing agent, 2-mercaptoethanol was selected to aid in the thiol-ene click crosslinking reactions by reducing the resulting disulphide bonds to free thiols and thus aiding in the formation of crosslinks.

7.3.1.4 Thiol-ene Click Photo Crosslinking of $PGSLP_{1000}$-Nor 1 with Reducing Agent

A reducing agent was used to investigate if a previous gelation study (Section 7.3.1.1) was unsuccessful due to sulphide bond formation.

A solution of $PGSLP_{1000}$-Nor 1, 2,2'-(Ethylenedioxy)diethanethiol, 2-mercaptoethanol and Irgacure 2959 was made up in deionised H_2O with wt % of 10, 2,1 and 1 respectively. A second mixture was made up of the same formulation without the Irgacure 2959 to be used as a control. These mixtures were then incubated in a shaker-water bath at 60°C for 2 h. The vials were then exposed to UV light over a period of 60 min. No change in viscosity was observed and a colour change from a clear solution to a milkier fluid was observed as in previous experiments (Sections 7.3.1.1 and 7.3.1.2). The same procedure was repeated with an increased dithiol wt % of 6 %, with no observable change in viscosity. The increased dithiol wt % procedure was repeated with the solvent being changed to methanol, no changes were observed in either the viscosity or colour.

7.3.1.5 Thiol-ene Click Photo Crosslinking of $PGSLP_{1000}$-Nor 2 with Reducing Agent

A reducing agent was used to investigate if a previous gelation study with a different batch of functionalised polymer (Section 7.3.1.2) was unsuccessful due to sulphide bond formation.

A solution of $PGSLP_{1000}$-Nor 2, 2,2'-(Ethylenedioxy)diethanethiol, 2-mercaptoethanol and Irgacure 2959 was made up in deionised H_2O with wt % of 10, 2, 1 and 1 respectively. A second mixture was made up of the same formulation without the Irgacure 2959 to be used as a control. These mixtures were then incubated in a shaker-water bath at 60°C for 2 h. The vials were then exposed to UV light over a period of 60 min. No change in viscosity was observed and a colour change from a clear solution to a milkier fluid was observed as in previous experiments (Sections 7.3.1.1 and 7.3.1.2). The same procedure was repeated with an increased dithiol wt % of 6 %, again with no observable change in viscosity. The increased dithiol wt % procedure was repeated with the solvent being changed to methanol, no changes were observed in either the viscosity or colour.

7.3.2 Thiol-ene Click Photo Crosslinking of PGS-Nor

As no crosslinking was successful with the hydrophilic derivates of PGS, an investigation into the viability of the crosslinking mechanism was carried out (Figure 7.3)

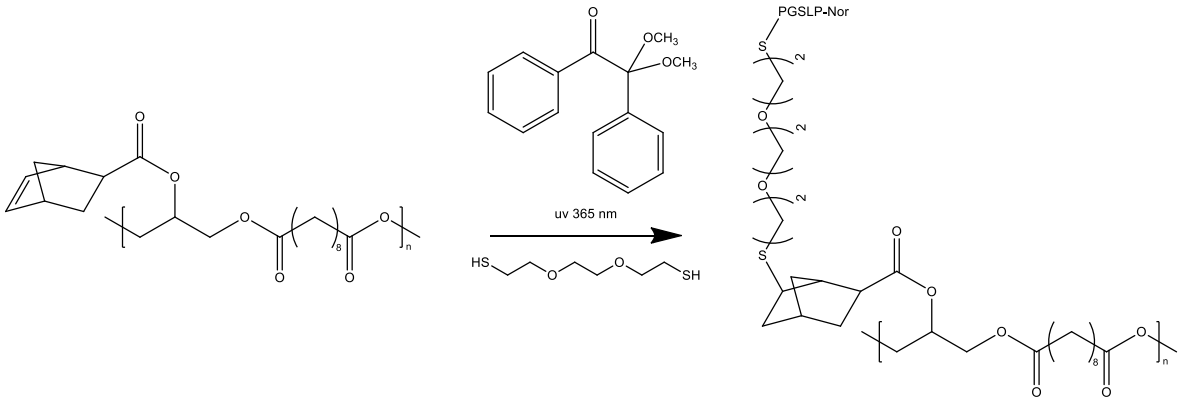

Figure 7.3 Photocrosslinking of PGS-Nor, using 2,2'-(Ethylenedioxy)diethanethiol as a crosslinker and DMPA as a photoinitiator.

Previous modification of PGS with norbornene moieties had already proven successful, and so this material was used in a crosslinking experiment in an attempt to from an organo-gel.

7.3.2.1 Thiol-ene Click Photo Crosslinking of PGS-Nor

PGS-Nor was used to determine if the functionalisation rate of PGSLP-Nor was causing a lack of gel formation in previous photo crosslinking studies (Sections 7.3.1.1 to 7.3.1.5).

A solution of PGS-Nor, 2,2'-(Ethylenedioxy)diethanethiol, and Irgacure 2959 was made up in methanol with wt % of 10, 2 and 1 respectively. A second mixture was made up of the same formulation without the Irgacure 2959 to be used as a control. These mixtures were then incubated in a shaker-water bath at 60°C for 2 h. The vials were then exposed to UV light over a period of 60 min. No change in viscosity was observed.

7.3.2.2 Thiol-ene Click Photo Crosslinking of PGS-Nor with Reducing Agent

As in previous cases (Section 7.3.1.3, 7.3.1.4 and 7.3.1.5) the possibility of disulphide formation warranted an approach using a reducing agent, 2-mercaptoethanol was again used. A solution of PGS-Nor, 2,2'-(Ethylenedioxy)diethanethiol, 2-mercaptoethanol and Irgacure 2959 was made up in methanol with wt % of 10, 2, 1 and 1 respectively. A second mixture was made up of the same formulation without the Irgacure 2959 to be used as a control. These mixtures were then incubated in a shaker-water bath at 60°C for 2 h. The vials were then exposed to UV light over a period of 60 min. No change in viscosity was observed.

7.3.3 Photo Crosslinking of PGSLP Derivatives

Acrylated materials were also used in crosslinking investigations (Figure 7.4) for the formation of elastomeric gels due to lack of gel formation using thiol-ene click photo crosslinking protocols, thought to be due to the presence of difficult to remove coupling by-products in the product.

Acrylated forms of $PGSLP_{1000}$ were initially investigated as a potential gel forming polymer. Following a lack of gelation, formulation variation was explored to determine if polymer fraction was too low for successful gel formation.

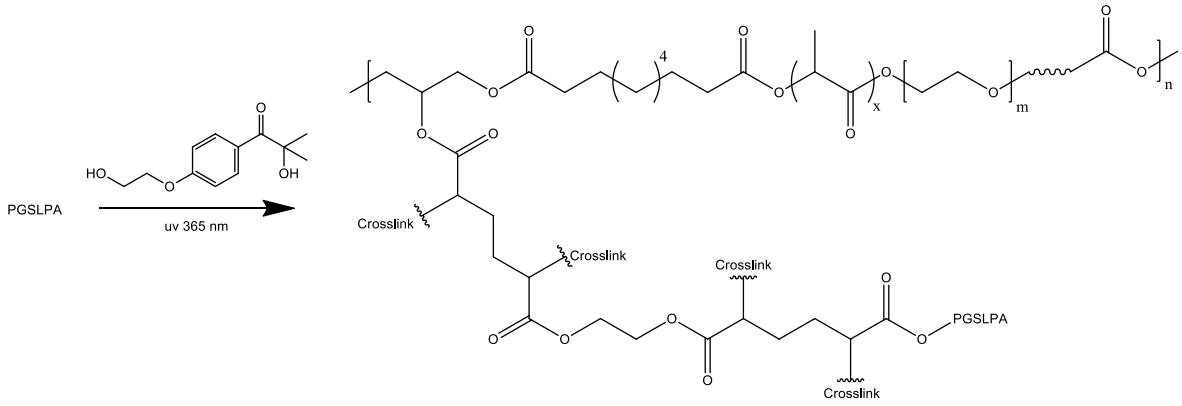

Figure 7.4 Photocrosslinking of PGSLPA, using PEGDA as a crosslinker and Irganure 2959 as a photoinitiator.

An increased glycerol form of PGSLP was prepared, functionalised with a norbornene moiety, and used in a photo crosslinking investigation. The aim was to determine if low potential sites for crosslinking reactions to take place was the limiting factor in gel formation, increasing the hydroxyl content of the polymers structure enables higher potential grafting rate of photo crosslinking functionality, allowing for increased crosslink density within the gel. A PGSLP form with increased glycerol and sebacic acid content was used to determine if an increase in the linear chain length of the polymer, as well as an increase in potential crosslinking sites would enable gel formation.

All previous investigations had yielded no gel formation and so a change to the photoinitiator was also considered. PGSLP is soluble in both water and methanol and so the photoinitiator was changed from Irgacure 2959 to 2,2-Dimethoxy-2-phenylacetophenone (DMPA). Finally, a novel, acrylated polymer was synthesised with an increased Mw PEG which formed gel after increasing the fractions of polymer and crosslinker.

7.3.3.1 Photo Crosslinking of $PGSLP_{1000}A$

An acrylate functionalised form of PGSLP was used to investigate gel formation using a diacrylate terminated PEG crosslinker.

A solution of $PGSLP_{1000}A$, PEG_{8000} diacrylate and Irgacure 2959 was made up in deionised H_2O with wt % of 10, 1 and 1 respectively. A second mixture without Irgacure 2959 was made up to act as a control. A third mixture was made up with the formulation but without the PEG_{8000} diacrylate, this was to investigate the potential for self-curing properties of the polymer. The mixtures were incubated in a shaker-water bath at 60°C for 2 h. Following incubation, the vials were exposed to UV light over a period of 60 min. No change in viscosity was observed in any of the mixtures. This procedure was repeated with the solvent changed from deionised H_2O to methanol, again no observable change in viscosity.

7.3.3.2 Photo Crosslinking of $PGSLP_{1000}A$, $PGSLP_{1000}$-Nor 1 and $PGSLP_{1000}$-Nor 2

As all crosslinking thus far had proven unsuccessful, efforts were made to investigate whether gelation was occurring, but the degree was too small to be detected in terms of viscosity. A large increase in the wt % of the crosslinker from 1 % to 10 % was used in new formulations, both with and without reducing agents resulting in the formulations in Table 7.1.

Table 7.1 Photo crosslinking matrix 1.

Polymer	Polymer wt %	Crosslinker wt %	Reducing agent wt %	Irgacure 2959 wt %
$PGSLP_{1000}A$	10	10	0	1
$PGSLP_{1000}A$	10	10	0	0
$PGSLP_{1000}$-Nor 1	10	10	1	1
$PGSLP_{1000}$-Nor 1	10	10	0	1
$PGSLP_{1000}$-Nor 1	10	10	0	0
$PGSLP_{1000}$-Nor 2	10	10	1	1
$PGSLP_{1000}$-Nor 2	10	10	0	1
$PGSLP_{1000}$-Nor 2	10	10	0	0

These formulations were incubated at 60°C for 2 h and then exposed to UV radiation. All formulations resulted in no observable changes in viscosity and therefore no gel formation.

7.3.3.3 Thiol-ene Click Photo Crosslinking of PG^SLP_{1000}-Nor

Increasing the glycerol content of the PGSLP material would increase the potential sites for grafting of photo crosslinking functionality, this would increase the number of potential crosslinking sites yielding a gel with increased crosslink density – producing a gel with an increased modulus.

A solution of PG^SLP_{1000}-Nor, 2,2'-(Ethylenedioxy)diethanethiol, 2-mercaptoethanol and Irgacure 2959 prepared in deionised H_2O with wt % of 10, 10, 1 and 1 respectively. A second mixture without Irgacure 2959 was made up to act as a control. A third mixture was made up with the formulation but without the 2,2'-(Ethylenedioxy)diethanethiol, this was to investigate the potential for self-curing properties of the polymer. The mixtures were incubated in a shaker-water bath at 60°C for 2 h. Following incubation, the vials were exposed to UV light over a period of 60 min. No change in viscosity was observed in any of the mixtures. This procedure was repeated with the solvent changed from deionised H_2O to methanol. No changes in viscosity were observed.

7.3.3.4 Thiol-ene Click Photo Crosslinking of PG^S^LP_{1000}-Nor

Increasing the glycerol and sebacic acid content of the PGSLP material would increase the potential sites for grafting of photo crosslinking functionality, as well as providing more space between the crosslinking sites that could be filled with a reinforcement phase.

A solution of PG^S^LP_{1000}-Nor, 2,2'-(Ethylenedioxy)diethanethiol, 2-mercaptoethanol and Irgacure 2959 was made up in deionised H_2O with wt % of 10, 10, 1 and 1 respectively. A second mixture without Irgacure 2959 was made up to act as a control. A third mixture was made up with the formulation but without the 2,2'-(Ethylenedioxy)diethanethiol, this was to investigate the potential for self-curing properties of the polymer. The mixtures were incubated in a shaker-water bath at 60°C for 2 h. Following incubation, the vials were exposed to UV light over a period of 60 min. No change in viscosity was observed in any of the mixtures. This procedure was repeated with the solvent changed from deionised H_2O to methanol. No changes in viscosity were observed.

7.3.3.5 Photo Crosslinking Investigation Using an Alternative Photoinitiator Molecule.

Successful modification of the various polymers produced had yielded no gelation upon exposure to UV radiation, variation of the formulations and introduction of reducing agents had otherwise had no effect on the gelation behaviour. Changing of the previously used photoinitiator, Irgacure 2959 to 2,2-Dimethoxy-2-phenylacetophenone (DMPA) was investigated to see its effect on the crosslinking. The crosslinking formulations were all incubated at 60°C for 2 h before being exposed to UV radiation.

Table 7.2 Photo crosslinking matrix 2. Investigation of photoinitiator molecule.

Polymer	Polymer wt %	Crosslinker wt %	Reducing agent wt %	DMPA wt %	Solvent
PGSA	10	5	0	1	Deionised H_2O
PGSA	10	5	0	1	Methanol
PGS-Nor	10	5	1	1	Deionised H_2O
PGS-Nor	10	5	1	1	Methanol
$PGSLP_{1000}A$	10	5	0	1	Deionised H_2O
$PGSLP_{1000}A$	10	5	0	1	Methanol
$PGSLP_{1000}$-Nor 1	10	5	1	1	Deionised H_2O
$PGSLP_{1000}$-Nor 1	10	5	1	1	Methanol
$PGSLP_{1000}$-Nor 2	10	5	1	1	Deionised H_2O
$PGSLP_{1000}$-Nor 2	10	5	1	1	Methanol
$PG\text{^}SLP_{1000}A$	10	5	0	1	Deionised H_2O
$PG\text{^}SLP_{1000}A$	10	5	0	1	Methanol
$PG\text{^}SLP_{1000}$-Nor	10	5	1	1	Deionised H_2O
$PG\text{^}SLP_{1000}$-Nor	10	5	1	1	Methanol
$PG\text{^}S\text{^}LP_{1000}A$	10	5	0	1	Deionised H_2O
$PG\text{^}S\text{^}LP_{1000}A$	10	5	0	1	Methanol
$PG\text{^}S\text{^}LP_{1000}$-Nor	10	5	1	1	Deionised H_2O
$PG\text{^}S\text{^}LP_{1000}$-Nor	10	5	1	1	Methanol

Following incubation, the vials were exposed to UV light over a period of 60 min. No change in viscosity was observed in any of the mixtures.

7.3.3.5.1 Increased PEG Length Photo crosslinking

Following the lack of gelation in the different formulations that were studied, an increase in the chain length of the elastomeric material was explored as a means to increase the likelihood of gelation (Table 7.3). Instead of PEG_{1000} the elastomer was synthesised with PEG_{8000}. This molecular weight was chosen as it matched the chain length of the intended crosslinking molecule.

Table 7.3 Photo crosslinking matrix 3. Investigation of polymer chain length.

Polymer	Polymer wt %	Crosslinker wt %	Photoinitiator	Photoinitiator wt %	Solvent
$PGSLP_{8000}AL$	10	5	Irgacure 2959	1	Deionised H_2O
$PGSLP_{8000}AL$	10	5	DMPA	1	Methanol
$PGSLP_{8000}AS$	10	5	Irgacure 2959	1	Deionised H_2O
$PGSLP_{8000}AS$	10	5	DMPA	1	Methanol
PGSA	10	5	Irgacure 2959	1	Methanol
PGSA	10	5	DMPA	1	Methanol
PEGDA	10	0	Irgacure 2959	1	Deionised H_2O
PEGDA	10	0	DMPA	1	Methanol

Partial gel formation was observed with all formulations however none were observed to form a complete and stable gel and therefore there was no utility in measuring mechanical properties.

A separate crosslinking matrix (Table 7.4) was prepared with a more concentrated formulation being prepared, separate incubation of polymers, crosslinkers and photo initiators was also carried out at an increased temperature. A separate formulation was prepared containing only the crosslinker, PEGDA and a photoinitiator, to test the effectiveness of the PEGDA to homo-polymerise.

Table 7.4 Photo crosslinking matrix 4. Investigation of formulation concentrations.

Polymer	Polymer wt %	Crosslinker wt %	Photoinitiator	Photoinitiator wt %	Solvent
$PGSLP_{8000}AL$	20	20	Irgacure 2959	1	Deionised H_2O
$PGSLP_{8000}AL$	20	20	DMPA	1	Methanol
$PGSLP_{8000}AS$	20	20	Irgacure 2959	1	Deionised H_2O
$PGSLP_{8000}AS$	20	20	DMPA	1	Methanol
PGSA	20	20	Irgacure 2959	1	Methanol
PGSA	20	20	DMPA	1	Methanol
PEGDA	20	0	Irgacure 2959	1	Deionised H_2O
PEGDA	20	0	DMPA	1	Methanol

Following the UV crosslinking procedure as described in Section 3.2.8, the formulations all appeared to have formed complete gels except the PEGDA formulations, with the ability to upturn the sample vials containing the complete gels and for them to remain in place. These gels appeared complete

and stable with no running liquid content. Resulting samples were therefore tested to determine their mechanical properties, such as elastic modulus, yield point and elastic modulus.

7.3.4 Compression to Failure Testing

Compression to failure is a useful procedure to establish a complete stress-strain relationship for a material through low strain to high strain environments. An Instron 3365 Universal Tester with a 500 N load cell in compression mode was used for compression to failure testing.

Elastomeric gels and composite structures (containing PGS-based fibre and hydrogels) were photo crosslinked using a Chromato-Vue C-71 UV viewing system (4 x 15-watt 365 nm UV tubes fitted). Samples were cut to 4 x 15 x 15 mm for testing. 4 different forms of testing samples were prepared (Figure 7.5).

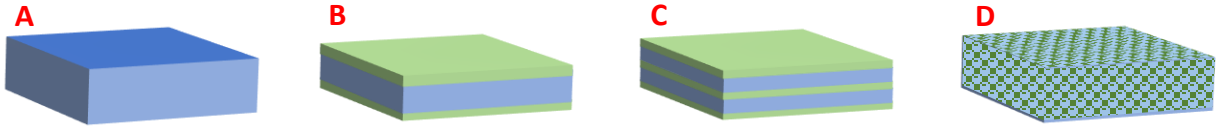

Figure 7.5 Gel and composite structural forms. A) 100 % elastomer, no reinforcement. B) Bilayer arrangement, elastomeric bulk phase with electrospun nonwoven laminated to faces. C) Trilayer arrangement, layer deposition of electrospun nonwoven and elastomeric bulk phase. D) Segmented electrospun nonwoven reinforced composite.

Preparation of gel A (Figure 7.5) was achieved by depositing an incubated, Irgacure 2959 photoinitiator doped elastomer formulation into a suitable mould, the mould was then transferred to the UV curing environment and cured over a period of 2 h to ensure complete gelation.

Construction of the composite materials B and C (Figure 7.5) was achieved by layer deposition, whereby a layer of electrospun nonwoven web was layered into a suitable mould. Deposition of the

incubated, Irgacure 2959 photoinitiator doped elastomer formulation on top of the nonwoven web followed by further steps of layering the electrospun nonwoven web and elastomer formulation until construction was complete. The mould was then transferred to the UV curing environment and cured over a period of 2 h to ensure complete gelation.

Composite form D (Figure 7.5) was constructed by cutting a nonwoven web into 2 x 1 mm lengths, these fibrous ‘slivers’ were then transferred to the elastomer formulation and homogenised using a magnetic stirrer at 200 rpm. Once homogenisation was achieved the formulation was doped with a photoinitiator (Irgacure2959) and transferred to a mould where it underwent curing.

Table 7.5 Composition and volume fractions for the four different constructions.

Sample	Composition	Wt/V %	Gel Volume Fraction %	Fibre Volume Fraction %
A Unreinforced gel	PGSLPA	25	100	0
	$PEGDA_{8000}$	10		
B Bilayer reinforced composite	PGSLPA	25	98.04	1.96
	$PEGDA_{8000}$	10		
	PGSLPA/PCL Electrospun nonwoven web ($2g/m^2$)	-		
C Trilayer reinforced composite	PGSLPA	25	97.09	2.91
	$PEGDA_{8000}$	10		
	PGSLPA/PCL Electrospun nonwoven web ($2g/m^2$)	-		
D Segmented electrospun nonwoven reinforced composite	PGSLPA	25	98.04	1.96
	$PEGDA_{8000}$	10		
	PGSLPA/PCL Nonwoven wen ($2g/m^2$)	5		

Owing to the synthesis of the elastomer with photocuring functionality being challenging, the physical and adhesion properties and the issues with photocuring, the decision was made to select a formulation that had previously been found to cure with the most frequent success. All elastomer formulations used for composite and gel formation were therefore comprised of 25 % wt/v PGSLPA, 10 % wt/v $PEGDA_{8000}$, and 2 % wt/v Irgacure 2959 in deionised water. Composite form D also had

nanofibrous material at 5 % wt/V, which equated to a 35 x 35 mm nonwoven web with an areal density of 2 g/m^2.

Compression testing was done at a strain rate of 1 mm/min until a limit of 450 N was reached, this was to ensure the sample was compressed to failure and the stopping point was determined by the force between the compression plates reaching a limit to prevent damaging the load cell. All compression testing was done in the same conditions.

7.3.5 Compression Fatigue Testing

Compression fatigue testing is important for materials that are intended to undergo cyclic strain, as the materials are intended to act as foot plantar implantable materials, they have to undergo cyclic strains to function efficiently. The materials were prepared exactly as previously described (Section 7.3.4). Testing was conducted using the same testing apparatus under the same conditions. A strain rate of 1 mm/min was used with a distance of 2.5 mm, this value being selected based upon compression to failure testing carried out previously (Section 7.4.8). A distance of 2.5 mm is a point still in the linear elastic portion of the stress-strain curves for the materials, before the yield point and where the materials are expected to perform in a clinical setting.

7.4 Results and Discussion

7.4.1 Thiol-ene Click Photo Crosslinking of $PGSLP_{1000}$-Nor

Photo-crosslinking of $PGSLP_{1000}$-Nor materials with a dithiol PEG crosslinker was attempted. The use of thiol-ene click chemistry as a means of curing materials is sought after due to the high reaction speeds and yields as well as the ‘green’ nature of the chemistry involved. PGSLP curing to produce elastomeric gels requires thermo-curing at temperatures above 180°C and under vacuum, these

conditions therefore, cannot be used in a physiological setting and so other routes of curing are required.

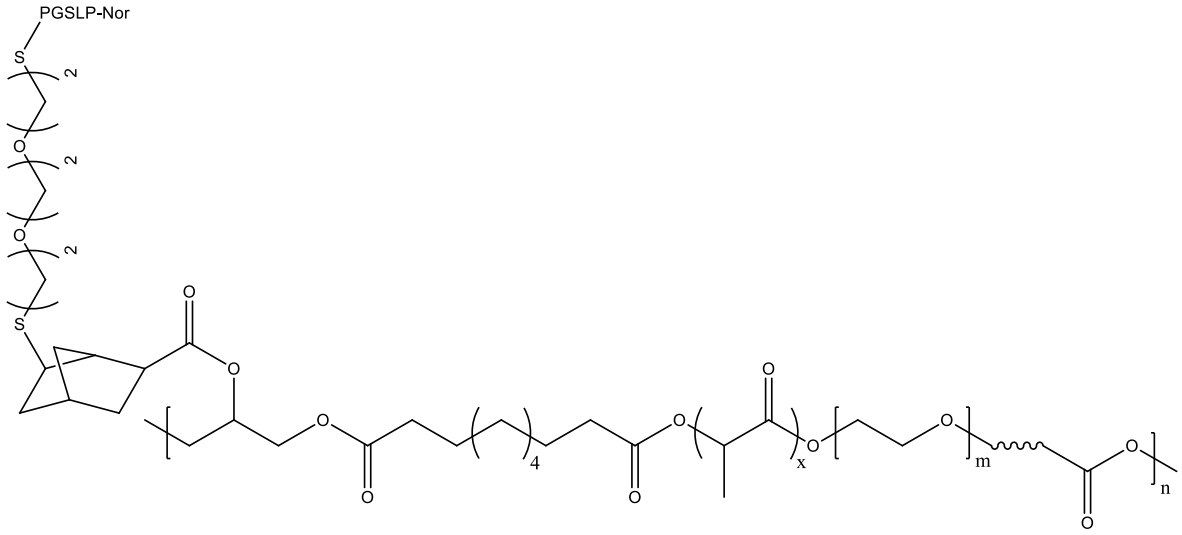

Figure 7.6 Proposed structure of PGSLP-Nor crosslinked matrix, using 2,2'-(Ethylenedioxy)diethanethiol as a crosslinker.

Figure 7.6 shows the proposed structure of the crosslinked PGSLP-Nor matrix, crosslinking between two norbornene functionalised polymer chains using a dithiol crosslinker.

7.4.1.1 Thiol-ene Click Photo Crosslinking of $PGSLP_{1000}$-Nor 1

A formulation of $PGSLP_{1000}$-Nor, a dithiol PEG crosslinker and photo initiator Irgacure 2959 was made up in a single vial. A secondary vial was made up in the same fashion without the Irgacure 2959, this was to investigate whether any homo-polymerisation occurred. These mixtures were incubated in a shaker-water bath at 60°C for 2 h to ensure complete dissolution. The vials were then placed under a UV light emitting at wavelength of 365 nm for 60 min. The vials were wrapped in aluminium foil for the entirety of this procedure until exposure to UV radiation.

Upon removal from UV radiation source the solutions were not visibly more viscous and thus no gelation had occurred, a colour changed was observed however as the solution turned from transparent to 'milky' white.

The experiment was repeated with an increased dithiol PEG crosslinker wt % however no visible increase in viscosity was observed, again a 'milky' white solution was present at the end of the UV exposure. This procedure was again repeated but with the solvent changed from deionised H_2O to methanol, this was to test whether the milky colour present at the end of the UV exposure was due to the components of the formulation precipitating as the solution cooled. The UV exposure didn't yield gelation or any increases in viscosity however the solution remained transparent through-out the procedure.

7.4.1.2 Thiol-ene Click Photo Crosslinking of $PGSLP_{1000}$-Nor 2

Photo-crosslinking of $PGSLP_{1000}$-Nor was attempted again, but with a different batch of modified polymer, this polymer was produced by the modified reaction protocol involving an extended chilling period in the freezer at -20°C. The same formulations as in the previous investigation (Section 7.4.1.1) was prepared, the original formulation in deionised H_2O, an increased dithiol PEG crosslinker formulation in deionised H_2O and an increased dithiol PEG crosslinker formulation in methanol. All vials were again wrapped in aluminium foil for the entirety of this procedure until exposure to UV radiation.

All formulations yielded no gelation and visible no increases in viscosity.

7.4.2 Thiol-ene Click Photo Crosslinking of $PGSLP_{1000}$-Nor with Reducing Agent

A possible reason for the lack of gelation in the photo-crosslinking investigations carried out could be the formation of disulphide bonds between the thiol groups present on the crosslinker. Reducing

agents decrease the probability of this bond formation and thus increase the probability of successful crosslinking in this case. 2-mercaptoethanol was selected to be used as the reducing agent in the thiol-ene click crosslinking reactions, by reducing the resulting disulphide bonds to free thiols, allowing them to undergo the expected thiol-ene click chemistry when exposed to UV radiation.

7.4.2.1 Thiol-ene Click Photo Crosslinking of $PGSLP_{1000}$-Nor 1 with Reducing Agent

The same crosslinking procedure was used, and the same formulations were made up as in previous investigations: the original formulation in deionised H_2O, an increased dithiol PEG crosslinker formulation in deionised H_2O and an increased dithiol PEG crosslinker formulation in methanol (Section 7.4.1.1). However, 1 wt % of reducing agent was introduced to the formulations. The vials containing the formulations were all wrapped in aluminium foil so as to prevent external stimuli.

Upon removal from the UV radiation source there was no visible increases in viscosity and the colour changes were similar to those of previous experiments without a reducing agent.

7.4.2.2 Thiol-ene Click Photo Crosslinking of $PGSLP_{1000}$-Nor 2 with Reducing Agent

A secondary batch of modified polymer was used in another crosslinking experiment to primarily to investigate whether the initial modified polymer used was too contaminated with DCC to enable crosslinking. The procedure and formulations (Section 7.4.1.1) were repeated with the alternate batch of norbornene modified polymer and the introduction of the reducing agent.

Removal from the UV source showed no formation of gels and no visible increases in viscosity again.

7.4.3 Thiol-ene Click Photo Crosslinking of PGS-Nor

Due to the inability of the norbornene modified PGSLP materials to successfully form gels, a previously modified PGS based material (Section 4.3.2.6) was used with the crosslinking procedure.

This was firstly to investigate whether the thiol-ene click chemistry was a viable option in producing gels, but secondly it was to determine whether the effective reactive groups were too low in the new PGSLP materials for successful formation of gels. The effective reactive groups are initially the exposed hydroxyl groups present in the polymeric structure, these are grafting sites where modification of the polymer takes place; whether it be the Steglich esterification to couple norbornene moieties to the backbone or where acrylation takes place by reacting with acryloyl chloride and thus grafting a reactive alkene group to the backbone. The reactive sites are then modified to introduce functionality, in this case photo crosslinking, this functional group of the polymer reacts directly with the crosslinker molecule to form a chemical bond and causing gelation.

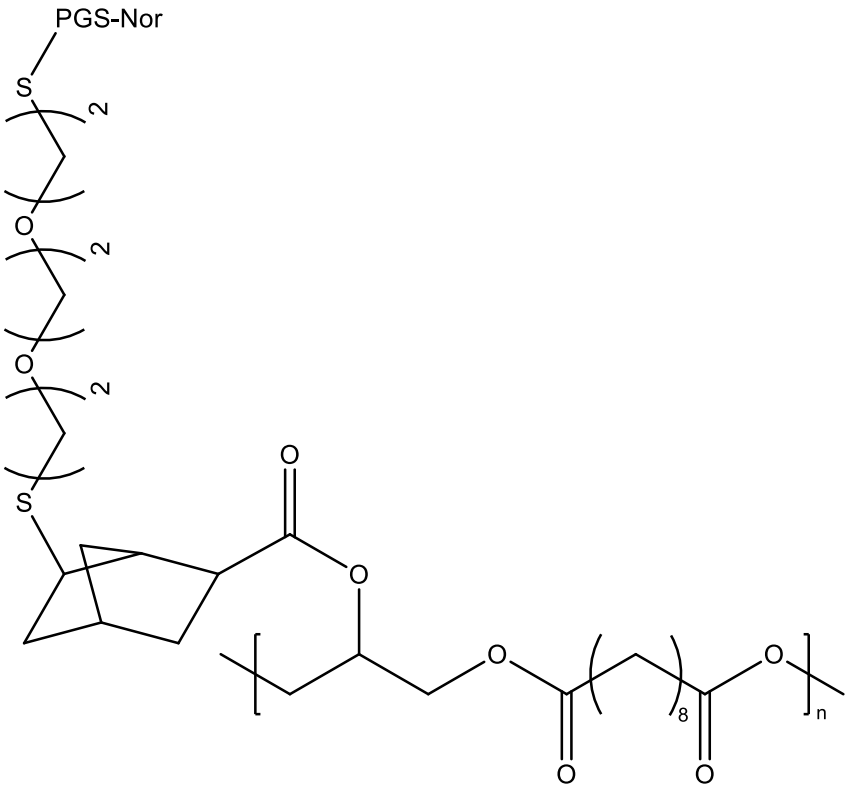

Figure 7.7 Proposed structure of PGS-Nor crosslinked matrix, using 2,2'-(Ethylenedioxy)diethanethiol as a crosslinker.

Figure 7.7 shows the proposed structure of the crosslinked PGS-Nor matrix, crosslinking between two norbornene functionalised polymer chains using a dithiol crosslinker.

7.4.3.1 Thiol-ene Click Photo Crosslinking of PGS-Nor

Reaction procedure was mimicked from previous crosslinking experiments, detailed in Section 7.3.1.1, with PGS-Nor substituted for PGSLP-Nor. The vials were wrapped in aluminium foil and incubated at 60°C for 2 h. After exposure to UV radiation for 60 min the vials were removed, as with previous experiments there was had been no gelation occurring and no increase in viscosity was observed.

7.4.3.2 Thiol-ene Click Photo Crosslinking of PGS-Nor with Reducing Agent

A reason for the lack of gelation occurring in the thiol-ene click reactions could be the formation of disulphide bonds, these bonds can be reduced to free thiols by a reducing agent. The same procedure previously described (Section 7.3.1.1) using the same formulations with a 1 wt % of 2-mercaptoethanol reducing agent dope was employed.

No visible change in viscosity was observed.

7.4.4 Photo Crosslinking of $PGSLP_{1000}A$

As was always intended, an acrylated form of the polymer was used in testing, although thiol-ene click chemistry would be favourable, the lack of gel formation using the norbornene modified polymers meant that gel formation using acrylated derivates was required.

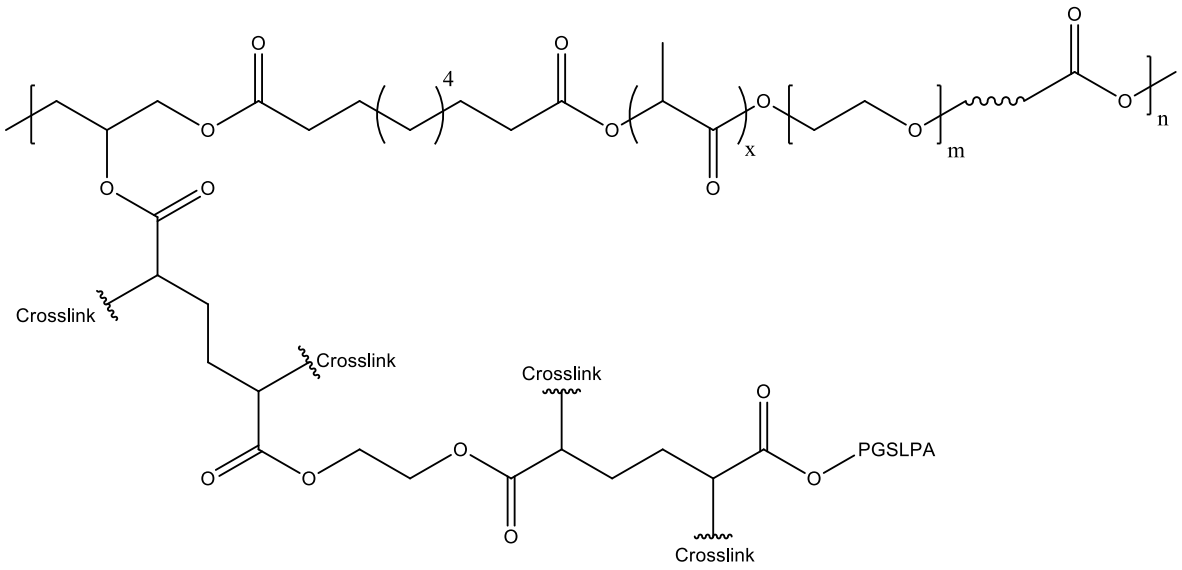

Figure 7.8 Proposed structure of PGSLPA crosslinked matrix, using PEGDA as a crosslinker.

Figure 7.8 shows the proposed structure of the crosslinked PGSLPA matrix, highlighting the highly branched nature of the photo crosslinked gel.

7.4.4.1 Photo Crosslinking of $PGSLP_{1000}A$

A formulation of $PGSLP_{1000}A$, PEG_{8000} diacrylate and photo initiator Irgacure 2959 was made up in a single vial. A secondary vial was made up in the same fashion without the Irgacure 2959, this was to investigate whether any homo-polymerisation occurred, which is likely in the case of acrylated materials. These mixtures were incubated in a shaker-water bath at 60°C for 2 h to ensure complete dissolution. The vials were then placed under a UV light emitting at wavelength of 365 nm for 60 min. The vials were wrapped in aluminium foil for the entirety of this procedure until exposure to UV radiation.

After removal from the UV radiation source the solutions were not observed to be more viscous. The experiment was repeated with the solvent changed from deionised H_2O to methanol, this however didn't lead to gel formation.

7.4.5 Photo Crosslinking of $PGSLP_{1000}A$, $PGSLP_{1000}$-Nor 1 and $PGSLP_{1000}$-Nor 2

After multiple attempts with all materials to form a gel, an investigation into whether gelation was occurring but on such a small scale that it was not observable was carried out. The wt % of crosslinker used in the experiments was increased 10-fold from 1 to 10 wt %. With the norbornene modified polymer formulations being replicated with and without 2-mercaptoethanol as a reducing agent (Table 7.1).

All formulations did not yield any gel formation, no observable increase in viscosity was observed.

7.4.5.1 Thiol-ene Click Photo Crosslinking of PG^SLP_{1000}-Nor

A formulation of PG^SLP_{1000}-Nor, a dithiol PEG crosslinker, reducing agent and photo initiator Irgacure 2959 was made up in a single vial. A secondary vial was made up in the same fashion without the Irgacure 2959. These mixtures were incubated in a shaker-water bath at 60°C for 2 h to ensure complete dissolution. The vials were then placed under a UV light emitting at wavelength of 365 nm for 60 min. The vials were wrapped in aluminium foil for the entirety of this procedure until exposure to UV radiation.

Upon removal from UV radiation source the solutions were not visibly more viscous and thus no gelation had occurred. The experiment was repeated with an increased dithiol PEG crosslinker wt % however no visible increase in viscosity was observed. Repetition of this experiment with the solvent changed from deionised H_2O to methanol also yielded no increase in viscosity and thus no gelation.

7.4.5.2 Thiol-ene Click Photo Crosslinking of PG^S^LP_{1000}-Nor

A formulation of PG^S^LP_{1000}-Nor, a dithiol PEG crosslinker, reducing agent and photo initiator Irgacure 2959 was made up in a single vial. A secondary vial was made up in the same fashion without the Irgacure 2959. These mixtures were incubated in a shaker-water bath at 60°C for 2 h to

ensure complete dissolution. The vials were then placed under a UV light emitting at wavelength of 365 nm for 60 min. The vials were wrapped in aluminium foil for the entirety of this procedure until exposure to UV radiation.

Upon removal from UV radiation source the solutions were not visibly more viscous and thus no gelation had occurred. The experiment was repeated with an increased dithiol PEG crosslinker wt % however no visible increase in viscosity was observed. Repetition of this experiment with the solvent changed from deionised H_2O to methanol also yielded no increase in viscosity and thus no gelation.

7.4.6 Photo Crosslinking Investigation Using an Alternative Photo Initiator Molecule.

Numerous polymer derivatives had undergone modification without producing any gels upon exposure to UV light, formulation variations and introduction of a reducing agent in the case of the norbornene functionalised polymer had no effect on the photo crosslinking behaviour. The decision was made to investigate whether the photo initiator, Irgacure 2959 was the reason behind the unsuccessful attempts to produce a gel. Changing of the previously used photo-initiator, Irgacure 2959 to 2,2-Dimethoxy-2-phenylacetophenone (DMPA) was investigated to see its effect on the crosslinking.

A matrix for photo crosslinking (Table 7.2) to investigate this change in photo initiators was used. No gelation was observed and so it was concluded that the photoinitiators used weren't an issue, the issue was with the materials or formulations themselves. The norbornene modified polymers exhibited no gelation behaviour but considering the modification protocol is prone to hydrolysis of the activated carboxylic acid species, and the difficulty in removing the DCC coupling by-products it was determined these were the primary factors in the inability to form gels.

7.4.7 Increased PEG Length Photo Crosslinking

To investigate if the material was an issue a new derivative was synthesised, with an increased chain length. Initially a PEG_{100000} was intended to be substituted for PEG_{1000} in the synthesis, as a large increase in chain length would give a good indication of whether the chain length of the acrylated polymer was the issue in gel formation. However, upon application of heat and stirring for the initial mixing step of the polycondensation it was observed that the stirring was no longer functional, and the reaction was a failure. Without stirring the reaction could not mix properly, meaning that polycondensation would occur between the physical boundaries of the different reagents and that synthesis of a homogenous polymer would be impossible. Increasing the polymer chain length was instead achieved by substituting the PEG_{1000} in the synthesis step with PEG_{8000}, this molecular weight was chosen as it directly related to the chosen crosslinker. A photo crosslinking matrix (Table 7.3) was devised and tested.

Partial gel formation was observed with all formulations however, no formulations were observed to form a complete and stable gel. The gels produced were unsuitable for mechanical testing due to their structural integrity being so weak that they could not hold their shape and instead acted more like a viscous fluid.

To investigate if the formulation component concentrations were an issue in gel formation another photo crosslinking matrix (Table 7.4) was prepared but with increased concentrations of previous formulations used. Both Irgacure 2959 and DMPA were also used in these formulations to determine their efficacy of initiating higher concentration solutions. A formulation of PEG_{8000} diacrylate (PEGDA) and photo initiator only was prepared to test the effectiveness of PEGDA to homo-

polymerise.

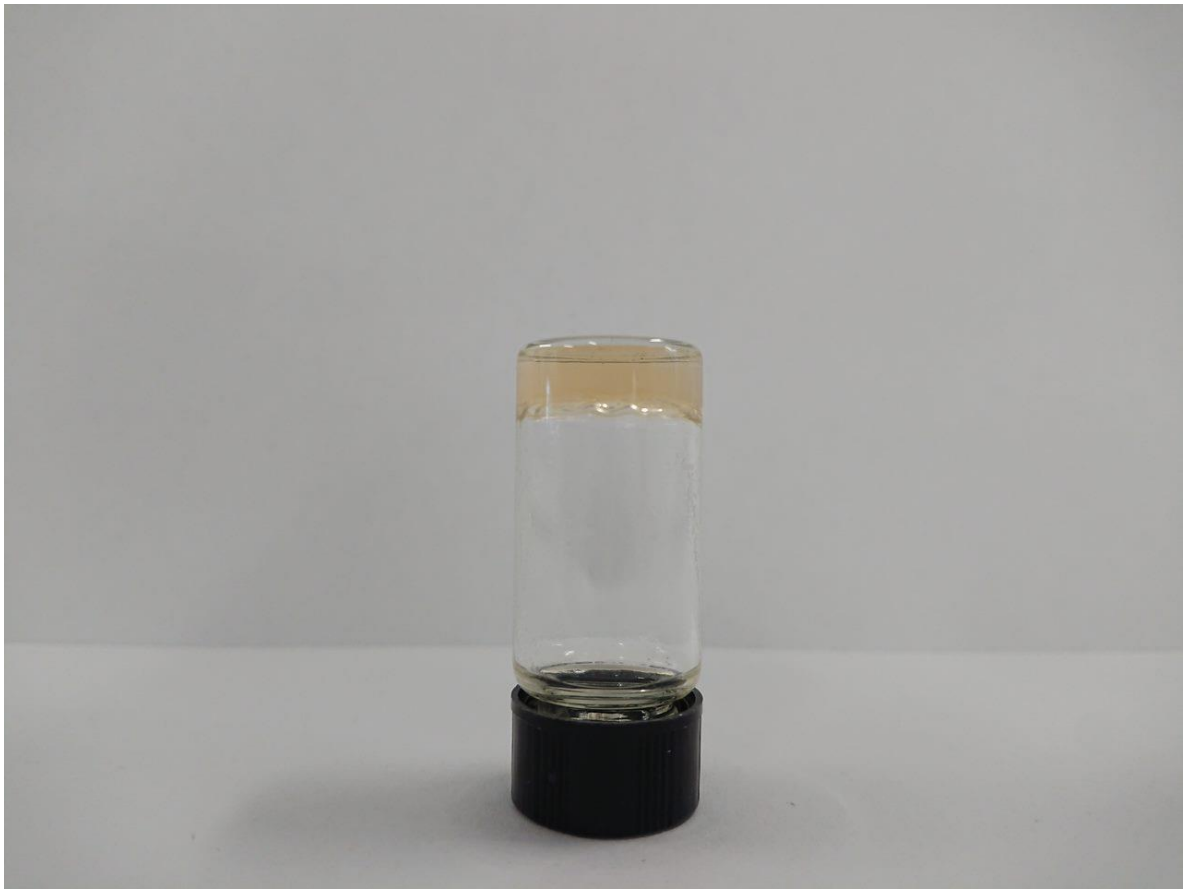

Figure 7.9 Complete gel formation of $PGSLP_{8000}A$

The PEGDA only formulation was observed to show partial gel formation, with significant volumes of free-flowing fluid. The $PGSLP_{8000}A$ and PGSA formulation all successfully formed gels (Figure 7.9), giving an indication that a combination of polymer chain length and concentration were hindering the formation of gels in previous tests, however this also contrasts sharply with the norbornene modified polymers which were all unsuccessful in the formation of gels but as stated previously this is likely to do with the inclusion of large amounts of by-products in the formulations alongside the relative inefficiency of the reaction pathway.

7.4.8 Compression to Failure Testing

Compression to failure testing enables a full strain behaviour profile to be generated and provides an indication of how the bulk material will perform in a desired application. The materials tested are not expected to undergo compression to failure in their intended clinical application, instead they are expected to undergo cyclic compression in the linear elastic portion of their stress-strain profile.

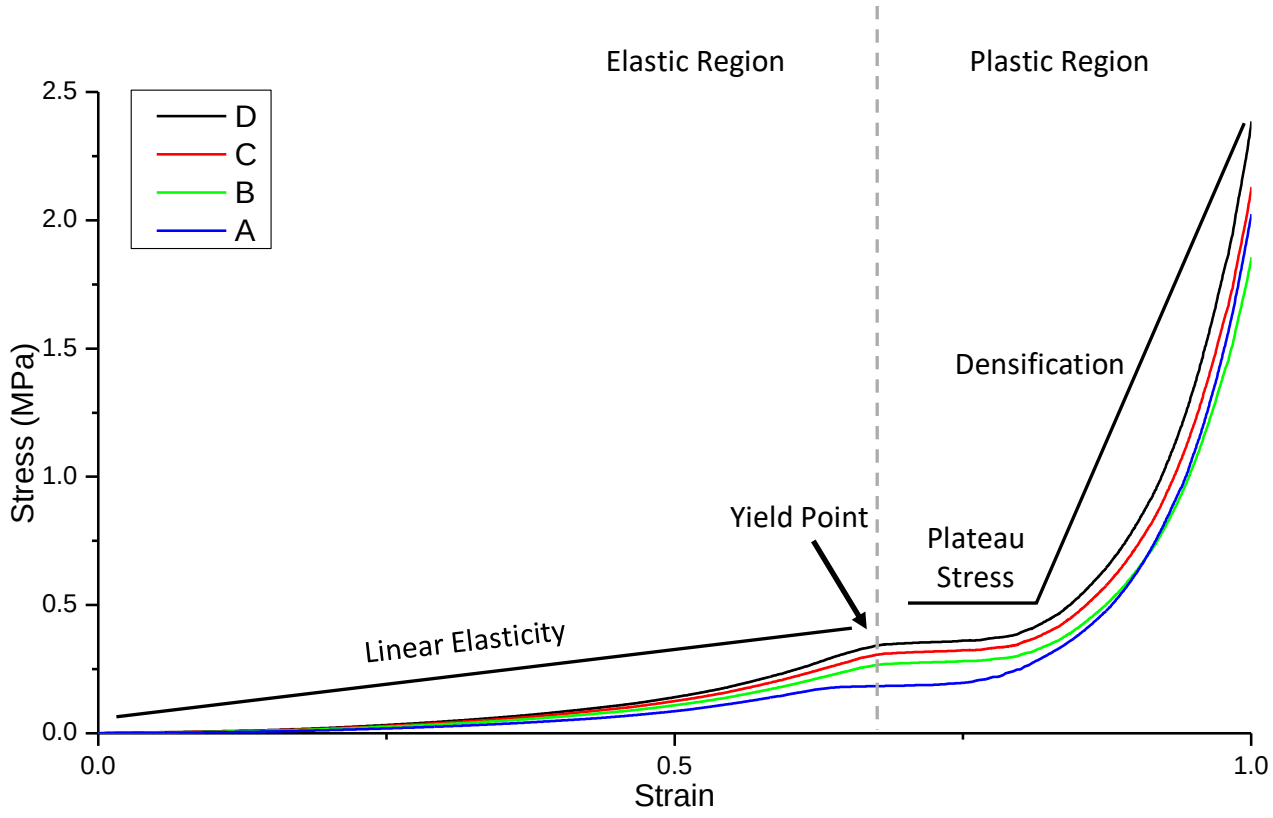

Figure 7.10 Complete compression stress-strain curve for gel and composite constructions. A) 100 % elastomer, no reinforcement. B) Bilayer arrangement, elastomer with electrospun nonwoven laminated to faces. C) Trilayer arrangement, layer deposition of electrospun nonwoven and elastomeric bulk phase. D) Segmented electrospun nonwoven reinforced composite.

Figure 7.10 shows the complete stress-strain compression profile for all four compositions. Inclusion of a fibre reinforcement phase increases the stress response of the construct, allowing it to absorb more energy before permanent deformation occurs. The segmented electrospun nonwoven reinforced composite showed the largest increase in mechanical strength, at 0.6 strain the stress of the composite was 58.5 %, 28.5 % and 12.0% % greater than that of an unreinforced hydrogel, bilayer and trilayer composite respectively.

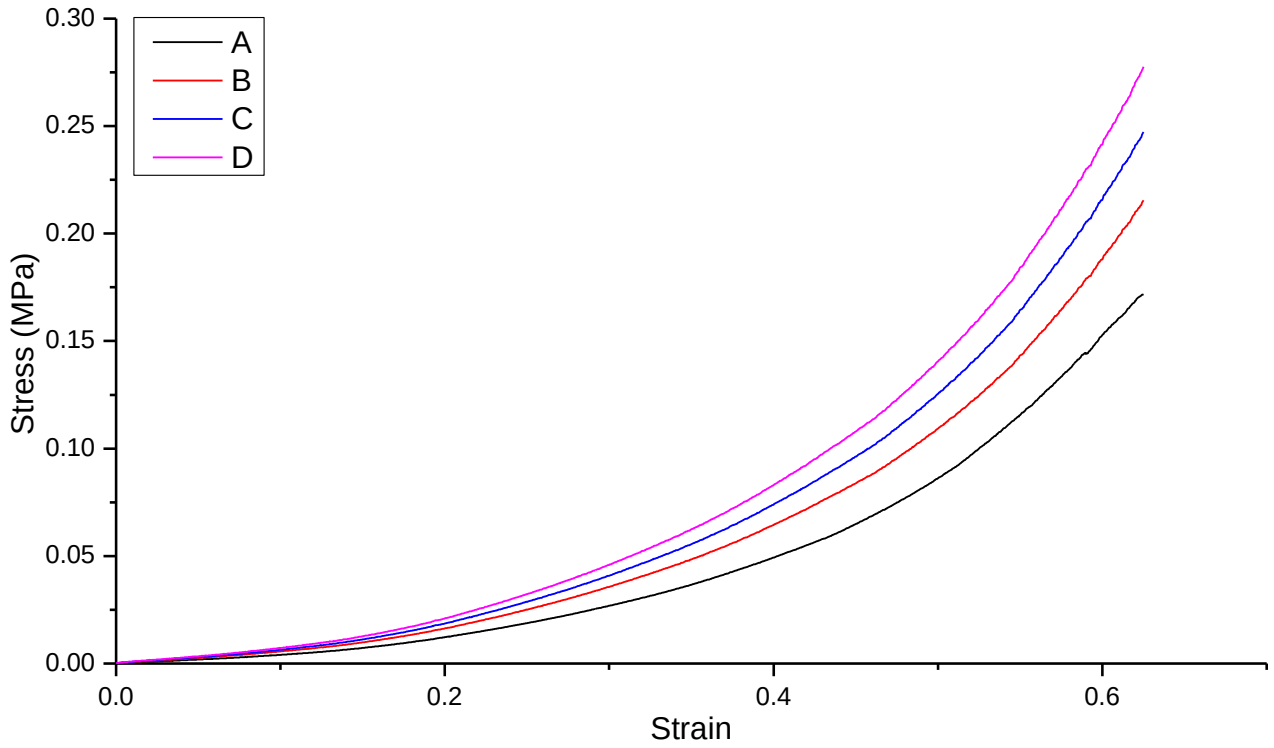

Figure 7.11 Initial linear elasticity portion of compression stress-strain curve for gel and composite constructions. A) 100 % elastomer, no reinforcement. B) Bilayer arrangement, elastomer with electrospun nonwoven laminated to faces. C) Trilayer arrangement, layer deposition of electrospun nonwoven and elastomeric bulk phase. D) Segmented electrospun nonwoven reinforced composite.

Figure 7.11 shows the linear portion of the stress-strain curve profile for all four compositions. The end point was selected before the yield point of the material, and this was then used in further fatigue testing. This linear portion of the stress-strain curve was also used to calculate the elastic modulus.

Table 7.6 Composition and strain related elastic modulus data for the four different constructions.

Sample	Composition	Wt/V %	Strain	E (MPa)	Eσ (MPa)
A Unreinforced gel	PGSLPA	25	0.1	0.040	0.028
			0.2	0.061	0.013
			0.3	0.089	0.021
	$PEGDA_{8000}$	10	0.4	0.123	0.031
			0.5	0.172	0.019
			0.6	0.254	0.019
B Bilayer reinforced composite	PGSLPA	25	0.1	0.057	0.041
			0.2	0.081	0.021
	$PEGDA_{8000}$	10	0.3	0.119	0.026
			0.4	0.161	0.042
	PGSLPA/PCL Electrospun nonwoven web ($2g/m^2$)	-	0.5	0.218	0.034
			0.6	0.313	0.023
C Trilayer reinforced composite	PGSLPA	25	0.1	0.064	0.044
			0.2	0.093	0.020
	$PEGDA_{8000}$	10	0.3	0.136	0.028
			0.4	0.184	0.047
	PGSLPA/PCL Electrospun nonwoven web ($2g/m^2$)	-	0.5	0.250	0.037
			0.6	0.359	0.012
D Segmented electrospun nonwoven reinforced composite	PGSLPA	25	0.1	0.073	0.053
			0.2	0.104	0.028
	$PEGDA_{8000}$	10	0.3	0.153	0.036
			0.4	0.207	0.057
	PGSLPA/PCL Electrospun nonwoven web ($2g/m^2$)	5	0.5	0.281	0.049
			0.6	0.402	0.038

Table 7.6 shows the composition and elastic modulus of the composites at strain rates 0.1 – 0.6. Elastic modulus of the segmented electrospun nonwoven reinforced composite , D, is significantly ($P<0.05$) increased compared to the unreinforced and bilayer constructions, with the modulus being 28.7 - 80.4 %, 28.5 - 71.3 %, 28.7 - 70.8 %, 28.7 - 68.2 %, 28.66 - 63.4 %, 28.5 % higher at strain 0.1 – 0.6 respectively, the largest increases being between construction A and D. T-test analysis showed

that the trilayer reinforced composite was not significantly different than the segmented electrospun nonwoven reinforced composite

7.4.9 Compression Fatigue Testing

The compression fatigue strain limit was deduced from the linear portion of the compression failure test, whereby a limit of 2.5 mm deformation was selected as it was before the yield point of the materials. During initial testing a cycle number of 15 was selected as the hysteresis response was maintained from 12 cycles in most cases.

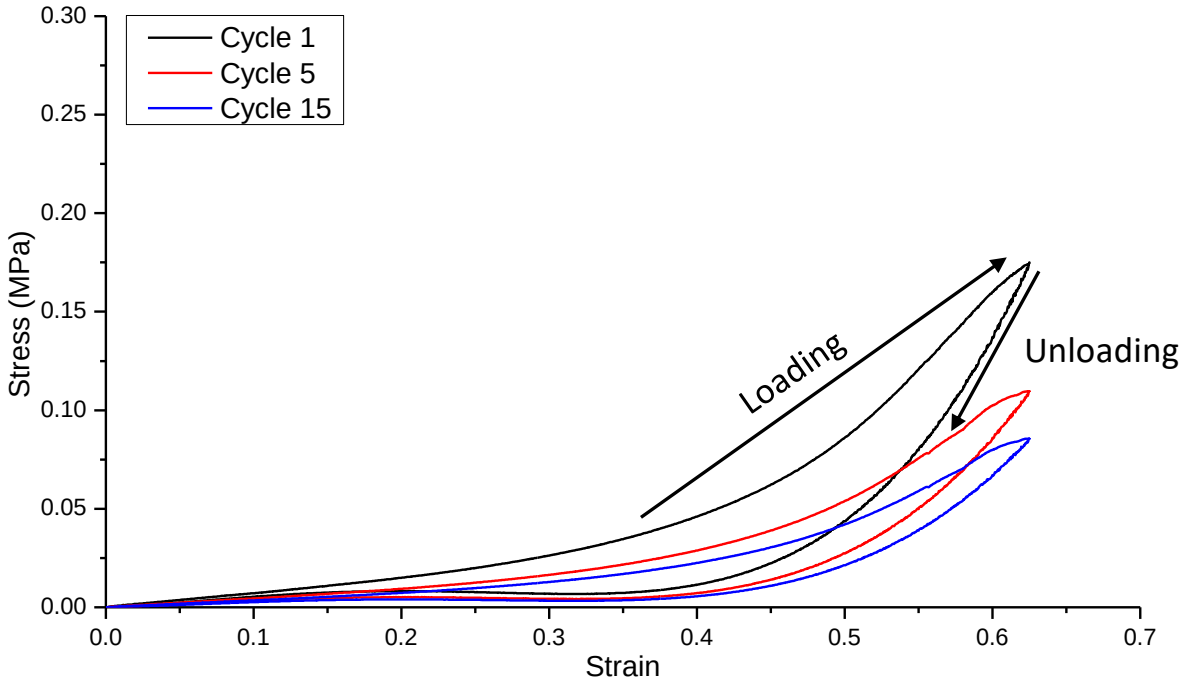

Figure 7.12 Compression fatigue stress-strain curve for unreinforced composite, A.

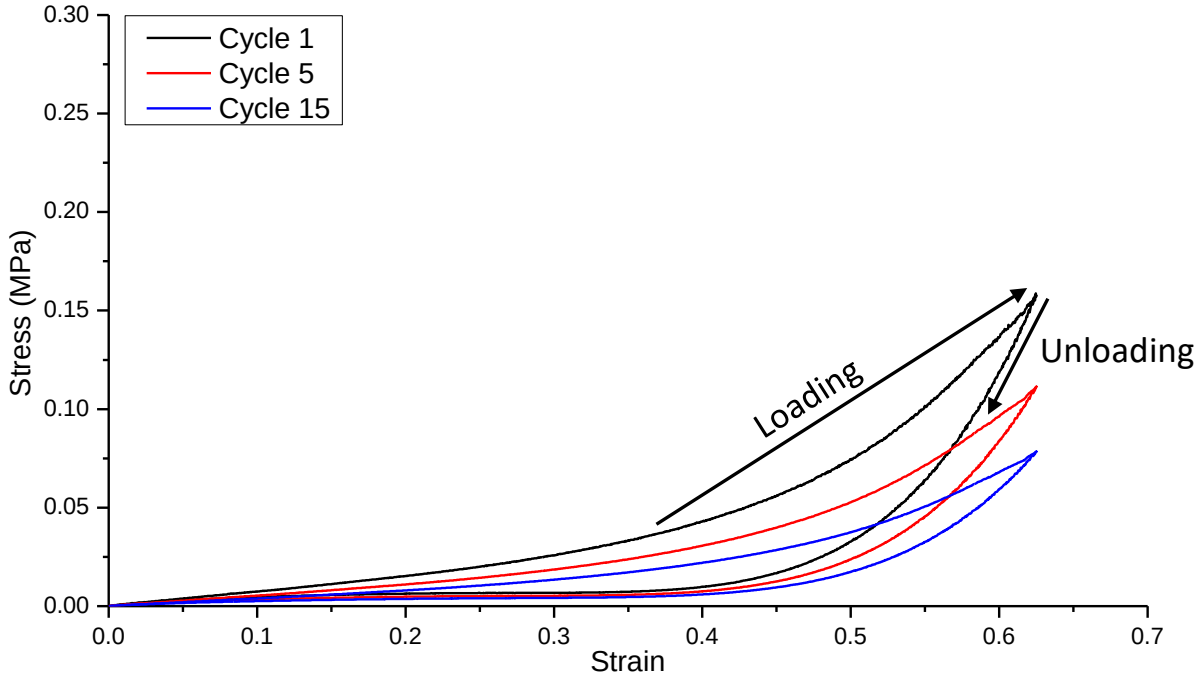

Figure 7.13 Compression fatigue stress-strain curve for bilayer reinforced composite, B.

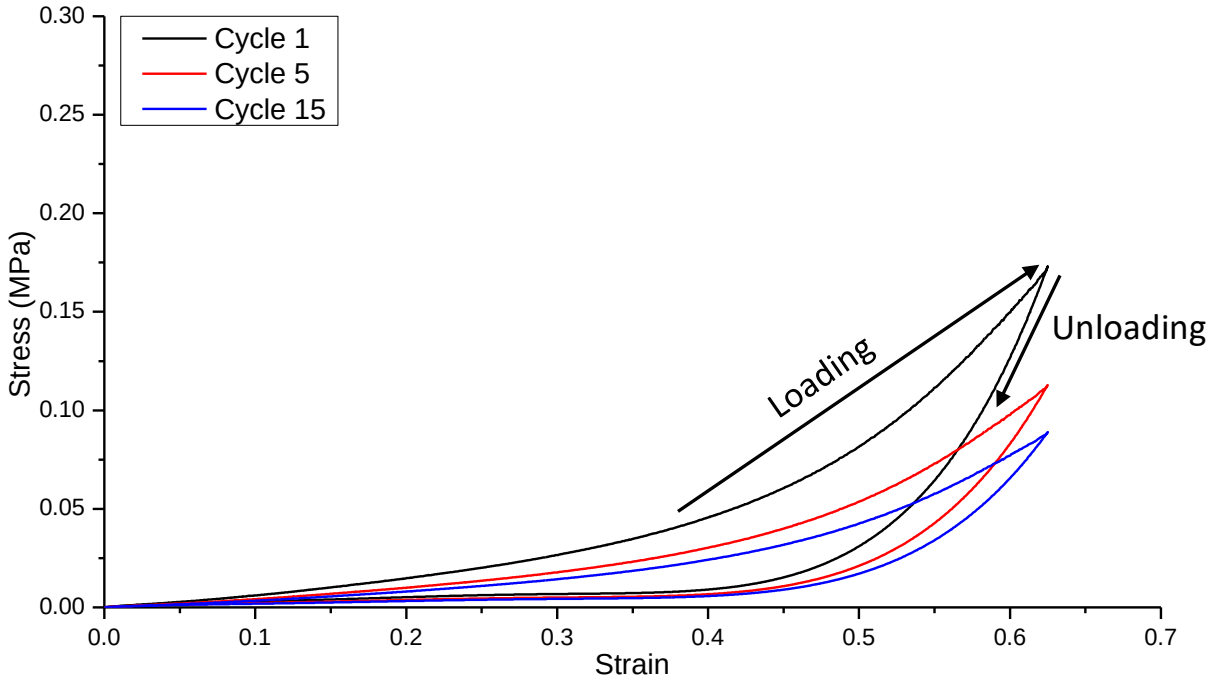

Figure 7.14 Compression fatigue stress-strain curve for trilayer composite, C.

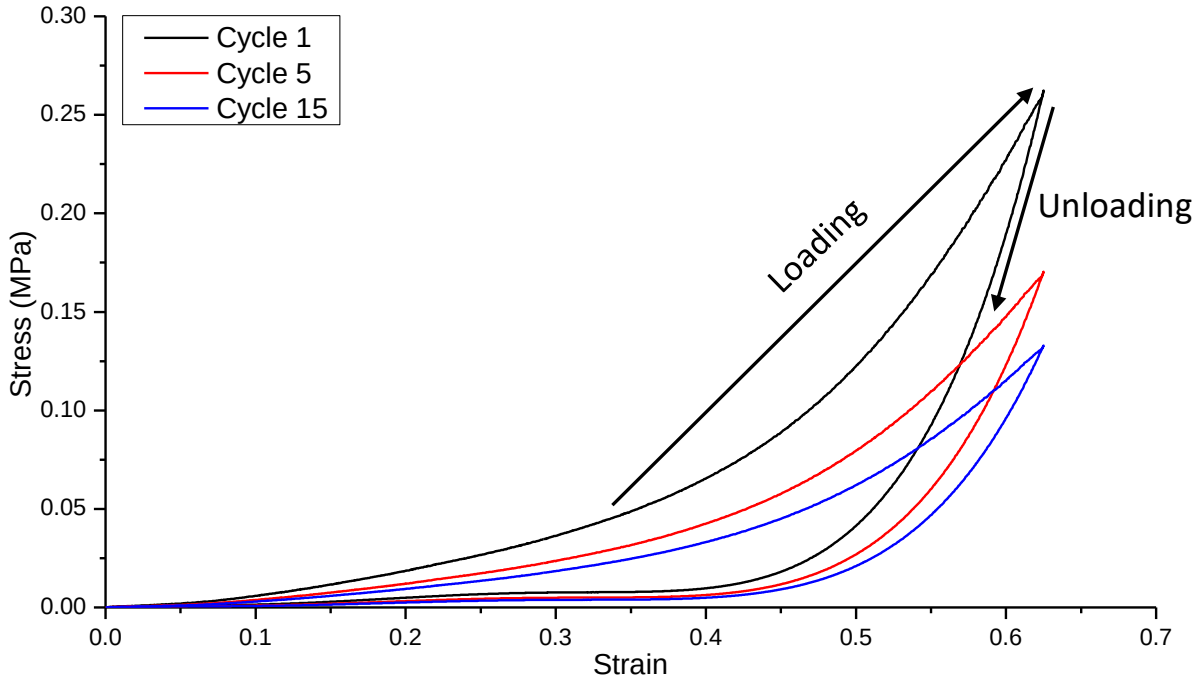

Figure 7.15 Compression fatigue stress-strain curve for segmented electrospun nonwoven reinforced composite, D.

Figure 7.12, Figure 7.13, Figure 7.14, and Figure 7.15 show the hysteresis response of constructions A, B, C and D respectively. The hysteresis response shows clear elastomeric behaviour, with the deformation energy being absorbed and the material returning to its original shape – evidenced by the response returning to 0 strain, 0 stress upon unloading. The response of all the materials follows the same trend, whereby a decreased hysteresis response is observed at 50 % maximum stress at cycle 15.

Comparison of the maximum stress at cycle 1 and cycle 5 of the materials shows that the bilayer construction, B, had the smallest decrease in maximum stress at 29.9 %, compared to 37.3 %, 34.8 % and 35.0 % for constructions A, C and D respectively. However, cycle 15 shows no significant

differences (P>0.05) in terms of maximum stress, with decreases of 51.1 %, 50.6 %, 48.6 % and 49.3 % for constructions A, B, C and D respectively.

Table 7.7 Dissipated energy of the four composites, data calculated through integration of the hysteresis response in cycle 1, 5 and 15.

Sample	Cycle 1 Dissipated Energy	Cycle 5 Dissipated Energy	Cycle 15 Dissipated Energy
A Unreinforced gel	0.047	0.029	0.023
B Bilayer reinforced composite	0.041	0.029	0.021
C Trilayer reinforced composite	0.043	0.028	0.023
D Segmented electrospun nonwoven reinforced composite	0.061	0.040	0.031

Energy dissipation for the four composites was calculated using OrginPro 8.5, integration analysis was used to generate values for the area of hysteresis loops for cycles 1, 5 and 15 (Table 7.7). There are no significant (P<0.05) differences in energy dissipation between constructions A, B and C however, the segmented electrospun nonwoven reinforced composite, D, shows significant increases in energy dissipation across all cycles. This is likely due to the orientation of the fibre reinforcement phase. Segmented electrospun nonwoven reinforced composite allows for strain to be distributed evenly throughout the composite structure, combined with the increase in maximum stress the composite can dissipate significantly more energy than other constructions.

7.5 Summary

Fibre reinforced composites comprised of PGS-based electrospun fibres and hydrogels, both with photocuring capabilities were successfully formed into three different constructions. Bilayer and trilayer constructions improve mechanical properties when compared with unreinforced gels, with significant ($P<0.05$) increases in maximum stress and modulus. segmented electrospun nonwoven reinforced composites outperformed other constructions, having a far greater maximum stress achieved during compression testing.

Compression fatigue testing showed that all constructions displayed similar elastic responses to strain, with the hysteresis responses following the same trend. Ultimately the hysteresis responses plateaued, with the maximum stress observed at cycle 15 being nearly 50 % for all tested samples.

Comparison of the modulus with literature values reported for fat pad tissue, which ranges from 0.1 MPa to 1.5 MPa, show that the modulus of the composite constructions produced falls within this range. The material was visibly elastic and was capable of undergoing deformation before returning to its original shape.

Hysteresis energy dissipation calculations showed that no significant improvements in energy dissipation were observed with a bilayer and trilayer construction compared to an unreinforced hydrogel. Reinforcement with a segmented electrospun nonwoven phase did however provide a large increase to energy dissipation, showing that mimicking a natural physiological tissue structure is beneficial with regards to improving maximum stress and energy dissipation.

Conclusions

At present, treatment of foot plantar defects involves silicone injections directly into the wound cavity, which compensates for the lack of tissue by providing mechanical support but does not enable any regenerative healing capacity. In an alternative approach, this work aimed to explore alternative elastomeric materials based on PGS, including variants with an elastomeric material was synthesised with photocuring functionality.

The key aims of the work as indicated in Chapter 1 were to review biocompatible elastomeric materials, suitable for the replacement of silicone that is currently used in a clinical setting as a treatment for fat pad loss due to diabetic ulceration. To design, manufacture and characterise a biocompatible, elastomeric material that can be reinforced with a fibre phase. This composite would be capable of delivery by injection where curing *in situ* would prevent invasive surgical procedures. Finally to characterise the materials degradation, physical and mechanical properties, which are relevant to clinical requirements.

Chapter 2 critically reviewed literature in relation to the clinical challenges with treating foot plantar defects (cavity wounds) and highlighted the lack of a regenerative approach, which is not feasible using current materials such as PDMS. Alternative elastomer materials were also reviewed, which showed that while some materials possess suitable ultimate strength, their elastomeric response was limited and so the material would not respond as a natural tissue would. Simulation of a natural tissues response to strain is a key requirement in successful implant devices, and so it was established that elastomers based on PGS could have potential for treatment of foot plantar defects, provided their mechanical properties could be appropriately modulated.

Other provisions regarding material choice also showed PGS to be an advantageous candidate due to its biocompatibility, potential to promote tissue regeneration, and economic considerations, *i.e.* the constituent reagents involved in the synthesis of PGS are food additives readily available which allows for a low-cost treatment that could potentially have a large impact on a patient's quality of life.

Chapter 3 summarised the experimental methods and equipment used in this work. ^{1}H NMR analysis was used to confirm molecular structures of synthesised products, ^{1}H NMR spectra were analysed using MestreNova® Research Lab software. FTIR analysis was used qualitatively to determine the success of modification protocols, analysis of spectra was conducted using Bruker OPUS 7.0 software. Scanning electron microscopy was used to evaluate nanofibrous webs produced using an electrospinning procedure, micrographs were then analysed using ImageJ processing software to determine fibre diameter and porosity of the samples. Differential scanning calorimetry and thermogravimetric analysis was used to characterise produced materials. Due to the properties of the elastomers produced in this work some materials were unsuitable for analysis as thermally driven polycondensation would take place during heating cycles.

Chapter 4 details the synthesis and modification protocols of PGS. Initial modification protocols were first tested with a model polymer, poly(vinyl alcohol-*co*-ethylene), to ensure suitability before being used on PGS. Acrylation protocols of the model polymer revealed a solvent interaction with the reagents, causing the production of a HCl vapour which reacted with the triethylamine present in the reaction mixture, forming an ammonium salt which nullified the modification process. Introduction of a different photo crosslinking functionality to the model polymer was achieved with the grafting of a norbornene moiety to the molecular structure. Steglich esterification was investigated as a suitable modification technique. Using DCC as a coupling reagent and DMAP as a

scavenger a norbornene carboxylic acid was grafted to the polymer structure, confirmed by ^{1}H NMR and FTIR analysis.

PGS synthesis was then achieved, followed by modification with the protocols used with the model polymer. Initial attempts to synthesise the polymer yielded a fully crosslinked material, that while elastic was unsuitable for further modification due to its insolubility. Solubility issues warranted a change in synthesis protocol. The synthesis followed two steps, linear chain formation then crosslinking, therefore the decision was made to synthesis the linear chains, oligo(glycerol sebacate), and attempt to modify it. Changing the solvent from DMSO to Dichloromethane for the modification with a norbornene carboxylic acid was successful, with the molecular structure being confirmed by ^{1}H NMR analysis. A beneficial side effect of the solvent change was the ability to remove large amounts of DCC urea, a by-product of the coupling reaction. ^{1}H NMR and FTIR analysis showed that while large amounts of DCC urea had been removed from the product, there was a significant presence in the final product – evidenced by the physical appearance of the material.

Acrylation of PGS is highly desirable, as it allows for crosslinking without the use of the high temperatures required during synthesis, ^{1}H NMR analysis showed that the modification had been successful with the presence of the three different proton environments corresponding to the acrylate functional group. PGS was synthesised with varied curing times to allow for materials with different potential reactive sites. Modulating the degree of modification of the polymer enabled some control over the crosslinked polymers properties.

Although the synthetic route involving DCC coupling was shown to be successful, the presence of urea by-products is highly detrimental in terms of clinical applications. Acrylation was far more successful as the reaction was high yield with low contamination, the introduced acrylate

functionality allows for photo crosslinking and gel formation, while the initial polymer synthesis involves no solvent or harmful chemicals.

Chapter 5 aimed to explore the potential synthesis of a water soluble, PGS based material capable of *in situ* curing. Inclusion of PEG and lactic acid improved the hydrophilicity of PGS, allowing the material to be used in an aqueous solution, which is desirable for the intended application where injection with other solvent systems would be harmful.

Initial synthesis routes involved a short chain PEG molecule, which produced viscous fluid products that were extremely difficult to handle. Removal from reaction vessels was a time-consuming process involving heating the polymer to reduce its viscosity. The produced materials were however readily soluble in water. Inclusion of catalysts in the synthesis procedure reduced the time needed for the polymerisation step.

Modifications to the molecular structure were conducted using the same procedures as were used on PGS, norbornene grafting and acrylation were investigated to determine if the modification techniques were suitable for the PGSLP material. As PGSLP was water soluble an effort was made to try and extract the material from a DCC urea contaminated product, extractions with water were separated, combined, and reduced which yielded a viscous fluid. Contrasting with the PGS, the materials physical appearance didn't indicate the presence of DCC urea. A relatively low yield was thought to be caused by interactions between the DCC urea and PGSLP, causing the polymer to crash out of solution and be removed during extraction.

^{1}H NMR analysis confirmed that modification of the polymer was successful, with the presence of the proton peaks associated with the alkene bond of the norbornene functional group. The presence of DCC urea by-products however were also shown to be present through analysis of the ^{1}H NMR spectrum.

Acrylation of PGSLP followed the same procedure that had been shown to be successful with PGS. ^{1}H NMR analysis confirmed the modification procedure was successful, the new material, PGSLPA was collected as a fine white powder and was still water soluble. Crosslinking investigations detailed in Chapter 7 ran alongside material synthesis and modification experiments, enabling a fluid approach to synthesis alterations. Increased glycerol and sebacic acid content materials were synthesised to increase the number of potential modification sites on the polymers structure. Increasing the absolute number of crosslinking sites would allow for materials to be produced with increased crosslink density – which would enable material properties such as maximum stress and elastic modulus to be modulated. Increasing the glycerol content produced a material far more problematic to handle and use for future experimentation, viscosity was greatly increased due to the increased crosslink density, in turn making handling and transfer of the polymer extremely difficult. Increasing both glycerol and sebacic acid content produced a material with increased viscosity and crystalline agglomerations, the agglomerations were likely unreacted sebacic acid and were removed by dialysis, as acrylation of the impure material would only serve to modify the terminal hydroxyl groups.

Increasing the PEG chain length used in the synthesis of the PGSLP material was intended to allow for easier crosslinking of the material, this would also allow the material to more easily be used to produce nanofibres by electrospinning. Increasing the PEG chain length from 1000 Mw to 100000 Mw was unsuccessful. Upon heating an extremely viscous mass in the reaction vessel was formed causing stirring to become non-functional. The reaction was abandoned as reaction conditions could not be met.

Following this, increasing the PEG chain length from 1000 Mw to 8000 Mw was investigated and successfully completed, this PEG chain length of 8000 Mw coincided with the Mw of the diacrylate PEG intended for use in crosslinking investigations. Differing the reaction times involved in the

synthesis of this novel material allowed for different degrees of crosslinking in the polymerisation, which enabled modulation of degree of modification. A long and short curing time polymer was synthesised and acrylated, upon reaction completion, the products were collected as viscous brown fluids, contrasting with the fine white powders collected in previous PGS and PGSLP acrylation reactions. This was assumed to be due to the increase in PEG chain length, solid particulates were present in the material and so dialysis was used to purify the material. This had the secondary benefit of removing the catalysts used for synthesis, producing a pure PGSLPA material that could then be used in electrospinning and gel formation investigations.

Chapter 6 describes the production of novel nanofibrous webs containing PGSLP. Initial electrospinning procedures involved trying to spin PGSLP in HFIP, however this proved unsuccessful with regard to producing nanofibres. Instead, a film was deposited onto the collection plate that could not be removed due to the physical properties, the film behaved similarly to the synthesis products in that it was a viscous fluid without any inherent strength.

Commixing with PCL allowed for nanofibrous webs to be produced, as the PCL acted as a carrier material. Spinning of PEG 1000 Mw containing PGSLP derivatives was unsuccessful, likely due to the low molecular weight of the PGSLP material causing weak chain entanglement. For the first time, novel electrospun nanofibrous webs containing PGSLP were produced, using an electrospinning solution comprised of 5 % wt/v PGSLP and 5 % wt/v PCL_{80000}, at operational voltage 20 kV, with a syringe tip to collector distance of 15 cm and flow rate of 1 mL h^{-1}. Successful nanofibre formation was observed with PEG 8000 Mw containing PGSLP derivatives, this was further confirmed by SEM analysis that showed fibre diameters and porosity values consistent with nanofibrous webs.

Separate investigations were conducted whereby gelatin was commixed with PGSLP as an alternative carrier material. A challenge that was observed with spinning of PGSLP and gelatin was

gel formation in the needle tip, which caused intermittent blockages. Gelling was also observed within the syringe, causing increased back pressure at the syringe pump. This was mitigated by reducing the volume of spinning solution held in the syringe, and therefore the residence time prior to extrusion but was still unsuccessful in producing a uniform nonwoven web. Electrospraying was also observed, producing a non-uniform web due to droplet formation, suggesting chain entanglement in the solution was inadequate, which is necessary to consistently form fibres.

Electrospinning of acrylated forms of PGSLP allows for crosslinking functionality to be included in the fibre reinforcement phase, increasing the interfacial interaction behaviour in a composite material. Electrospinning of PGSLPA and a photoinitiator proved successful, novel electrospun nanofibrous webs containing a photo active form of PGSLP were produced, allowing for crosslinking to occur post spinning. A 5 % wt/v PGSLPA and 5 % wt/v PCL_{80000}, at operational voltage 20 kV, with a syringe tip to collector distance of 15 cm and flow rate of 1 mL h^{-1} was used to successfully form the nonwoven web. Tensile testing of the produced nonwoven webs showed that the novel fibres outperformed PCL and PGS based webs in terms of maximum extension. Maximum stress was decreased for all PGSLP derivatives however, due to the increase in maximum extension the materials displayed a far higher work of rupture.

Chapter 7 examines the combination of the novel PGSLPA elastomer and PGSLPA nanofibrous webs. Photo crosslinking of various synthesised materials was achieved, norbornene and acrylate functionalised derivates of PGS and PGSLP were investigated for their ability to produce gels.

Thiol-ene click photo crosslinking is an attractive method of forming gels due to its high reaction speed and yields. Investigations using a PEG dithiol reagent yielded no gel formation with any formulations involving norbornene functionalised PGS and $PGSLP_{1000}$. Procedures were altered with increased dithiol content to encourage gel formation but were unsuccessful. Disulphide bond

formation was thought to be a hindering factor in the formation of gels and so a reducing agent was employed to alleviate the disulphide bond formation by reducing them to free thiols, this however didn't yield any successful gel formation. Where applicable solvent changes from deionised water to methanol were also investigated to determine if organogel formation was possible. The conclusion was that by-products present in the polymers from DCC coupling reactions was stopping gel formation by interacting with the crosslinking reagents or directly with the polymer.

Acrylated forms of PGS and $PGSLP_{1000}$ were also investigated as potential gel forming materials. PGS and PGSLP derivatives were incubated with a diacrylate PEG crosslinker however no gelation was observed. As all crosslinking had thus far proven unsuccessful, an effort was made to determine if gelation had occurred but at such a small degree that it was not observable. To investigate this all the formulations had increased quantities of crosslinker added. This however also yielded no observable gelation behaviour.

An alternative photoinitiator molecule was selected to see its effects on the crosslinking behaviour. DMPA was selected as it was readily soluble in methanol. All crosslinking reactions produced no visible gelation, with increased crosslinker content and increased reducing agent content having no impact.

Increased PEG chain length PGSLPA derivates were then investigated, as a way of determining if molecular chain length of the polymer was causing an issue with crosslinking. The chain length of PEG was increased from 1000 to 8000 Mw. Formulations of $PGSLP_{8000}A$ and PGSA were made up with both Irgacure 2959 and DMPA, once incubated and exposed to UV light all formulations were observed to have undergone partial gel formation. Increasing the concentrations of the formulations yielded complete gel formation, gels produced were stable with no fluid content.

Compression testing was then carried out on four different elastomeric constructs, where the bulk amorphous gel phase used a formulation known to undergo successful photo crosslinking. Fibre reinforcement in different forms was used in three constructs with one construct being a pure gel sample. Layer deposition was employed in two samples, forming a bilayer and trilayer composite, the third fibre reinforced composite had segmented electrospun nonwoven content. Segmented electrospun nonwoven reinforced composite represent a more natural structure, as biological tissues have a more randomly orientated fibre reinforcement phase within their extracellular matrix.

Compression to failure testing showed that all fibre reinforced composites outperform unreinforced hydrogels, with the segmented electrospun nonwoven composite performing best. The produced composites displayed elastic modulus values within the range of reported modulus values for plantar fat pad tissue. Compression fatigue testing showed that all constructs experience a similar degree of maximum stress decrease, which was achieved after 12 cycles. Hysteresis energy dissipation analysis showed that no significant difference was found between the unreinforced, bilayer reinforced, and trilayer reinforced composites, only the segmented electrospun nonwoven orientated fibre reinforced composite performed better.

A critical review of literature related to elastomeric materials for the replacement of silicone was conducted, with the down selection of PGS as a suitable candidate for development. Development of a hydrophilic derivative of PGS, PGSLP was conducted, and manufacture of fibre reinforced, injectable, photo-curing composites was successful. The assembled composite structures and the comprising materials were characterised to evaluate their physical and mechanical properties.

Recommendations for Further Work

Further development of the composite systems produced could involve alterations to the formulation component concentrations. In this work a known formulation was used to produce all composite structure bulk phase gels, changing the functionalised PGSLP and crosslinker concentrations would drastically alter the composite structures elastic modulus, energy dissipation and hysteresis response. Alterations to the volume fractions of the gel and fibre reinforcement phases would provide an avenue of investigation into creating a composite material with tuneable mechanical properties, that would better reflect the need of the intended implant recipient.

Further investigation into the degradation behaviour of the materials produced in this work would be key to understanding the materials potential applications. Cytotoxicity degradation studies to determine the products of degradation and their effect on endogenous tissue could provide insight into possible issues with biocompatibility.

Investigations into the use of the material as a regenerative scaffold would be insightful. The material was designed as a structural support composite for diabetic patients but may have applications in other clinical settings as a regeneration scaffold, provided cell penetration and proliferation are sufficient. Impregnation of the composite materials with endogenous tissue and study of their growth in the structure could provide understanding of the regenerative capacity of the material.

Inclusion of therapeutic molecules within the composite structure could provide some clinical benefit as a multi-faceted approach to treating a diabetic ulcer, inclusion of an antimicrobial therapeutic molecule into the amorphous phase or by direct modification of the molecular

structure with function antimicrobial moieties could allow for the underlying chronic infection to be treated while also allowing tissue regeneration of the low plantar tissue.

References

1. Turns, M. The diabetic foot: an overview for community nurses. *British Journal of Community Nursing.* 2012, **17**(9), pp.422-433.
2. Brem, H. and Tomic-Canic, M. Cellular and molecular basis of wound healing in diabetes. *The Journal of Clinical Investigation.* 2007, **117**(5), pp.1219-1222.
3. Jeffcoate, W.J. et al. Unresolved issues in the management of ulcers of the foot in diabetes. *Diabetic Medicine.* 2008, **25**(12), pp.1380-1389.
4. Vinik, A.I. Diabetic neuropathy: pathogenesis and therapy. *The American Journal of Medicine.* 1999, **107**(2, Supplement 2), pp.17-26.
5. Macfarlane, R.M. and Jeffcoate, W.J. Factors contributing to the presentation of diabetic foot ulcers. *Diabetic Medicine.* 1997, **14**(10), pp.867-870.
6. Rebolledo, F. et al. *The Pathogenesis of the Diabetic Foot Ulcer: Prevention and Management.* 2011.
7. Chen, H. et al. Electrospun 3D Fibrous Scaffolds for Chronic Wound Repair. *Materials.* 2016, **9**(4), p.272.
8. Turner, N.J. and Badylak, S.F. The Use of Biologic Scaffolds in the Treatment of Chronic Nonhealing Wounds. *Advances in Wound Care.* 2015, **4**(8), pp.490-500.
9. Grigoriadis, G. et al. Material properties of the heel fat pad across strain rates. *Journal of the Mechanical Behavior of Biomedical Materials.* 2017, **65**, pp.398-407.
10. Bowling, F.L. et al. Liquid Silicone to Mitigate Plantar Pedal Pressure: A Literature Review. *J Diabetes Sci Technol.* 2010, **4**(4), pp.846-852.
11. Wearing, S.C. and Smeathers, J.E. The heel fat pad: mechanical properties and clinical applications. *Journal of Foot and Ankle Research.* 2011, **4**(1), p.I14.
12. van Deursen, R. Mechanical Loading and Off-Loading of the Plantar Surface of the Diabetic Foot. *Clinical Infectious Diseases.* 2004, **39**(Supplement_2), pp.S87-S91.
13. Balkin, S.W. and Kaplan, L. Injectable silicone and the diabetic foot: a 25-year report. *The Foot.* 1991, **1**(2), pp.83-88.
14. van Schie, C.H. et al. The effect of silicone injections in the diabetic foot on peak plantar pressure and plantar tissue thickness: a 2-year follow-up. *Arch Phys Med Rehabil.* 2002, **83**(7), pp.919-23.
15. Garrido, L. et al. In vivo degradation of silicones. *Magn Reson Med.* 1993, **29**(6), pp.839-43.
16. Bowling, F.L. et al. Liquid silicone to mitigate plantar pedal pressure: a literature review. *J Diabetes Sci Technol.* 2010, **4**(4), pp.846-52.
17. Jahss, M.H. et al. Investigations into the Fat Pads of the Sole of the Foot: Anatomy and Histology. *Foot & Ankle.* 1992, **13**(5), pp.233-242.
18. Hsu, C.-C. et al. Diabetic effects on microchambers and macrochambers tissue properties in human heel pads. *Clinical Biomechanics.* 2009, **24**(8), pp.682-686.
19. Pai, S. and Ledoux, W.R. The compressive mechanical properties of diabetic and non-diabetic plantar soft tissue. *Journal of Biomechanics.* 2010, **43**(9), pp.1754-1760.
20. Kassab, G.S. and Sacks, M. *Structure-Based Mechanics of Tissues and Organs.* 2016.
21. Aerts, P. et al. The mechanical properties of the human heel pad: A paradox resolved. *Journal of Biomechanics.* 1995, **28**(11), pp.1299-1308.
22. Kinoshita, H. et al. In vivo examination of the dynamic properties of the human heel pad. *Int J Sports Med.* 1993, **14**(6), pp.312-9.

23. Bennett, M.B. and Ker, R.F. The mechanical properties of the human subcalcaneal fat pad in compression. *J Anat.* 1990, **171**, pp.131-8.
24. Ledoux, W.R. and Blevins, J.J. The compressive material properties of the plantar soft tissue. *Journal of Biomechanics.* 2007, **40**(13), pp.2975-2981.
25. Franz, S. et al. Immune responses to implants – A review of the implications for the design of immunomodulatory biomaterials. *Biomaterials.* 2011, **32**(28), pp.6692-6709.
26. Williams, D.F. On the mechanisms of biocompatibility. *Biomaterials.* 2008, **29**(20), pp.2941-2953.
27. Gorbet, M.B. and Sefton, M.V. Biomaterial-associated thrombosis: roles of coagulation factors, complement, platelets and leukocytes. *Biomaterials.* 2004, **25**(26), pp.5681-5703.
28. Anderson, J.M. Inflammatory response to implants. *ASAIO Trans.* 1988, **34**(2), pp.101-7.
29. Wilson, C.J. et al. Mediation of Biomaterial–Cell Interactions by Adsorbed Proteins: A Review. *Tissue Engineering.* 2005, **11**(1-2), pp.1-18.
30. Ratner, B.D. The engineering of biomaterials exhibiting recognition and specificity. *Journal of Molecular Recognition.* 1998, **9**(5-6), pp.617-625.
31. Anderson, J.M. Chapter II.2.2 - Inflammation, Wound Healing, and the Foreign-Body Response. In: Ratner, B.D. et al. eds. *Biomaterials Science (Third Edition)*. Academic Press, 2013, pp.503-512.
32. Katari, R. et al. Tissue Engineering and Regenerative Medicine: Semantic Considerations for an Evolving Paradigm. *Frontiers in Bioengineering and Biotechnology.* 2014, **2**, p.57.
33. Reddig, P.J. and Juliano, R.L. Clinging to life: cell to matrix adhesion and cell survival. *Cancer and Metastasis Reviews.* 2005, **24**(3), pp.425-439.
34. Zhao, D. et al. Understanding cell homing-based tissue regeneration from the perspective of materials. *Journal of Materials Chemistry B.* 2015, **3**(37), pp.7319-7333.
35. Hiraoka, Y. et al. In Situ Regeneration of Adipose Tissue in Rat Fat Pad by Combining a Collagen Scaffold with Gelatin Microspheres Containing Basic Fibroblast Growth Factor. *Tissue Engineering.* 2006, **12**(6), pp.1475-1487.
36. Degasne, I. et al. Effects of Roughness, Fibronectin and Vitronectin on Attachment, Spreading, and Proliferation of Human Osteoblast-Like Cells (Saos-2) on Titanium Surfaces. *Calcified Tissue International.* 1999, **64**(6), pp.499-507.
37. Webster, T.J. et al. Specific proteins mediate enhanced osteoblast adhesion on nanophase ceramics. *J Biomed Mater Res.* 2000, **51**(3), pp.475-483.
38. Webster, T.J. et al. Mechanisms of Enhanced Osteoblast Adhesion on Nanophase Alumina Involve Vitronectin. *Tissue Engineering.* 2001, **7**(3), pp.291-301.
39. Berthiaume, F. et al. Tissue Engineering and Regenerative Medicine: History, Progress, and Challenges. *Annual Review of Chemical and Biomolecular Engineering.* 2011, **2**(1), pp.403-430.
40. Sultana Phd Ceng Csci, N. *Biodegradable PHBV Polymer-Based Scaffolds for Bone Tissue Engineering.* 2013.
41. Köse, G.T. et al. Tissue engineered cartilage on collagen and PHBV matrices. *Biomaterials.* 2005, **26**(25), pp.5187-5197.
42. Longo, U.G. et al. Tendon augmentation grafts: a systematic review. *British Medical Bulletin.* 2010, **94**(1), pp.165-188.
43. Hirooka, A. et al. Augmentation with a Gore-Tex patch for repair of large rotator cuff tears that cannot be sutured. *Journal of Orthopaedic Science.* 2002, **7**(4), pp.451-456.
44. Baier Leach, J. et al. Photocrosslinked hyaluronic acid hydrogels: natural, biodegradable tissue engineering scaffolds. *Biotechnol Bioeng.* 2003, **82**(5), pp.578-89.

45. Chevallay, B. and Herbage, D. Collagen-based biomaterials as 3D scaffold for cell cultures: applications for tissue engineering and gene therapy. *Medical and Biological Engineering and Computing.* 2000, **38**(2), pp.211-218.
46. Zhang, R. and Ma, P.X. Poly(alpha-hydroxyl acids)/hydroxyapatite porous composites for bone-tissue engineering. I. Preparation and morphology. *J Biomed Mater Res.* 1999, **44**(4), pp.446-55.
47. Nair, L.S. and Laurencin, C.T. Biodegradable polymers as biomaterials. *Progress in Polymer Science.* 2007, **32**(8), pp.762-798.
48. Badylak, S.F. et al. Extracellular matrix as a biological scaffold material: Structure and function. *Acta Biomater.* 2009, **5**(1), pp.1-13.
49. Olenius, M. The first clinical study using a new biodegradable implant for the treatment of lips, wrinkles, and folds. *Aesthetic Plast Surg.* 1998, **22**(2), pp.97-101.
50. Moyle, G.J. et al. A randomized open-label study of immediate versus delayed polylactic acid injections for the cosmetic management of facial lipoatrophy in persons with HIV infection. *HIV Med.* 2004, **5**(2), pp.82-7.
51. Foumenteze, J.P. et al. Hyaluronic Acid Filler Injections Under the Metatarsal Heads Provide a Significant and Long-Lasting Improvement in Metatarsalgia From Wearing High-Heeled Shoes. *Dermatologic Surgery.* 2018, **44**(7), pp.994-1001.
52. Ballin, A.C. et al. Dermal Fillers: An Update. *American Journal of Clinical Dermatology.* 2015, **16**(4), pp.271-283.
53. Funt, D. and Pavicic, T. Dermal fillers in aesthetics: an overview of adverse events and treatment approaches. *Clinical, Cosmetic and Investigational Dermatology.* 2013, **6**, pp.295-316.
54. Richert, L. et al. Improvement of Stability and Cell Adhesion Properties of Polyelectrolyte Multilayer Films by Chemical Cross-Linking. *Biomacromolecules.* 2004, **5**(2), pp.284-294.
55. Shiratori, S.S. and Rubner, M.F. pH-Dependent Thickness Behavior of Sequentially Adsorbed Layers of Weak Polyelectrolytes. *Macromolecules.* 2000, **33**(11), pp.4213-4219.
56. Dubas, S.T. and Schlenoff, J.B. Polyelectrolyte Multilayers Containing a Weak Polyacid: Construction and Deconstruction. *Macromolecules.* 2001, **34**(11), pp.3736-3740.
57. Fery, A. et al. Nanoporous Thin Films Formed by Salt-Induced Structural Changes in Multilayers of Poly(acrylic acid) and Poly(allylamine). *Langmuir.* 2001, **17**(13), pp.3779-3783.
58. Tan, S.H. et al. Oxygen plasma treatment for reducing hydrophobicity of a sealed polydimethylsiloxane microchannel. *Biomicrofluidics.* 2010, **4**(3), p.032204.
59. Chaiwong, C. et al. Effect of plasma treatment on hydrophobicity and barrier property of polylactic acid. *Surface and Coatings Technology.* 2010, **204**(18), pp.2933-2939.
60. Klee, D. et al. Surface modification of a new flexible polymer with improved cell adhesion. *Journal of Materials Science: Materials in Medicine.* 1994, **5**(9), pp.592-595.
61. Li, X. et al. Surface modification with fibronectin or collagen to improve the cell adhesion. *Applied Surface Science.* 2008, **255**(2), pp.459-461.
62. Grinnell, F. and Phan, T.V. Deposition of fibronectin on material surfaces exposed to plasma: Quantitative and biological studies. *Journal of Cellular Physiology.* 2005, **116**(3), pp.289-296.
63. Van Agthoven, J.F. et al. Structural basis for pure antagonism of integrin αVβ3 by a high affinity form of fibronectin. *Nature structural & molecular biology.* 2014, **21**(4), pp.383-388.
64. Redick, S.D. et al. Defining Fibronectin's Cell Adhesion Synergy Site by Site-Directed Mutagenesis. *The Journal of Cell Biology.* 2000, **149**(2), pp.521-527.

65. Chluba, J. et al. Peptide Hormone Covalently Bound to Polyelectrolytes and Embedded into Multilayer Architectures Conserving Full Biological Activity. *Biomacromolecules.* 2001, **2**(3), pp.800-805.
66. Leguen, E. et al. Bioactive coatings based on polyelectrolyte multilayer architectures functionalized by embedded proteins, peptides or drugs. *Biomolecular Engineering.* 2007, **24**(1), pp.33-41.
67. Mendelsohn, J.D. et al. Rational Design of Cytophilic and Cytophobic Polyelectrolyte Multilayer Thin Films. *Biomacromolecules.* 2003, **4**(1), pp.96-106.
68. Stuckey, D.J. et al. Magnetic resonance imaging evaluation of remodeling by cardiac elastomeric tissue scaffold biomaterials in a rat model of myocardial infarction. *Tissue Eng Part A.* 2010, **16**(11), pp.3395-402.
69. Ker, R.F. The time-dependent mechanical properties of the human heel pad in the context of locomotion. *The Journal of Experimental Biology.* 1996, **199**(7), p.1501.
70. Meyers, M.A. and Chawla, K.K. *Mechanical Behavior of Materials.* 2 ed. Cambridge: Cambridge University Press, 2008.
71. Fontanella, C.G. et al. Biomechanical behavior of plantar fat pad in healthy and degenerative foot conditions. *Medical & Biological Engineering & Computing.* 2016, **54**(4), pp.653-661.
72. Case, J. et al. 1 - Tension and compression: direct stresses. In: Case, J. et al. eds. *Strength of Materials and Structures (Fourth Edition)*. London: Butterworth-Heinemann, 1999, pp.12-54.
73. NDT Resource Centre. *Toughness.* [Online]. 2018. [Accessed 22 Aug]. Available from: https://www.nde-ed.org/EducationResources/CommunityCollege/Materials/Mechanical/Toughness.htm
74. Callister, W.D. and Rethwisch, D.G. *Materials science and engineering : an introduction.* 2014.
75. Horath, L. *Fundamentals of materials science for technologists: properties, testing, and laboratory exercises.* Waveland Press, 2017.
76. Callister, W.D. and Rethwisch, D.G. *Fundamentals of materials science and engineering.* Wiley London, UK:, 2000.
77. Chen, Q. et al. Elastomeric biomaterials for tissue engineering. *Progress in Polymer Science.* 2013, **38**(3), pp.584-671.
78. Hiki, S. et al. Synthesis and characterization of hydroxy-terminated [RS]-poly(3-hydroxybutyrate) and its utilization to block copolymerization with l-lactide to obtain a biodegradable thermoplastic elastomer. *Polymer.* 2000, **41**(20), pp.7369-7379.
79. Curtis, J. and Colas, A. Chapter II.5.18 - Medical Applications of Silicones A2 - Ratner, Buddy D. In: Hoffman, A.S. et al. eds. *Biomaterials Science (Third Edition)*. Academic Press, 2013, pp.1106-1116.
80. Curtis, J. and Colas, A. Chapter II.5.18 - Medical Applications of Silicones. In: Ratner, B.D. et al. eds. *Biomaterials Science (Third Edition)*. Academic Press, 2013, pp.1106-1116.
81. Owen, M.J. Elastomers: Siloxane. In: Buschow, K.H.J. et al. eds. *Encyclopedia of Materials: Science and Technology*. Oxford: Elsevier, 2001, pp.2480-2482.
82. De Nicola, R.R. Permanent Artificial (Silicone) Urethra. *The Journal of Urology.* 1950, **63**(1), pp.168-172.
83. Smelser, G.K. and Ozanics, V. Importance of atmospheric oxygen for maintenance of the optical properties of the human cornea. *Science.* 1952, **115**(2980), pp.140-1.
84. Papas, E.B. The significance of oxygen during contact lens wear. *Contact Lens and Anterior Eye.* 2014, **37**(6), pp.394-404.

85. Santerre, J.P. et al. Understanding the biodegradation of polyurethanes: From classical implants to tissue engineering materials. *Biomaterials.* 2005, **26**(35), pp.7457-7470.
86. Zdrahala, R.J. and Zdrahala, I.J. Biomedical Applications of Polyurethanes: A Review of Past Promises, Present Realities, and a Vibrant Future. *J Biomater Appl.* 1999, **14**(1), pp.67-90.
87. Zdrahala, R.J. Small caliber vascular grafts. Part II: Polyurethanes revisited. *J Biomater Appl.* 1996, **11**(1), pp.37-61.
88. Abraham, G.A. et al. Bioresorbable poly(ester-ether urethane)s from L-lysine diisocyanate and triblock copolymers with different hydrophilic character. *J Biomed Mater Res A.* 2006, **76**(4), pp.729-36.
89. Gorna, K. and Gogolewski, S. Biodegradable porous polyurethane scaffolds for tissue repair and regeneration. *J Biomed Mater Res A.* 2006, **79**(1), pp.128-38.
90. Schoental, R. Carcinogenic and Chronic Effects of 4,4′-Diaminodiphenylmethane, an Epoxyresin Hardener. *Nature.* 1968, **219**, p.1162.
91. Cardy, R.H. Carcinogenicity and Chronic Toxicity of 2,4-Toluenediamine in F344 Rats2. *JNCI: Journal of the National Cancer Institute.* 1979, **62**(4), pp.1107-1116.
92. Zdrahala, R.J. et al. Polyether-based thermoplastic polyurethanes. I. Effect of the hard-segment content. *Journal of Applied Polymer Science.* 1979, **24**(9), pp.2041-2050.
93. Oertel, G. and Abele, L. *Polyurethane Handbook: Chemistry, Raw Materials, Processing, Application, Properties.* Hanser, 1994.
94. Guan, J. et al. Synthesis, characterization, and cytocompatibility of elastomeric, biodegradable poly(ester-urethane)ureas based on poly(caprolactone) and putrescine. *J Biomed Mater Res.* 2002, **61**(3), pp.493-503.
95. Anderson, A.J. and Dawes, E.A. Occurrence, metabolism, metabolic role, and industrial uses of bacterial polyhydroxyalkanoates. *Microbiol Rev.* 1990, **54**(4), pp.450-72.
96. Sudesh, K. et al. Synthesis, structure and properties of polyhydroxyalkanoates: biological polyesters. *Progress in Polymer Science.* 2000, **25**(10), pp.1503-1555.
97. Lu, J. et al. Mini-Review: Biosynthesis of Poly(hydroxyalkanoates). *Polymer Reviews.* 2009, **49**(3), pp.226-248.
98. Kaufman, E.E. et al. Regulation and properties of an NADP+ oxidoreductase which functions as a gamma-hydroxybutyrate dehydrogenase. *J Neurochem.* 1983, **40**(6), pp.1639-46.
99. Romero, L.A. et al. Effects of serum and endotoxin in experimental lung injury. *Journal of Pediatric Surgery.* 1990, **25**(8), pp.846-849.
100. Spitalsky, Z. and Bleha, T. Elastic properties of poly(hydroxybutyrate) molecules. *Macromol Biosci.* 2004, **4**(6), pp.601-9.
101. Dufresne, A. and Vincendon, M. Poly(3-hydroxybutyrate) and Poly(3-hydroxyoctanoate) Blends: Morphology and Mechanical Behavior. *Macromolecules.* 2000, **33**(8), pp.2998-3008.
102. Martin, D.P. and Williams, S.F. Medical applications of poly-4-hydroxybutyrate: a strong flexible absorbable biomaterial. *Biochemical Engineering Journal.* 2003, **16**(2), pp.97-105.
103. Choi, J. and Lee, S.Y. Factors affecting the economics of polyhydroxyalkanoate production by bacterial fermentation. *Applied Microbiology and Biotechnology.* 1999, **51**(1), pp.13-21.
104. Neises, B. and Steglich, W. Simple Method for the Esterification of Carboxylic Acids. *Angewandte Chemie International Edition in English.* 1978, **17**(7), pp.522-524.
105. Bruggeman, J.P. et al. Biodegradable Poly(polyol sebacate) Polymers. *Biomaterials.* 2008, **29**(36), pp.4726-4735.
106. Wang, Y. et al. In vivo degradation characteristics of poly(glycerol sebacate). *Journal of Biomedical Materials Research Part A.* 2003, **66A**(1), pp.192-197.

107. Liang, S.-L. et al. The mechanical characteristics and in vitro biocompatibility of poly(glycerol sebacate)-Bioglass® elastomeric composites. *Biomaterials.* 2010, **31**(33), pp.8516-8529.
108. Chen, Q.-Z. et al. An elastomeric patch derived from poly(glycerol sebacate) for delivery of embryonic stem cells to the heart. *Biomaterials.* 2010, **31**(14), pp.3885-3893.
109. Loh, X.J. et al. Poly(glycerol sebacate) biomaterial: synthesis and biomedical applications. *Journal of Materials Chemistry B.* 2015, **3**(39), pp.7641-7652.
110. Chen, Q.-Z. et al. Biomaterials in cardiac tissue engineering: Ten years of research survey. *Materials Science and Engineering: R: Reports.* 2008, **59**(1), pp.1-37.
111. Nijst, C.L.E. et al. Synthesis and Characterization of Photocurable Elastomers from Poly(glycerol-co-sebacate). *Biomacromolecules.* 2007, **8**(10), pp.3067-3073.
112. Gerecht, S. et al. A porous photocurable elastomer for cell encapsulation and culture. *Biomaterials.* 2007, **28**(32), pp.4826-4835.
113. E., H.C. and N., B.C. Thiol–Ene Click Chemistry. *Angewandte Chemie International Edition.* 2010, **49**(9), pp.1540-1573.
114. Lowe, A.B. Thiol-ene "click" reactions and recent applications in polymer and materials synthesis. *Polymer Chemistry.* 2010, **1**(1), pp.17-36.
115. ten Brummelhuis, N. et al. Thiol–Ene Modification of 1,2-Polybutadiene Using UV Light or Sunlight. *Macromolecules.* 2008, **41**(24), pp.9946-9947.
116. Justynska, J. et al. Toward a toolbox of functional block copolymers via free-radical addition of mercaptans. *Polymer.* 2005, **46**(26), pp.12057-12064.
117. Justyna, J. and Helmut, S. Modular Synthesis of Functional Block Copolymers. *Macromolecular Rapid Communications.* 2004, **25**(16), pp.1478-1481.
118. Mahdavi, A. et al. A biodegradable and biocompatible gecko-inspired tissue adhesive. *Proceedings of the National Academy of Sciences.* 2008, **105**(7), pp.2307-2312.
119. Yang, J. et al. Novel Citric Acid-Based Biodegradable Elastomers for Tissue Engineering. *Advanced Materials.* 2004, **16**(6), pp.511-516.
120. Yang, J. et al. Synthesis and evaluation of poly(diol citrate) biodegradable elastomers. *Biomaterials.* 2006, **27**(9), pp.1889-1898.
121. Di Lullo, G.A. et al. Mapping the ligand-binding sites and disease-associated mutations on the most abundant protein in the human, type I collagen. *J Biol Chem.* 2002, **277**(6), pp.4223-31.
122. Gosline, J. et al. Elastic proteins: biological roles and mechanical properties. *Philosophical Transactions of the Royal Society of London. Series B: Biological Sciences.* 2002, **357**(1418), p.121.
123. Muiznieks, L.D. and Keeley, F.W. Molecular assembly and mechanical properties of the extracellular matrix: A fibrous protein perspective. *Biochimica et Biophysica Acta (BBA) - Molecular Basis of Disease.* 2013, **1832**(7), pp.866-875.
124. Cox, B.A. et al. Communication: Coacervation of tropoelastin results in fiber formation. *J Biol Chem.* 1974, **249**(3), pp.997-8.
125. Wright, E.R. et al. Thermoplastic Elastomer Hydrogels via Self-Assembly of an Elastin-Mimetic Triblock Polypeptide. *Advanced Functional Materials.* 2002, **12**(2), pp.149-154.
126. Bellingham, C.M. et al. Recombinant human elastin polypeptides self-assemble into biomaterials with elastin-like properties. *Biopolymers.* 2003, **70**(4), pp.445-455.
127. Jawad, H. et al. Nanocomposite Elastomeric Biomaterials for Myocardial Tissue Engineering Using Embryonic Stem Cell-derived Cardiomyocytes. *Advanced Engineering Materials.* 2010, **12**(12), pp.B664-B674.

128. Medalia, A.I. and Kraus, G. 8 - Reinforcement of Elastomers by Particulate Fillers A2 - Mark, James E. In: Erman, B. and Eirich, F.R. eds. *Science and Technology of Rubber (Second Edition)*. San Diego: Academic Press, 1994, pp.387-418.
129. Chen, Q. et al. Elastomeric nanocomposites as cell delivery vehicles and cardiac support devices. *Soft Matter.* 2010, **6**(19), pp.4715-4726.
130. Qiu, H. et al. A citric acid-based hydroxyapatite composite for orthopedic implants. *Biomaterials.* 2006, **27**(34), pp.5845-5854.
131. Chen, Q. et al. A comparative study on in vitro enzymatic degradation of poly(glycerol sebacate) and poly(xylitol sebacate). *RSC Advances.* 2012, **2**(10), pp.4125-4134.
132. Liang, S.-L. et al. In Vitro enzymatic degradation of poly (glycerol sebacate)-based materials. *Biomaterials.* 2011, **32**(33), pp.8486-8496.
133. Mehdizadeh, M. and Yang, J. Design Strategies and Applications of Tissue Bioadhesives. *Macromol Biosci.* 2013, **13**(3), pp.271-288.
134. Mizrahi, B. et al. Elasticity and safety of alkoxyethyl cyanoacrylate tissue adhesives. *Acta Biomater.* 2011, **7**(8), pp.3150-7.
135. Bhagat, V. and Becker, M.L. Degradable Adhesives for Surgery and Tissue Engineering. *Biomacromolecules.* 2017, **18**(10), pp.3009-3039.
136. Joan, F.J.I. et al. Introduction of Flexible Cyanoacrylates in Sutureless Gastric Closure. *Surgical Innovation.* 2016, **23**(5), pp.490-497.
137. Xu, L. et al. A cross-linking strategy provides a new generation of biodegradable and biocompatible cyanoacrylate medical adhesives. *Journal of Materials Chemistry B.* 2016, **4**(23), pp.4147-4155.
138. Lim, J.I. et al. The adhesive properties of prepolymerized allyl 2-cyanoacrylate/poly L-3,4-dihydroxyphenylalanine for use as bioglue. *Materials Letters.* 2012, **81**(Supplement C), pp.251-253.
139. Lee, Y.J. et al. Biocompatibility of a Novel Cyanoacrylate Based Tissue Adhesive: Cytotoxicity and Biochemical Property Evaluation. *PLOS ONE.* 2013, **8**(11), p.e79761.
140. Kureha, T. et al. Water-immiscible bioinert coatings and film formation from aqueous dispersions of poly(2-methoxyethyl acrylate) microspheres. *Colloids and Surfaces B: Biointerfaces.* 2017, **155**(Supplement C), pp.166-172.
141. Schacht, E.H. Polymer chemistry and hydrogel systems. *Journal of Physics: Conference Series.* 2004, **3**(1), p.22.
142. Illeperuma, W.R.K. et al. Fiber-reinforced tough hydrogels. *Extreme Mechanics Letters.* 2014, **1**, pp.90-96.
143. Peppas, N.A. et al. Hydrogels in Biology and Medicine: From Molecular Principles to Bionanotechnology. *Advanced Materials.* 2006, **18**(11), pp.1345-1360.
144. Gong, J.P. et al. Double-Network Hydrogels with Extremely High Mechanical Strength. *Advanced Materials.* 2003, **15**(14), pp.1155-1158.
145. Agrawal, A. et al. Strong fiber-reinforced hydrogel. *Acta Biomater.* 2013, **9**(2), pp.5313-5318.
146. Lee, S. et al. The effects of varying poly(ethylene glycol) hydrogel crosslinking density and the crosslinking mechanism on protein accumulation in three-dimensional hydrogels. *Acta Biomater.* 2014, **10**(10), pp.4167-4174.
147. Okay, O. General Properties of Hydrogels. In: Gerlach, G. and Arndt, K.-F. eds. *Hydrogel Sensors and Actuators: Engineering and Technology*. Berlin, Heidelberg: Springer Berlin Heidelberg, 2010, pp.1-14.
148. Omidian, H. et al. *Swelling and Crosslink Density Measurements for Hydrogels.* 1994.

149. Jordan, J. et al. Experimental trends in polymer nanocomposites—a review. *Materials Science and Engineering: A.* 2005, **393**(1), pp.1-11.
150. Hussain, F. et al. Review article: Polymer-matrix Nanocomposites, Processing, Manufacturing, and Application: An Overview. *Journal of Composite Materials.* 2006, **40**(17), pp.1511-1575.
151. Tjong, S.C. Structural and mechanical properties of polymer nanocomposites. *Materials Science and Engineering: R: Reports.* 2006, **53**(3), pp.73-197.
152. Yang, J. et al. Cellulose Nanocrystals Mechanical Reinforcement in Composite Hydrogels with Multiple Cross-Links: Correlations between Dissipation Properties and Deformation Mechanisms. *Macromolecules.* 2014, **47**(12), pp.4077-4086.
153. Gaharwar, A.K. et al. Highly Extensible, Tough, and Elastomeric Nanocomposite Hydrogels from Poly(ethylene glycol) and Hydroxyapatite Nanoparticles. *Biomacromolecules.* 2011, **12**(5), pp.1641-1650.
154. McCullen, S.D. et al. Fiber-reinforced scaffolds for tissue engineering and regenerative medicine: use of traditional textile substrates to nanofibrous arrays. *Journal of Materials Chemistry.* 2010, **20**(40), pp.8776-8788.
155. Mauck, R.L. et al. Engineering on the straight and narrow: the mechanics of nanofibrous assemblies for fiber-reinforced tissue regeneration. *Tissue Eng Part B Rev.* 2009, **15**(2), pp.171-93.
156. Li, D. and Xia, Y. Electrospinning of Nanofibers: Reinventing the Wheel? *Advanced Materials.* 2004, **16**(14), pp.1151-1170.
157. Reneker, D.H. and Yarin, A.L. Electrospinning jets and polymer nanofibers. *Polymer.* 2008, **49**(10), pp.2387-2425.
158. Teo, W.-E. and Ramakrishna, S. Electrospun nanofibers as a platform for multifunctional, hierarchically organized nanocomposite. *Composites Science and Technology.* 2009, **69**(11), pp.1804-1817.
159. Kedem, S. et al. Composite Polymer Nanofibers with Carbon Nanotubes and Titanium Dioxide Particles. *Langmuir.* 2005, **21**(12), pp.5600-5604.
160. Zhu, Y. et al. Multifunctional Carbon Nanofibers with Conductive, Magnetic and Superhydrophobic Properties. *ChemPhysChem.* 2006, **7**(2), pp.336-341.
161. Hu, G. et al. Anatase TiO2 nanoparticles/carbon nanotubes nanofibers: preparation, characterization and photocatalytic properties. *Journal of Materials Science.* 2007, **42**(17), pp.7162-7170.
162. Chronakis, I.S. Novel nanocomposites and nanoceramics based on polymer nanofibers using electrospinning process—A review. *Journal of Materials Processing Technology.* 2005, **167**(2), pp.283-293.
163. Yeo, L.Y. and Friend, J.R. Electrospinning carbon nanotube polymer composite nanofibers. *Journal of Experimental Nanoscience.* 2006, **1**(2), pp.177-209.
164. Ayutsede, J. et al. Carbon Nanotube Reinforced Bombyx mori Silk Nanofibers by the Electrospinning Process. *Biomacromolecules.* 2006, **7**(1), pp.208-214.
165. Cohen, Y. and Pyckhout-Hintzen, W. *From Carbon Nanotube Dispersion to Composite Nanofibers.* 2005.
166. Kannan, P. et al. *Deformation of Isolated Single-Wall Carbon Nanotubes in Electrospun Polymer Nanofibres.* 2007.
167. Jo, E. et al. Core-Sheath Nanofibers Containing Colloidal Arrays in the Core for Programmable Multi-Agent Delivery. *Advanced Materials.* 2009, **21**(9), pp.968-972.

168. Yang, Y. et al. Release pattern and structural integrity of lysozyme encapsulated in core–sheath structured poly(dl-lactide) ultrafine fibers prepared by emulsion electrospinning. *European Journal of Pharmaceutics and Biopharmaceutics.* 2008, **69**(1), pp.106-116.
169. Chan, K.H.K. and Kotaki, M. Fabrication and morphology control of poly(methyl methacrylate) hollow structures via coaxial electrospinning. *Journal of Applied Polymer Science.* 2009, **111**(1), pp.408-416.
170. Bas, O. et al. Enhancing structural integrity of hydrogels by using highly organised melt electrospun fibre constructs. *European Polymer Journal.* 2015, **72**(Supplement C), pp.451-463.
171. Shin, Y.M. et al. Experimental characterization of electrospinning: the electrically forced jet and instabilities. *Polymer.* 2001, **42**(25), pp.09955-09967.
172. Guan, J. et al. Biodegradable poly(ether ester urethane)urea elastomers based on poly(ether ester) triblock copolymers and putrescine: synthesis, characterization and cytocompatibility. *Biomaterials.* 2004, **25**(1), pp.85-96.
173. Guelcher, S.A. et al. Synthesis, mechanical properties, biocompatibility, and biodegradation of polyurethane networks from lysine polyisocyanates. *Biomaterials.* 2008, **29**(12), pp.1762-1775.
174. Fromstein, J.D. and Woodhouse, K.A. Elastomeric biodegradable polyurethane blends for soft tissue applications. *Journal of Biomaterials Science, Polymer Edition.* 2002, **13**(4), pp.391-406.
175. Avella, M. et al. Review Properties of blends and composites based on poly(3-hydroxy)butyrate (PHB) and poly(3-hydroxybutyrate-hydroxyvalerate) (PHBV) copolymers. *Journal of Materials Science.* 2000, **35**(3), pp.523-545.
176. Meyers, M.A. et al. Biological materials: Structure and mechanical properties. *Progress in Materials Science.* 2008, **53**(1), pp.1-206.
177. Theron, A. et al. Electrostatic Field-Assisted Alignment of Electrospun Nanofibres. *Nanotechnology.* 2001, **12**, p.384.
178. Li, D. et al. Electrospinning of Polymeric and Ceramic Nanofibers as Uniaxially Aligned Arrays. *Nano Lett.* 2003, **3**(8), pp.1167-1171.
179. Li, D. et al. Electrospinning Nanofibers as Uniaxially Aligned Arrays and Layer-by-Layer Stacked Films. 2004, **16**(4), pp.361-366.
180. Gao, J. et al. Macroporous elastomeric scaffolds with extensive micropores for soft tissue engineering. *Tissue Eng.* 2006, **12**(4), pp.917-25.
181. Motlagh, D. et al. Hemocompatibility evaluation of poly(glycerol-sebacate) in vitro for vascular tissue engineering. *Biomaterials.* 2006, **27**(24), pp.4315-4324.
182. Gerecht, S. et al. A porous photocurable elastomer for cell encapsulation and culture. *Biomaterials.* 2007, **28**(32), pp.4826-35.
183. Yeh, Y.-C. et al. Norbornene-modified poly(glycerol sebacate) as a photocurable and biodegradable elastomer. *Polymer Chemistry.* 2017, **8**(34), pp.5091-5099.
184. Jordan, A. et al. A solvent-reagent selection guide for Steglich-type esterification of carboxylic acids. *Green Chemistry.* 2021, **23**(17), pp.6405-6413.
185. Jia, Y. et al. Synthesis and characterization of poly(glycerol sebacate)-based elastomeric copolyesters for tissue engineering applications. *Polymer Chemistry.* 2016, **7**(14), pp.2553-2564.
186. Vogt, L. et al. Poly(Glycerol Sebacate) in Biomedical Applications—A Review of the Recent Literature. *Advanced Healthcare Materials.* 2021, **10**(9), p.2002026.
187. Bosworth, L.A. and Downes, S. Physicochemical characterisation of degrading polycaprolactone scaffolds. *Polymer Degradation and Stability.* 2010, **95**(12), pp.2269-2276.

188. Manoukian, O.S. et al. Biodegradable Polymeric Injectable Implants for Long-Term Delivery of Contraceptive Drugs. *Journal of Applied Polymer Science.* 2018, **135**(14), p.46068.
189. Ker, R.F. The design of soft collagenous load-bearing tissues. *Journal of Experimental Biology.* 1999, **202**(23), p.3315.
190. Cornwell, K.G. et al. Extracellular Matrix Biomaterials for Soft Tissue Repair. *Clin Podiatr Med Surg.* 2009, **26**(4), pp.507-523.
191. Li, X. et al. Biocomposites reinforced by fibers or tubes as scaffolds for tissue engineering or regenerative medicine. *J Biomed Mater Res A.* 2014, **102**(5), pp.1580-94.
192. Moffat, K.L. et al. Novel nanofiber-based scaffold for rotator cuff repair and augmentation. *Tissue Eng Part A.* 2009, **15**(1), pp.115-26.
193. Li, X. et al. Collagen-based scaffolds reinforced by chitosan fibres for bone tissue engineering. *Polymer International.* 2005, **54**(7), pp.1034-1040.
194. Geethamma, V.G. et al. Short coir fiber-reinforced natural rubber composites: Effects of fiber length, orientation, and alkali treatment. *Journal of Applied Polymer Science.* 1995, **55**(4), pp.583-594.
195. Caves, J.M. et al. The use of microfiber composites of elastin-like protein matrix reinforced with synthetic collagen in the design of vascular grafts. *Biomaterials.* 2010, **31**(27), p.10.1016/j.biomaterials.2010.05.014.
196. Slivka, M.A. et al. Porous, resorbable, fiber-reinforced scaffolds tailored for articular cartilage repair. *Tissue Eng.* 2001, **7**(6), pp.767-80.
197. Fu, S.-Y. et al. 5 - Strength of short fibre reinforced polymers. In: Fu, S.-Y. et al. eds. *Science and Engineering of Short Fibre Reinforced Polymer Composites*. Woodhead Publishing, 2009, pp.80-118.
198. Pan, N. Theoretical determination of the optimal fiber volume fraction and fiber-matrix property compatibility of short fiber composites. *Polymer Composites.* 1993, **14**(2), pp.85-93.
199. Department of Materials Science and Engineering. *Mechanics of Composites.* [Online]. 2018. [Accessed 3 Sep]. Available from: http://www.mse.mtu.edu/~drjohn/my4150/class2/class2.html
200. Wang, X. et al. Additive manufacturing of ceramics from preceramic polymers: A versatile stereolithographic approach assisted by thiol-ene click chemistry. *Additive Manufacturing.* 2019, **27**, pp.80-90.